ไบโอคอนจูเกตระหว่างอนุพันธ์กรดซินนามิกและเคอร์ซิทอลเพื่อเป็นสารต้านอนุมูลอิสระและสารยับยั้งแอลฟากลูโคซิเดส และการสังเคราะห์อนุพันธ์ของสารประกอบซัลฟีนาไมด์จากไทออลประเภทต่างๆโดยใช้ไฮเปอร์เวเลนซ์ไอโอดีน(III)เป็นรีเอเจนต์

นายเอกพล รัตนางกูร

วิทยานิพนธ์นี้เป็นส่วนหนึ่งของการศึกษาตามหลักสูตรปริญญาวิทยาศาสตรดุษฎีบัณฑิต
สาขาวิชาเคมี ภาควิชาเคมี
คณะวิทยาศาสตร์ จุฬาลงกรณ์มหาวิทยาลัย
ปีการศึกษา 2557

CINNAMIC ACID DERIVATIVES/QUERCITOL BIOCONJUGATES AS ANTIOXIDANT AND α-GLUCOSIDASE INHIBITOR AND SYNTHESIS OF SULFENAMIDE DERIVATIVES FROM THIOLS USING HYPERVALENT IODINE(III) REAGENTS

Mr. Eakkaphon Rattanangkool

A Dissertation Submitted in Partial Fulfillment of the Requirements
for the Degree of Doctor of Philosophy Program in Chemistry
Department of Chemistry
Faculty of Science
Chulalongkorn University
Academic Year 2014

Thesis Title	CINNAMIC ACID DERIVATIVES/QUERCITOL BIOCONJUGATES AS ANTIOXIDANT AND α-GLUCOSIDASE INHIBITOR AND SYNTHESIS OF SULFENAMIDE DERIVATIVESFROM THIOLS USING HYPERVALENT IODINE(III) REAGENTS
By	Mr. Eakkaphon Rattanangkool
Field of Study	Chemistry
Thesis Advisor	Assistant Professor Sumrit Wacharasindhu, Ph.D.
Thesis Co-Advisor	Associate Professor Preecha Phuwapraisirisan, Ph.D.

Accepted by the Faculty of Science, Chulalongkorn University in Partial Fulfillment of the Requirements for the Doctoral Degree

.....Dean of the Faculty of Science
(Professor Supot Hannongbua, Dr.rer.nat.)

THESIS COMMITTEE

.....Chairman
(Assistant Professor Warinthorn Chavasiri, Ph.D.)

.....Thesis Advisor
(Assistant Professor Sumrit Wacharasindhu, Ph.D.)

.....Thesis Co-Advisor
(Associate Professor Preecha Phuwapraisirisan, Ph.D.)

.....Examiner
(Professor Tirayut Vilaivan, D.Phil.)

.....Examiner
(Associate Professor Pornthep Sompornpisut, Ph.D.)

.....External Examiner
(Poonsakdi Ploypradith, Ph.D.)

เอกพล รัตนางกูร : ไบโอคอนจูเกตระหว่างอนุพันธ์กรดซินนามิกและเคอร์ซิทอลเพื่อเป็นสารต้านอนุมูลอิสระและสารยับยั้งแอลฟากลูโคซิเดส และการสังเคราะห์อนุพันธ์ของสารประกอบซัลฟีนาไมด์จากไทออลประเภทต่างๆโดยใช้ไฮเปอร์เวเลนซ์ไอโอดีน(III)เป็นรีเอเจนต์ (CINNAMIC ACID DERIVATIVES/QUERCITOL BIOCONJUGATES AS ANTIOXIDANT AND α-GLUCOSIDASE INHIBITOR AND SYNTHESIS OF SULFENAMIDE DERIVATIVESFROM THIOLS USING HYPERVALENT IODINE(III) REAGENTS) อ.ที่ปรึกษาวิทยานิพนธ์หลัก: ผศ. ดร.สัมฤทธิ์ วัชรสินธุ์, อ.ที่ปรึกษาวิทยานิพนธ์ร่วม: รศ. ดร.ปรีชา ภูวไพรศิริศาล, หน้า.

งานวิจัยนี้แบ่งออกเป็น 2 ส่วน (1) การสังเคราะห์สารออกฤทธิ์จาก (+)-*proto*-quercitol ซึ่งเป็นสารที่แยกได้จากธรรมชาติ และ (2) การศึกษาวิธีการสังเคราะห์อนุพันธ์ของซัลฟีนาไมด์และผลิตภัณฑ์ที่เกี่ยวข้องโดยใช้ไฮเปอร์เวเลนต์ไอโอดีน(III) โดยในงานวิจัยแรกเกี่ยวข้องกับการสังเคราะห์ระหว่าง carbasugar และอนุพันธ์ของกรดซินนามิกโดยผลิตภัณฑ์ที่ได้นำมาทดสอบฤทธิ์การยับยั้งกลูโคซิเดสและฤทธิ์การต้านอนุมูลอิสระ ในงานนี้สามารถสังเคราะห์สารได้ทั้งหมด 31 อนุพันธ์คืออนุพันธ์เอสเตอร์ (2.1ER-2.8ES) และอนุพันธ์เอไมด์ (2.1AR-2.8AS) สารทั้งหมดได้ถูกพิสูจน์เอกลักษณ์และทดสอบฤทธิ์การยับยั้งแอลฟากลูโคซิเดสในยีสต์และในลำไส้เล็กของหนู (มอลเทสและซูเครส) โดยสารสังเคราะห์ที่สามารถยับยั้งแอลฟากลูโคซิเดสในลำไส้เล็กของหนูได้ มีค่า IC_{50} อยู่ที่ 0.41-527.41 ไมโครโมลาร์ ซึ่งมีฤทธิ์ยับยั้งแอลฟากลูโคซิเดสได้ดีกว่าอนุพันธ์กรดซินนามิกตั้งต้น 1.2-208 เท่า จากสารผลิตภัณฑ์ทั้งหมดสาร 2.8AS แสดงฤทธิ์การยับยั้งมอลเทสได้ดีที่สุดโดยมีค่า IC_{50} อยู่ที่ 0.41 ไมโครโมลาร์ ออกฤทธิ์ใกล้เคียงกับยารักษาโรคเบาหวาน acarbose และ voglibose (ค่า IC_{50} อยู่ที่ 1.5 และ 0.25 ไมโครโมลาร์ตามลำดับ) ในขณะเดียวกันยังคงมีฤทธิ์การต่อต้านอนุมูลอิสระ SC_{50} อยู่ที่ 0.07 มิลลิโมลาร์ ซึ่งมีค่าใกล้เคียงกับสารมาตรฐาน BHA (SC_{50} อยู่ที่ 0.10 มิลลิโมลาร์) นอกจากนี้ได้ศึกษากลไกการยับยั้งระหว่างมอลเทสและ 2.8AS พบว่า 2.8AS เป็นสารยับยั้งแบบไม่แข่งขัน ดังนั้นจึงได้ทำการศึกษาเพิ่มเติมโดยวิธีการจำลองโมเลกุลเพื่อยืนยันการทดลองข้างต้น พบว่า 2.8AS สามารถจับกับมอลเทสได้ที่ บริเวณอัลโลสเตอริกซึ่งอยู่บนส่วนที่เป็นตัวเร่งปฏิกิริยาและเป็นคนละตำแหน่งกับบริเวณเร่งซึ่งเป็นบริเวณที่ acarbose จับนอกจากนี้การศึกษาการตอบสนองแบบเสริมฤทธิ์กันระหว่าง 2.8AS และ acarbose ในการยับยั้งมอลเทส พบว่ามีฤทธิ์การยับยั้งที่เพิ่มขึ้น 1.1-5.7 เท่าเมื่อเทียบกับการใช้ acarbose ตัวเดียว ดังนั้นจากผลการศึกษาข้างต้นคาดว่าการใช้ยาและ 2.8AS ร่วมกันจะสามารถช่วยลดระดับน้ำตาลในกระแสเลือดได้

ในงานวิจัยที่สองเน้นการพัฒนาการสังเคราะห์สารประกอบซัลฟีนาไมด์ โดยอนุพันธ์ซัลฟีนาไมด์ถูกสังเคราะห์ขึ้นจากการทำปฏิกิริยาระหว่างอนุพันธ์ไทออลกับไฮเปอร์เวเลนต์ไอโอดีน(III) และเอมีนได้ผลผลิต 43–90 เปอร์เซ็นต์ การศึกษาครั้งนี้ถูกนำมาประยุกต์ใช้กับอินโดลซึ่งเป็นตัวแทนสารกลุ่มอะโรมาติกที่อุดมด้วยอิเล็กตรอนและสามารถสร้างพันธะซัลเฟอร์–คาร์บอนได้ในปฏิกิริยาแบบขั้นตอนเดียว โดยประโยชน์ของการศึกษาในครั้งนี้คือการใช้ตัวทำปฏิกิริยา (ดีไอบี) ที่มีความเป็นพิษต่ำ ราคาถูก รวมทั้งปฏิกิริยาการสังเคราะห์เป็นปฏิกิริยาที่ไม่รุนแรงคือ สามารถทำได้ที่อุณหภูมิห้อง ตัวทำละลายไม่จำเป็นต้องกลั่น และเป็นระบบเปิด

ภาควิชา เคมี ลายมือชื่อนิสิต .....

สาขาวิชา เคมี ลายมือชื่อ อ.ที่ปรึกษาหลัก .....

ปีการศึกษา 2557 ลายมือชื่อ อ.ที่ปรึกษาร่วม .....

5272661223 : MAJOR CHEMISTRY
KEYWORDS: GLUCOSIDASE / CAFFEIC ACID / MULTIFUNCTIONAL DRUG / ISOFERULIC ACID / DIABETES MELLITUS / HYPERVALENT COMPOUNDS / IODINE / SULFUR / HETEROCYCLES / SULFENAMIDE

EAKKAPHON RATTANANGKOOL: CINNAMIC ACID DERIVATIVES/QUERCITOL BIOCONJUGATES AS ANTIOXIDANT AND α-GLUCOSIDASE INHIBITOR AND SYNTHESIS OF SULFENAMIDE DERIVATIVESFROM THIOLS USING HYPERVALENT IODINE(III) REAGENTS. ADVISOR: ASST. PROF. SUMRIT WACHARASINDHU, Ph.D., CO-ADVISOR: ASSOC. PROF. PREECHA PHUWAPRAISIRISAN, Ph.D., pp.

In this research, we focus on two distinct research themes: (1) bioactive compound from natural (+)-*proto*-quercitol and (2) synthetic methodology for the synthesis of sulfenamides and related compounds using hypervalent iodine(III). The first project involves structural modification of natural carbasugar with cinnamic acid derivatives to enhance their glucosidase inhibitory and antioxidant property. In this work, 31 novel compounds (quercityl-cinnamate derivatives (2.1ER-2.8ES) and quercityl-cinnamamide derivatives (2.1AR-2.8AS)) were prepared, fully characterized and investigated for their α-glucosidase inhibitory effect against baker's yeast and rat intestine (maltase and sucrase) *in vitro*. Most compounds potentially inhibit α-glucosidase from rat intestine with IC_{50} value in the range of 0.41-527.41 μM, which are 1.2-208 times greater than corresponding starting cinnamic acid derivatives. Of the prepared compounds, 2.8AS possesses the highest maltase inhibitory activity with an IC_{50} value of 0.41 μM, which is equipotent to some clinically used antidiabetic drugs, acarbose and voglibose (IC_{50} = 1.5 and 0.25 μM, respectively). In addition, its radical scavenging ability (SC_{50} = 0.07 mM) is comparable to that of commercial antioxidant BHA (SC_{50} = 0.10 mM). In addition, kinetic study revealed that mechanistically, 2.8AS is non-competitive inhibitor for maltase. Moreover, docking analysis confirmed that 2.8AS could bind to the maltase in an allosteric site on the catalytic domain, which is different from the pocket site (active site) of acarbose. For synergistic effect of 2.8AS, inhibitory activity against maltase exerted by a mixture of acarbose and 2.8AS was significantly improved up to 1.1-5.7 times, when compared with acarbose alone. The outcome of this research suggests that this combination may provide a significant clinical benefit in delaying postprandial hyperglycemia.

The aim of the second project is to develop an efficient synthetic methodology for sulfenamide. Treatment of hypervalent iodine(III) to thiols in the presence of amines provides the corresponding sulfenamides in fair to good yields (43–90%). The methodology is successfully extended to indole as a representative of an electron-rich aromatic compound, allowing a successful construction of an S–C bond in a one-pot fashion. The key benefits of this reaction include lower toxicity, low cost of DIB reagent, and mild reaction conditions (room temperature, undried solvents and open flask).

Department:	Chemistry	Student's Signature	.....
Field of Study:	Chemistry	Advisor's Signature	.....
Academic Year:	2014	Co-Advisor's Signature	.....

ACKNOWLEDGEMENTS

The author would like to express my sincere appreciation to my advisor, Assistant Professor Dr. Sumrit Wacharasindhu and co-advisor, Associate Professor Dr. Preecha Phuwapraisirisan, Department of Chemistry, Faculty of Science, Chulalongkorn University, for excellent instruction, great valuable advice, kind guidance and support throughout the course of this research.

In addition, many thanks to the Chairperson: Assistant Professor Dr. Warinthorn Chavasiri, Department of Chemistry, Faculty of Science, Chulalongkorn University; the thesis examiners: Professor Dr. Tirayut Vilaivan and Associate Professor Dr. Pornthep Sompornpisut, Department of Chemistry, Faculty of Science, Chulalongkorn University and Dr. Poonsakdi Ploypradith for their invaluable discussion and suggestion.

I also especially thank Associate Professor Dr. Pornthep Sompornpisut and Mr Chirayut Supunyabut for his kind assistance, advice, and for all of his tireless efforts in computational study.

Moreover, special thanks to member in Natural Products Research Unit and Material Advancement via Proficient Synthesis group, Department of Chemistry, Faculty of Science, Chulalongkorn University for their generosity, help and good friendship. And I also thank to Dr. Wisuttaya Worawalai and Dr. Thanakorn Damsud for technical assistance and for all of the greatest memories.

I wish to thank Chulalongkorn University Dutsadi Phiphat Scholarship for granting in partial financial support to conduct this research.

Finally, I am deeply grateful to my family for their love and encouragement throughout my Ph.D. study.

CONTENTS

Page

Page

Page

Page

LIST OF TABLES

LIST OF FIGURES

LIST OF SCHEMES

LIST OF ABBREVIATIONS

acetone-d_6	deuterated acetone
brm	broad multiplet (NMR)
brs	broad singlet (NMR)
calcd	calculated
^{13}C NMR	carbon-13 nuclear magnetic resonance
$CDCl_3$	deuterated chloroform
CD_3OD	deuterated methanol
COSY	correlated spectroscopy
DBU	1,8-diazabicyclo[5.4.0]undec-7-ene
DIB	(diacetoxy)iodo benzene
DIPEA	*N,N*-diisopropylethylamine
DMF	*N,N*-dimethylformamide
DMAP	4-(dimethylamino)pyridine
DM	diabetes mellitus
ddd	doublet of doublet of doublet (NMR)
dt	doublet of triplet (NMR)
d	doublet (NMR)
dd	doublet of doublet (NMR)
2D NMR	two dimensional nuclear magnetic resonance
1D NMR	one dimensional nuclear magnetic resonance
ESIMS	electrospray ionization mass spectrometry
equiv	equivalent (s)
g	gram (s)
^{1}H NMR	proton nuclear magnetic resonance

HRESIMS	high-resolution electrospray ionization mass spectrometry
Hz	Hertz
h	hour (s)
IC_{50}	concentration required for 50% inhibition *in vitro*
IDDM	insulin-dependent diabetes mellitus
*i*PrOH	isopropanol
J	coupling constant
min	minute (s)
mg	milligram (s)
mL	milliliter (s)
mmol	millimole (s)
m/z	mass per charge
m	multiplet (NMR)
MsCl	mesyl chloride
M.W.	molecular weight
M	molar
NIDDM	non-insulin-dependent diabetes mellitus
PNP-G	p-nitrophenyl-**α**-D-glucopyranoside
rt	room temperature
s	singlet (NMR)
TFA	trifluoroacetic acid
THF	tetrahydrofuran
TMS	tetramethylsilane
TsCl	*p*-toluenesulfonyl chloride
TLC	thin layer chromatography
U	unit

UV	ultraviolet
δ	chemical shift
δ_C	chemical shift of carbon
δ_H	chemical shift of proton
°C	degree Celsius
vmax	maximum wave number
µL	microliter (s)
µM	micromolar (s)
% yield	percent yield

CHAPTER I

INTRODUCTION

1.1 Diabetes mellitus (DM) disease

1.1.1 Introduction

Over the last century, diabetes mellitus (DM) is becoming a major public health problem because of changes in human behavior and lifestyle. The outbreak of diabetes mellitus can be found worldwide and the numbers of diabetes mellitus patients are increasing around the world. The prevalence of diabetes mellitus has reached epidemic proportions and has affected 6.4% of adults worldwide in 2010 [1, 2]. The worldwide evaluation of the disease in 2010 indicated the increasing number of cases by 46% [3] (Figure 1.1) from 2000 and will reach a number of 144% over the next 30 years [4].

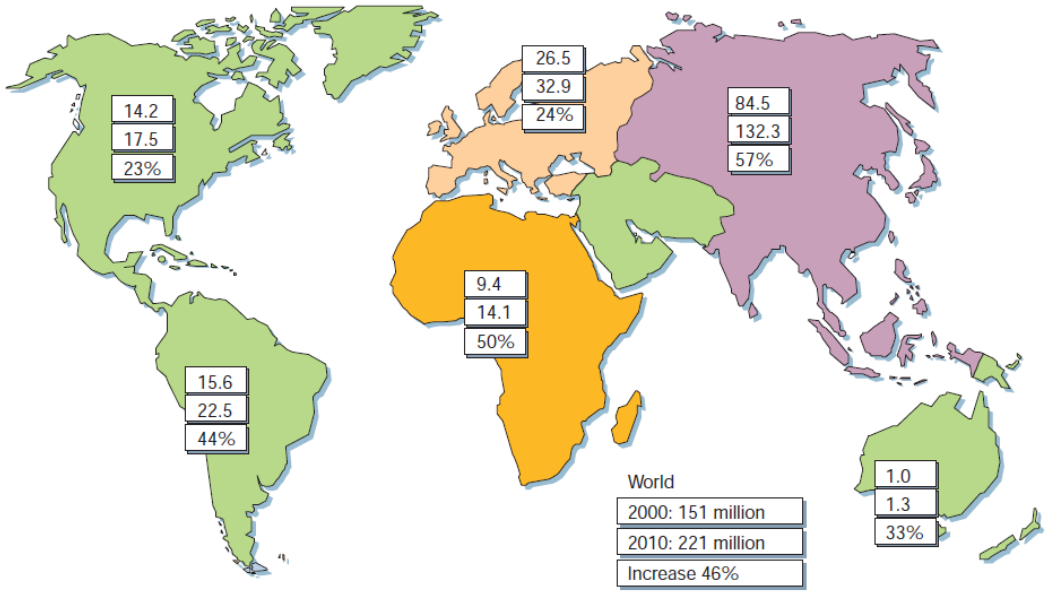

Figure 1.1 Numbers of people with diabetes (in millions) for 2000 and 2010 (top and middle values, respectively), and the percentage increase [3].

DM usually related to diabetic patients is a group of metabolic disorders characterized by high blood glucose levels (postprandial hyperglycemia) or elevated blood glucose levels.

Generally, the metabolic process of carbohydrate in small intestine involves the breakdown of carbohydrates to monosaccharide (glucose) which is then adsorbed into the cells of the intestine to blood vessels. β-Cells of pancreas normally release insulin hormone when glucose level is increasing to transport glucose into the cells. If β-cells of pancreas cannot secrete insulin hormone or promote the binding of insulin of the insulin receptor, this normally leads to a DM symptom (Figure 1.2).

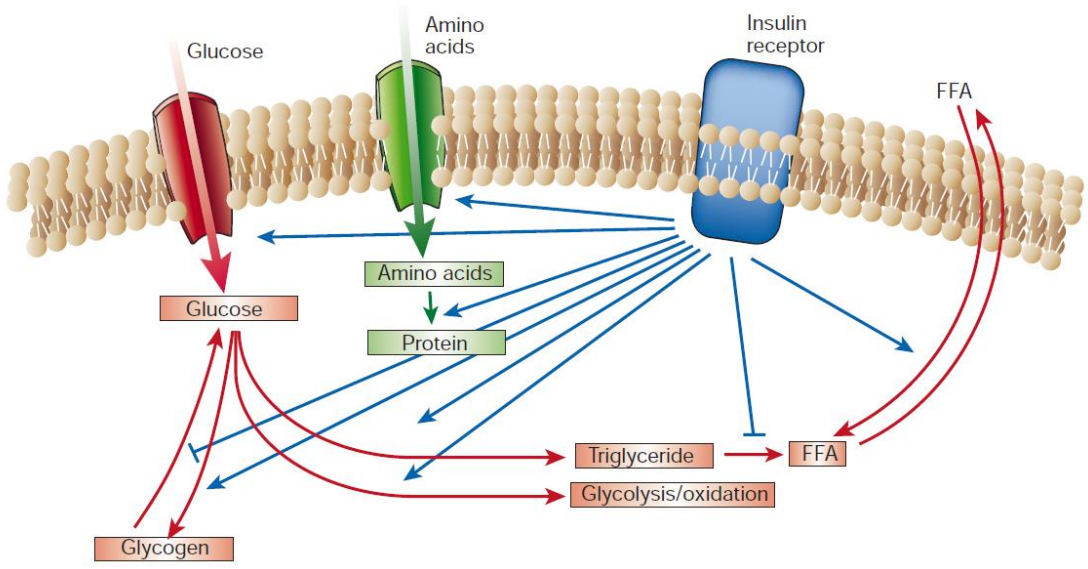

Figure 1.2 The regulation of carbohydrate metabolism by insulin [5].

There are two main types of diabetes (Figure 1.3). Type I diabetes is due mainly to autoimmune-mediated damage of pancreatic β-cell islets, resulting in absolute insulin deficiency. Type II diabetes, accounts for over 95% around the world which is higher than the frequency of type I diabetes. Type II diabetes is characterized by insulin resistance and/or irregular insulin secretion. People with type II diabetes are not reliant on exogenous insulin, but may require it to control blood

glucose level. Currently, we have several drugs to treat type II diabetic patients, each with unique molecular to lower blood glucose levels. A key approach for treating type II diabetic patients is to delay the postprandial hyperglycemia by decreasing the rate of carbohydrate digestion through the inhibition of α-glucosidase [6, 7].

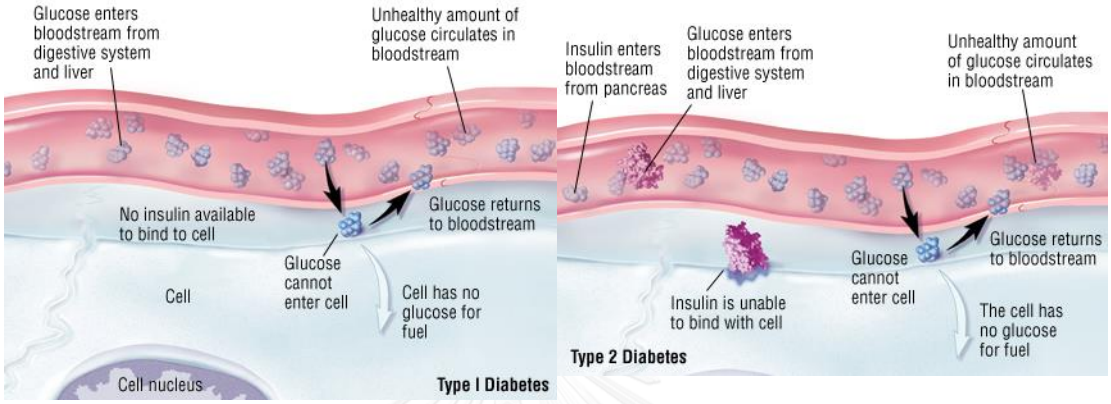

Figure 1.3 Causes of diabetes: type I DM (http://www.drugs.com/health-guide/type-1-diabetes-mellitus.html) and type II DM (http://www.drugs.com/health-guide/type-2-diabetes-mellitus.html).

1.1.2 α-Glucosidase inhibitors

Glycosidase inhibitors are clinically employed as anti-hyperglycemic [8] and anti-influenza agents [9] and have ability to treat viral [10], bacterial, and fungal infections [11], as well as a range of other ailments, including Gaucher's disease [12] and cancer[13].

Glucosidases are specific for the cleavage of glycosidic bonds (1-4 or 1-6 linkage) depending on the number, position, or configuration of the hydroxyl groups on the sugar molecule. Thus, α-glucosidases are able to catalyze the cleavage of α-glycosidic bonds through α-linkages at the anomeric center, such as hydrolysing α-1,4-glycosidic bond of oligosaccharide to D-glucose (Figure 1.4). α-Glucosidase inhibitors slow down the rate of oligosaccharide digestion and retard D-glucose absorption, thereby lowering blood glucose levels. Usually, α-glucosidase inhibitors

are used as oral anti-diabetic drugs by preventing the hydrolysis of oligosaccharide to D-glucose in diabetes mellitus type II patients.

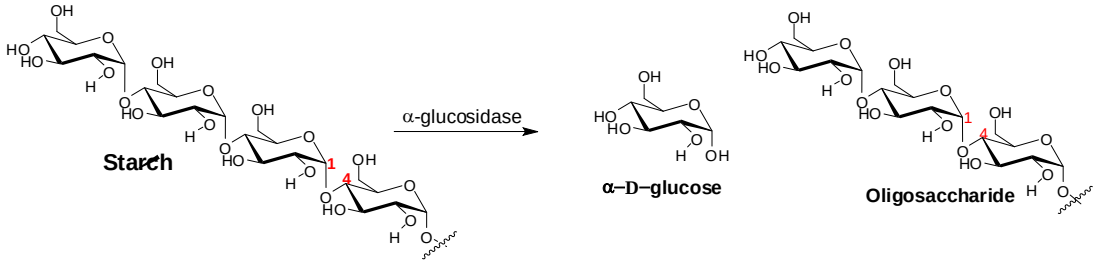

Figure 1.4 Hydrolysis of oligosaccharides (starch) with α-glucosidase.

Nowadays, there there are only a few drugs for the treatment of type II diabetes, such as (1) acarbose (Precose® or Glucobay® or Prandase®, Figure 1.5, **1.1**), which was discovered in a target-directed screening of soil bacteria *Actinoplanes* sp. by researchers at the Bayer company in 1970s and was first launched in 1990 [14]. Voglibose (Basen®, Figure 1.5, **1.2**), which exhibited the highest potency against maltase and sucrase, has been developed for treating diabetes mellitus type II by a Japanese company since 1994. From some current reports, voglibose displayed 20-30 times higher inhibition against maltase and sucrase than acarbose [15]. Miglitol (Glyset®, Figure 1.5, **1.3**), was synthesized starting from the naturally occurring 1-deoxynojirimycin and was first approved in 1996.

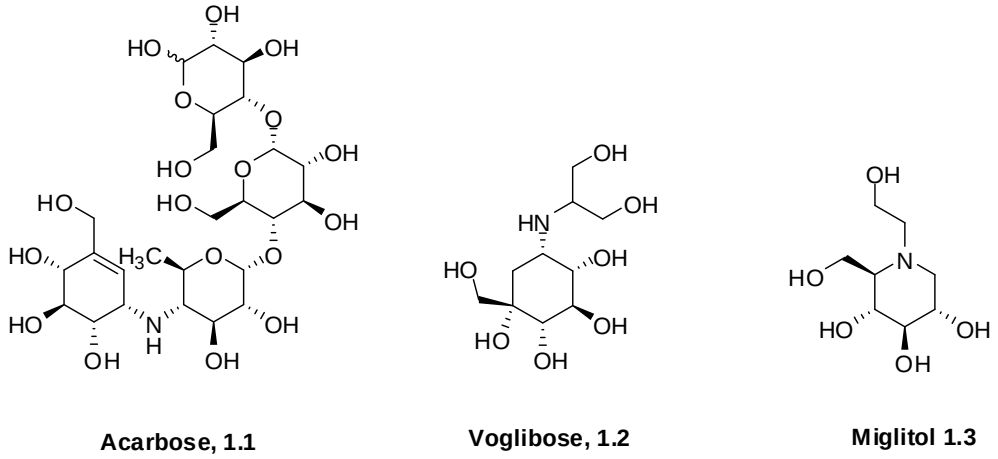

Figure 1.5 Structure of acarbose (**1.1**), voglibose (**1.2**) and miglitol (**1.3**).

Usually, the available drugs have an aminocyclitol or iminosugar as a core structure [16]. Currently, some research groups exposed the new groups or new compounds for anti-diabetic drug.

Sulfonium-sulfate thiosugars

Salacinol (**1.4**) (Figure 1.6), is among the first sulfonium-sulfate inhibitors which were discovered from the dried roots and stems of *Salacia reticulata* by Yoshikawa and co-workers in 1997 [17]. Compound **1.4** exhibited several α-glucosidase inhibitory activities on rat intestine, including those against maltase, sucrase and isomaltase (K_i = 0.31, 0.32 and 0.47 μM, respectively) [17, 18].

Kotalanol (**1.6**) (Figure 1.6), was another bioactive component that was found in the aqueous extracts of *Salacia reticulata*, and exhibited higher α-glucosidase inhibitory activity (K_i = 0.23 and 0.18 μg/mL for maltase and sucrase, respectively) than salacinol (**1.5**) (K_i = 0.31 and 0.32 μg/mL for maltase and sucrase, respectively) [19].

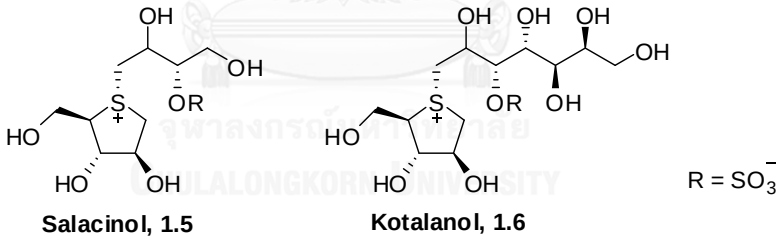

Figure 1.6 Structures of salacinol (**1.5**) and kotalanol (**1.6**).

Marine organosulfates

Penarolide sulfates A_1 (**1.7**) and A_2 (**1.8**) as seen in Figure 1.7 were isolated from a marine sponge *Penares* sp. and their core structures with absolute configurations were determined to be the unique 30- and 31-membered macrolide, respectively. These compounds inhibited yeast α-glucosidase with IC_{50} values of 1.2 and 1.5 μg/mL, respectively [20].

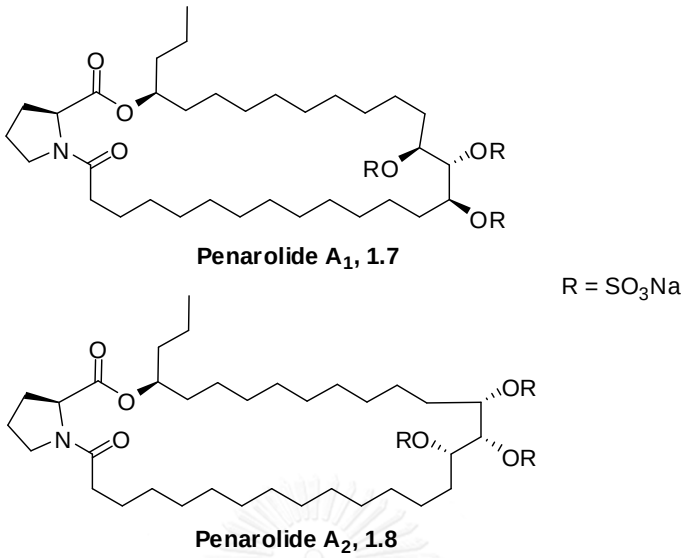

Figure 1.7 Structure of penarolide sulfates A_1 (**1.7**) and A_2 (**1.8**).

Other types

Derivatives of the benzothiazole skeleton derivatives (**1.9a**-**1.9t**) were synthesized, as sshown in Scheme 1.1. A all synthesized compounds were tested for yeast α-glucosidase inhibitory activity by Choudhary and co-workers [21]. (E)-*N'*-(4-Chlorobenzylidene)-4-(benzo[d]thiazol-2-yl)benzohydrazide (**1.9o**), as shown in Figure 1.8, showed the most potent inhibitory activity against yeast α-glucosidase with IC_{50} value 5.31 μM, which was 170 times greater than acarbose (906 μM).

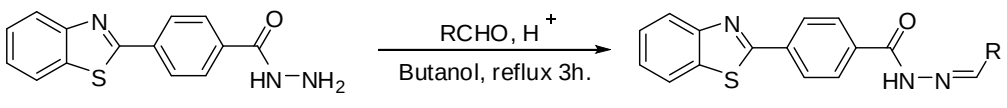

1.9 **1.9a**-**1.9t**

Scheme 1.1 Synthesis of various benzothiazole derivatives by treating compound **1.9** with various aryl-aldehydes derivatives (**1.9a**-**1.9t**.).

2-Allylamino-4-methylsulfanyl-butyric acid (**1.10**) (Figure 1.8) was synthesized and fully characterized by Palvannan and co-workers [22]. Compound **1.10** was

evaluated for the DPPH radical scavenging activity and also against yeast α-amylase and α-glucosidase inhibition *in vitro*. Compound **1.10** showed α-amylase and α-glucosidase inhibitory activity with IC_{50} values of 51.2 and 45.6 μg/mL, respectively. In addition, compound **1.10** displayed DPPH radical activity of 44.1 μg/mL.

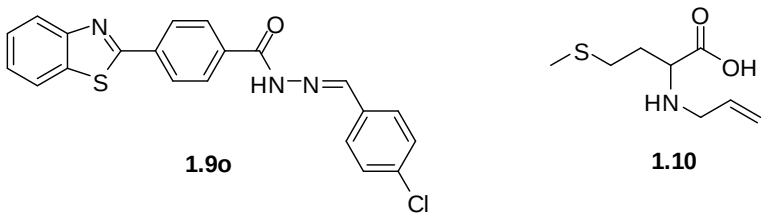

1.9o **1.10**

Figure 1.8 Structure of **1.9o** and 4-methyl sulfanyl butyric acid (**1.10**).

From the point of view, all of the bioactive compounds having in only single component. And during the past few decades, many groups have provided some evidences suggesting that excess plasma glucose drives the overproduction of superoxide radicals and other reactive oxygen species, all of which were implicated in the impairment of the cells via oxidative stress and accounting for the pathogenesis of all diabetic complications [23-25].

Therefore, anti-diabetic drugs possessing anti-hyperglycemic effect and radical scavenging ability would be beneficial for type II diabetic therapy.

1.2 Bioconjugation technique

The fundamental aspect of bioconjugation simply involves the attachment of one molecule to another, usually through a covalent bond, to create a complex comsisting of both molecules linked together (Figure 1.9).

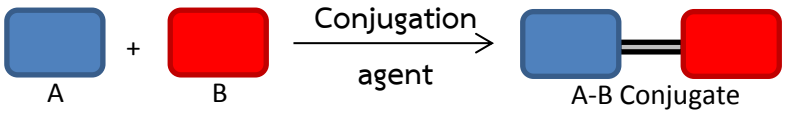

Figure 1.9 Forming a basis conjugate involves the reaction of two molecules.

Usually, at least one of the molecules is of biological activity or is a fragment or derivative of a biomolecule. In some cases, the conjugate that is formed is entirely synthetic, but its use is directed toward biological or life science application [26]. Common types of bioconjugation reactions are coupling of protein, lipid, amino acid or sugar.

Literature reviews on bioconjugated compounds:

Seven novel conjugated compounds encompassing ferulic acid and *myo*-inositol residues were synthesized and examined for their structures and biological activities by Taniguchi, H. and co-workers in 2000 [27]. The TPA (12-*O*-tetradecanoylphorbol-13-acetate)-induced superoxide (O_2^-) generation inhibitory activity was evaluated on human promyelocytic leukemia cells (HL-60 cells). Compound **1.11** showed the strongest anti-oxidant activity on HL-60 cells of 98 percent, which was 7 times greater than that of the starting material ferulic acid. The other derivatives displayed lower than 30 percent of antioxidant activity (Figure 1.10).

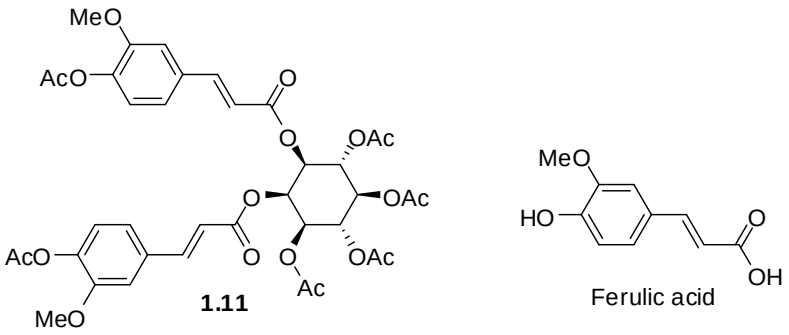

Figure 1.10 The derivative (**1.11**) and ferulic acid.

In 2001 Misra, K. and co-workers synthesized curcumin bioconjugates by coupling with amino acid or nucleotide analogues at methylene carbon (1,3-dione) and studied thier antibacterial activities [28]. 2'-Deoxy-2'-curcuminyluridin (Figure 1.11, **1.12**) exhibited MIC values against *Micrococcus cocci* and *Staphylococcus aureus* of 3.75 and 7.50 μmol/mL, respectively, but the parent compound (curcumin) did not exhibit any significant antibacterial activity even at 10 mM. Moreover, compound **1.12** possessed a partition coefficient of 3.0, while that of curcumin was 3.2. Thus, these results showed that a bioconjugated compound may have quite improved water solubility.

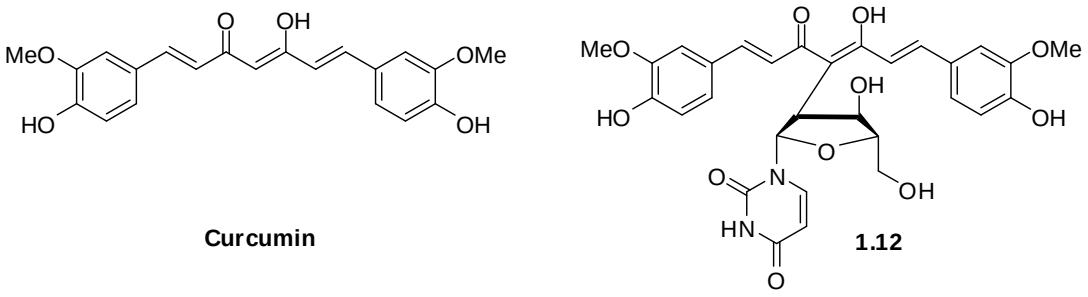

Figure 1.11 Curcumin and 2'-deoxy-2'-curcuminyluridin (**1.12**)

Moreover, six daunorubicin derivatives consistong of uncommon sugars were synthesized and tested against cancer cells by Wang, P. G. and co-workers in 2005

[29]. The conjugates were evaluated for cytotoxicity against colon cancer cells (SW620 cells) by an MTS assay. The results showed that the aglycon of daunorubicin without sugar or uncommon sugar moiety has 70–100-fold lower activity than daunorubicin analogues with uncommon sugars. Compound **1.13** showed the lowest IC_{50} value of 104 nM, which is 20 times greater than that of aglycon of daunorubicin (>2,000 nM) as shown in Figure 1.12.

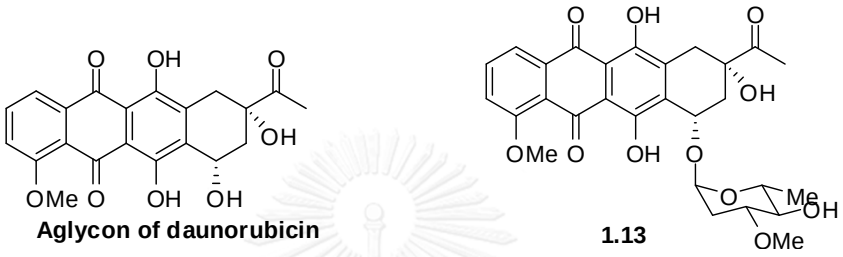

Figure 1.12 Aglycon of daunorubicin and compound **1.13**.

In 2009 Lee, Y. S. and co-workers [30] prepared some bioconjugated compounds of the glucose-flavone types which were evaluated for their antioxidant activity (Figure 1.13). The quercetin 3-*O*-methyl ether series (**1.14a** and **1.14b**) exhibited superoxide radical scavenging activities (IC_{50} = 10.24, 12.77 μM, respectively) as compared to the parent compound **1.14** (IC_{50} = 17.39 μM). Besides, the superoxide radical scavenging activity of the luteolin series (**1.15a** and **1.15b**) were increased two-fold by conjugation with a glucose group (IC_{50} = 3.28, 3.53 μM, respectively) versus luteolin (IC_{50} = 8.66 μM) while a commercial antioxidant ascorbic acid (IC_{50} >300 μM) was used as a reference.

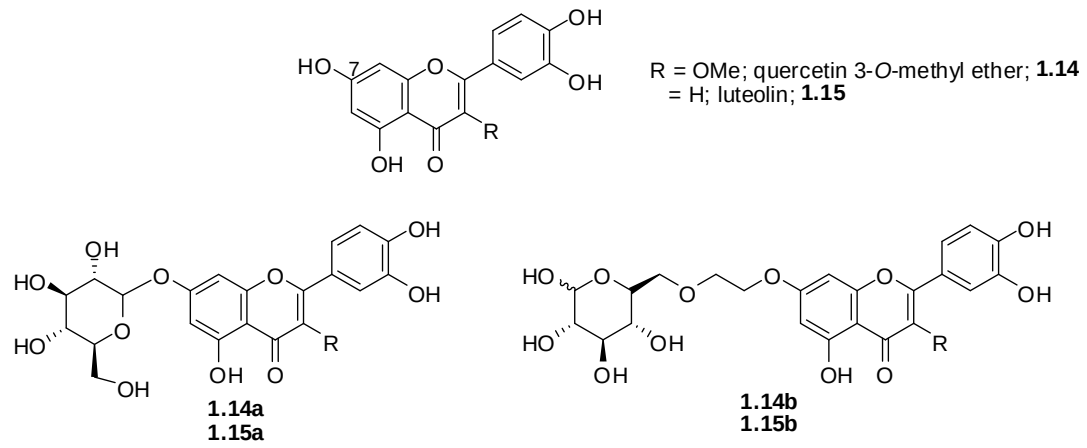

Figure 1.13 Glucose-flavones conjugates.

In addition, 7-*O*-cinnamoylmorroniside (Figure 1.14, **1.17**) was synthesized and evaluated for its anti-inflammatory activity using human umbilical vein endothelial cells (HUVECs) by Koketsu, M. and co-workers [31]. Compound **1.17** inhibited the expression of E-selectin by the stimulation of TNF-α, with in IC_{50} value of 49.3 μM which was comparable to that of harpagoside (**1.16**) (a reference anti-inflammatory agent) (IC_{50} value of 88.2 μM), but the parent compound (morroniside) showed normally no activity.

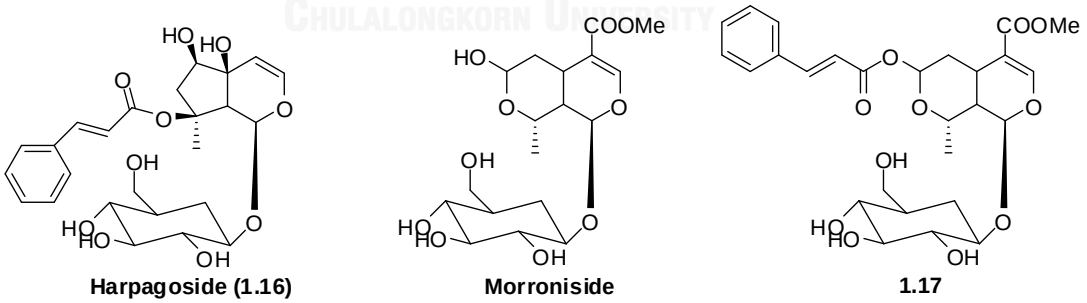

Figure 1.14 Harpagoside (**1.16**), morroniside and 7-*O*-cinnamoylmorroniside (**1.17**).

Furthermore, fumagillin derivatives were synthesized and evaluated for their antiangiogenic anticancer activities using calf pulmonary artery endothelial cells (CPAE) by No, K. T. and co-workers in 2000 [32] (Figure 1.15). The results indicated

that the antiproliferation activity of the *trans*-cinnamic acid ester derivative (**1.18b**) was 10,000 fold greater than these of the *cis*-cinnamic acid ester derivative (**1.18d**) and phenylalkanoic acid ester derivative (**1.18c**). Moreover, the potency of **1.18b** compound on endothelial cell is more than 1,000 times greater than that of TNP-470 (**1.18a**) which was clinically developed for treating cancers as an anti-angiogenic agent [33].

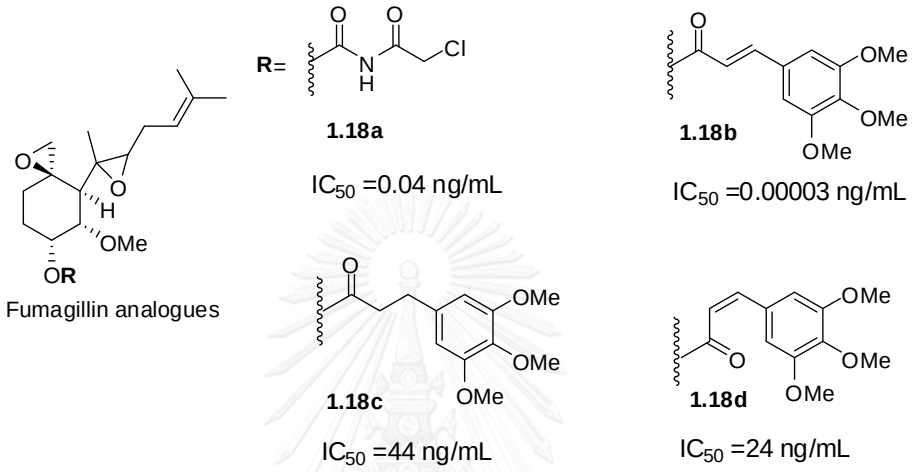

Figure 1.15 Fumagillin derivatives.

In 2011 Baltas, M. and co-workers [34] prepared a number of cinnamic acid derivatives which possessed encouraging anti-tuberculosis (anti-TB) activities (MIC) and cytotoxic activities. The MIC value of **1.19** against *Mycobacterium tuberculosis* strain ($H_{37}Rv$) of 0.04 μM was 1,800 times greater than that of isoniazid (INH), a frontline anti-TB drug, with the IC_{50} value of 729 μM as shown in Figure 1.16.

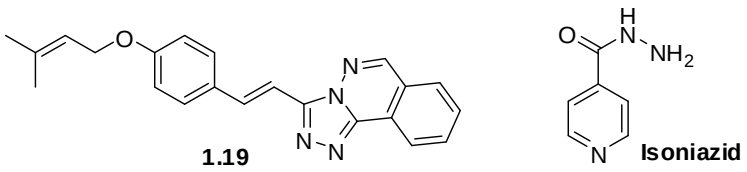

Figure 1.16 Compound **1.19** and isoniazid.

Additionally, Zeng, A. and co-workers reported the preparation of *N*-substituted aminomethyl-β-D-glucopyranoside derivatives using their parent compounds as starting material *via* reductive amination (Scheme 1.2) or acylation

(Scheme 1.3). All synthesized compounds were tested for α-glucosidase inhibitory activity. Most of them inhibited α-glucosidase greater than a parent compound (**1.20**). Of all synthesized compounds, **1.24a** (IC_{50} = 2.3 μM) and **1.24e** (IC_{50} = 5.1 μM) were the most potent, inhibiting yeast α-glucosidase and maltase in rat intestine, respectively [35].

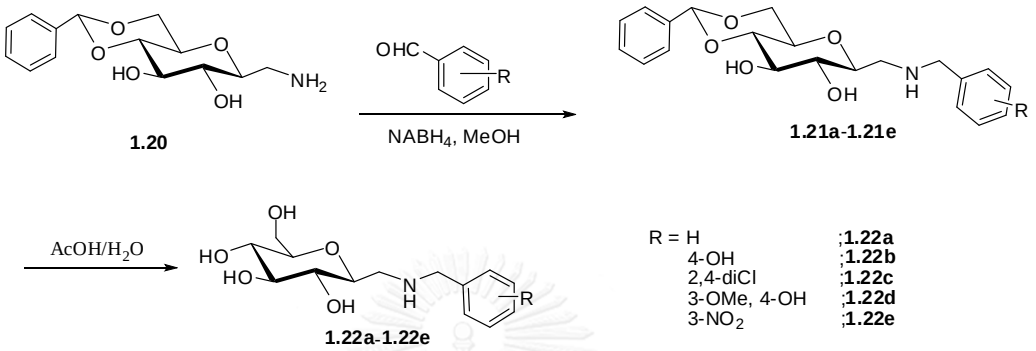

Scheme 1.2 Synthesis of sugar-amines **1.22a**-**1.22e**.

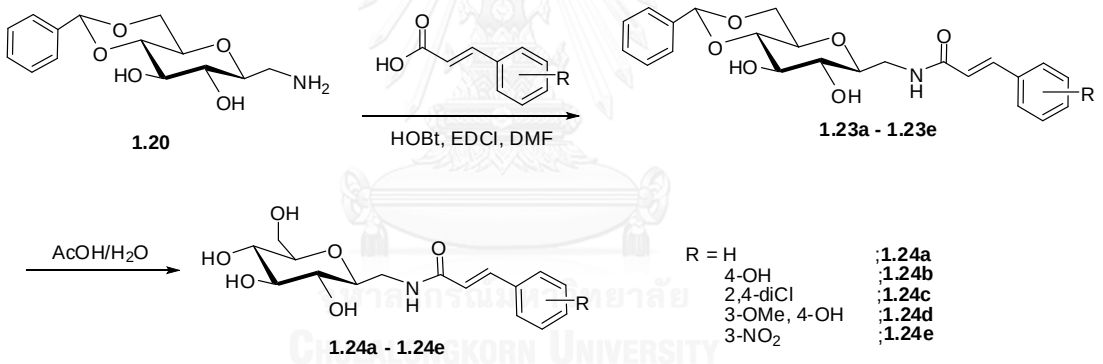

Scheme 1.3 Synthesis of sugar-amides **1.24a**-**1.24e**.

The conventional conjugated compounds shown above were prepared by combining oxy-sugars or uncommon oxy-sugars with a bio-active compound. Over the last decade, cyclitols or carbasugars are defined as polyhydroxy-substituted cycloalkenes or cycloalkanes that can be classified into four major groups namely inositols (**1.25**), quercitols (**1.26**), conduritols (**1.27**) and quinic acids (**1.28**) [36] (Figure 1.17). All types were studied and the analogues of these sugars were investigated for bio-activities. Some of the compounds exhibited inhibitory activities against various

glycosidases [37, 38] including anti-bacterial [39] and potential anticancer activities [40].

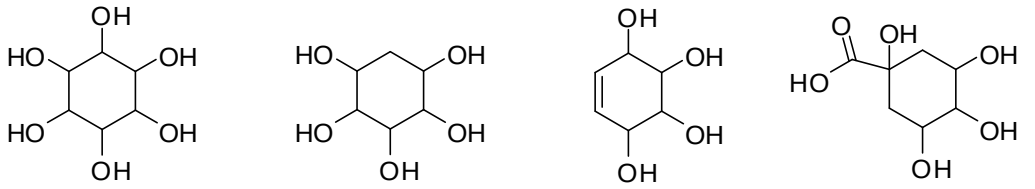

Figure 1.17 Structures of certain natural cyclitols.

In our research group, Wacharasindhu, S. and co-workers [38] were successful to synthesize 5-amino-1,2,3,4-cyclohexanetetrols (*R*- and *S*- configuration) from naturally available (+)-*proto*-quercitol *via* compound **1.30** as a chiral building block. 5*R*- and 5*S*-Aminocyclitols showed inhibition against yeast α-glucosidase with IC_{50} values of 12.5 and 2,890 μM, respectively.

In next few years, Phuwapraisirisan, P. [41] and co-workers developed an efficient method for the synthesis of (+)-conduritol F, (+)-*chiro*- and (+)-*epi*-inositols (Scheme 1.4) from naturally available (+)-*proto*-quercitol and evaluated their α-glucosidase inhibitory effects. Of the synthesized compounds, (+)-conduritol F showed the greatest inhibition against type I α-glucosidase with an IC_{50} value of 86.1 μM, which is 5-fold greater than that of acarbose. Moreover, *N*-substituted aminoquercitols [42] (Scheme 1.5) were prepared starting from compound **1.29** and then tested for its α-glucosidase inhibitory activity. Synthetic compounds showed IC_{50} values against maltase in rat small intestine in a range of 0.24–290 μM. Of the compounds examined, the highest inhibition was observed with IC_{50} of 0.24 μM, whereas acarbose was 6 times less active (IC_{50} 1.50 μM).

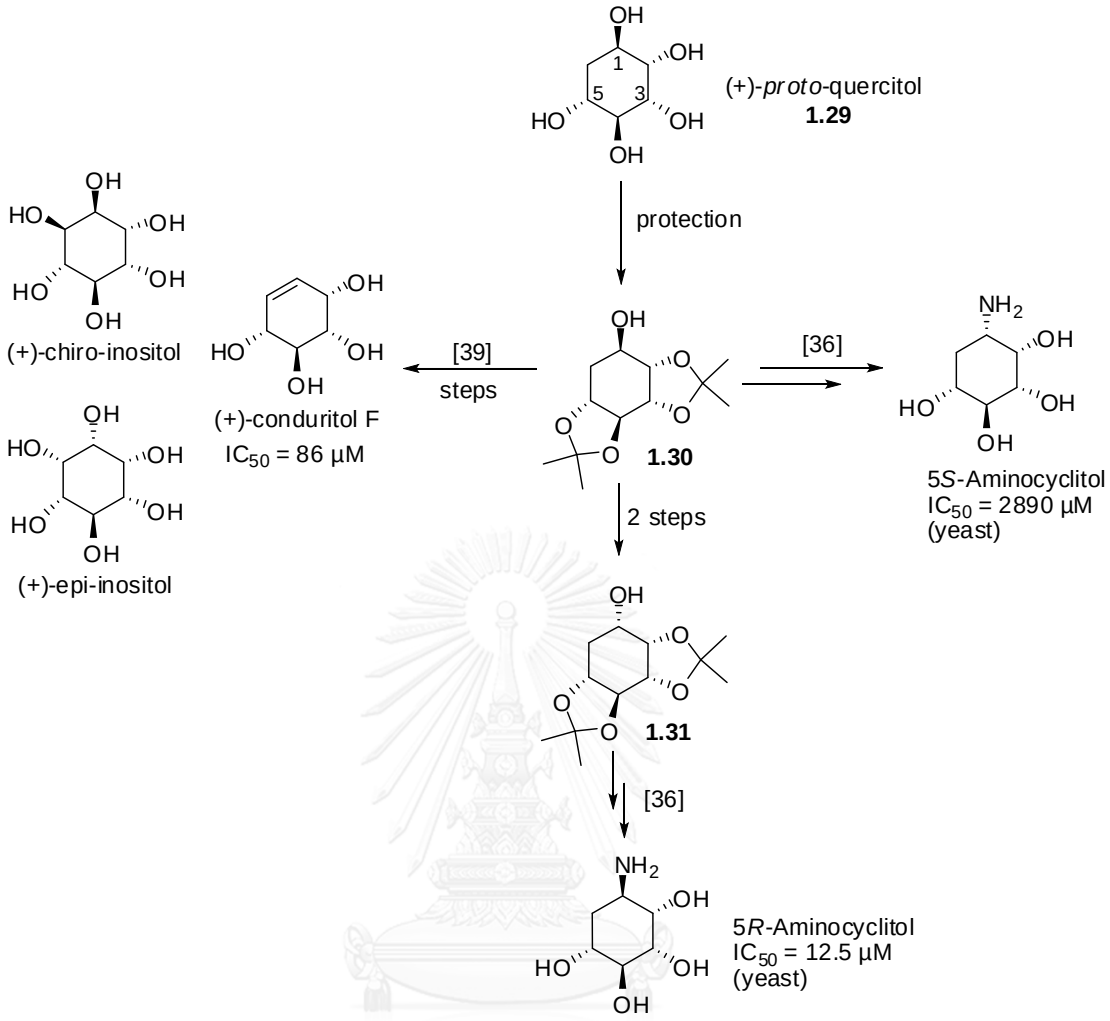

Scheme 1.4 Synthesis of aminoquercitols, (+)-conduritol F and inositols.

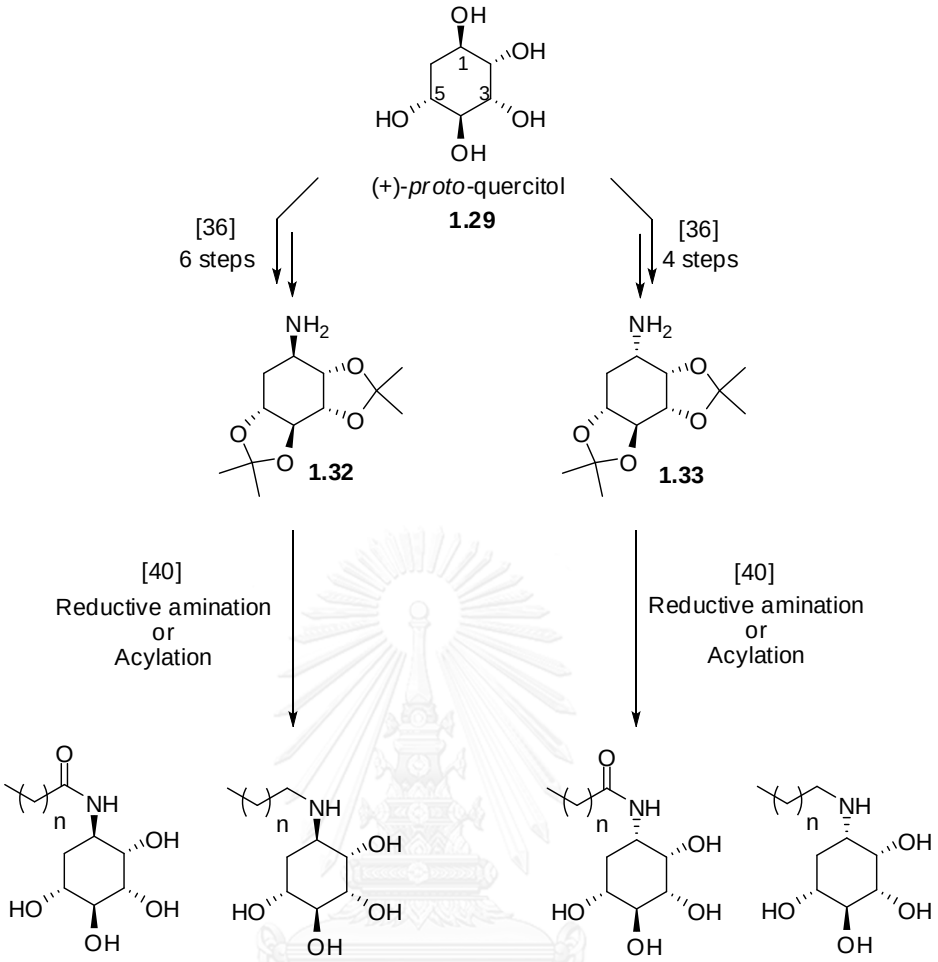

Scheme 1.5 Synthesis of *N*-acyl aminoquercitols and *N*-alkyl aminoquercitols

To the best of our knowledge, the use of bioconjugated compound as antidiabetic agents in multifunctional activities (anti-hyperglycemic effect and radical scavenging) has not been performed and most of α-glucosidase inhibitors were classified as competitive type. Therefore in this research, we have focused on the synthesis of cinnamic acid derivatives/quercitol bioconjugates in the hope that it will have not only multifunctional activities, but also create new inhibitory mechanism for rat small intestine α-glucosidase (maltase).

1.3 Objectives

In this research, we have focused on the synthesis of bioconjugated compounds containing cinnamic acid derivatives (CADs) and (+)-*proto*-quercitol through amide or ester linkage. We hope that the combination of two active moieties would afford bioconjugates with improved activities.

All synthesized compounds were initially screened for DPPH radical-scavenging using BHA as a positive control and α-glucosidase inhibitory activity using enzymes from baker's yeast (Type I) and rat small intestine (Type II). Kinetic analysis and synergistic effect of the active compounds against rat intestine maltase and sucrase were determined by Lineweaver–Burk plot and a plausible mechanism was also proposed involve allosteric site of α-glucosidase (NtMGAM) with the strongest α-glucosidase inhibitor by molecular docking.

CHAPTER II

BIOCONJUGATED (AMINO)QUERCITOL WITH CINNAMIC ACID DERIVATIVES: SYNTHESIS, BIO-ACTIVITY ASSAYS, KINETIC STUDY AND COMPUTATIONAL STUDY

2.1 Compound design

Based on the previous reports, aminocyclitols are a group of natural products possessing significant relevance in medicinal chemistry as they are structural components of α-glucosidase inhibitors as seen in Figure 2.1 [38, 42, 43]. In the course of our research on new α-glucosidase inhibitors, we recently reported the synthesis and inhibitory effects of aminoquercitols from naturally available (+)-*proto*-quercitol (Figure 2.1). The results revealed that aminoquercitols could improve inhibitory activity. Moreover, our previous results could provide necessary data on the structural requirement for designing other potent α-glucosidase inhibitors. Therefore, we herein extended our study by connecting quercitol core with other bioactive residues in order to create multiple activities within one single analogue. Inspired by chlorogenic acid and its analogues, a well-recognized natural product having both potent antioxidant [44, 45] and antidiabetic activities [46], the structures contained cinnamic acid derivatives and quinic acid as seen in Figure 2.2a were desighed. Therefore, we planned to synthesize some novel bioconjugate analogues possessing cinnamic moiety and quercitol core (Figure 2.2b). This would result in not only the improvement of each activity, but also alter the mode of inhibition.

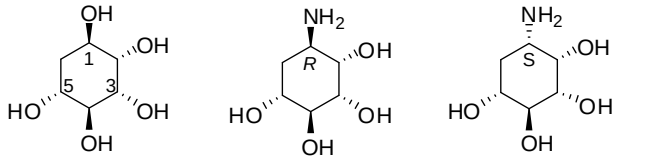

(+)-*proto*-quercitol
1.29, NI

5*R*-Aminocyclitol
IC_{50} = 12.5 µM
(Baker's yeast)

5*S*-Aminocyclitol
IC_{50} = 2890 µM
(Baker's yeast)

Figure 2.1 Structure of (+)-*proto*quercitol, 5*R*-aminocyclitol and 5*S*-aminocyclito.

a)

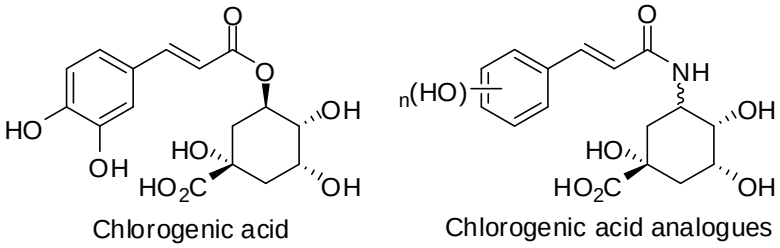

b)

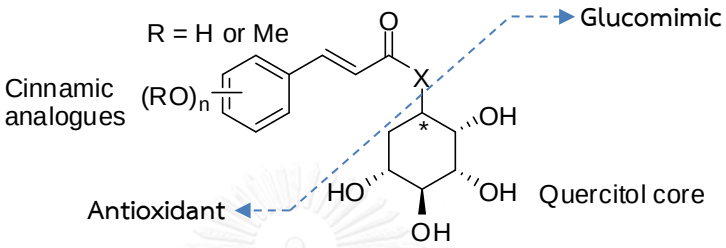

Figure 2.2 a) Structures of chlorogenic acid its analogues, b) a designed cinnamic acid derivatives/quercitol encompassing antioxidant and glucomimic residues.

In this work, the structure–activity relationship of the synthesized compounds and mechanism underlying α-glucosidase inhibitory effect of the most potent inhibitor and molecular docking analysis will be fully investigated.

2.2 Synthesis of queritylcinnamates and quercitylcinnamamides

2.2.1 Synthesis of bis-acetonides (**1.30**, **1.31**) and aminobis-acetonides (**1.32**, **1.33**)

*2.2.1.1 Isolation of (+)-proto-quercitol (**1.29**)*

(+)-*proto*-Quercitol (**1.29**) utilized in this study was isolated from the stems of *Arfeuillea arborescens* using the previously described method with slight modification [38]. The MeOH extract, after partitioning with hexane and CH_2Cl_2, was concentrated to afford the desired quercitol (ca. 1.0%) as colorless crystals. In this research, the structure and relative configuration were confirmed by NMR technique which correspond to the previous report from our group [38]. The absolute configurations of all the stereogenic centers of (+)-*proto*-quercitol (**1.29**) has been addressed based on the previous report as shown in Scheme 2.1.

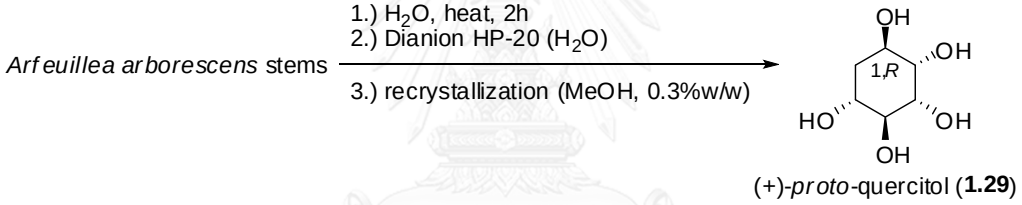

Scheme 2.1 Isolation of (+)-*proto*-quercitol.

*2.2.1.2 Conversion of (+)-proto-quercitol (**1.29**) to (amino)bis-acetonides (**1.30**-**1.33**)*

In order to investigate the effect of C1 configuration on inhibitory effect, it is necessary to prepare bis-acetonide derivatives as seen in Scheme 2.2.

All four derivatives (**1.30**-**1.33**) were prepared from (+)-*proto*-quercitol (**1.29**) as demonstrated in Scheme 2.2. Briefly, protection of two diols in (+)-*proto*-quercitol (**1.30**) with dimethoxypropane gave the target alcohol **1.30** in 79% yield. The alcohol epimer **1.31** was also synthesized from **1.30** through oxidation using acetic anhydride/DMSO followed by $LiAlH_4$ reduction, yielding the desired product in 42% yield.

The amine acetonide derivatives (**1.32** and **1.33**) were synthesized from **1.31** and **1.30**, respectively. Initially, mesylation with $MeSO_2Cl$ followed by azidation with

NaN_3 gave rise to the formation of azide derivatives (79 and 84% yields, respectively). Finally, $LiAlH_4$ reduction of azide derivatives gave the desired products **1.32** and **1.33** in 43 and 81% yields, respectively as white solids.

.

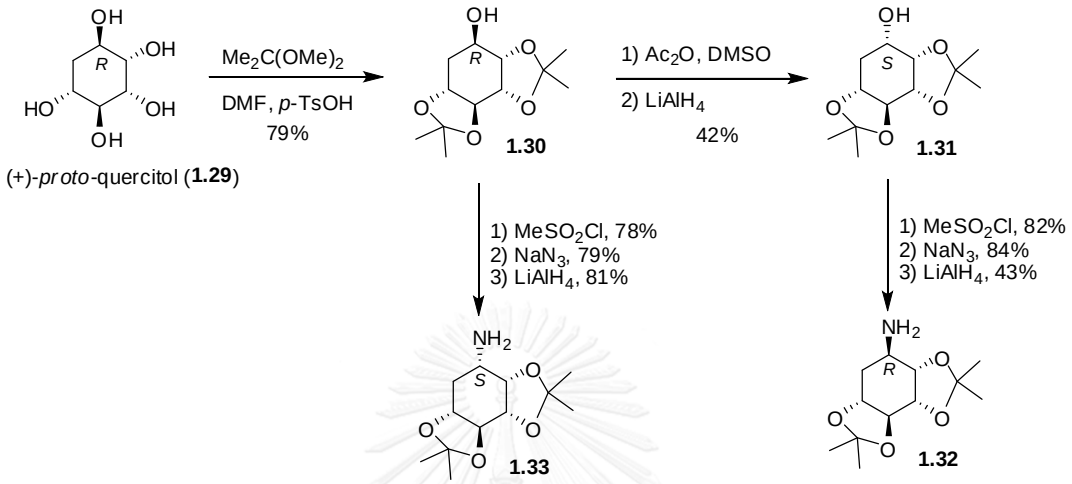

Scheme 2.2 Synthesis of bis-acetonide (**1.30** and **1.31**) and amino bis-acetonide (**1.32** and **1.33**).

2.2.2 Synthesis of quercitylcinnamates (ester compound)

With the chiral coupling partners **1.30** and **1.31** in hands**,** the quercitylcinamates **2.1ER**-**2.8ES** were prepared as depicted in Scheme 2.3. For the esters **2.1ER**-**2.8ER** and their epimers **2.1ES**-**2.8ES**, the synthetic route was straight forward involving the direct coupling reaction between alcohol **1.31** or **1.32** with the corresponding cinnamic derivatives **2.1**-**2.5.** The ester bond formation was achieved using *N*,*N*′-dicyclohexylcarbodiimide (DCC) as an activator and 4-dimethylaminopyridine (DMAP) as a catalyst, giving 9 corresponding ester compounds (**2.1ERp**-**2.5ERp**) in 67-85% yields. Finally, removal of acetonide group in ester **2.1ERp**-**2.5ERp** underwent smoothly upon treatment with Amberlyst-15 in methanol to give the desired esters **2.1ER**-**2.5ER** in 56-73% yields (Scheme 2.3).

On the other hand, esterification of caffeic acid (**2.6**), ferulic acid (**2.7**) and isoferulic acid (**2.8**) required additional protection step because free phenolic

group(s) of cinnamic acid (**2.6**-**2.8**) could interfere with the ester coupling reaction. Our initial effort on direct coupling was unsuccessful and all cinnamic acids (**2.6**-**2.8**) could not be dissolved in CH_2Cl_2, which is the best solvent for this Steglich esterification. Therefore, the silylation of **2.6**-**2.8** with *tert*-butyldimethylsilyl chloride (TBDMSCl) was conducted not only to protect the reactive phenolic group(s) but also improve the solubility of the acids **2.6**-**2.8** in CH_2Cl_2. Therefore, the syntheses of ester **2.6ERp**-**2.8ESp** were accomplished by ester bond formation of protected cinnamic derivatives (**2.6**-**2.8**) with the chiral alcohol **1.30** or **1.31**. Lastly, the double deprotection of silyl and acetonide groups in **2.6ERp**-**2.8ESp** with TBAF followed by the addition of Amberlyst-15 resulted in the formation of esters **2.6ER**-**2.8ES** in 42-49% yields as white solids (Scheme 2.3).

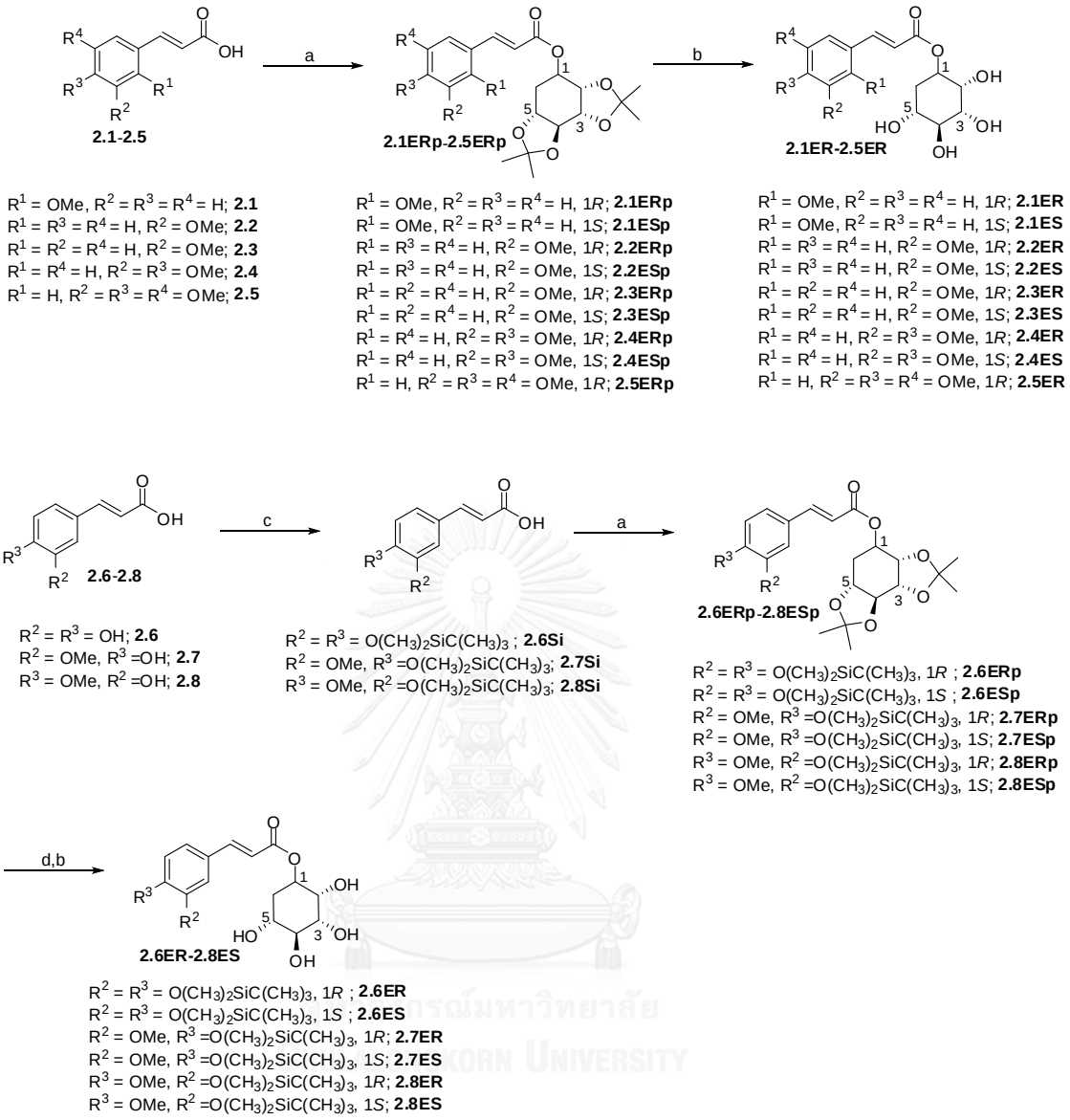

Scheme 2.3 Synthesis of quercitylcinnamates. Reagents and conditions: (a) **1.30** or **1.31**, DCC, DMAP, CH_2Cl_2, 0 $^{\circ}$C to rt; (b) Amberlyst-15, MeOH; (c) TBDMSCl, imidazole, DMF, rt; (d) TBAF, THF, rt.

To confirm the structure of all target compounds **2.1ER-2.8ES**, the HRESIMS analysis and NMR spectroscopy were performed and their spectra were shown in Figure A.1-A.30 in the Appendix section.

Of all synthesized **2.1ER**-**2.8ES**, the molecular weights correspond well with the required HRESIMS data (Appendix section, Figure A.63-A.93). For NMR analysis data we selected compound **2.2ER** and **2.2ES** and compared with starting material **1.29** and epimer **1.29**, as an example (Figure 2.3).

^{1}H NMR data of **2.2ER** and **2.2ES** showed signals of α,β-unsaturated protons at δ_H 7.65 (d, *J* = 16.0 Hz, 1H) and 6.52 (d, *J* = 16.0 Hz, 1H) for **2.2ER** and δ_H 7.72 (d, *J* = 16.0 Hz, 1H) and 6.54 (d, *J* = 16.0 Hz, 1H) for **2.2ES** (Figure 2.3). For proton on aromatic ring, those signals showed multiplet peak in a range of 7.00-7.50 ppm for both compounds. The methine proton (H-C1) of **2.2ER** and **2.2ES** were observed at δ_H 5.11 (brs, 1H, H-C1) and 4.85 (m, 1H, H-C1), respectively. Moreover, a splitting pattern of methylene protons (H-C6) in final compounds (**2.1ER**-**2.8ES**) around δ_H 1.99-2.01 ppm are different from their carbasugar start materials (**1.29** and epimer **1.29**) around δ_H 2.02-1.86 ppm. Proton signals change from two sets of multiplet in starting materials into a single set of multiplet in all ester compounds (**2.1ER**-**2.8ES**).

.

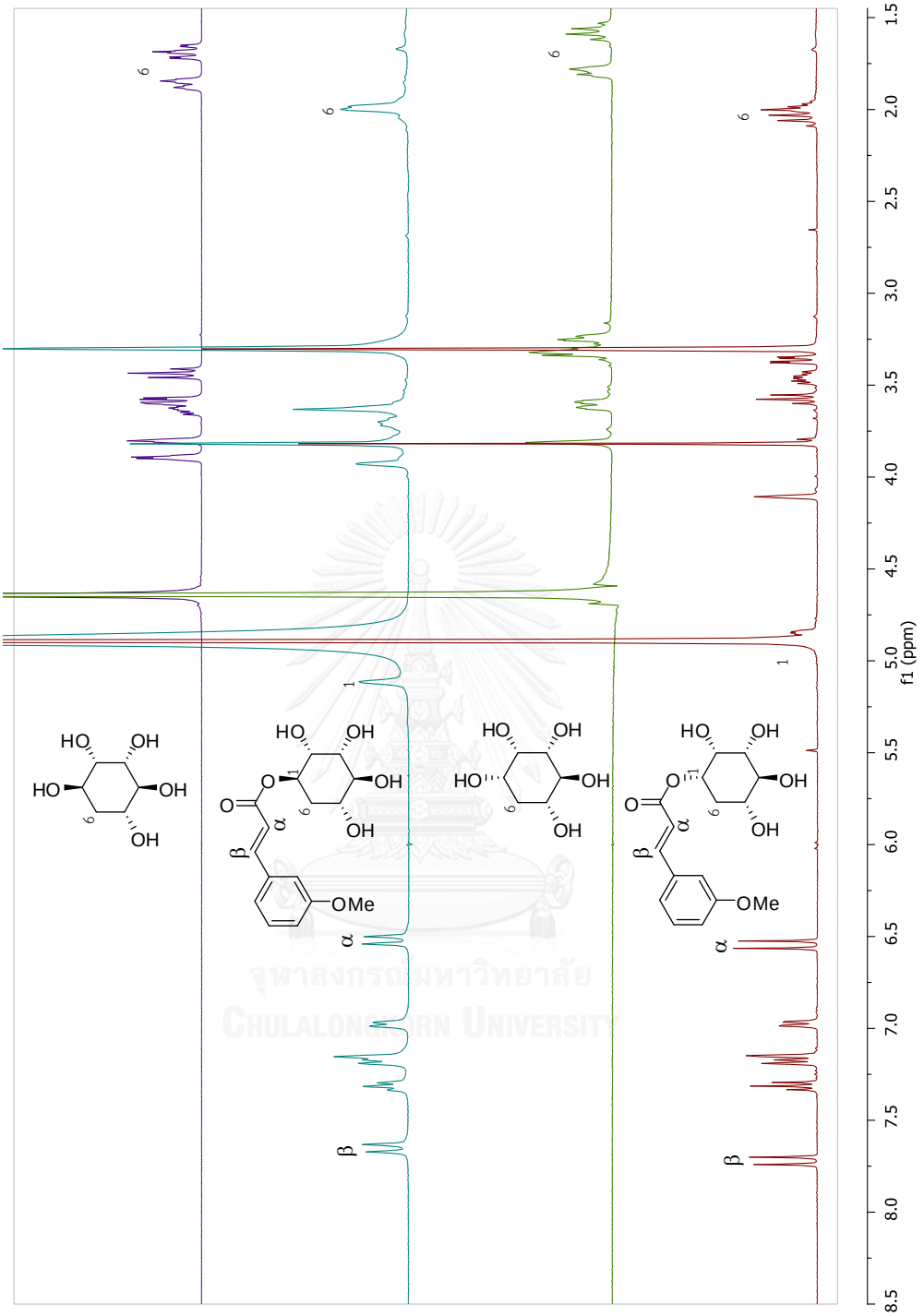

Figure 2.3 Shown a stacking of **1.29**, **2.2ER**, epimer **1.29** and **2.2ES** ^{1}H NMR in CD_3OD.

Interestingly, for all ester target compounds in *R*-configuration such as **2.2ER**, a signal which is assignable to methine proton (H-C1) appeared at 5.10-5.11 ppm. However, in case of *S*-configuration, a methine proton (H-C1) appeared at a slightly lower field at 4.80-4.85 ppm. Our hypotheses relied on the optimized 3D molecular structure, which was depicted in Figure 2.4. The hydrogen atom at methine proton (H-C1) in *R*-configuration was located on an axial position, close to an oxygen atom (O1) with the distance of 2.65 Å. This suggested that high downfield effect from the oxygen (O1) might result in the high chemical shift of **2.2ER**. On the other hand, hydrogen atom at methine proton (H-C1) in *S*-configuration, which was located on an equatorial position, might not be significantly affected by the neighboring groups. Therefore, methine proton (H-C1) of ester series of *R*-configuration (**2.1ER**-**2.8ER**) displayed higher chemical shifts in comparison with *S*-configuration series (**2.1ES**-**2.8ES**) as shown in Appendix section (Figure A.1-A.30)

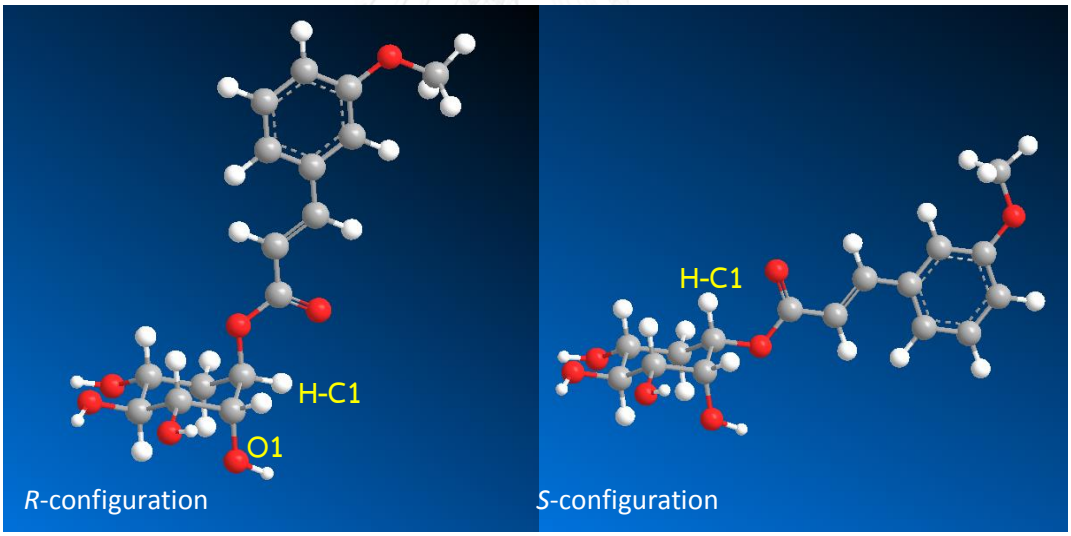

Figure 2.4 Shown optimized 3D molecular structure of **2.2ER** (*R*-configuration) (left) and **2.2ES** (*S*-configuration) (right).

2.2.3 Synthesis of aminoquercitylcinnamamides (amide compound)

2.2.3.1 Coupling reaction between aminobis-acetonides and cinnamic acid derivatives

Next, we synthesized cinnamic acid bioconjugates (**2.1AR**-**2.8AS**) from aminobis-acetonides (**1.32** and **1.33**) coupling with cinnamic derivatuves (**2.1**-**2.8**) as seen in Scheme 2.4.

Synthetic procedures for **2.1AR**-**2.8AS** compounds are straight forward involving the direct amide coupling reaction between amines (**1.32**, **1.33**) and the corresponding cinnamic derivatives **2.1**-**2.8** without any protection of phenolic group(s) on cinnamic derivatives (**2.6**-**2.8**). Unlike the previous synthetic method, the amide bond formation proceeds a lot faster than the ester bond formation. In the presence of 3-(ethylimonomethyleneamino)-*N*,*N*-dimethylpropan-1-amine (EDCI), 1-hydroxybenzotriazole (HOBt) and 4-dimethylaminopyridine (DMAP), the amide coupling reaction between cinnamic acids (**2.1**-**2.8**) and amines (**1.33** and **1.34**) under went smoothly under reflux condition to give **2.1ARp**-**2.8ASp** in 56-78% yields (Scheme 2.4) without any ester by-products. Finally, cleavage of the two acetonide protecting groups in **2.1ARp**-**2.8ASp** under acidic condition generated the target quercitylcinnamamides **2.1AR**-**2.8AS** in 72-85% yields as seen in Scheme 2.4.

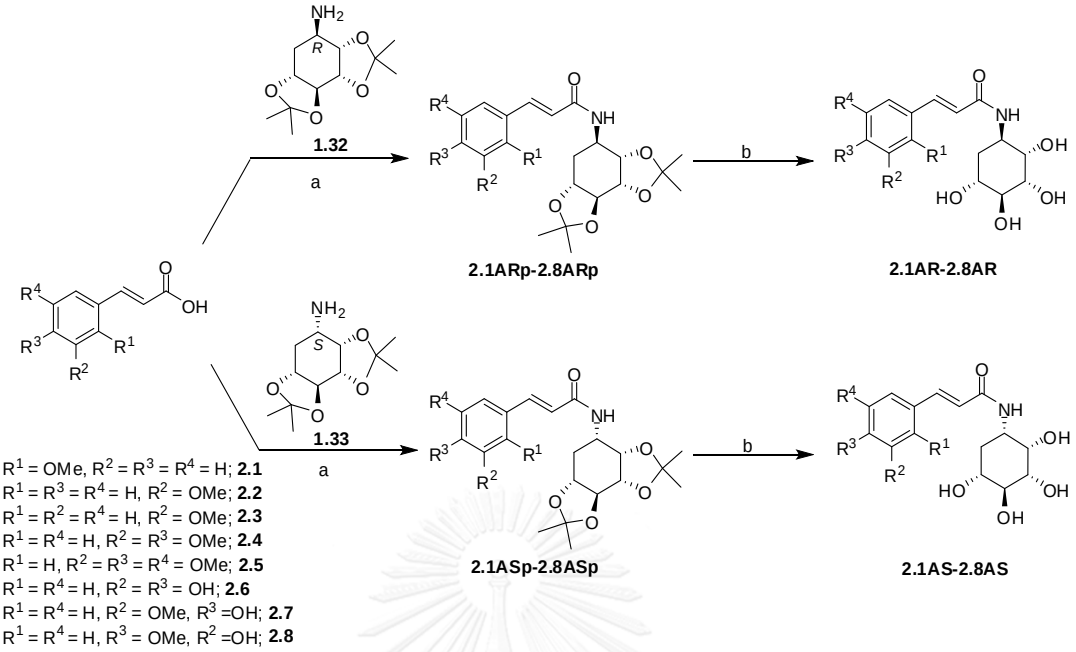

Scheme 2.4 Synthesis of quercitylcinnamamides. *Reagents and conditions*: (a) EDCI, HOBt, DMAP, DMF, reflux overnight; (b) Amberlyst-15 in MeOH.

Of all synthesized 16 conjugates compounds (**2.1AR**-**2.8AS**), the molecular weights correspond well with the required HRESIMS data (Appendix section). For NMR analysis data, we selected compound **2.6AR** and **2.6AS** as an example (Figure 2.5).

^{1}H NMR data of **2.6AR** and **2.6AS** showed signals of α,β-unsaturated protons at δ_H 7.40 (d, *J* = 15.6 Hz, 1H) and 6.47 (d, *J* = 15.6 Hz, 1H) in **2.6AR** and δ_H 7.39 (d, *J* = 15.6 Hz, 1H) and 6.44 (d, *J* = 15.6 Hz, 1H) in **2.6AS**. For protons on aromatic ring, they displayed signals in a range of 6.75-7.02 ppm.

In addition, *R*-derivatives (**2.6AR**) showed signals assignable to methylene protons (H-C6) as two sets of multiplet at δ_H 2.00 (m, 1H, H-C6) and 1.86 (m, 1H, H-C6). While **2.6AS**, which is *S*-derivatives, gave a single set of multiplet for methylene proton (H-C6) at δ_H 1.86 (m, 2H, H-C6). This phenomenal were found in all amide derivatives when we performed the NMR analysis in CD_3OD. The explanation from this observation is still unclear.

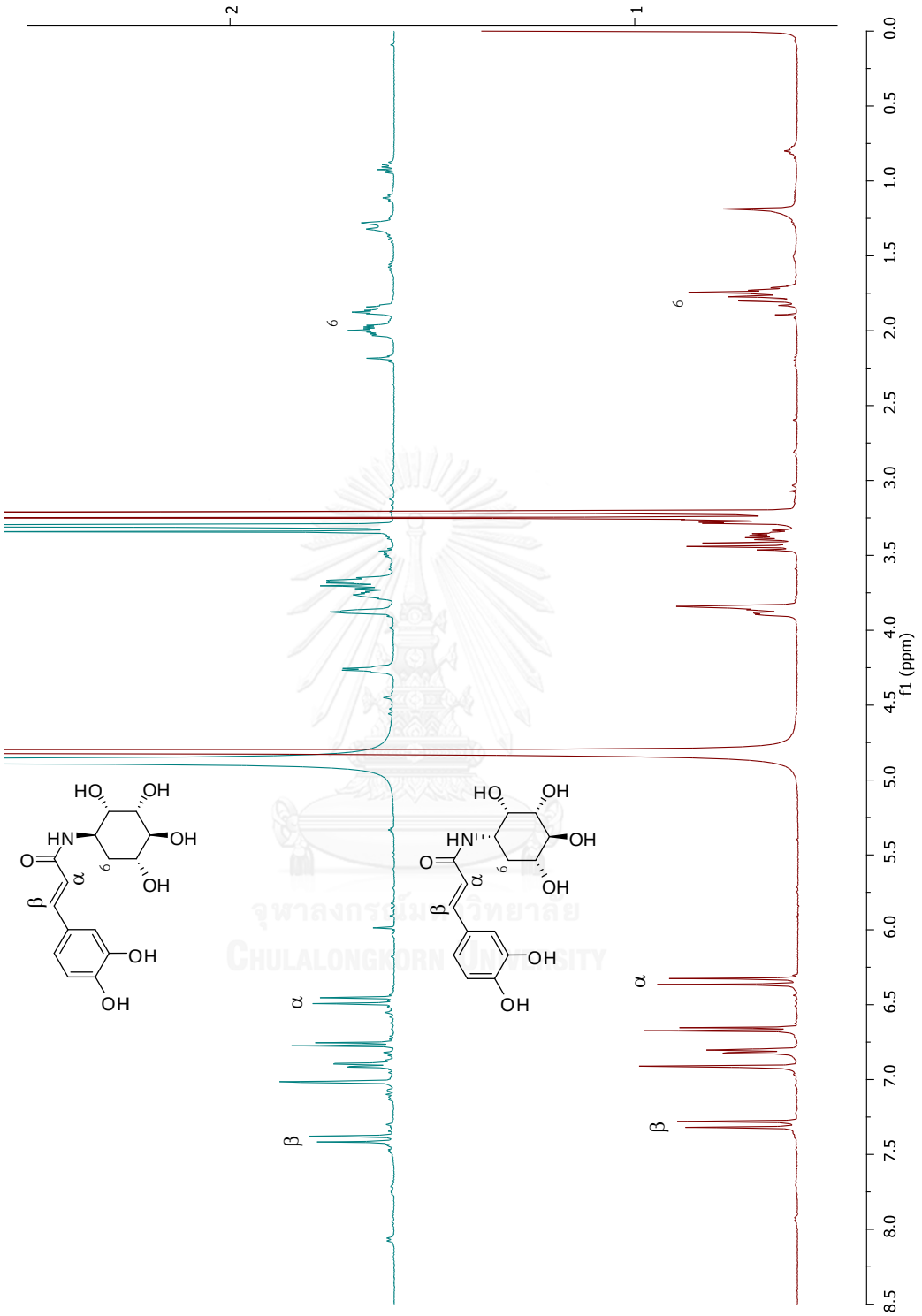

Figure 2.5 Shown a stacking of **2.6AR** and **2.6AS** ^{1}H NMR in CD_3OD.

2.3 Bio-activity assays

2.3.1 α-Glucose inhibitory activity of **2.1ES**-**2.8ER** ester

For the evaluation of α-glucosidase inhibitory activity of quercitylcinnamates conjugate, **2.1ER**-**2.8ES** were compared with the commercial antidiabetic drug, acarbose, and their parent cinnamic analogues (**2.1**-**2.8**) as the reference (Figure 2.6).

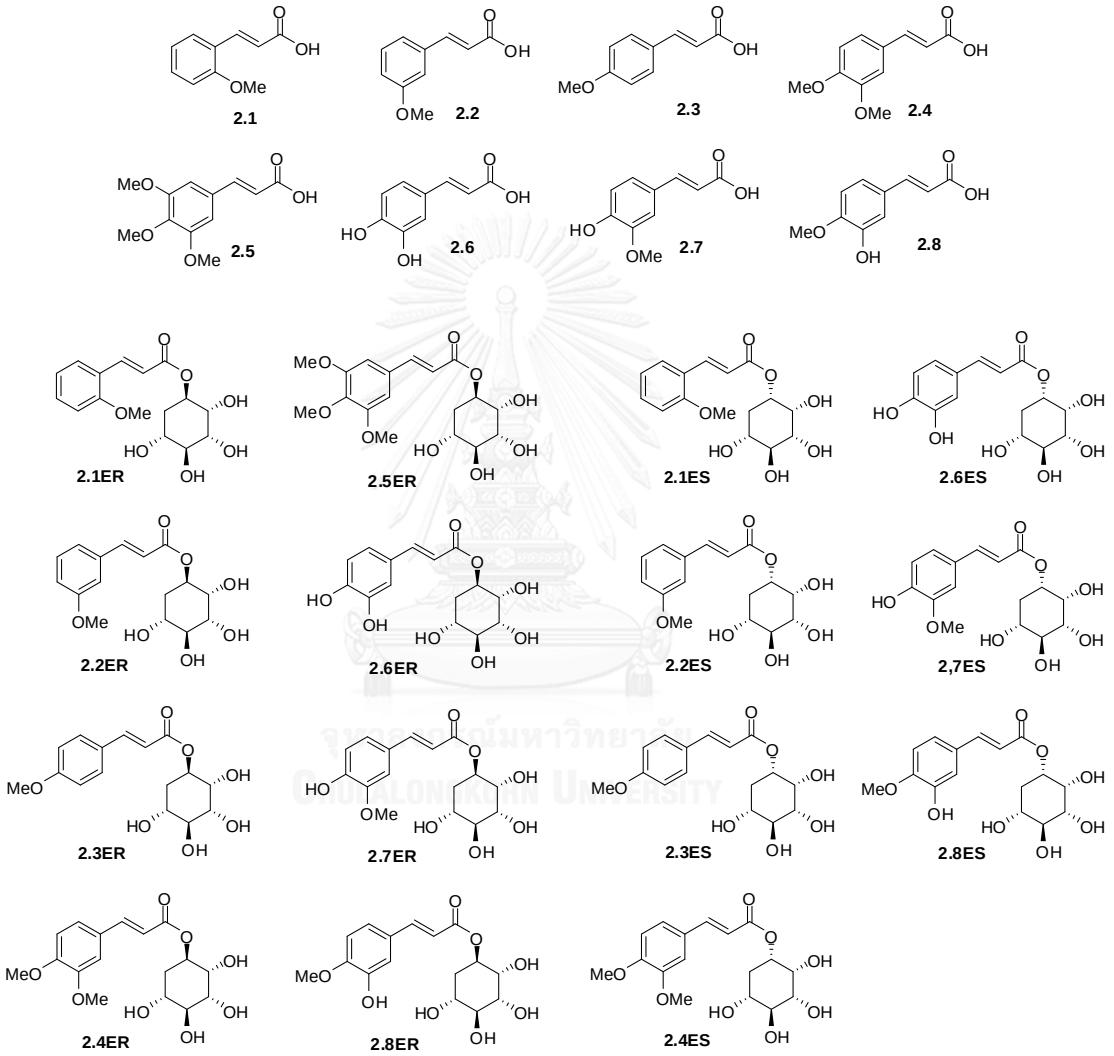

Figure 2.6 Structure of cinnamic acid analogues (**2.1**-**2.8**) and **2.1ER**-**2.8ES**.

We utilized the conventional assays using the enzyme derived from baker's yeast [47] and rat small intestine [48] and the data were summarized in Table 2.1.

For α-glucosidase inhibitory activity, all tested compounds showed no inhibition against yeast α-glucosidase (type I α-glucosidase) but some of which

inhibited maltase and sucrase, type II α-glucosidases from rat intestine. The bioconjugates **2.6ER**-**2.8ES**, whose structures are composed of caffeoyl, ferulyl and isoferulyl moieties, respectively, displayed inhibitory effects in range of 5.31–954.08 μM, whereas **2.1ER**-**2.5ER** showed inactivity property. Notably, their cinnamoyl cores in **2.6ER**-**8ES**, which is different from those of **2.1ER**-**2.5ER** in having at least one phenolic group showed better activity, suggesting that phenolic moiety possibly involved in exerting the observed inhibition. It was likely that the more phenolic group in cinnamoyl moiety, the more potent inhibition observed. This result was similar to previous report from Adisukwattana and co-workers when parent compounds **2.6** ,**2.7** and **2.8** were tested against α-glucosidase from rat intestine [49]. This trend was obviously found in **2.6ER**, whose inhibition against maltase was more potent than those of **2.7ER** (10 times) and **2.8ER** (4 times); while **2.8ER** showed only two times more potent than **2.7ER**.

Further inspection of two quercityl residues (**1.30** and **1.31**), installed in the active bioconjugates, on inhibitory effect revealed significant difference in inhibition. Bioconjugates **2.6ER**, **2.7ER** and **2.8ER**, all of which generated from natural quercitol **1.30**, showed inhibitory effect 3-94 times more potent than their corresponding C1 epimers (**2.6ES**, **2.7ES** and **2.8ES**). The difference in inhibitory potency among epimeric analogues were strikingly observed in **2.6ER**, whose inhibition against maltase and sucrose were 93 and 22 times more potent than **2.6ES**. Compared to their corresponding cinnamic precursors (**2.6**, **2.7** and **2.8**), **2.6ER**, **2.7ER** and **2.8ER** showed more improved inhibitory effects (4-6 times), whereas their epimeric analogues (**2.6ES**, **2.7ES** and **2.8ES**) displayed reverse trend. The observed results suggested that *R* configuration of C1 in quercityl moiety was also associated with exerting inhibitory effect, in addition to the presence of more phenolic groups in cinnamoyl residues.

The pronounced inhibitions raised by *R* configuration of C1 were also supported by a similar trend observed in our previous report of *N*-alkyl aminoquercitols as seen in Chapter 1.2.2 [42]. Of bioconjugates synthesized, **2.6ER** showed most potent inhibition against both maltase and sucrase with IC_{50} values of 5.31 and 43.65 μM, respectively.

Table 2.1 α-Glucose inhibitory effect of quercitylcinnamates (**2.1ES-2.8ER**)

Entry	Compound	α-Glucosidase inhibitory effect (IC_{50}, μM)		
		Baker's yeast glucosidase	Maltase[a]	Sucrase[a]
1	**2.1ES**	NI[b]	NI	NI
2	**2.1ER**	NI	NI	NI
3	**2.2ES**	NI	NI	NI
4	**2.2ER**	NI	NI	NI
5	**2.3ES**	NI	NI	NI
6	**2.3ER**	NI	NI	NI
7	**2.4ES**	NI	NI	NI
8	**2.4ER**	NI	NI	NI
9	**2.5ER**	NI	NI	NI
10	**2.6**	ND	34.69 ± 0.74	37.45 ± 0.62
11	**2.6ES**	NI	487.48 ± 0.50	954.08 ± 0.50
12	**2.6ER**	NI	5.31 ± 0.10	43.65 ± 0.30
13	**2.7**	ND	305.89 ± 0.34	81.88 ± 0.48
14	**2.7ES**	NI	21.07 ± 0.15	171.43 ± 0.35
15	**2.7ER**	NI	51.93 ± 0.20	67.21 ± 0.20
16	**2.8**	ND[c]	81.83 ± 0.15	32.18 ± 0.19
17	**2.8ES**	NI	367.15 ± 0.42	805.48 ± 0.65
18	**2.8ER**	NI	20.81 ± 0.14	53.00 ± 0.32
19	Acarbose	403.9 ± 0.40	1.50	2.30

[a] α-glucosidase was obtained from rat small intestine.

[b] No inhibition (inhibitory effect less than 30% at 10 mg/mL for baker's yeast and at 1 mg/mL for maltase and sucrase).

[c] Not determined.

2.3.2 α-Glucose inhibitory activity of **2.1AS-2.8AR** amide

Similarly, the amide derivative **2.1AS-2.8AR** (Figure 2.6) were tested against α-glucosidase activity using aforementioned methods and compared with antidiabetic drug, acarbose and voglibose (Table 2.2). All synthetic compounds did not inhibit yeast α-glucosidase (type I α-glucosidase) and rat small intestine glucosidase (maltase and sucrose, type II α-glucosidase), but **2.6AS-2.8AR**, whose structures encompassing caffeoyl, ferulyl and isoferulyl moieties, potent inhibition against both maltase and sucarse in range of 0.41–269.45 μM was observed. The results was similar to above section, indicating that a number of hydroxyl group(s) played an important role in α-glucosidase potency [50]. The effects of chirality at C-1 position were found in amide series as well. In contrast, *S*-configuration in aminoquercityl moiety series (**2.7AS** and **2.8AS**) showed stronger inhibitory activity against maltase more than those of *R*-configuration (**2.7AR** and **2.8AR**) except in **2.6AS** and **2.6AR** cases. Nevertheless, their inhibitory effects on sucrase displayed equal activities among quercitylcinnamamides having *S*- or *R*- configurations. Bioconjugates **2.8AS** and **2.7AS** showed the inhibition of maltase more potent than those of **2.8AR** (145 times) and **2.7AR** (67 times), respectively. Compared to their corresponding parent cinnamic analogues (**2.7** and **2.8**), **2.7AS** and **2.8AS** showed more enhancement against maltase (199 and 208 times, respectively), whereas their epimer analogues (**2.7AR** and **2.8AR**) showed lower enhancement against maltase (1 and 3 times, respectively). Compound **2.8AS** showed the IC_{50} value toward maltase in 0.41 μM, which considered as the most potent compound in this work. While the tested compound in amide series (**2.6AS**, **2.7AS**, **2.8AS**, **2.6AR** and **2.7AR**) exhibited weak to medium potency in the range of 1.47-181.32 μM.

It is our goal to create the antidiabetic agent so the comparative evaluation with the current antidiabetic drug, acarbose and voglibose, were investigated. Our best compound, **2.8AS**, displayed better activity against maltase in comparison with acarbose (IC_{50} = 1.50 μM) and found in the same range with voglibose (IC_{50} = 0.25 μM)

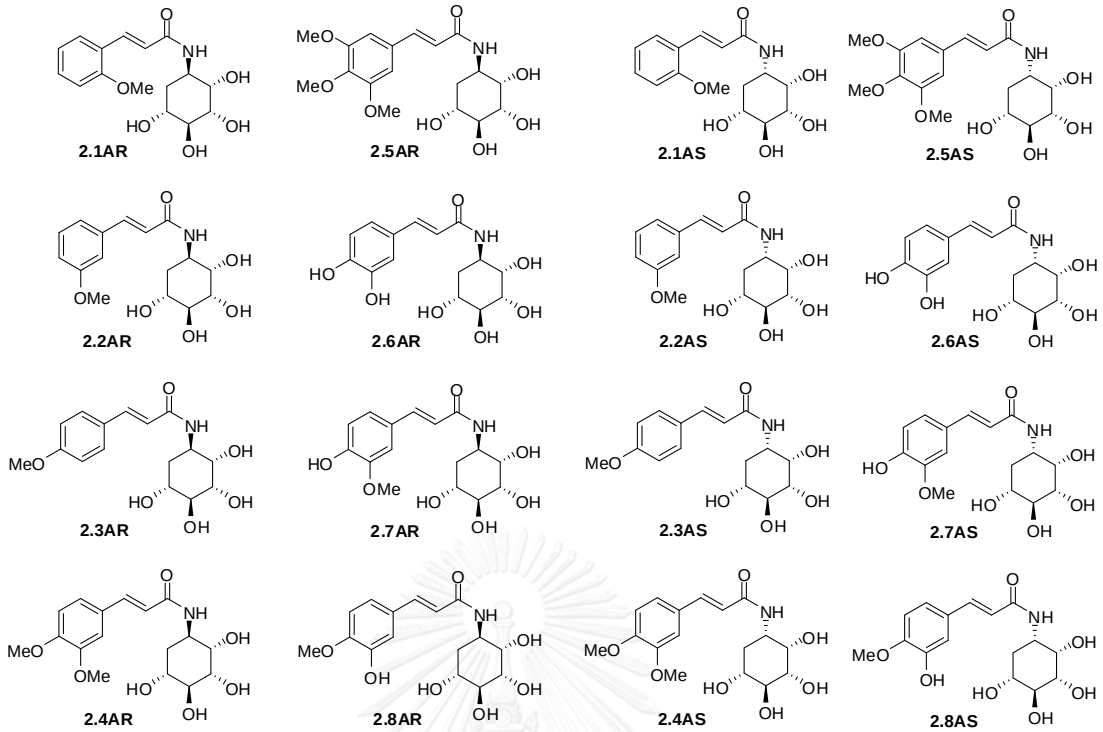

Figure 2.7 Structure of **2.1AR**-**2.8AS**.

Table 2.2 α-Glucose inhibitory effect of quercitylcinnamamides (**2.1AR-2.8AS**)

Entry	Compound	α-Glucosidase inhibitory effect (IC_{50}, μM)		
		Baker's yeast glucosidase	Maltase[a]	Sucrase[a]
1	**2.1AS**	NI[b]	NI	NI
2	**2.1AR**	NI	NI	NI
3	**2.2AS**	NI	NI	NI
4	**2.2AR**	NI	NI	NI
5	**2.3AS**	NI	NI	NI
6	**2.3AR**	NI	NI	NI
7	**2.4AS**	NI	NI	NI
8	**2.4AR**	NI	NI	NI
9	**2.5AS**	NI	NI	NI
10	**2.5AR**	NI	NI	NI
11	**2.6**	ND[c]	34.69 ± 0.74	37.45 ± 0.62
12	**2.6AS**	NI	181.32 ± 0.22	114.15 ± 0.55
13	**2.6AR**	NI	70.88 ± 015	31.88 ± 0.32
14	**2.7**	ND	305.89 ± 0.34	81.88 ± 0.48
15	**2.7AS**	NI	1.47 ± 0.28	45.13 ± 0.11
16	**2.7AR**	NI	98.23 ± 0.22	269.45 ± 0.25
17	**2.8**	ND	81.83 ± 0.15	32.18 ± 0.19
18	**2.8AS**	NI	0.41 ± 0.07	52.04 ± 0.27
19	**2.8AR**	NI	59.71 ± 0.38	30.32 ± 0.43
20	Acarbose	403.9 ± 0.40	1.50 ± 0.14	2.30 ± 0.02
21	Voglibose	ND[c]	0.25	0.094

[a] α-glucosidase was obtained from rat small intestine.

[b] No inhibition (inhibitory effect less than 30% at 10 mg/mL for baker's yeast and at 1 mg/mL for maltase and sucrase).

[c] Not determined.

To gain more insight into structure-activity relationship (SAR), all of the active compounds in ester and amide series having a phenolic group at *para*- and/or *meta*-position(s) in cinnamic moiety were compared and the data were shown in Figure 2.8. It was found that the chirality of C1 position and bond linkages strongly affected on α-glucosidase inhibitory activity.

In general, in the present of *S*-configuration at C1 position, amide series (**2.6AS**-**2.8AS**) showed better activity toward α-glucosidase in maltase in comparison with ester series (**2.6ES**-**2.8ES**). In contrast, amide series containing *R*-configuration at C1 position possessed a weaker α-glucosidase activity than ester series.

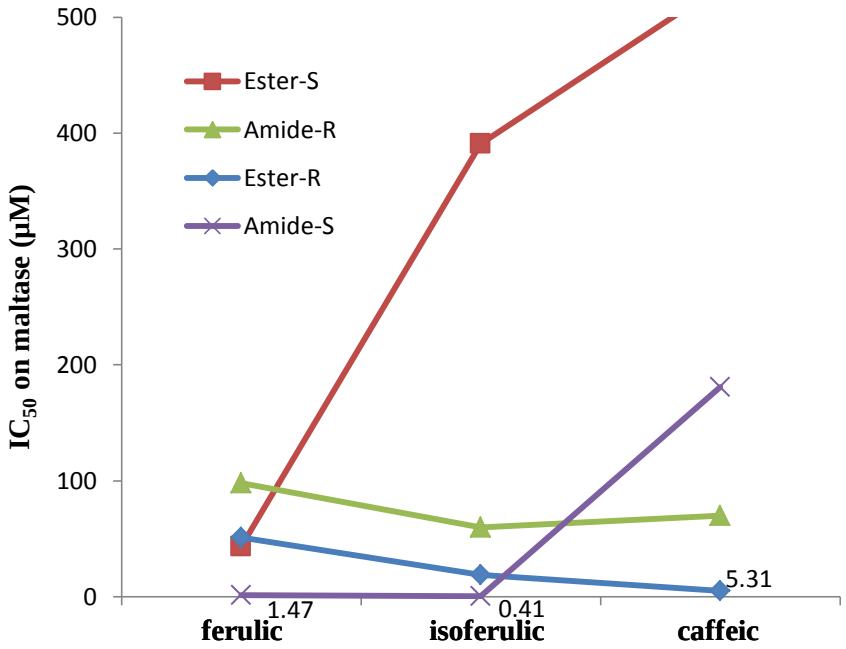

Figure 2.8 A trend of IC_{50} values of potent compounds.

2.2.3 DPPH radical scavenging ester and amide

As for antioxidation activity of all synthesized ester bioconjugates, it was tested against DPPH radical scavenging assay and the results were summarized in Table 2.3. Among all eight cinnamic acid derivatives (**2.1**-**2.8**), there are only three compounds possessing a good antioxidant activity that has been reported [49], such

as caffeic acid (**2.6**), ferulic acid (**2.7**) and isoferulic acid (**2.8**). Therefore, we selected those compounds and tested toward DPPH radical scavenging and compared with our bioconjugated compounds. For ester series, only **2.6ER** showed a good antioxidant property, while in amide series, only **2.6AS**-**2.8AR** exhibited a good to excellent antioxidant activity. These results indicated that those cinnamic moieties played important role for antioxidant activity in bioconjugated compounds.

Table 2.3 Radical scavenging activity of quercitylcinnamates (**2.1ES**-**2.8ER**) and quercitylcinnamamides (**2.1AS**-**2.8AR**).

Entry	Compound	Radical scavenging (SC_{50}, mM)	Entry	Compound	Radical scavenging (SC_{50}, mM)
1	**2.1ES**	NS[a]	21	**2.1AS**	NS[a]
2	**2.1ER**	NS	22	**2.1AR**	NS
3	**2.2ES**	NS	23	**2.2AS**	NS
4	**2.2ER**	NS	24	**2.2AR**	NS
5	**2.3ES**	NS	25	**2.3AS**	NS
6	**2.3ER**	NS	26	**2.3AR**	NS
7	**2.4ES**	NS	27	**2.4AS**	NS
8	**2.4ER**	NS	28	**2.4AR**	NS
9	**2.5ES**	ND[b]	29	**2.5AS**	NS
10	**2.5ER**	NS	30	**2.5AR**	NS
11	**2.6**	0.15	31	**2.6**	0.15
12	**2.6ES**	NS	32	**2.6AS**	0.06
13	**2.6ER**	0.11	33	**2.6AR**	0.04
14	**2.7**	0.15	34	**2.7**	0.15
15	**2.7ES**	NS	35	**2.7AS**	0.06
16	**2.7ER**	NS	36	**2.7AR**	0.07
17	**2.8**	0.15	37	**2.8**	0.15
18	**2.8ES**	NS	38	**2.8AS**	0.07
19	**2.8ER**	NS	39	**2.8AR**	1.17
20	BHA[c]	0.10			

[a] No scavenging (inhibitory effect less than 50% at concentration of 10 mg/mL).

[b] Not determined.

[c] BHA = butylated hydroxyanisole

To simplify the antioxidant data, we selected only bioconjugates derived from the known cinnamic derivatives (**2.6**, **2.7** and **2.8**) having a good antioxidant activity as seen in Figure 2.8 and compared with their parent cinnamic acid analogues. For ester series, only **2.6ER** showed a good radical scavenging activity toward DPPH with SC_{50} value of 0.11 mM (Table 2.3, entry 13 and Figure 2.9, caffeic moiety). It was comparable to that of its parent cinnamic analogue, caffeic acid (SC_{50} = 0.15 mM) and standard antioxidant BHA (SC_{50} 0.10 mM) (Table 2.3, entry 20). On the other hand, the amide series having phenolic group(s) (**2.6**-**2.8**) displayed a good antioxidant activity (Table 2.3, entries 32-39). Those compounds showed SC_{50} value in range of 0.04–1.17 mM. Based on this result, it suggested that the use of amide linkage can maintain the activity of their corresponding cinnamic acid moiety (SC_{50} = 0.15 mM). Surprisingly, most of compounds showed even better activity than their mother compounds (**2.6**, **2.7** and **2.8**) as seen in case of **2.6AS**, **2.6AR**, **2.AS**, **2.7AR**, and **2.8AS** and showed comparable activity with the standard antioxidant BHA (SC_{50} 0.10 mM).

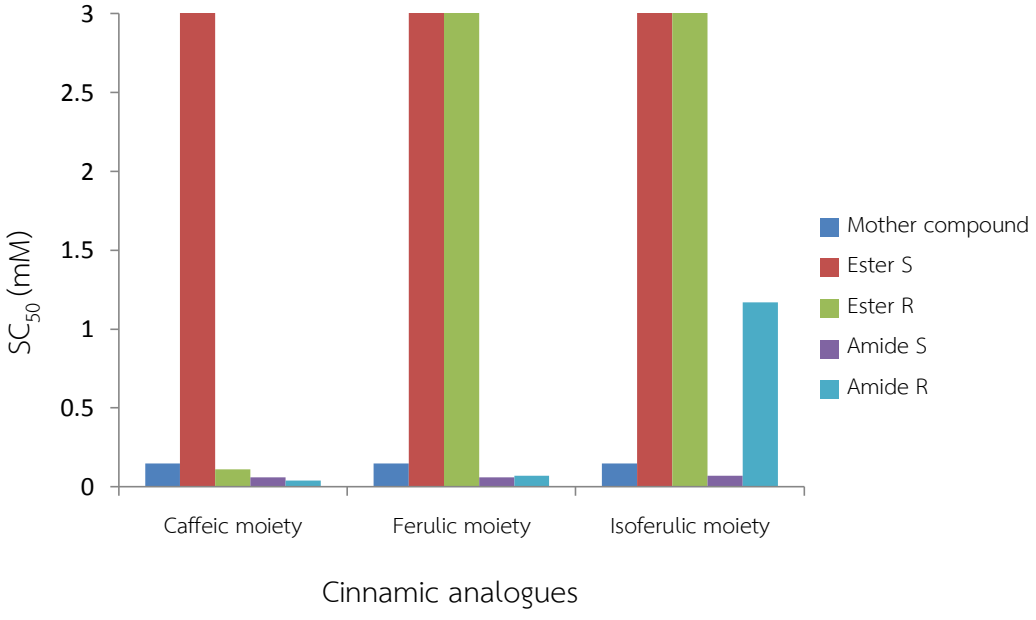

Figure 2.9 A trend of SC_{50} values of potent compounds

2.3.4 Mechanism underlying inhibitory effect of **2.6ER** and **2.8AS** against rat intestinal α-glucosidase

Currently, there are a numerous reports on the α-glucosidase inhibitor drugs and the active compounds for against α-glucosidase in rat small intestine in a present as shown in Figure 2.10 [35, 39, 51, 52]. Structurally, the core structures of those compounds are either carbasugar or sugar, which were identified as competitive inhibitor of maltase in rat small intestine. In general, the mode of enzyme inhibition can be divided into 4 categories as seen in Table 2.4. The competitive mode suggests that binding of the inhibitor to the active site on the enzyme prevents binding of the substrate. While non-competitive inhibitor bind the enzyme at allosteric sites and reduces the activity of the enzyme. However, our conjugated compounds are composed of carbasugar (**1.31**, **1.32**, **1.33** and **1.34**) and cinnamic acid analogues (**2.1**-**2.8**). Among cinnamic acid analogue, caffeic, ferulic and isoferulic acid were reported as mixed competitive inhibitor for α-glucosidase in rat small intestine [49]. Therefore, it is very important to investigate on the kinetic of enzyme inhibition activity of all prepared compounds in order to identify the mode of inhibition.

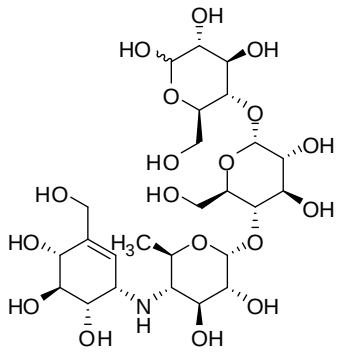

Acarbose
IC_{50} ; maltase (rat) 1.50 μM

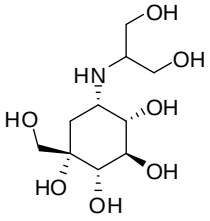

Voglibose
IC_{50} ; maltase (rat) 0.25 μM

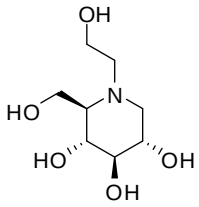

Miglitol
IC_{50} ; maltase (rat) 1.3 μM

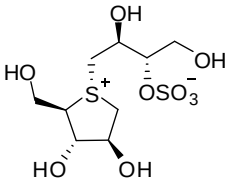

Salacinol
IC_{50} ; maltase (rat) 5.2 μM

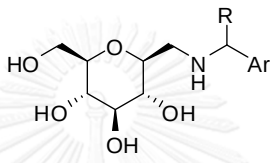

Sugar-amines
IC_{50} ; maltase (rat) 160-1326 μM

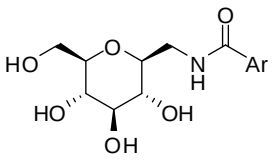

Sugar-amides
IC_{50} ; maltase (rat) 5.1-1014 μM

Figure 2.10 Examples of useful α-glucosidase inhibitor for type II diabetes [35, 39, 51, 52].

Table 2.4 Inhibition mechanism

Type of inhibition	K_m	V_{max}	Intersection
Competitive	increased	unchanged	Y axis, Y>0
Non-competitive	unchanged	decreased	X axis, X<0
Uncompetitive	decreased	decreased	No intersection
Mixed	increased	decreased	Second quadrant

Of all synthesized compounds, we chose the most potent compound in each series for further kinetic investigation. For ester series we selected **2.6ER** possessing α-glucosidase from maltase and DPPH radical scavenging activity in 5.31 μM and 0.11 mM, respectively. In addition, the most potent in amide series is **2.8AS** having α-glucosidase from maltase and DPPH radical scavenging activity in 0.41 μM and 0.07

mM, respectively. In order to obtain further evidence of the nature of inhibition exerted by compound **2.6ER** and **2.8AS**, a kinetic analysis of the enzyme inhibition activity was assayed using reaction condition described in a Chapter 3.8.

*2.3.4.1 Kinetic study of quercitylcaffeate (**2.6ER**)*

The Lineweaver—Burk plot of initial velocity versus maltose concentrations in the presence of different concentrations of **2.6ER** gave a series of straight lines, all of which intersected within the second quadrant (Figure 2.11a). The analysis showed that V_{max} decreased with increasing K_m in the presence of increasing concentrations of **2.6ER**. This behavior [53] indicated that **2.6ER** inhibits maltase by two different pathways; competitively forming enzyme-inhibitor (EI) complex and interrupting enzyme-substrate (ES) intermediate by forming enzyme-substrate-inhibitor (ESI) complex in non-competitive manner. To gain insightful pathway in which **2.6ER** preferentially proceeded, binding affinities of EI and ESI complexes were determined. Secondary plot of slope against concentration of **2.6ER** (Figure 2.11b) showed EI dissociation constant (K_i) of 23.8 μM while ESI dissociation constant (K'_i) of 64.5 μM was also deduced from secondary plot of intercept against concentration of **2.6ER** (Figure 2.11c). A lower dissociation constant of K_i pointed out stronger binding between enzyme and **2.6ER** and suggested preferred competitive over non-competitive manners. In addition, inhibitory mechanism of **2.6ER** toward sucrase was also determined using similar methodology. Apparently, **2.6ER** also inhibited sucrase through mixed-inhibition (Figure 2.12a); in which competitive mode (K_i 22.4 μM, Figure 2.12b) was preferred over non-competitive manner (K'_i 47.5 μM, Figure 2.12c).

(a)

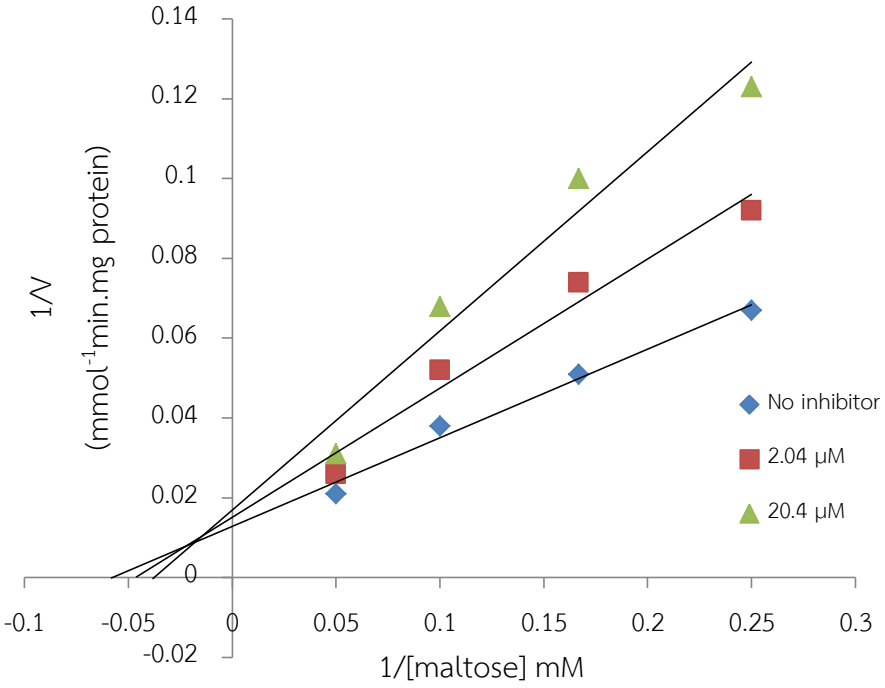
0.14
0.12
0.1
0.08
0.06
0.04
0.02
0
-0.02
-0.1
-0.05
0
0.05
0.1
0.15
0.2
0.25
0.3
1/V
(mmol-1min.mg protein)
1/[maltose] mM
No inhibitor
2.04 µM
20.4 µM

(b)

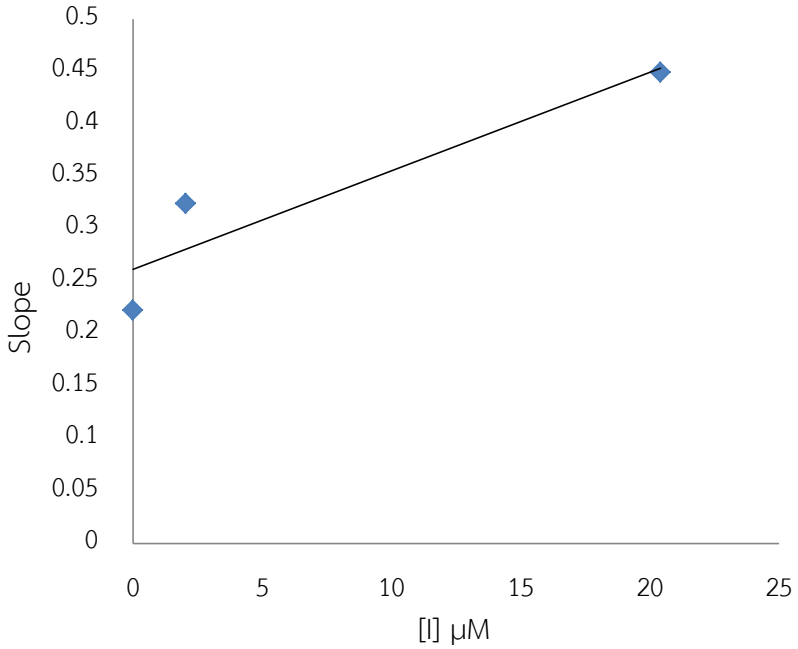
0.5
0.45
0.4
0.35
0.3
0.25
0.2
0.15
0.1
0.05
0
0
5
10
15
20
25
Slope
[I] µM

(c)

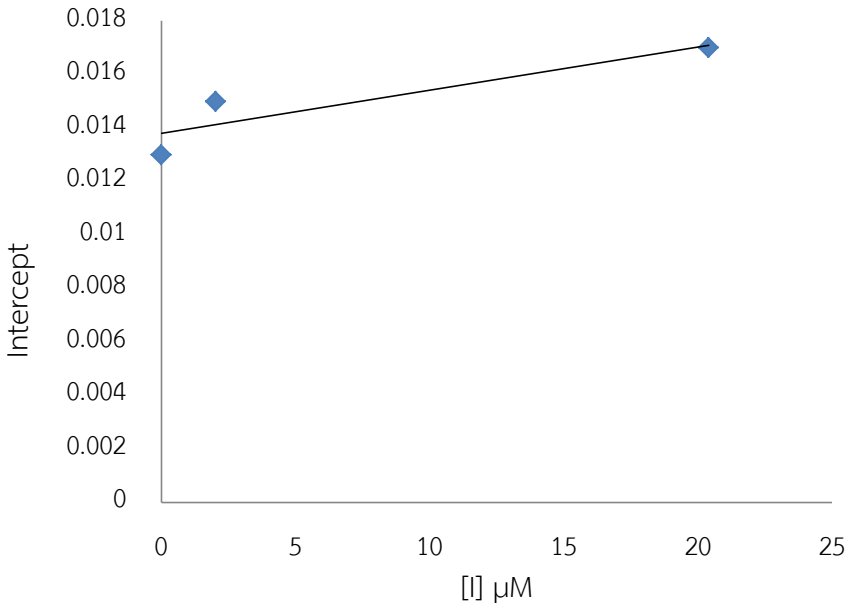

Figure 2.11 (a) Lineweaver–Burk plots for inhibitory activity of **2.6ER** against maltase, (b) Secondary plot of slope vs [I] determination of Ki of **2.6ER** against maltase and (c) Secondary plot of slope vs [I] determination of K′i of **2.6ER** against maltase.

(a)

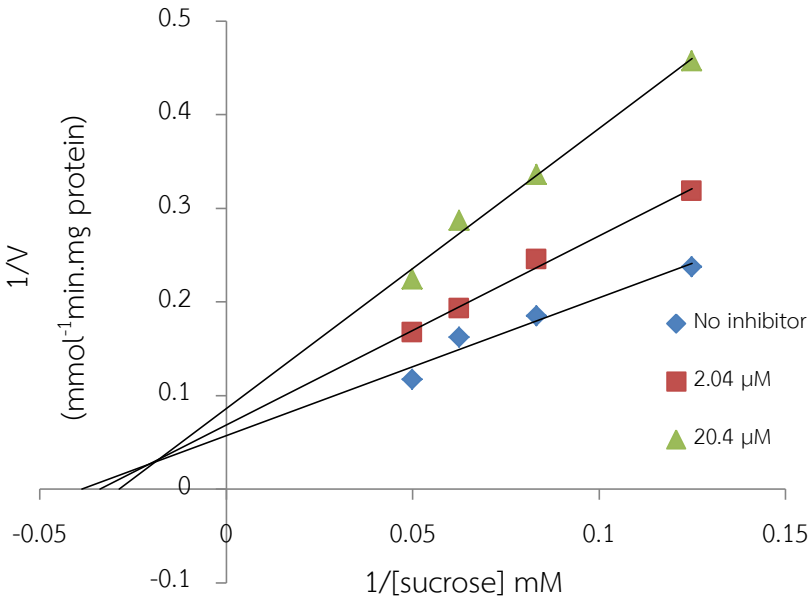

(b)

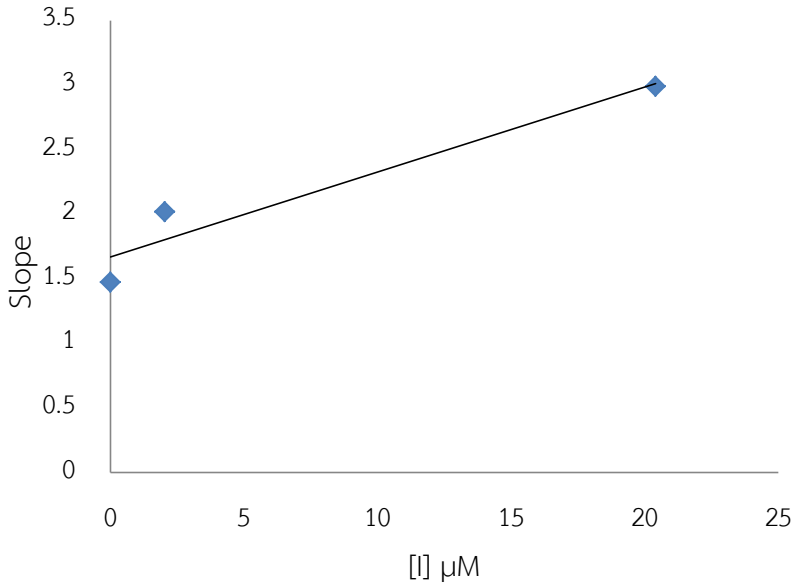

(c)

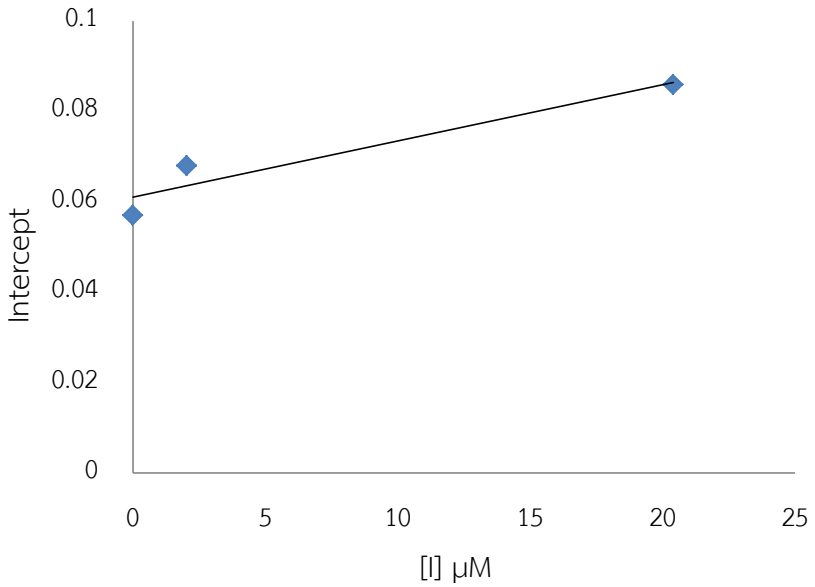

Figure 2.12 (a) Lineweaver–Burk plots for inhibitory activity of **2.6ER** against sucrase, (b) Secondary plot of slope *vs* [I] determination of K_i of **2.6ER** against sucrase and (c) Secondary plot of slope *vs* [I] determination of K'_i of **2.6ER** against sucrase.

Finally, based on Lineweaver–Burk plots and secondary plot, we summarized all the dissociation constants (K_m, K_i and K'_i) and mode of inhibition for against maltase and sucrase in Table 2.5.

Table 2.5 Kinetic data of α-glucosidase inhibition of **2.6ER**.

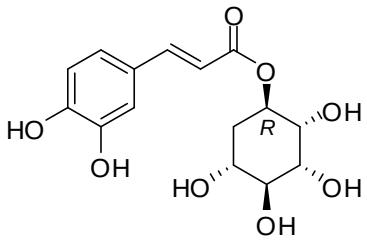

α-glucosidase	Inhibition type	K_i (μM)	K'_i (μM)	K_m (mM)
Maltase	Mixed-inhibition	23.8	64.5	17.3
Sucrase	Mixed-inhibition	22.4	47.5	25.9

*2.3.4.2 Kinetic study of aminoquercitylisoferulamide (**2.8AS**)*

In order to obtain further evidence, we investigated kinetic study of **2.8AS** which is the most potent inhibtor in our research against maltase in rat intestine, using Lineweaver–Burk plots. The Lineweaver–Burk plots of the initial velocity versus maltose concentration in the presence of different concentrations of **2.8AS** revealed a series of straight lines; all of which intersected at X-axis in second quadrant (Figure. 2.13a). The analysis demonstrated that K_m did not change while V_{max} decreased in the presence of increasing concentration of **2.8AS**. This behavior indicated that **2.8AS** inhibited maltase in a non-competitive manner. To the best of our knowledge, this is the first synthetic non-competitive inhibitor for α-glucosidase in rat small intestine for maltase.

To determine the binding affinity of ESI complex, the secondary plot of slope of lines in Lineweaver–Burk relation versus the inhibitor concentration was performed as shown in Figure 2.13b-c. The kinetics revealed that EI dissociation constant (K_i) and while ESI dissociation constant (K'_i) are 6.5 and 6.2 μM, respectively. This results suggested that **2.8AS** inhibits maltase by binding to the allosteric binding site of maltase to form either enzyme-inhibitor (EI) complex or enzyme-inhibitor-substrate (EIS) complex equally effective as shown in Figure 2.14.

(a)

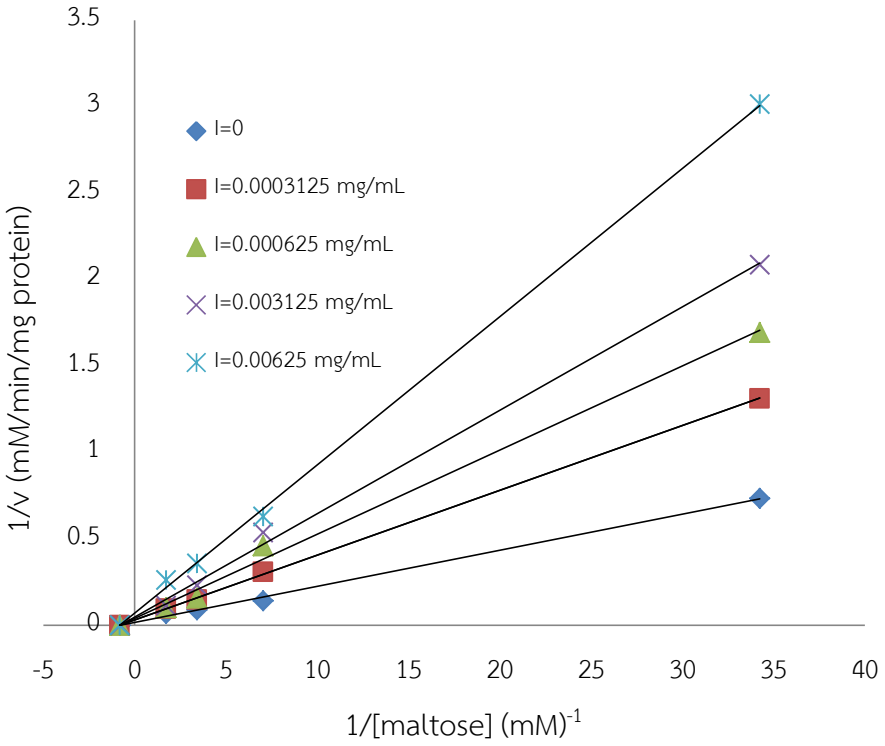
3.5
3
2.5
2
1.5
1
0.5
0
-5
0
5
10
15
20
25
30
35
40
1/v (mM/min/mg protein)
1/[maltose] (mM)-1
I=0
I=0.0003125 mg/mL
I=0.000625 mg/mL
I=0.003125 mg/mL
I=0.00625 mg/mL

(b)

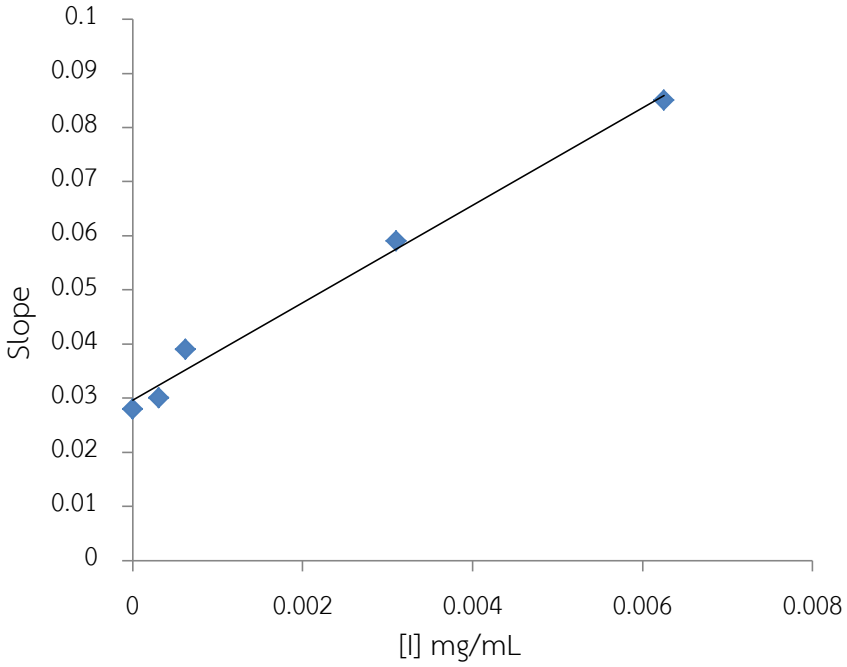
0.1
0.09
0.08
0.07
0.06
0.05
0.04
0.03
0.02
0.01
0
0
0.002
0.004
0.006
0.008
Slope
[I] mg/mL

(c)

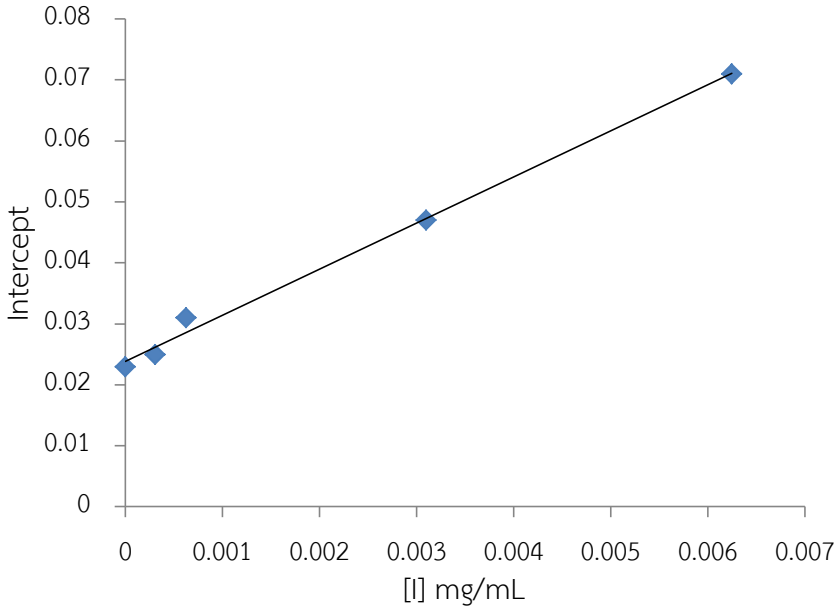

Figure 2.13 (a) Lineweaver–Burk plots for inhibitory activity of **2.8AS** against maltase, (b) Secondary plot of slope *vs* [I] determination of K_i of **2.8AS** against maltase and (c) Secondary plot of slope *vs* [I] determination of K'_i of **2.8AS** against maltase.

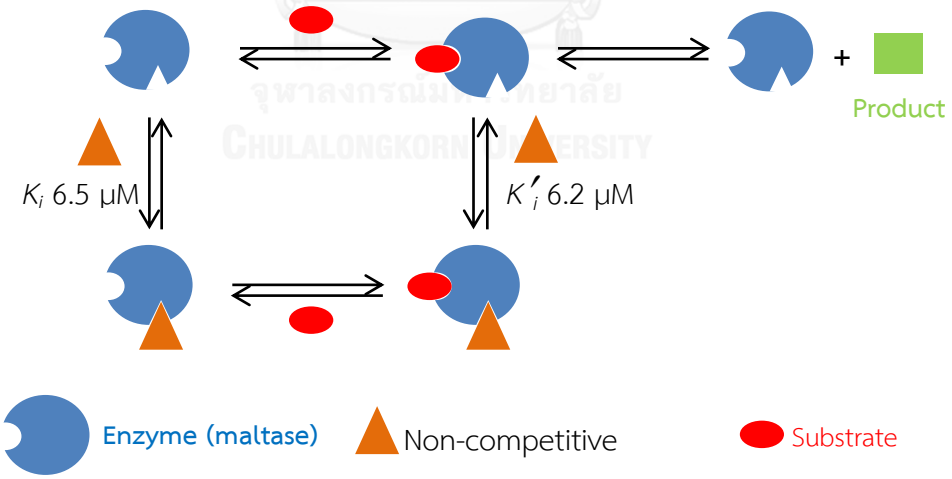

Figure 2.14 Proposed inhibitory mechanism of **2.8AS** against maltase.

Based on the above discussion, **2.8AS** was identified as a non-competitive inhibitor which was different from the commercially drug acarbose, which is a competitive inhibitor. Therefore, the use of both **2.8AS** and acarbose may result in

greater potency due to the possibility to form a strong complex between enzyme–**2.8AS**–acarbose, which retarded the conversion of enzyme or substrate.

2.3.5 Synergistic effect of acarbose by non-competitive inhibitor (**2.8AS**)

Usage of multiple drugs with different mechanisms or mode of action may also direct the effect against single target, multiple targets or multiple diseases simultaneously [54]. The possible outcomes for synergitic effects are 1) increasing the therapeutic effect, 2) decreasing the dosage but increasing or preserving the same activity to avoid toxicity, 3) slowing down the development of drug resistance, and 4) supplying selective synergism resistance target (or efficacy synergism) versus host (or toxicity antagonism). As **2.8AS** was a non-competitive inhibitor of rat intestinal α-glucosidase, it is of interest to study whether it may interact synergistically on α-glucosidase when combined with acarbose. A mixture of acarbose under varying concentrations (0.0003125-0.0625 mg/mL) and fixed concentration of **2.8AS** (0.000625 mg/mL) were tested against α-glucosidase (Figure 2.15). Notably, the 0.000625 mg/mL of **2.8AS** alone showed lower than 10% inhibitory activity and IC_{50} of acarbose is 0.001 mg/mL. The mixtures showed a greater inhibitory effect than acarbose alone in all concentrations. The inhibitory enhancements were found to be in the range of 1.1-5.7 times. Interestingly, the grater enhancement of inhibition was observed when the dose of acarbose (0.0003125 and 0.000625 mg/mL) in the mixtures is below its IC_{50} value while the effect decreased with higher concentrations of the acarbose (0.003125, 0.00625 and 0.0625 mg/mL) in the mixture. To our delight, 0.0003125 mg/mL of acarbose and 0.000625 mg/mL of **2.8AS** dosage gave 57% inhibitory activity whereas acarbose alone possessed IC_{50} at 0.001 mg/mL. The results suggested that the dosage of acarbose could be reduced from 0.001 to 0.0003125 mg/mL while maintaining the inhibitory activity at the IC_{50} level of acarbose. This results suggested that the mixture of acarbose and **2.8AS** provided a significant clinical benefit in delaying postprandial hyperglycemia. The intake amount of **2.8AS**

that is required together with low dose of acarbose also needs further investigation in type II diabetic patients.

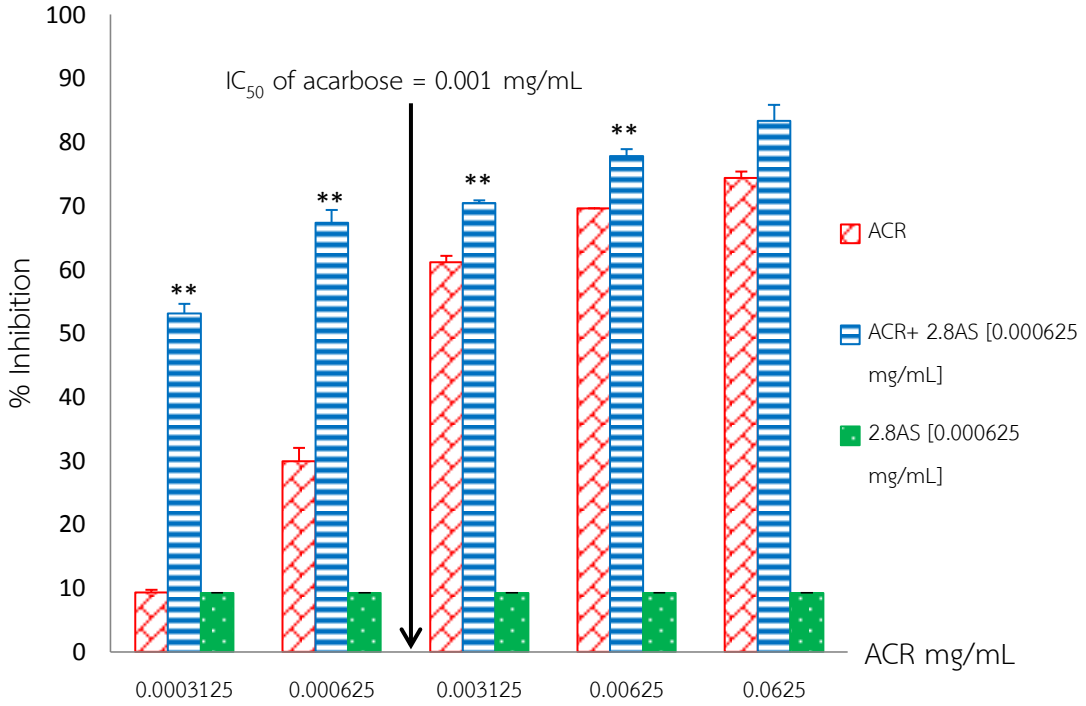

Figure 2.15 The percentage intestinal inhibition of acarbose and its combination with **2.8AS** (0.000625 mg/ml). Results are expressed as mean ± SEM, n = 3. **p<0.01 compared to acarbose alone.

2.4 Molecular docking of 1*S*-aminoquercitylisoferulamide (2.8AS)

Based on the above section, to prove our hypothesis and to confirm the kinetic results, a molecular docking study was further investigated in this section.

2.4.1 Homology model of rat NtMGAM

Even though the crystal structure of human *N*-terminal maltase-glucoamylase (NtMGAM) was first reported in 2008 [55], no such crystal structure for the maltase from rat small intestine was reported. Therefore in this work, we need to create a homology structure of N-terminal maltase-glucoamylase from rat small intestine.

A homology structure of *N*-terminal maltase-glucoamylase (NtMGAM) as shown in Figure 2.16a (white), from rat small intestine was first built based on the crystal structure of human NtMGAM (PDB: code 2QLY) as shown in Figure 2.16a (cyan). The model displayed the perfect structural superposition between the rat (white) and human (cyan) NtMGAM, suggesting the high accuracy of our simulated model with 0.23 Å RMSD (82.4% sequence identity). Both models were used receptor models in the protein-ligand docking process.

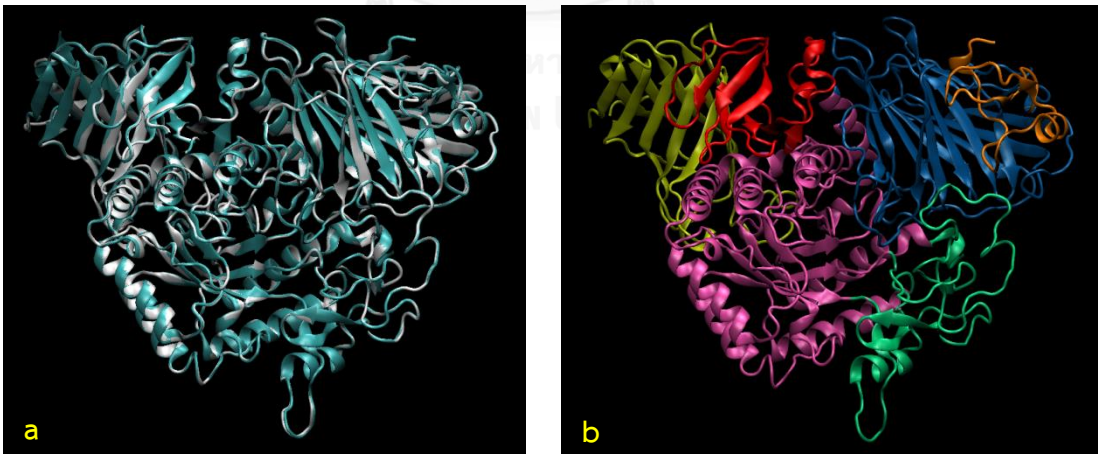

Figure 2.16 The 3D structure of rat and human NtMGAM were displayed in Newcartoon mode. (a) The homology model of rat NtMGAM (white) superposed with the crystal structure of human NtMGAM (cyan), (b) NtMGAM (2QLY). Individual domains are colored as follows: trefoil Type-P domain (brown), N-terminal domain (blue), catalytic $(\beta/\alpha)_8$ domain (mauve), catalytic domain Insert 1 and 2 (green),

proximal C-terminal domain (ProxC) (red), distal C-terminal domain (DistC) (yellow) [55].

2.4.2 The docking of X-ray human NtMGAM model and compound **2.8AS**

A crystal structure of human NtMGAM-acarbose complex provides important information useful for validation of our docking methodology. To test ability of docking method to correctly predict the binding pose of acarbose in the human NtMGAM binding site, the inhibitor present in the X-ray structure was removed and the docked back into the binding pocket. The binding pose of the ligand obtained from the docking result was very similar to that of the reported crystal structure of the human NtMGAM-acarbose complex (PDB: code 2QMJ) (Figure 2.17a). All further docking runs were performed using docking parameters that gave the most accurate reproduction of the inhibitor binding pose.

Next, a molecular docking of the compound **2.8AS** binding to human NtMGAM was carried out. The results showed that compound **2.8AS** appeared to bind to different sites other than the active site of the protein in NtMGAM-acarbose complex (Figure 2.16). This is in agreement with experimental data in which the compound **2.8AS** was reported to show the non-competitive inhibitory activity.

A further analysis of the top-ranked binding poses of **2.8AS** (on the basis of the binding energy) as seen in Table 2.6, which is obtained from automated docking studies provided seven potential allosteric sites (Figure 2.17b). Pose A (including rank 1 and 3) exhibited the lowest binding energy of -6.4 $\pm$ 0.7 kcal/mole and showed the binding poses of **2.8AS** in the catalytic domain (pink new cartoon), which is different from the binding site of acarbose**.** On the other hand, other poses (Pose B to F) showed the binding pose of **2.8AS** out of the catalytic domain of NtMGAM, which can be neglected as seen in Figure 2.17b.

Table 2.6 Average energy values from the top ranked binding poses of **2.8AS** on human NtMGAM.[a]

Position	Average Energy ± SD (kcal/mole)
Pose A (humanNtMGAM) (rank 1, 3)	-6.4 ± 0.7
Pose B (humanNtMGAM) (rank 2)	-6.0 ± 0.2
Pose C (humanNtMGAM) (rank 4, 7, 9)	-5.3 ± 0.7
Pose D (humanNtMGAM) (rank 8)	-5.0 ± 0.5
Pose E (humanNtMGAM) (rank 5)	-4.9 ± 0.4
Pose F (humanNtMGAM) (rank 6)	-4.9 ± 0.3
Pose G (humanNtMGAM) (rank 10)	-4.7 ± 0.3

[a] For more information see Appendix Table

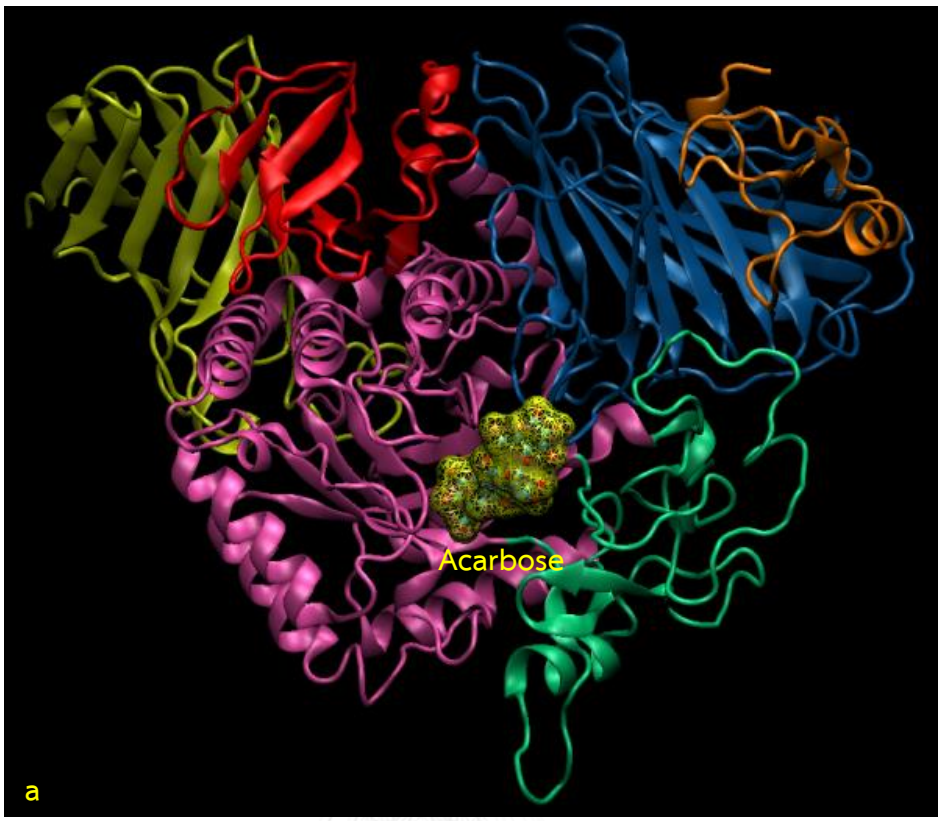
Acarbose
a

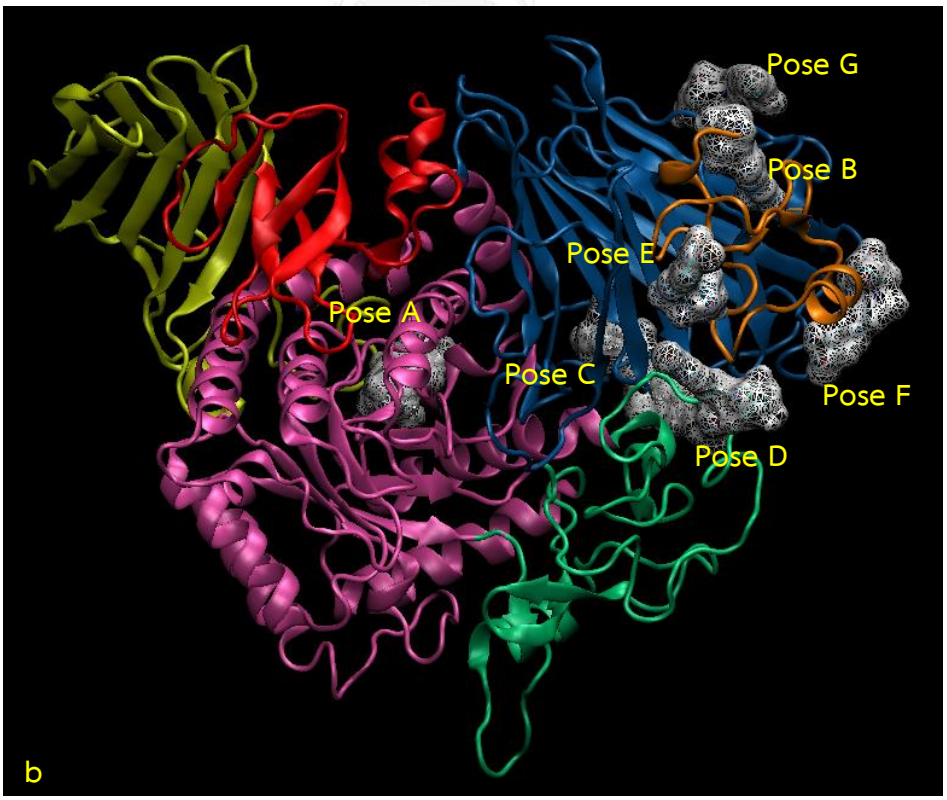
Pose G
Pose B
Pose E
Pose A
Pose C
Pose F
Pose D
b

Figure 2.17 Predicted binding site of **2.8AS** on 2QLY. Molecular docking results for compound acarbose and **2.8AS**. (a) Shown bonding poses of acarbose (yellow molecular surface) and (b) Shown binding poses of **2.8AS** (white molecular surface)

2.4.3 The docking of homology rat NtMGAM model and compound **2.8AS**

Similarly, an analysis of the top ten ranked binding poses gave five candidate sites for the non-competitive inhibition of compound **2.8AS** on the rat NtMGAM. Pose A (including rank 2 and 3) and Pose D (including rank 8 and 9) contained the binding energy of -5.2 $\pm$ 0.7 and -4.6 ± 0.3 kcal/mole, respectively (Table 2.7). Both poses were found in the catalytic domain (pink new cartoon), which were not in the same pocket site as NtMGAM-acarbose complex (Figure 2.18a). Even though pose E (rank 1) showed the lowest binding energy (-6.3 ± 0.7 kcal/mole), it gave the highest distance value of the center of the cluster to the center of the binding site (43.5 Å). Moreover, other poses (Pose B and C) showed the binding poses, which were out of the catalytic domain of NtMGAM as seen in Figure 2.18b. Therefore, poses B, C and E can be ruled out from our cluster in this model.

Table 2.7 Average energy values from the top ranked binding poses of **2.8AS** on homology rat NtMGAM

Position	Average Energy ± SD (kcal/mole)
Pose A (ratNtMGAM) (rank 2, 3)	-5.2 ± 0.7
Pose B (ratNtMGAM) (rank 4, 5 ,10)	-4.7 ± 0.4
Pose C (ratNtMGAM) (rank 6, 7)	-4.7 ± 0.4
Pose D (ratNtMGAM) (rank 8, 9)	-4.6 ± 0.3
Pose E (ratNtMGAM) rank 1	-6.3 ± 0.7

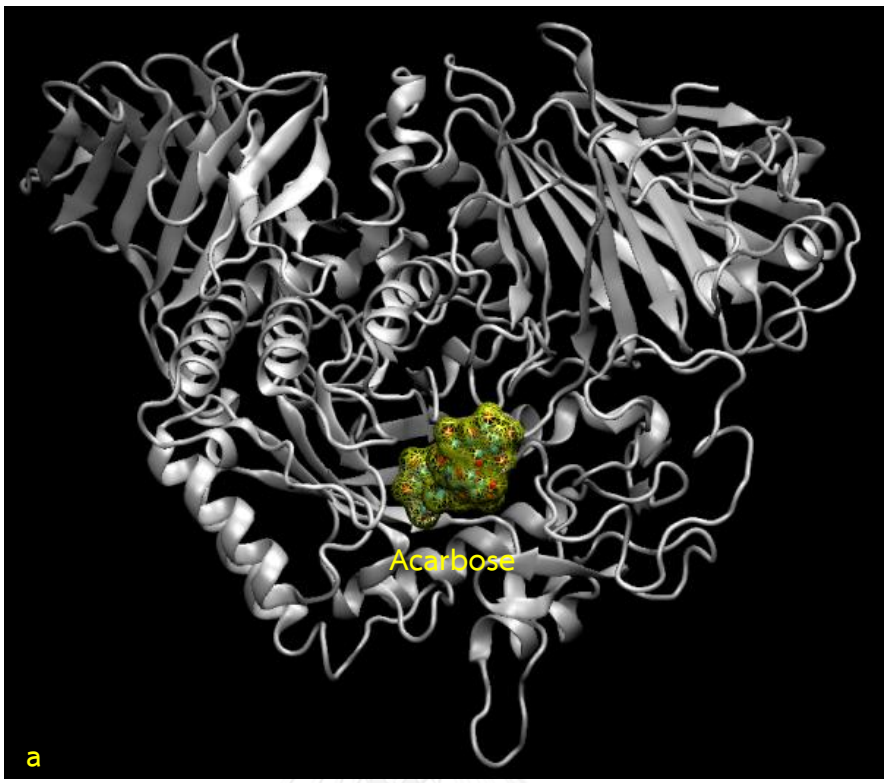
Acarbose
a

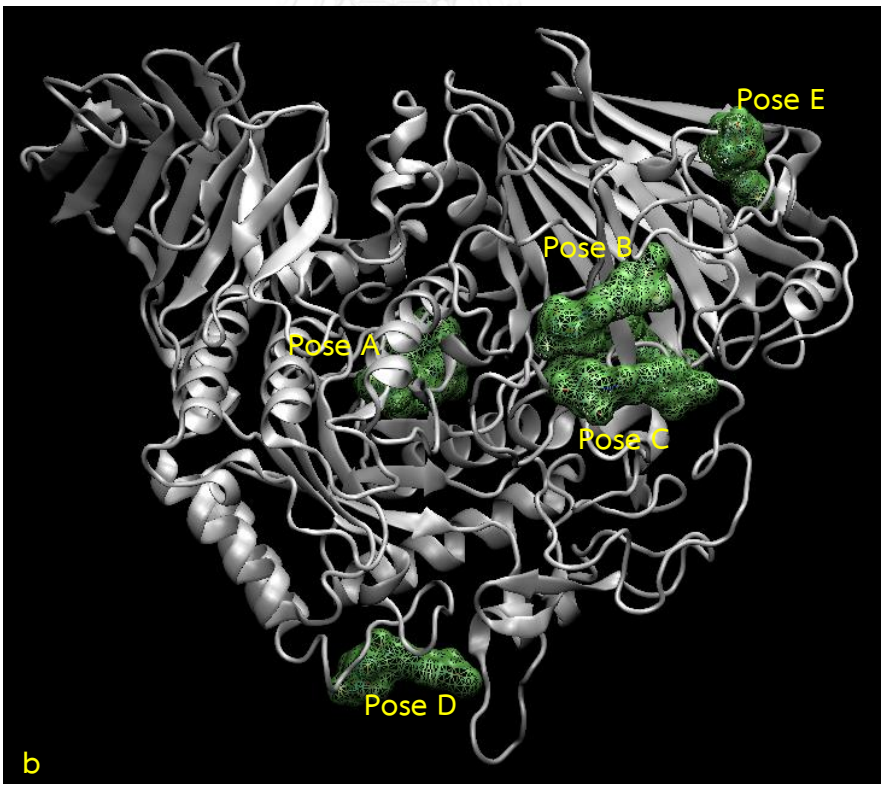
Pose E
Pose B
Pose A
Pose C
Pose D
b

Figure 2.18 Predicted binding pocket of **2.8AS** on homology model (white new cartoon model). Molecular docking results for compound acarbose and **2.8AS**. (a) Shown site pocket of acarbose (yellow molecular surface) and (b) Shown binding pocket overlaid with **2.8AS** (green molecular surface).

In order to find the most plausible allosteric site of NtMGAM-**2.8AS**, the overlay between human NtMGAM-**2.8AS** and rat NtMGAM-**2.8AS** was analyzed (Figure 2.19). Evaluation of the docking analysis predicted that the two systems revealed the consistency between the predicted binding pose of human NtMGAM-**2.8AS** and that of rat NtMGAM-**2.8AS**. A white dash rectangular as seen in Figure 2.19 indicated the same binding pose between pose A (humanNtMGAM) and pose A (ratNtMGAM) in catalytic domain, suggesting a highly plausible allosteric site. Obviously, those binding sites of compound **2.8AS** to the *N*-terminal maltase (NtMGAM) (both human and rat) were in the different pocket when compared with that of acarbose (yellow molecular surface). These results were consistent with a kinetic study of **2.8AS** (Chapter 2.3.4.2), which suggested the binding in the non-competitive manner.

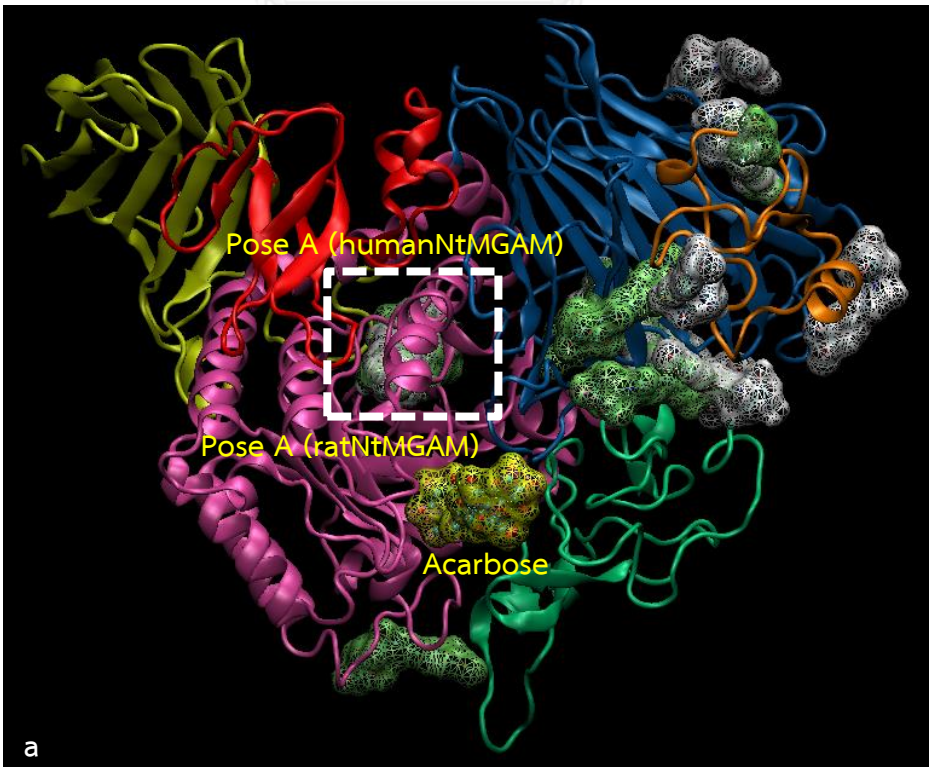

Figure 2.19 Overlap between results from docking **2.8AS**-2QLY (white molecular surface) and **2.8AS**-homology model (green molecular surface). Individual domains are colored.

Moreover, Fpocket web server (http://fpocket.sourceforge.net) was used to predict allosteric binding pocket of human (PDB: 2QLY) and homology rat *N*-terminal maltase (NtMGAM). Fpocket is an online open source protein (cavity) detection algorithm based on the Voronoi tessellation [56] and utilized α-spheres concept [57]. Target protein 3D structure was submitted to Fpocket server for automated pocket prediction. Fpocket predicted 42 binding pockets in the submitted human *N*-terminal maltase, while 52 binding pockets of homology rat *N*-terminal maltase were observed as seen in Appendix Table A.3. Top three ranks of human and homology rat prediction pockets were shown in Figure 2.20a and 2.20b, respectively.

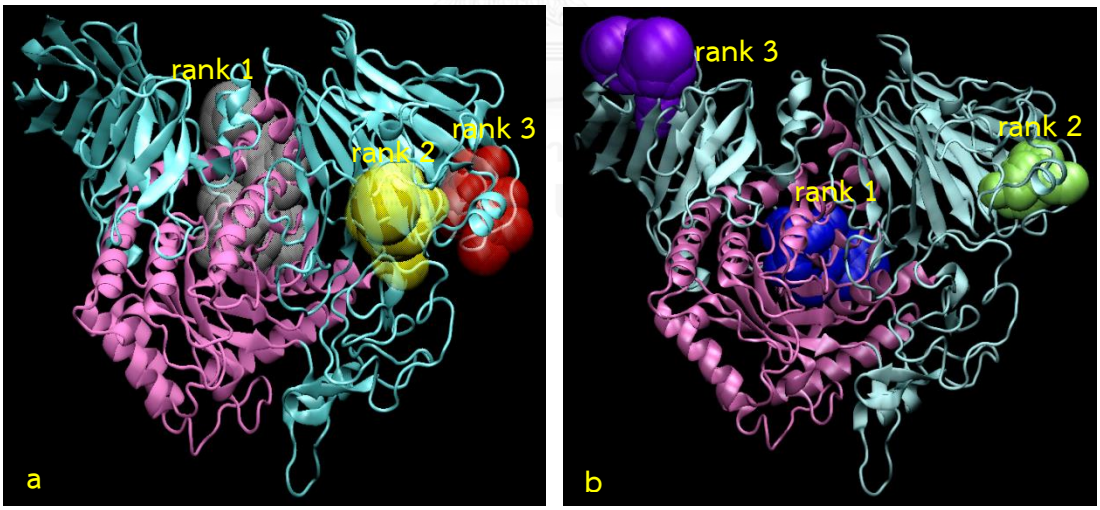

Figure 2.20 Cavities found by fpocket. (a) Top 3 results out of 42 possible binding sites from human; (b) Top 3 results out of 52 possible binding sites from homology rat.

The first ranked docking prediction from human (yellow licoline structure) and homology rat *N*-terminal maltase (lime licoline structure) corresponded to the first ranked prediction of the allosteric pocket on the catalytic domain (PDB 2QLY) as seen in Figure 2.21.

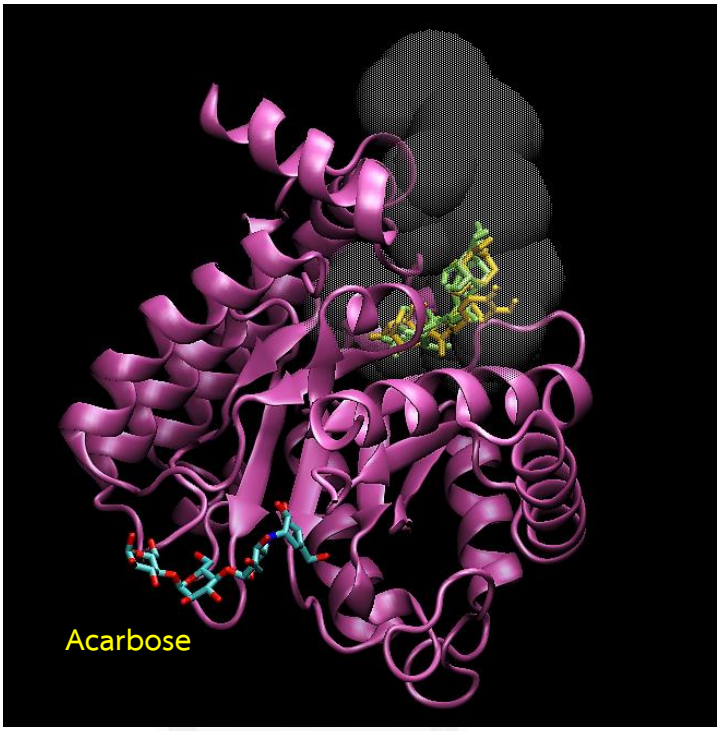

Figure 2.21 Overlap between the first ranked results from docking **2.8AS**-2QLY (yellow licoline structure), **2.8AS**-homology model (lime licoline structure), cavity binding pocket (white cloud) and acarbose on catalytic domain.

From the above results, we have also discovered new allosteric sites on maltase, which have never been reported before and those pockets are located on positions different from those of the acarbose's catalytic site. Based on the docking simulation from **2.8AS**-maltase human and **2.8AS**-maltase homology rat complexes comparing with Fpocket results, it suggested a new potential allosteric binding site of maltase. These results supported the non-competitive manner of our kinetic investigations (Chapter 2.3.4.2).

We hypothesized that after the formation of **2.8AS**-maltase complex, the 3D structure of the active site on maltase would change, thus prohibiting the binding between maltose substrate and maltase.

Thus, the new potential allosteric site can be used for future rational drug design for new and potent selective α-glucosidase inhibitors.

CHAPTER III

Experimental section

3.1 General experiment procedures

All moisture-sensitive reactions were carried out under a nitrogen atmosphere. All solvents were distilled prior to use. HRESIMS spectra were obtained from a micrOTOF Bruker mass spectrometer. ^{1}H and ^{13}C NMR spectra were recorded ($CDCl_3$, CD_3OD and DMSO-d_6 as solvents) at 400 and 100 MHz, respectively, on a Varian Mercury^{+} 400 NMR spectrometer. Chemical shifts were reported in ppm downfield from TMS or solvent residue. Thin layer chromatography (TLC) was performed on pre-coated Merck silica gel 60 F254 plates (0.25 mm thick layer) and visualized under 254 nm UV followed by dipping in $KMnO_4$ solution. Column chromatography was conducted using Merck silica gel 60 (70–230 mesh) or Sephadex LH-20

3.2 Isolation of (+)-*proto*-quercitol

Our improved method of isolation of (+)-*proto*-quercitol (**1.29**) was applied [41, 42]. Generally, ground stems (1.0-1.2 kg) of *A. arborescens* were boiled with water (2×4 L) for 2 h. The combined decoction was filtered, concentrated to a half volume and partitioned twice with equal volume of CH_2Cl_2 to remove lipophilic matters. The aqueous layer was diluted with water in a ratio of 2:1 and applied onto a Diaion HP20 column (1 kg) equilibrated with water. The column was excessively eluted with water (11 L), and the aqueous elutes were lyophilized to yield white powder. More purified (+)-*proto*-quercitol (**1.29**, 1.0%w/w) was obtained upon crystallization using hot MeOH.

3.3 Synthesis of (amino)bis-acetonides 1.30, 1.31, 1.32 and 1.33

(amino)Bis-acetonides were synthesized using our previous methods [38, 41, 42], yielding **1.30** (79%), **1.31** (42%), **1.32** (43%) and **1.33** (81%). The ^{1}H and ^{13}C NMR data were matched well the reports.

3.4 General synthesis of quercitylcinnamates

3.4.1 General protection of phenolic group

A solution of **2.6**, **2.7** or **2.8** (1 eq, 2.57 mmol), imidazole (10 eq: 1 OH group) and tert-butyldimethylsilyl chloride (TBDMSCl) (10 eq: 1 OH group) in *N*,*N*-dimethylformamide (DMF, 15 mL) in a 50 mL round buttom(ed) flask. The mixture was stirred at room temperature for 1 h under N_2 gas. The reaction mixture was washed with water (3×20 mL) and the organic portion was extracted with ethyl acetate (EtOAc) (3×20 mL). The organic layer was washed with saturated aqueous NaCl, followed by dried over Na_2SO_4. After filtration and removal of the solvent under reduced pressure, the crude product was purified by silica gel column to afford 6Si, 7Si and 8Si in 74, 82 and 79% yields, respectively.

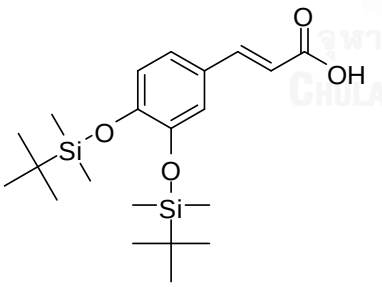

3,4-Di-O-tert-butyldimetylsilylcaffeic acid (**2.6Si**); white powder; ^{1}H NMR ($CDCl_3$, 400 MHz) δ 7.46 (d, *J* = 15.8 Hz, 1H), 6.83 (d, *J* = 8.8 Hz, 1H), 6.81 (s, 1H), 6.62 (d, *J* = 8.8 Hz, 1H), 6.03 (d, *J* = 15.8 Hz, 1H), 0.77 (d, *J* = 4.5 Hz, 18H), 0.00 (d, *J* = 3.2 Hz, 12H)

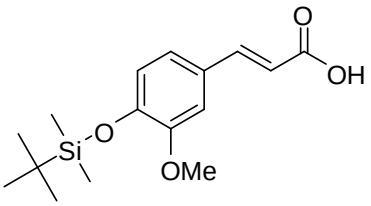

4-O-tert-Butyldimetylsilylferulic acid (**2.7Si**); white powder; ^{1}H NMR ($CDCl_3$, 400 MHz) δ 7.65 (d, *J* = 15.9 Hz, 1H), 6.98 (d, *J* = 8.6 Hz, 1H), 6.95 (s, 1H), 6.79 (d, J = 8.6 Hz, 1H), 6.24 (d, *J* = 15.9 Hz, 1H), 3.78 (s, 3H), 0.93 (s, 9H), 0.11 (s, 6H)

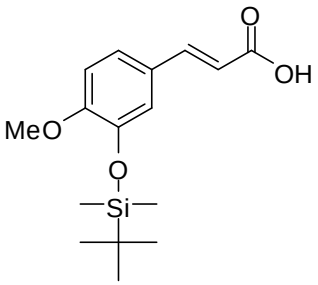

4-O-tert-Butyldimetylsilylisoferulic acid (**2.8Si**); white powder; ^{1}H NMR ($CDCl_3$, 400 MHz) δ 7.66 (d, *J* = 15.7 Hz, 1H), 6.97 (d, *J* = 8.8 Hz, 1H), 6.95 (s, 1H), 6.79 (d, *J* = 8.8 Hz, 1H), 6.20 (d, *J* = 15.7 Hz, 1H), 3.78 (s, 3H), 0.93 (s, 9H), 0.11 (s, 6H)

3.4.2 General coupling reaction between bis-acetonides and cinnamic or silylated cinnamate derivatives

To a solution of **2.1, 2.2, 2.3, 2.4** and **2.5** (2.5 eq) in CH_2Cl_2 (5 mL) were added dicyclohexylcarbodimine (DCC, 2.7 eq) and 4-dimethylaminopyridine (DMAP, catalytic amount). The reaction mixture was stirred at 0 °C for 30 min. **1.30** or **1.31** (1 eq) in CH_2Cl_2 was added dropwise at room temperature under N_2 gas. The product was filtrated and solvent was removed under reduced pressure. The crude product was subsequently purified by silica gel column to afford bis-acetonides **2.1ERp**-**2.5ERp**.

To a solution of **2.6Si**, **2.7Si** and **2.8Si** (11 eq) in CH_2Cl_2 (10 mL) were added DCC (12 eq) and DMAP (catalytic amount). The reaction mixture was stirred at 0 °C for 30 min. **1.30** or **1.31** (1 eq) in CH_2Cl_2 was added dropwise at room temperature under N_2 gas. The bis-acetonides **2.6ERp**-**2.8ESp** were obtained after purification using silica gel column.

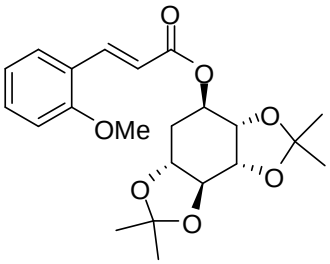

2.1ERp; 75% yield of pale yellow oil; ^{1}H NMR ($CDCl_3$, 400 MHz) δ 7.94 (d, *J* = 16.1 Hz, 1H), 7.43 (d, *J* = 7.6 Hz, 1H), 7.30 (t, *J* = 7.5 Hz, 1H), 6.90 (t, *J* = 7.5 Hz, 1H), 6.85 (d, *J* = 7.6 Hz, 1H), 6.46 (d, *J* = 16.1 Hz, 1H), 5.47 (m, 1H), 4.30 (m, 1H), 4.23 (m, 1H), 3.83 (s, 3H), 3.66 (m, 1H), 3.54 (m, 1H), 2.16 (m, 1H), 2.04 (m, 1H), 1.46 (s, 3H), 1.38 (s, 6H), 1.30 (s, 3H).

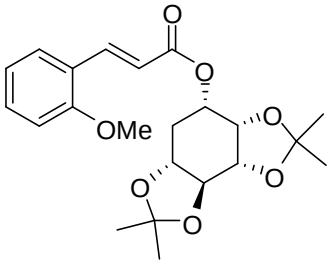

2.1ESp; 72% yield of colorless wax; ^{1}H NMR ($CDCl_3$, 400 MHz) δ 7.98 (d, *J* = 16.1 Hz, 1H), 7.45 (d, *J* = 7.5 Hz, 1H), 7.29 (t, *J* = 7.6 Hz, 1H), 7.19 (s, 1H), 6.90 (t, *J* = 7.6 Hz, 1H), 6.85 (d, *J* = 7.5 Hz, 1H), 6.55 (d, *J* = 16.1 Hz, 1H), 5.30 (m, 1H), 4.37 (m, 1H), 4.23 (m, 1H), 3.84 (m, 4H), 3.44 (m, 1H), 2.36 (m, 1H), 1.93 (m, 2H), 1.47 (s, 3H), 1.40 (s, 3H), 1.38 (s, 3H), 1.30 (s, 3H).

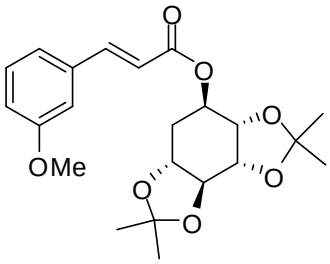

2.2ERp; 79% yield of colorless wax; ^{1}H NMR ($CDCl_3$, 400 MHz) δ 7.61 (d, *J* = 16.0 Hz, 1H), 7.24 (t, *J* = 7.9 Hz, 1H), 7.06 (d, *J* = 7.5 Hz, 1H), 6.98 (s, 1H), 6.89 (d, *J* = 7.5 Hz, 1H), 6.36 (d, *J* = 16.0 Hz, 1H), 5.45 (m, 1H), 4.30 (m, 1H), 4.23 (m, 1H), 3.77 (s,

3H), 3.66 (m, 1H), 3.56 (m, 1H), 2.15 m, 1H), 2.06 (m, 1H), 1.46 (s, 3H), 1.39 (s, 6H), 1.20 (s, 3H).

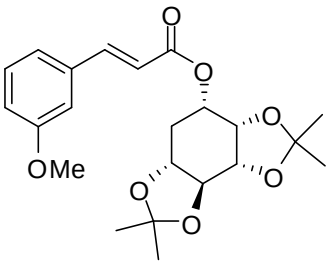

2.2ESp; 76% yield of colorless oil; ^{1}H NMR ($CDCl_3$, 400 MHz) δ 7.65 (d, *J* = 16.0 Hz, 1H), 7.24 (t, *J* = 7.9 Hz, 1H), 7.07 (d, *J* = 7.5 Hz, 1H), 6.99 (s, 1H), 6.89 (d, *J* = 7.5 Hz, 1H), 6.45 (d, *J* = 16.0 Hz, 1H), 5.31 (m, 1H), 4.38 (m, 1H), 4.24 (m, 1H), 3.83 (m, 1H), 3.77 (s, 3H), 3.45 (m, 1H), 2.38 (m, 1H), 1.92 (m, 1H), 1.47 (s, 3H), 1.40 (s, 3H), 1.38 (s, 3H), 1.30 (s, 3H).

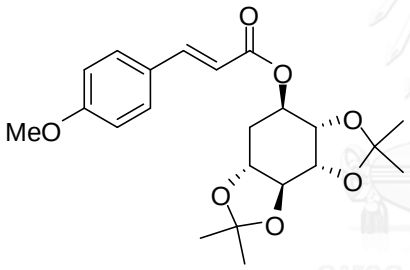

2.3ERp; 83% yield of colorless viscous oil; ^{1}H NMR ($CDCl_3$, 400 MHz) δ 7.60 (d, *J* = 16.0 Hz, 1H), 7.42 (d, *J* = 8.7 Hz, 2H), 7.19 (s, 4H), 6.84 (d, *J* = 8.7 Hz, 2H), 6.24 (d, *J* = 16.0 Hz, 1H), 5.45 (m, 1H), 4.30 (m, 1H), 4.23 (m, 1H), 3.78 (s, 3H), 3.65 (m, 1H), 3.54 (m, 1H), 2.15 (m, 1H), 2.05 (m, 1H), 1.47 (s, 3H), 1.39 (s, 6H), 1.31 (s, 3H).

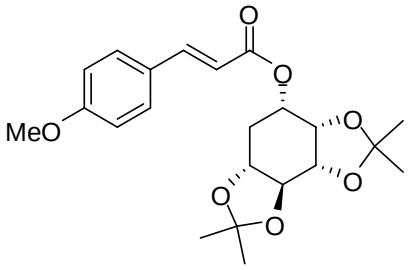

2.3ESp; 72% yield of colorless wax;^{1}H NMR ($CDCl_3$, 400 MHz) δ 7.69 (d, *J* = 15.9 Hz, 1H), 7.49 (d, *J* = 8.4 Hz, 2H), 6.90 (d, *J* = 8.4 Hz, 2H), 6.38 (d, *J* = 15.9 Hz, 1H),

5.35 (m, 1H), 4.43 (m, 1H), 4.30 (m, 1H), 3.87 (m, 1H), 3.83 (s, 3H), 3.50 (m, 1H), 2.43 (m, 1H), 1.98 (m, 1H), 1.53 (s, 3H), 1.46 (s, 3H), 1.44 (s, 3H), 1.36 (s, 3H).

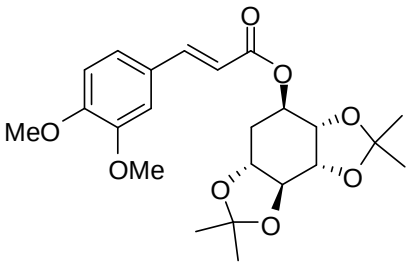

2.4ERp; 78% yield of colorless oil; ^{1}H NMR ($CDCl_3$, 400 MHz) δ 7.64 (d, *J* = 15.9 Hz, 1H), 7.11 (d, *J* = 8.3 Hz, 1H), 7.05 (s, 1H), 6.87 (d, *J* = 8.3 Hz, 1H), 6.30 (d, *J* = 15.9 Hz, 1H), 5.52 (m, 1H), 4.36 (m, 1H), 4.30 (m, 1H), 3.92 (s, 9H), 3.72 (m, 1H), 3.61 (m, 1H), 2.21 (m, 1H), 2.12 (m, 1H), 1.53 (s, 3H), 1.45 (s, 6H), 1.37 (s, 3H).

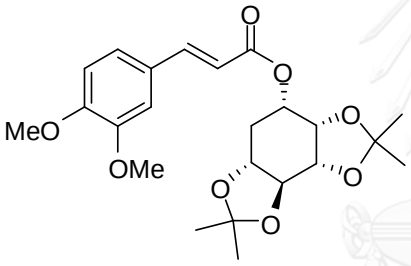

2.4ESp; 81% yield pale yellow oil; ^{1}H NMR ($CDCl_3$, 400 MHz) δ 7.62 (d, *J* = 15.8 Hz, 1H), 7.05 (d, *J* = 8.2 Hz, 1H), 7.01 (s, 1H), 6.81 (d, *J* = 8.2 Hz, 1H), 6.33 (d, *J* = 15.8 Hz, 1H), 5.31 (s, 1H), 4.38 (m, 1H), 4.24 (m, 1H), 3.83 (m, 7H), 3.45 (m, 2H), 2.37 (m, 1H), 1.90 (m, 1H), 1.48 (s, 3H), 1.40 (s, 3H), 1.38 (s, 3H), 1.30 (s, 3H).

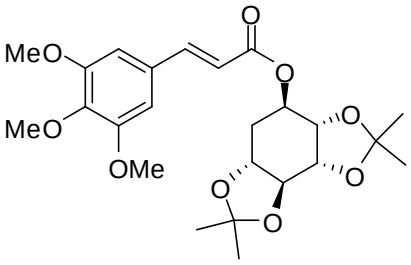

2.5ERp; 85% yield of colorless viscous oil; ^{1}H NMR ($CDCl_3$, 400 MHz) δ 7.56 (d, *J* = 15.9 Hz, 1H), 6.69 (s, 2H), 6.28 (d, *J* = 15.9 Hz, 1H), 5.45 (m, 1H), 4.31 (m, 1H), 4.24 (m, 1H), 3.82 (s, 9H), 3.66 (m, 1H), 3.54 (m, 1H), 2.21 (m, 1H), 2.12 (m, 1H), 1.47 (s, 3H), 1.39 (s, 6H), 1.31 (s, 3H).

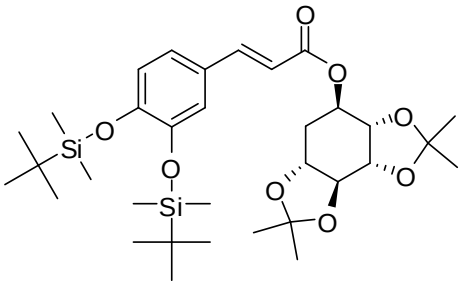

2.6ERp; 67% yield of colorless oil; ^{1}H NMR ($CDCl_3$, 400 MHz) δ 7.37 (d, *J* = 15.9 Hz, 1H), 6.80 (d, *J* = 8.7 Hz, 1H), 6.78 (s, 1H), 6.61 (d, *J* = 8.7 Hz, 1H), 6.00 (d, *J* = 15.9 Hz, 1H), 5.30 (m, 1H), 4.17 (m, 1H), 4.09 (m, 1H), 3.51 (m, 1H), 3.40 (m, 1H), 2.00 (m, 1H), 1.91 (m, 1H), 1.32 (s, 3H), 1.24 (s, 6H), 1.16 (s, 3H), 0.78 (s, 18H), 0.00 (s, 12H).

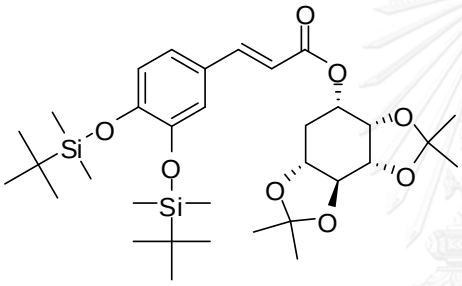

2.6ESp; 77% yield of pale yellow oil; ^{1}H NMR ($CDCl_3$, 400 MHz) δ 7.56 (d, *J* = 15.9 Hz, 1H), 6.96 (d, *J* = 8.7 Hz, 1H), 6.94 (s, 1H), 6.75 (d, *J* = 8.7 Hz, 1H), 6.25 (d, *J* = 15.9 Hz, 1H), 5.29 (brs, 1H), 4.44 (m, 1H), 4.23 (m, 1H), 3.30 (m, 1H), 3.43 (m, 1H), 2.36 (m, 1H), 1.92 (s, 1H), 1.48 (s, 3H), 1.40 (s, 3H), 1.38 (s, 3H), 1.30 (s, 3H), 0.91 (s, 18H), 0.14 (s, 12H).

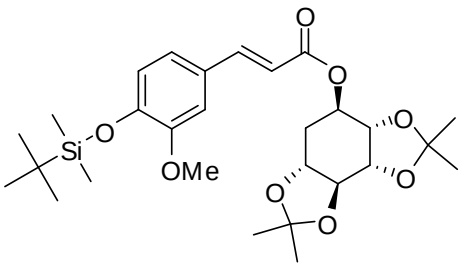

2.7ERp; 68% yield of colorless oil ^{1}H NMR ($CDCl_3$, 400 MHz) δ 7.47 (d, *J* = 15.8 Hz, 1H), 6.86 (d, *J* = 7.2 Hz, 2H), 6.85 (s, 1H), 6.80 (d, *J* = 7.2 Hz, 1H), 6.12 (d, *J* = 15.8 Hz, 1H), 5.35 (m, 1H), 4.20 (m, 1H), 4.12 (m, 1H), 3.67 (s, 3H), 3.55 (m, 1H), 3.44 (m,

1H), 2.05 (m, 1H), 1.94 (m, 1H), 1.36 (s, 3H), 1.28 (s, 6H), 1.18 (m, 1H), 0.82 (s, 9H), 0.00 (s, 6H).

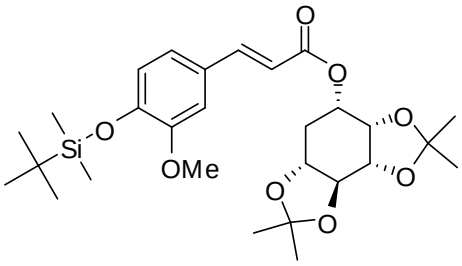

2.7ESp; 69% yield of colorless oil; ^{1}H NMR ($CDCl_3$, 400 MHz) δ 7.50 (d, *J* = 15.9 Hz, 1H), 6.86 (d, *J* = 7.6 Hz, 1H), 6.83 (s, 1H), 6.67 (d, *J* = 7.6 Hz, 1H), 6.21 (d, *J* = 15.9 Hz, 1H), 5.20 (m, 1H), 4.27 (m, 1H), 4.13 (m, 1H), 3.72 (m, 1H), 3.67 (s, 3H), 3.34 (m, 1H), 2.27 (m, 1H), 1.81 (m, 1H), 1.37 (s, 3H), 1.30 (s, 3H), 1.27 (s, 3H), 1.20 (s, 3H), 0.82 (s, 9H), 0.00 (s, 6H).

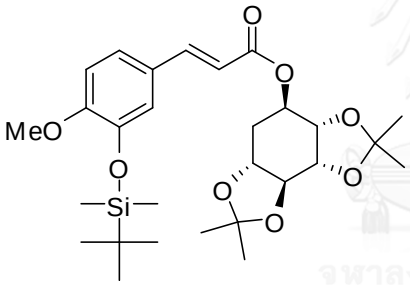

2.8ERp; 81% yield of pale yellow oil; ^{1}H NMR ($CDCl_3$, 400 MHz) δ 7.44 (d, *J* = 15.9 Hz, 1H), 6.94 (d, *J* = 8.2 Hz, 1H), 6.89 (s, 1H), 6.68 (d, *J* = 8.2 Hz, 1H), 6.08 (d, *J* = 15.9 Hz, 1H), 5.35 (m, 1H), 4.21 (m, 1H), 4.14 (m, 1H), 3.68 (s, 3H), 3.56 (m, 1H), 3.45 (m, 1H), 2.10 – 1.91 (m, 2H), 1.37 (s, 3H), 1.29 (s, 6H), 1.21 (s, 3H), 0.83 (s, 9H), 0.00 (s, 6H).

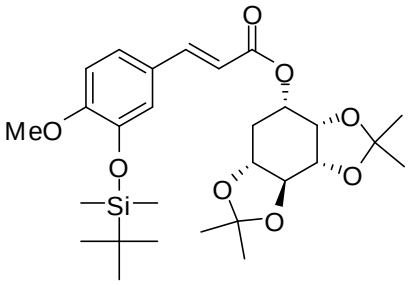

2.8ESp; 79% yield of colorless oil; ^{1}H NMR ($CDCl_3$, 400 MHz) δ 7.48 (d, *J* = 15.9 Hz, 1H), 6.95 (dd, *J* = 8.3, 2.0 Hz, 1H), 6.90 (d, *J* = 2.0 Hz, 1H), 6.68 (d, *J* = 8.3 Hz, 1H), 6.18 (d, *J* = 15.9 Hz, 1H), 5.20 (m, 1H), 4.28 (m, 1H), 4.13 (m, 1H), 3.72 (m, 1H), 3.68 (s, 3H), 3.34 (m, 1H), 2.27 (m, 1H), 1.83 (m, 1H), 1.38 (s, 3H), 1.30 (s, 3H), 1.28 (s, 3H), 1.21 (s, 3H), 0.84 (s, 9H), 0.00 (s, 6H).

3.4.3 General deprotection of silyl group and bis-acetonides

Deprotection of **2.6ERp**-**2.8ESp**, which contained both silyl groups and bis-acetonides, was performed as follow. To a solution of **2.6ERp** (1 eq) in tethahydrofuran (THF) was added TBAF/THF 1.0 M (2 eq: 1 OTBDMS). The mixture was stirred at room temperature for 3 h. The reaction mixture was washed with water (10 mL) and the organic layer was extracted with ethyl acetate (EtOAc) (3 $\times$ 15 mL) followed by being dried over Na_2SO_4. After filtration and removal of the solvent under reduced pressure, the crude product was dissolved in methanol (MeOH) and Amberlyst-15 (0.5 g: 0.1 mmol) was added into the solution. The reaction mixture was stirred at room temperature for 5 h. After filtration and removal of the solvent under reduced pressure the crude product was purified by Sephadex LH-20 eluted with MeOH to afford **2.6ER**. Compounds **2.6ESp**-**2.8ESp** were treated using aforementioned procedures to yield corresponding products **2.6ES**-**2.8ES**, respectively.

For deprotection of **2.1ERp**-**2.5ERp**, which contained only bis-acetonides, general procedures were conducted as follow. To a methanolic solution of **2.1ERp** was added Amberlyst-15 (0.5 g: 0.1 mmol), and the reaction mixture was stirred at room temperature for 5 h. After filtration and removal of the solvent under reduced pressure, the crude product was purified by Sephadex LH-20 eluted with MeOH to afford **2.1ER**. Compounds **2.1ESp**-**2.5ERp** were transformed, using the above procedures, to corresponding products **2.1ES**-**2.5ER**, respectively.

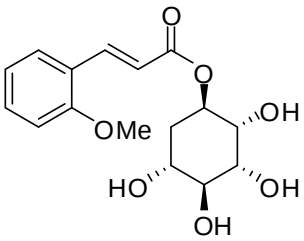

1R-Quercityl-2-methoxycinnamate (**2.1ER**) 75% yield of colorless oil; ^{1}H NMR (CD_3OD, 400 MHz) δ 7.97 (d, *J* = 16.2 Hz, 1H), 7.56 (d, *J* = 6.8 Hz, 1H, Ar-H), 7.38 (t, *J* = 7.4 Hz, 1H, Ar-H), 7.03 (d, *J* = 6.8 Hz, 1H, Ar-H), 6.96 (t, *J* = 7.4 Hz, 1H, Ar-H), 6.53 (d, *J* = 16.2 Hz, 1H), 5.10 (m, 1H, H-C1), 3.94 (brs, 1H), 3.89 (s, 3H, OMe), 3.84–3.60 (m, 3H), 1.99 (m, 2H, H-C6); ^{13}C NMR (CD_3OD, 100 MHz) δ 168.0, 160.0, 142.1, 133.2, 130.0, 124.2, 121.9, 118.8, 112.5, 76.0, 73.5, 72.9, 71.5, 70.8, 56.2, 32.9; HRESIMS *m/z* 347.1100 $[M + Na]^+$ (calcd for $[C_{16}H_{16}\ Na\ O_7]^+$ 347.1107).

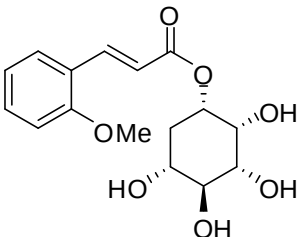

1S-Quercityl-2-methoxycinnamate (**2.1ES**) 79% yield of colorless oil; ^{1}H NMR (CD_3OD, 400 MHz) δ 7.92 (d, *J* = 16.2 Hz, 1H), 7.49 (dd, *J* = 8.0, 4.0 Hz, 1H, Ar-H), 7.28 (t, *J* = 7.5 Hz, 1H, Ar-H), 6.95 (d, *J* = 8.0 Hz, 1H, Ar-H), 6.88 (t, *J* = 7.5 Hz, 1H, Ar-H), 6.52 (d, *J* = 16.2 Hz, 1H), 4.85 (m, 1H, H-C1), 4.02 (s, 1H), 3.81 (s, 3H, OMe), 3.52–3.24 (m, 3H), 1.93 (m, 2H, H-C6); ^{13}C NMR (CD_3OD, 100 MHz) δ 168.6, 160.0, 142.0, 133.1, 130.0, 124.3, 121.9, 119.2, 112.5, 76.1, 73.6, 72.2, 71.5, 70.8, 56.1, 32.9; HRESIMS *m/z* 347.1108 $[M + Na]^+$ (calcd for $[C_{16}H_{20}NaO_7]^+$ 347.1107).

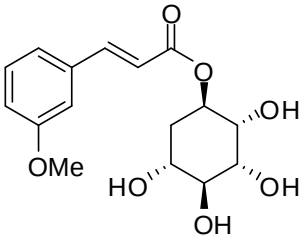

1R-Quercityl-3-methoxycinnamate (**2.2ER**) 85% yield of colorless oil; ^{1}H NMR (CD_3OD, 400 MHz) δ 7.65 (d, *J* = 16.0 Hz, 1H), 7.32 (t, *J* = 7.8 Hz, 1H, Ar-H), 7.18 (d, *J* =

7.8 Hz, 1H, Ar-H), 7.15 (s, 1H, Ar-H), 6.98 (d, *J* = 7.8 Hz, 1H, Ar-H), 6.52 (d, *J* = 16.0 Hz, 1H), 5.11 (brs, 1H, H-C1), 3.93 (brs, 1H), 3.82 (s, 3H, OMe), 3.76–3.55 (m, 3H), 1.99 (m, 2H, H-C6); ^{13}C NMR (CD_3OD, 100 MHz) δ 167.4, 161.6, 146.7, 137.0, 131.1, 121.9, 118.9, 117.6, 114.1, 75.9, 73.4, 73.0, 71.5, 70.8, 55.9, 32.9; HRESIMS *m/z* 347.1110 $[M + Na]^+$ (calcd for $[C_{16}H_{16}NaO_7]^+$ 347.1107).

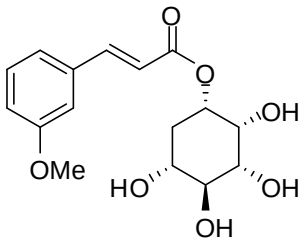

1S-Quercityl-3-methoxycinnamate (**2.2ES**) 73% yield of colorless oil; ^{1}H NMR (CD_3OD, 400 MHz) δ 7.72 (d, *J* = 16.0 Hz, 1H), 7.31 (t, *J* = 7.8 Hz, 1H, Ar-H), 7.18 (d, *J* = 8.2 Hz, 1H, Ar-H), 7.15 (s, 1H, Ar-H), 6.97 (dd, *J* = 8.2, 1.6 Hz, 1H, Ar-H), 6.54 (d, *J* = 16.0 Hz, 1H), 4.85 (m, 1H, H-C1), 4.11 (s, 1H), 3.82 (s, 3H, OMe), 3.64–3.33 (m, 3H), 2.01 (m, 2H, H-C6); ^{13}C NMR (CD_3OD, 100 MHz) δ 167.8, 161.6, 146.6, 137.2, 131.1, 121.8, 119.2, 117.4, 114.1, 76.1, 73.6, 72.2, 71.6, 70.8, 55.8, 32.9; HRESIMS *m/z* 347.1107 $[M + Na]^+$ (calcd for $[C_{16}H_{20}NaO_7]^+$ 347.1107).

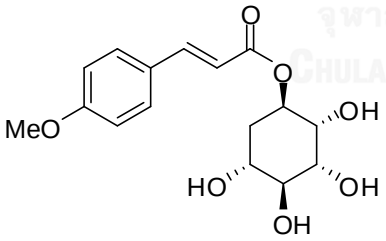

1R-Quercityl-4-methoxycinnamate (**2.3ER**) 78% yield of white solid; ^{1}H NMR (CD_3OD, 400 MHz) δ 7.64 (d, *J* = 15.9 Hz, 1H), 7.56 (d, *J* = 8.6 Hz, 2H, Ar-H), 6.95 (d, *J* = 8.6 Hz, 2H, Ar-H), 6.37 (d, *J* = 15.9 Hz, 1H), 5.11 (m, 1H, H-C1), 3.96–3.59 (m, 4H), 3.83 (s, 3H, OMe), 1.99 (m, 2H, H-C6); ^{13}C NMR (CD_3OD, 100 MHz) δ 167.8, 163.3, 146.6, 131.1, 131.1, 128.2, 115.9, 115.5, 115.5, 76.0, 73.5, 72.8, 71.5, 70.8, 55.9, 33.0; HRESIMS *m/z* 347.1104 $[M + Na]^+$ (calcd for $[C_{16}H_{20}NaO_7]^+$ 347.1107).

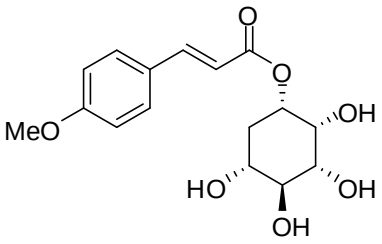

1S-Quercityl-4-methoxycinnamate *(**2.3ES**)* 78% yield of colorless oil; ^{1}H NMR (CD_3OD, 400 MHz) δ 7.61 (d, *J* = 15.9 Hz, 1H), 7.47 (d, *J* = 8.5 Hz, 2H, Ar-H), 6.86 (d, *J* = 8.5 Hz, 2H, Ar-H), 6.31 (d, *J* = 15.9 Hz, 1H), 4.85 (m, 1H, H-C1), 4.01 (s, 1H), 3.74 (s, 3H, OMe), 3.56–3.31 (m, 3H), 1.98-1.83 (m, 2H, H-C6); ^{13}C NMR (CD_3OD, 100 MHz) δ 168.3, 163.3, 146.5, 131.0, 131.0, 128.4, 116.2, 115.5, 115.5, 76.1, 73.6, 72.3, 71.4, 70.8, 55.9, 32.9; HRESIMS *m/z* 347.1103 $[M + Na]^+$ (calcd for $[C_{16}H_{20}NaO_7]^+$ 347.1107).

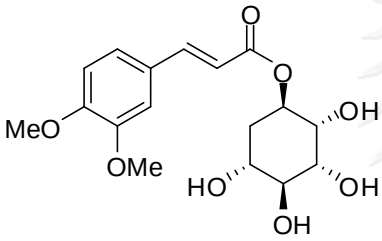

1R-Quercityl-3,4-dimethoxycinnamate *(**2.4ER**)* 85% yield of colorless oil; ^{1}H NMR (CD_3OD, 400 MHz) δ 7.62 (d, *J* = 15.9 Hz, 1H), 7.22 (s, 1H, Ar-H), 7.17 (d, *J* = 8.2 Hz, 1H, Ar-H), 6.97 (d, *J* = 8.2 Hz, 1H, Ar-H), 6.40 (d, *J* = 15.9 Hz, 1H), 5.11 (m, 1H, H-C1), 3.97–3.56 (m, 4H), 3.86 (s, 6H, 2×OMe), 2.00 (m, 2H, H-C6); ^{13}C NMR (CD_3OD, 100 MHz) δ 167.8, 153.0, 150.8, 146.9, 128.7, 124.2, 116.3, 112.7, 111.9, 76.0, 73.5, 72.9, 71.5, 70.8, 56.8, 56.5, 33.0; HRESIMS *m/z* 377.1203 $[M + Na]^+$ (calcd for $[C_{17}H_{22}NaO_8]^+$ 377.1212).

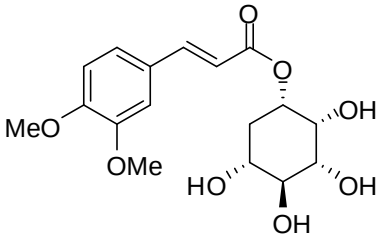

1S-Quercityl-3,4-dimethoxycinnamate *(**2.4ES**)* 79% yield of colorless oil; ^{1}H NMR (CD_3OD, 400 MHz) δ 7.60 (d, *J* = 15.9 Hz, 1H), 7.12 (s, 1H, Ar-H), 7.09 (d, *J* = 8.2 Hz, 1H, Ar-H), 6.88 (d, *J* = 8.2 Hz, 1H, Ar-H), 6.33 (d, *J* = 15.9 Hz, 1H), 4.82 (m, 1H, H-

C1), 4.01 (brs, 1H), 3.77 (s, 6H, 2×OMe), 3.52–3.25 (m, 3H), 2.05–1.85 (m, 2H, H-C6); ^{13}C NMR (CD_3OD, 100 MHz) δ 168.2, 152.9, 150.8, 146.7, 128.9, 124.0, 116.5, 112.7, 111.6, 76.1, 73.6, 72.3, 71.4, 70.8, 56.5, 56.5, 33.0; HRESIMS *m/z* 377.1209 $[M + Na]^+$ (calcd for $[C_{17}H_{22}NaO_8]^+$ 377.1212).

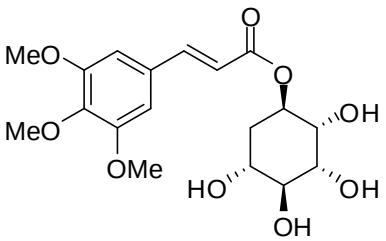

1R-Quercityl-3,4,5-trimethoxycinnamate *(***2.5ER***)* 83% yield of colorless oil; ^{1}H NMR (CD_3OD, 400 MHz) δ 7.62 (d, *J* = 15.9 Hz, 1H), 6.93(s, 1H, Ar-H), 6.91(s, 1H, Ar-H), 6.48 (d, *J* = 15.9 Hz, 1H), 5.12 (m, 1H, H-C1), 4.05–3.55 (m, 4H), 3.86 (s, 9H, 3×OMe), 2.00 (m, 2H, H-C6); ^{13}C NMR (CD_3OD, 100 MHz) δ 167.5, 154.9, 146.8, 146.4, 131.5, 118.1, 118.0, 106.9, 106.8, 76.0, 73.5, 73.0, 71.5, 70.8, 61.2, 56.8, 56.8, 33.0; HRESIMS *m/z* 407.1310 $[M + Na]^+$ (calcd for $[C_{18}H_{24}NaO_9]^+$, 407.1318).

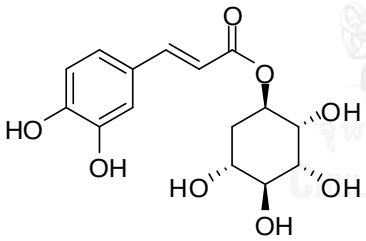

1R-Quercitylcaffeate *(***2.6ER***)* 84% yield of yellow oil; ^{1}H NMR (CD_3OD, 400 MHz) δ 7.45 (d, *J* = 15.9 Hz, 1H), 6.95 (d, *J* = 1.6 Hz, 1H, Ar-H), 6.86 (dd, *J* = 8.2, 1.6 Hz, 1H, Ar-H), 6.69 (d, *J* = 8.2 Hz, 1H, Ar-H), 6.16 (d, *J* = 15.9 Hz, 1H), 5.00 (m, 1H, H-C1), 3.83 (brs, 1H), 3.68–3.45 (m, 3H), 1.89 (m, 2H, H-C6); ^{13}C NMR (CD_3OD, 100 MHz) δ 168.0, 149.7, 147.4, 146.9, 127.7, 123.1, 116.6, 115.3, 114.9, 76.0, 73.5, 72.8, 71.6, 70.8, 32.9; HRESIMS *m/z* 325.0930 $[M - H]^-$ (calcd for $[C_{15}H_{17}O_8]^-$ 325.0923).

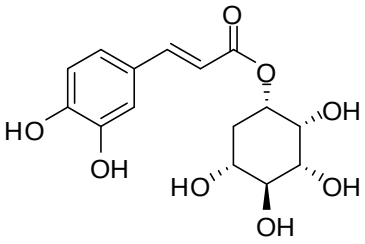

1S-Quercitylcaffeate (**2.6ES**) 84% yield of yellow oil; ^{1}H NMR (CD_3OD, 400 MHz) δ 7.51 (d, *J* = 15.9 Hz, 1H), 6.95 (d, *J* = 1.8 Hz, 1H, Ar-H), 6.88 (dd, *J* = 8.1, 1.8 Hz, 1H, Ar-H), 6.68 (d, *J* = 8.1 Hz, 1H, Ar-H), 6.20 (d, *J* = 15.9 Hz, 1H), 4.81 (m. 1H, H-C1), 4.00 (brs, 1H), 3.54–3.25 (m, 3H), 1.99-1.78 (m, 2H, H-C6); ^{13}C NMR (CD_3OD, 100 MHz) δ 168.5, 148.7, 147.3, 146.9, 127.8, 123.0, 116.5, 115.2, 115.2, 76.1, 73.6, 72.3, 71.3, 70.8, 32.9; HRESIMS *m/z* 349.0899 $[M + Na]^+$ (calcd for $[C_{15}H_{18}NaO_8]^+$ 349.0899).

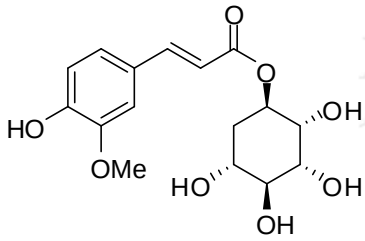

1R-Quercitylferurate (**2.7ER**) 79% yield of yellow less oil; ^{1}H NMR (CD_3OD, 400 MHz) δ 7.51 (d, *J* = 15.9 Hz, 1H), 7.11 (d, *J* = 1.6 Hz, 1H, Ar-H), 6.99 (dd, *J* = 8.2, 1.6 Hz, 1H, Ar-H), 6.72 (d, *J* = 8.2 Hz, 1H, Ar-H), 6.27 (d, *J* = 15.9 Hz, 1H), 5.01 (m, 1H, H-C1), 3.85–3.45 (m, 4H), 3.86 (s, 3H, OMe), 1.85 (m, 2H, H-C6); ^{13}C NMR (CD_3OD, 100 MHz) δ 168.0, 150.8, 149.4, 147.3, 127.6, 124.3, 116.5, 115.3, 111.8, 76.0, 73.4, 72.8, 71.5, 70.8, 56.5, 33.0; HRESIMS *m/z* 363.1057 $[M + Na]^+$ (calcd for $[C_{16}H_{20}NaO_8]^+$ 363.1056).

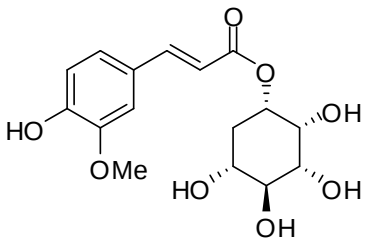

1S-Quercitylferurate (**2.7ES**) 79% yield of colorless oil; ^{1}H NMR (CD_3OD, 400 MHz) δ 7.58 (d, *J* = 15.9 Hz, 1H), 7.09 (s, 1H, Ar-H), 6.99 (d, *J* = 8.2 Hz, 1H, Ar-H), 6.72 (d, *J* = 8.2 Hz, 1H, Ar-H), 6.29 (d, *J* = 15.9 Hz, 1H), 4.73 (m, 1H, H-C1), 4.01 (brs, 1H), 3.79 (s, 3H, OMe), 3.52–3.23 (m, 3H), 1.99-1.84 (m, 2H, H-C6); ^{13}C NMR (CD_3OD, 100

MHz) δ 168.5, 150.7, 149.4, 147.2, 127.8, 124.1, 116.6, 115.6, 111.9, 76.1, 73.6, 72.4, 71.3, 70.9, 56.5, 32.9; HRESIMS *m/z* 363.1057 $[M + Na]^+$ (calcd for $[C_{16}H_{20}NaO_8]^+$ 363.1056).

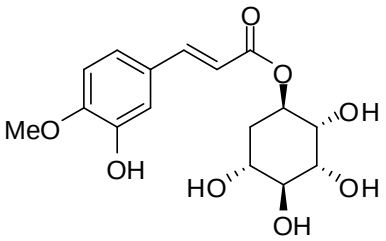

1R-Quercitylisoferulate (**2.8ER**) 76% yield of yellow oil; ^{1}H NMR (CD_3OD, 400 MHz) δ 7.56 (d, *J* = 15.9 Hz, 1H), 7.08 (s, 1H, Ar-H), 7.07 (d, *J* = 8.2 Hz, 1H, Ar-H), 6.95 (d, *J* = 8.2 Hz, 1H, Ar-H), 6.30 (d, *J* = 15.9 Hz, 1H), 5.10 (m, 1H, H-C1), 3.92 (s, 1H), 3.89 (s, 3H, OMe), 3.77–3.58 (m, 3H), 1.99 (m, 2H, H-C6); ^{13}C NMR (CD_3OD, 100 MHz) δ 167.8, 151.7, 148.0, 147.0, 128.8, 123.0, 115.9, 114.8, 112.6, 76.0, 73.4, 72.8, 71.5, 70.8, 56.4, 32.9; HRESIMS *m/z* 363.1054 $[M + Na]^+$ (calcd for $[C_{16}H_{20}NaO_8]^+$ 363.1056).

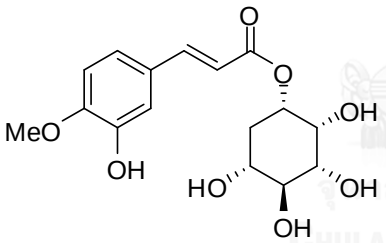

1S-Quercitylisoferulate (**2.8ES**) 64% yield of yellow oil; ^{1}H NMR (CD_3OD, 400 MHz) δ 7.54 (d, *J* = 15.9 Hz, 1H), 6.99 (s, 1H, Ar-H), 6.97 (d, *J* = 8.2 Hz, 1H, Ar-H), 6.85 (d, *J* =8.2 Hz, 1H, Ar-H), 6.25 (d, *J* = 15.9 Hz, 1H), 4.73 (m, 1H, H-C1), 4.00 (brs, 1H), 3.79 (s, 3H, OMe), 3.48 (t, *J* = 9.3 Hz, 1H), 3.41–3.32 (m, 1H), 3.26 (m, 1H), 1.92 (m, 2H, H-C6); ^{13}C NMR (CD_3OD, 100 MHz) δ 168.3, 151.6, 148.1, 146.9, 129.0, 122.8, 116.2, 114.8, 112.6, 76.1, 73.6, 72.3, 71.4, 70.9, 56.5, 32.9; HRESIMS *m/z* 363.1056 $[M + Na]^+$ (calcd for $[C_{16}H_{20}NaO_8]^+$ 363.1056).

3.5 General synthesis of quercitylcinnamamides

3.5.1 General coupling reaction between aminobis-acetonides and cinnamic acid derivatives

To a solution of **2.1**, **2.2**, **2.3**, **2.4**, **2.5**, **2.6**, **2.7** or **2.8** (2.5 eq) in DMF (3 mL) were added **1.32** or **1.33** (1.0 eq), HOBt (2.5 eq), EDCI (2.5 eq) and 4-dimethylaminopyridine (DMAP, catalytic amount). The reaction mixture was stirred at 115 ^{o}C overnight under N_2 gas. The crude product was subsequently purified by siliga gel column to afford **2.1ARp**-**2.8ASp** in 56-78% yields.

3.5.2 General deprotection of bis-acetonides

Deprotection of **2.1ARp** was dissolved in methanol (MeOH) and Amberlyst-15 (0.5 g: 0.1 mmol) was added into the solution. The reaction mixture was stirred at room temperature for 5h. After filtration and removal of the solvent under reduced pressure the crude product was purified by Sephadex-LH20 eluted with MeOH to afford **2.1AR** in 74% yield. **2.1ASp-2.8ASp** were treated using aforementioned procedures to yield corresponding products **2.1AS-2.8AS**, respectively in 72-85% yields

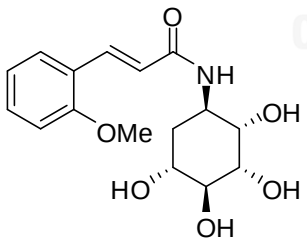

1*R*-Aminoquercityl-2-methoxycinnamamide (**2.1AR**). 74% yield of colorless oil; ^{1}H NMR (CD_3OD, 400 MHz) δ 7.76 (d, *J* = 15.9 Hz, 1H), 7.44 (dd, *J* = 8.3, 1.6 Hz, 1H), 7.25 (m, 1H), 6.93 (d, *J* = 8.3 Hz, 1H), 6.86 (t, *J* = 7.5 Hz, 1H), 6.66 (d, *J* = 15.9 Hz, 1H), 4.18 (m, 1H), 3.80 (s, 3H), 3.79 (m, 1H), 3.70–3.50 (m, 3H), 1.92 (m, 1H), 1.77 (m, 1H); ^{13}C NMR (CD_3OD, 100 MHz) δ 169.2, 159.7, 137.5, 132.2, 129.5, 125.0, 122.1, 121.8, 112.5, 75.0, 73.9, 72.6, 71.2, 56.1, 49.2, 33.2; HRESIMS *m/z* 346.1252 $[M + Na]^+$ (calcd for $[C_{16}H_{21}NNaO_6]^+$ 346.1261).

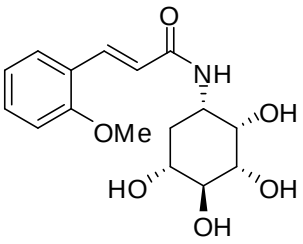

1*S*-Aminoquercityl-2-methoxycinnamamide (**2.1AS**). 80% yield of white solid; ^{1}H NMR (DMSO-d_6, 400 MHz) δ 7.88 (d, *J* = 7.9 Hz, 1H), 7.61 (d, *J* = 15.8 Hz, 1H), 7.47 (d, *J* = 7.4 Hz, 1H), 7.33 (t, *J* = 7.9 Hz, 1H), 7.04 (d, *J* = 8.4 Hz, 1H), 6.96 (t, *J* = 7.4 Hz, 1H), 6.77 (d, *J* = 15.8 Hz, 1H), 3.83 (s, 3H), 3.00–3.50 (m, 5H)*, 1.62 (m, 2H); ^{13}C NMR (DMSO–d_6, 100 MHz) δ 164.4, 157.4, 133.3, 130.7, 127.6, 123.4, 123.0, 120.6, 111.6, 74.4, 73.0, 71.1, 70.1, 55.5, 46.7, 33.1; HRESIMS *m/z* 324.1447 $[M + H]^+$ (calcd for $[C_{16}H_{22}NO_6]^+$ 324.1447). *determined by COSY

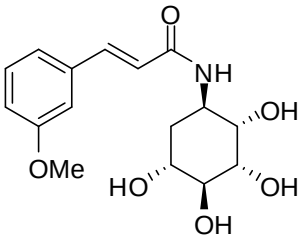

1*R*-Aminoquercityl-3-methoxycinnamamide (**2.2AR**). 78% yield of colorless oil; ^{1}H NMR (CD_3OD, 400 MHz) δ 7.50 (d, *J* = 15.7 Hz, 1H), 7.29 (t, *J* = 8.1 Hz, 1H), 7.12 (d, *J* = 8.1 Hz, 1H), 7.09 (s, 1H), 6.93 (dd, *J* = 8.1, 1.8 Hz, 1H), 6.68 (d, *J* = 15.7 Hz, 1H), 4.25 (m, 1H), 3.88 (m, 1H), 3.85 (s, 3H), 3.85–3.56 (m, 3H), 2.01 (m, 1H), 1.86 (m, 1H); ^{13}C NMR (CD_3OD, 100 MHz) δ 168.5, 161.6, 142.0, 137.7, 131.0, 122.1, 121.4, 116.6, 113.9, 75.0, 74.0, 72.5, 71.2, 55.8, 49.4, 33.2; HRESIMS *m/z* 324.1443 $[M + H]^+$ (calcd for $[C_{16}H_{22}NO_6]^+$ 324.1447).

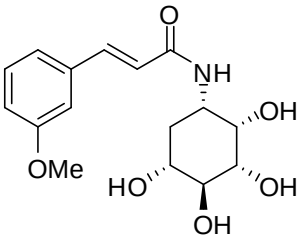

1*S*-Aminoquercityl-3-methoxycinnamamide (**2.2AS**). 84% yield of white solid; ^{1}H NMR (DMSO-d_6, 400 MHz) δ 7.86 (d, *J* = 8.o Hz, 1H), 7.34 (d, *J* = 15.7 Hz, 1H), 7.30 (t, *J* = 7.8 Hz 1H), 7.10 (d, *J* = 8.0 Hz, 2H), 7.09 (s, 1H), 6.91 (d, *J* = 7.8 Hz, 1H), 6.78 (d, *J* = 15.7 Hz, 1H), 4.85 (brs, 2H), 4.56 (brs, 2H), 3.75 (s, 3H), 3.10-3.50 (m, 5H)*, 1.72–1.49 (m, 2H); ^{13}C NMR (DMSO–d_6, 100 MHz) δ 164.0, 159.5, 138.3, 136.5, 129.9, 123.0, 119.9, 115.2, 112.4, 74.4, 73.0, 71.1, 70.1, 55.1, 46.7, 33.1; HRESIMS *m/z* 346.1267 [M + Na]$^{+}$ (calcd for $[C_{16}H_{21}NNaO_6]^{+}$ 346.1267). *determined by COSY

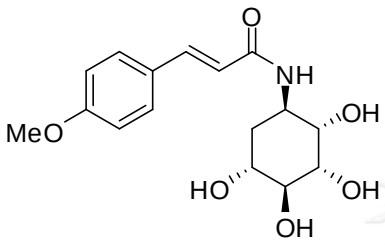

1*R*-Aminoquercityl-4-methoxycinnamamide (**2.3AR**). 72% yield of colorless oil; ^{1}H NMR (CD_3OD, 400 MHz) δ 7.50 (d, *J* = 15.7 Hz, 1H), 7.49 (d, *J* = 8.7 Hz, 2H), 6.92 (d, *J* = 8.7 Hz, 2H), 6.55 (d, *J* = 15.7 Hz, 1H), 4.27 (m, 1H), 3.89 (m, 1H), 3.80 (s, 3H), 3.78–3.60 (m, 3H), 2.02 (m, 1H), 1.86 (m, 1H); ^{13}C NMR (CD_3OD, 100 MHz) δ 169.0, 162.6, 141.9, 130.5, 130.5, 129.0, 129.0, 119.3, 115.4, 75.0, 74.0, 72.6, 71.2, 55.9, 49.5, 33.3; HRESIMS *m/z* 324.1436 [M + H]$^{+}$ (calcd for $[C_{16}H_{22}NO_6]^{+}$ 324.1447)

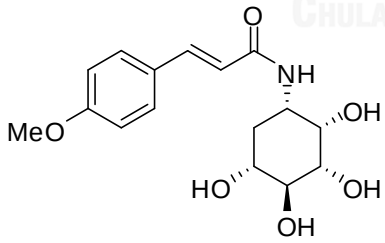

1*S*-Aminoquercityl-4-methoxycinnamamide (**2.3AS**). 81% yield of floral white solid; ^{1}H NMR NMR (DMSO-d_6, 400 MHz) δ 7.73 (d, *J* = 7.9 Hz, 1H), 7.43 (d, *J* = 8.1 Hz, 2H), 7.27 (d, *J* = 15.5 Hz, 1H), 6.90 (d, *J* = 8.1 Hz, 2H), 6.57 (d, *J* = 15.5 Hz, 1H), 4.78 (s, 1H), 4.57 (s, 1H), 4.48 (s, 2H), 3.71 (s, 3H), 3.31 (5H)*, 1.68–1.44 (m, 2H); ^{13}C NMR (DMSO–d_6, 100 MHz) δ 164.4, 160.2, 138.1, 138.1, 129.0, 127.6, 120.2, 120.2, 114.3, 74.4, 73.1, 71.1, 70.1, 55.2, 46.6, 33.2; HRESIMS *m/z* 346.1255 [M + Na]$^{+}$ (calcd for $[C_{16}H_{21}NNaO_6]^{+}$ 346.1267). *determined by COSY

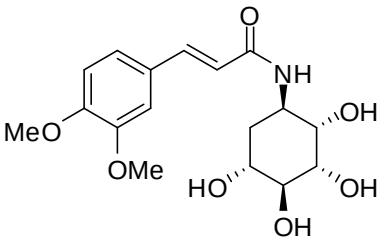

1*R*-Aminoquercityl-3,4-dimethoxycinnamamide (**2.4AR**). 82% yield of colorless oil; ^{1}H NMR (CD_3OD, 400 MHz) δ 7.38 (d, *J* = 15.7 Hz, 1H), 7.06 (s, 1H), 7.04 (d, *J* = 8.5 Hz, 1H), 6.87 (d, *J* = 8.5 Hz, 1H), 6.48 (d, *J* = 15.7 Hz, 1H), 4.17 (m, 1H), 3.76 (s, 6H), 3.82–3.70 (m, 1H), 3.70 - 3.50 (m, 3H), 1.92 (m, 1H), 1.76 (m, 1H); ^{13}C NMR (CD_3OD, 100 MHz) δ 167.4, 150.8, 149.3, 140.6, 128.0, 121.8, 118.2, 111.4, 110.0, 73.5, 72.4, 71.1, 69.7, 55.0, 55.01, 48.1, 31.8; HRESIMS *m/z* 376.1361 $[M + Na]^+$ (calcd for $[C_{17}H_{23}NNaO_7]^+$ 376.1372).

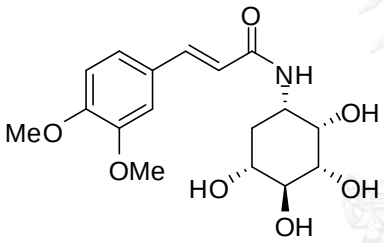

1*S*-Aminoquercityl-3,4-dimethoxycinnamamide (**2.4AS**). 85% yield of floral white solid; ^{1}H NMR (DMSO-d_6, 400 MHz) δ 7.70 (d, *J* = 8.1 Hz, 1H), 7.30 (d, *J* = 15.7 Hz, 1H), 7.13 (s, 1H), 7.07 (d, *J* = 8.2 Hz, 1H), 6.95 (d, *J* = 8.2 Hz, 1H), 6.66 (d, *J* = 15.7 Hz, 1H), 4.83 (s, 1H), 4.61 (s, 1H), 4.54 (s, 2H), 3.76 (s, 3H), 3.75 (s, 3H), 3.32 (5H)*, 1.61 (m, 2H); ^{13}C NMR (DMSO–d_6, 100 MHz) δ 164.3, 150.0, 148.9, 138.4, 127.9, 121.3, 120.4, 111.7, 109.9, 74.4, 73.0, 71.1, 70.1, 55.5, 55.4, 46.6, 33.2; HRESIMS *m/z* 354.1549 $[M + H]^+$ (calcd for $[C_{17}H_{24}NO_7]^+$ 354.1553). *determined by COSY

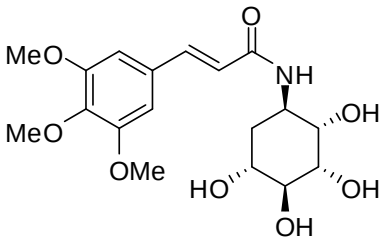

1*R*-Aminoquercityl-3,4,5-trimethoxycinnamamide (**2.5AR**). 85% yield of colorless oil; ^{1}H NMR (CD_3OD, 400 MHz) δ 7.37 (d, *J* = 15.7 Hz, 1H), 6.78 (s, 2H), 6.54 (d, *J* = 15.7 Hz, 1H), 4.18 (m, 1H), 3.78 (s, 9H), 3.75–3.50 (m, 4H), 1.91 (s, 1H), 1.77 (s, 1H); ^{13}C NMR (CD_3OD, 100 MHz) δ 168.7, 154.8, 142.0, 132.3, 132.3, 121.3, 106.3, 106.3, 75.0, 73.9, 72.6, 71.1, 61.2, 56.7, 56.7, 33.2; HRESIMS *m/z* 406.1479 $[M + Na]^+$ (calcd for $[C_{18}H_{25}NNaO_8]^+$ 406.1478).

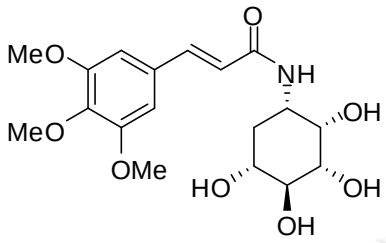

1*S*-Aminoquercityl-3,4,5-trimethoxycinnamamide (**2.5AS**). 79% yield of white solid; ^{1}H NMR (DMSO-d_6, 400 MHz) δ 7.75 (d, *J* = 8.2 Hz, 1H), 7.30 (d, *J* = 15.6 Hz, 1H), 6.87 (s, 2H), 6.73 (d, *J* = 15.6 Hz, 1H), 4.84 (s, 1H), 4.66 (s, 1H), 4.56 (s, 2H), 3.77 (s, 9H), 3.10-3.50 (m, 5H)*, 1.63 (m, 3H); ^{13}C NMR (DMSO–d_6, 100 MHz) δ 164.2, 153.0, 138.5, 138.5, 130.7, 130.7, 122.0, 104.9, 104.9, 74.4, 73.0, 71.9, 70.1, 60.1, 55.9, 55.9, 46.6, 33.1; HRESIMS *m/z* 406.1480 $[M + Na]^+$ (calcd for $[C_{18}H_{25}NNaO_8]^+$ 406.1478). *determined by COSY

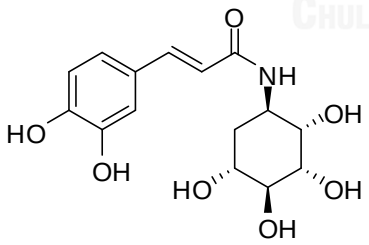

1*R*-Aminoquercitylcaffeamide (**2.6AR**). 81% yield of yellow oil; ^{1}H NMR (CD_3OD, 400 MHz) δ 7.40 (d, *J* = 15.6 Hz, 1H), 7.02 (s, 1H), 6.90 (d, *J* = 8.2 Hz, 1H), 6.75 (d, *J* = 8.2 Hz, 1H), 6.47 (d, *J* = 15.6 Hz, 1H), 4.26 (m, 1H), 3.87 (m, 1H), 3.82–3.60 (m, 3H), 2.00 (m, 1H), 186 (m, 1H); ^{13}C NMR NMR (CD_3OD, 100 MHz) δ 169.2, 148.8, 146.7, 142.6, 128.5, 122.2, 118.4, 116.5, 115.2, 74.9, 74.0, 72.6, 71.2, 49.2, 33.3; HRESIMS *m/z* 326.1238 $[M + H]^+$ (calcd for $[C_{15}H_{20}NO_7]^+$ 326.1240).

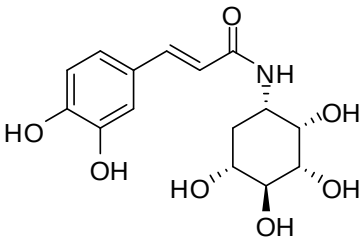

1*S*-Aminoquercitylcaffeamide (**2.6AS**). 77% yield of colorless oil; ^{1}H NMR (CD_3OD, 400 MHz) δ 7.39 (d, *J* = 15.7 Hz, 1H), 7.00 (d, *J* = 1.8 Hz, 1H), 6.90 (dd, *J* = 8.2, 1.8 Hz, 1H), 6.75 (d, *J* = 8.2 Hz, 1H), 6.44 (d, *J* = 15.7 Hz, 1H), 4.02–3.88 (m, 2H), 3.57–3.33 (m, 3H), 1.86 (m, 2H); ^{13}C NMR (CD_3OD, 100 MHz) δ 168.5, 148.8, 146.7, 142.5, 128.4, 122.2, 118.5, 116.5, 115.2, 76.1, 74.7, 72.7, 71.9, 49.5, 33.7; HRESIMS *m/z* 348.1060 $[M + Na]^+$ (calcd for $[C_{15}H_{19}NNaO_7]^+$ 348.1059).

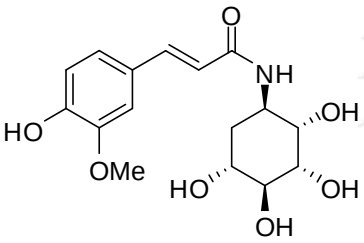

1*R*-Aminoquercitylferulamide (**2.7AR**). 79% yield of colorless oil; ^{1}H NMR (CD_3OD, 400 MHz) δ 7.36 (d, *J* = 15.7 Hz, 1H), 7.03 (d, *J* = 1.8 Hz, 1H), 6.94 (dd, *J* = 8.2, 1.8 Hz, 1H), 6.70 (d, *J* = 8.2 Hz, 1H), 6.43 (d, *J* = 15.7 Hz, 1H), 4.17 (m, 1H), 3.78 (s, 3H), 3.81–3.75 (m, 1H), 3.70–3.51 (m, 3H), 1.92 (m, 1H), 1.76 (m, 1H); ^{13}C NMR (CD_3OD, 100 MHz) δ 169.1, 149.9, 149.3, 142.4, 128.4, 123.3, 118.7, 116.5, 111.6, 75.0, 73.9, 72.6, 71.2, 56.4, 49.2, 33.2; HRESIMS *m/z* 340.1392 $[M + H]^+$ (calcd for $[C_{16}H_{22}NO_7]^+$ 340.1396).

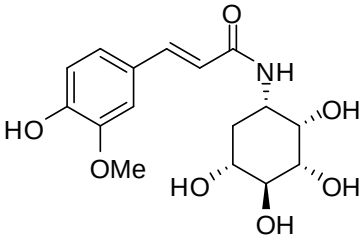

1*S*-Aminoquercitylferulamide (**2.7AS**). 75% yield of colorless oil; ^{1}H NMR (CD_3OD, 400 MHz) δ 7.46 (d, *J* = 15.6 Hz, 1H), 7.13 (s, 1H), 7.03 (d, *J* = 8.3 Hz, 1H), 6.79 (d, *J* = 8.3 Hz, 1H), 6.52 (d, *J* = 15.6 Hz, 1H), 4.04–3.89 (m, 2H), 3.87 (s, 3H), 3.60–3.33

(m, 3H), 1.88 (m, 2H); ^{13}C NMR (CD_3OD, 100 MHz) δ 168.5, 149.9, 149.4, 142.4, 128.4, 123.4, 118.8, 116.5, 111.7, 76.1, 74.6, 72.7, 71.8, 56.5, 48.6, 33.7; HRESIMS *m/z* 340.1383 $[M + H]^+$ (calcd for $[C_{16}H_{22}NO_7]^+$ 340.1396).

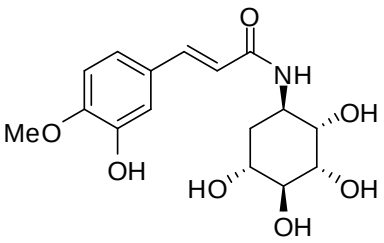

1*R*-Aminoquercitylferulamide (**2.8AR**). 72% yield of colorless oil; ^{1}H NMR (CD_3OD, 400 MHz) δ 7.45 (d, *J* = 15.7 Hz, 1H), 7.07 (d, *J* = 2.0 Hz, 1H), 7.02 (dd, *J* = 8.3, 2.0 Hz, 1H), 6.94 (d, *J* = 8.3 Hz, 1H), 6.54 (d, *J* = 15.7 Hz, 1H), 4.28 (m, 1H), 3.91 (s, 3H), 3.91 (m, 1H) 3.82–3.62 (m, 3H), 2.04 (m, 1H), 1.88 (m, 1H); ^{13}C NMR (CD_3OD, 100 MHz) δ 169.0, 150.9, 148.0, 142.2, 129.6, 122.2, 119.3, 114.6, 112.6, 75.0, 73.9, 72.6, 71.2, 56.5, 49.1, 33.2; HRESIMS *m/z* 362.1209 $[M + Na]^+$ (calcd for $[C_{16}H_{21}NNaO_7]^+$ 362.1216).

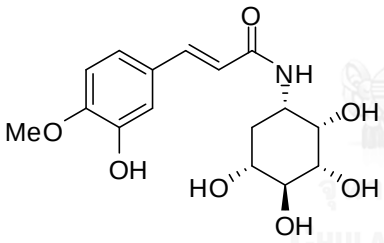

1*S*-Aminoquercitylferulamide (**2.8AS**). 74% yield of colorless oil; ^{1}H NMR (CD_3OD, 400 MHz) δ 7.34 (d, *J* = 15.7 Hz, 1H), 6.96 (d, *J* = 1.8 Hz, 1H), 6.92 (dd, *J* =8.3, 1.8 Hz, 1H), 6.84 (d, *J* = 8.3 Hz, 1H), 6.40 (d, *J* = 15.7 Hz, 1H) 3.94–3.82 (m, 2H), 3.79 (s, 3H), 3.50–3.30 (m, 3H), 3.31–3.24 (m, 1H), 1.83–1.69 (m, 2H); ^{13}C NMR (CD_3OD, 100 MHz) δ 168.3, 150.9, 148.0, 142.1, 129.6, 122.2, 119.5, 114.6, 112.6, 76.1, 74.7, 72.7, 71.9, 56.5, 48.8, 33.7; HRESIMS *m/z* 362.1215 $[M + Na]^+$ (calcd for $[C_{16}H_{21}NNaO_7]^+$ 362.1216).

3.6 α-Glucosidase inhibitory activity

Inhibitory activity of test compound against α-glucosidase from baker's yeast was assessed based on *p*-nitrophenoxide colorimetric method [47]. Briefly, A 10 mL of test compound (1 mg/mL in DMSO) was pre-incubated with 40 µL of α-glucosidase (0.1 U/mL in 0.1 M phosphate buffer, pH 6.9) at 37 °C for 10 min. The mixture was added with 50 µL substrate solution (1 mM *p*-nitrophenyl-α-D-glucopyranoside, PNPG) and incubated for additional 20 min. The resulting mixture was quenched by adding 100 µL of 1 M Na_2CO_3. *p*-Nitrophenoxide ion liberated from the enzymatic reaction was monitored at 405 nm by Bio-Rad 3550 microplate reader. The percentage inhibition was calculated by $[(A_0–A_1)/A_0] \times 100$, where A_1 and A_0 are the absorbance with and without the sample, respectively. The IC_{50} value was deduced from a plot of percentage inhibition versus sample concentration and acarbose and voglibose were used as a positive control. The inhibitory activity of the test compounds against α-glucosidases from rat intestine (as maltase and sucrase) was validated on the basis of glucose oxidase colorimetric method [48]. Maltase and sucrase was obtained from rat intestinal acetone powder (Sigma, St. Louis). Generally, the powder (1 g) was homogenized with 0.9% NaCl solution (30 mL). The aliquot containing both maltase and sucrase was obtained upon centrifugation (12,000 g) for 30 min. The test compound (1 mg/mL, 10 µL) was pre-incubated with crude enzyme solution (as maltase, 20 µL; as sucrase, 20 µL, respectively) at 37 °C for 10 min. The substrate solution (maltose: 0.58 µM, 20 µL; sucrose: 20 µM, 20 µL, respectively) in 0.1 M phosphate buffer (pH 6.9) was therefore added to the reaction mixture and incubated at 37 °C for additional 40 min. The mixture was heated in oven at 80 °C for 15 min to quench the reaction. The concentration of glucose released from the reaction mixture was determined by the glucose oxidase method using a commercial glucose assay kit (SU-GLLQ2, Human). The percentage inhibition was calculated using the above expression.

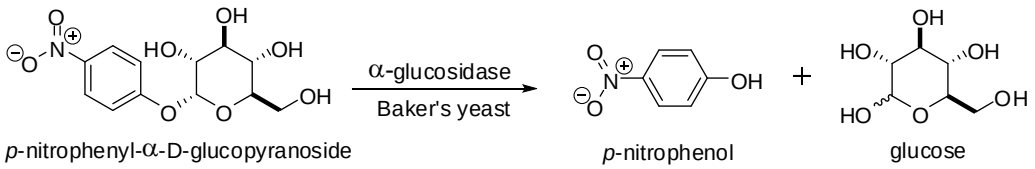

Figure 3.1. α-glucosidase inhibitory assay from baker's yeast.

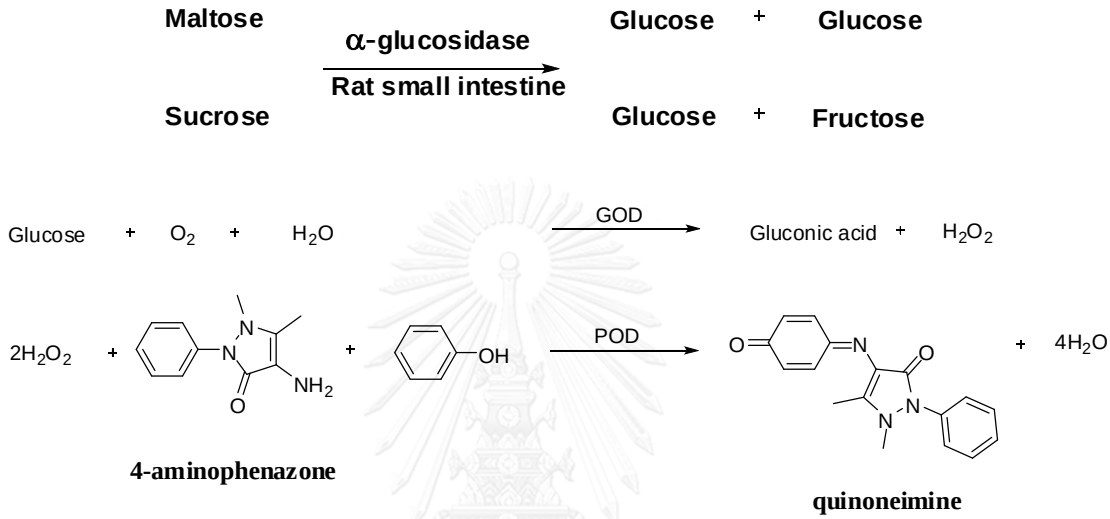

Figure 3.2 α-glucosidase inhibitory assay from rat small intestine.

3.7 DPPH radical scavenging

Radical scavenging activity was validated using DPPH colorimetric method [58]. Briefly, a sample solution (10 µL at concentrations of 0.1, 1.0 and 10.0 mg/mL) was added to 0.1 mM methanolic solution of DPPH (150 µL). The mixture was kept dark at room temperature in incubator shaker for 15 min. The absorbance of the resulting solution was measured at 517 nm with a 96-well microplate reader. The percentage scavenging was calculated by $[(A_0–A_1)/A_0] \times 100$, where A_0 is the absorbance without the sample whereas A_1 is the absorbance with the sample. The SC_{50} value was deduced from a plot of percentage scavenging versus sample concentration. BHA was used as a standard antioxidant.

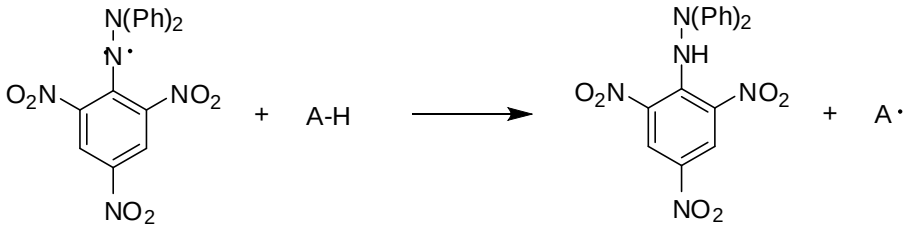

Figure 3.3 DPPH radical scavenging assay.

3.8 Kinetic study of α-glucosidase inhibition

The type of inhibition was investigated by analyzing enzyme kinetic data using aforementioned reactions. Maltase and sucrase activity were maintained at 0.45 and 0.09 U/mg proteins, respectively, in the presence of inhibitor (from 0 to 20.4 μM for **2.6ER** and 0 to 0.00625 mg/mL for **2.8AS**) at various concentrations of maltose ranging from 1.0 to 20.0 mM. A series of V_{max} and K_m values were obtained from Y intercepts and calculated by slope × V_{max}, respectively.

3.9 Combined effect of 8AS and acarbose on intestine α-glucosidase inhibitory activity

The various concentration of acarbose was combined with or without **2.8AS** at low concentration. The reaction was performed according to the above assay α-glucosidase inhibition activity from rat intestine). Results were expressed as a percentage inhibition of the corresponding control values (acarbose). The IC_{50} values were calculated from plots of log concentration of inhibitor concentration versus percentage inhibition curves by using Sigma Plot 9.0 (IL, USA). Statistical analysis was performed by Student's t test.

3.10 Homology modeling and molecular docking

3.10.1 Homology modeling

Although amino acid sequencing of α-glucosidases have been wildly discovered, a lot of the 3-dimentional structure is still unable to obtain such as that from rat small intestine. The homology modeling is one in the efficiency alternative method to construct the 3-dimentional structure without experimental require. Therefore, in this work the *Rattus norvegicus* rat intestinal maltase amino acid sequence (Acc. No. XP_008761090) was retrieved from the NCBI web server.

In addition to the N-terminal human maltase-glucomylase (PDB: 2QLY) template was chosen from result of BLAST search online method [59]. Finally, the 3-dimentional structure of the rat intestinal maltase was constructed from http://swissmodel.expasy.org [60-63] with 82.4% of sequence identity.

3.10.2 Molecular docking study

The molecular docking of the n-terminal human maltase-glucomylase (PDB: 2QLY) and ligands (**2.8AS**) was performed by using Autodock 4.2 with prior quantum geometry optimization of ligands, 6-31G [64]. The grid box size was set to be larger than the protein template to make sure that ligand can get into every possible binding site in the protein template. The potential binding sites were confirmed afterward by using Fpocket software (http://fpocket.sourceforge.net) [56, 57]. The docking was carried out by using the Lamarckian genetic algorithm (LGA) with ligand flexible mode and independently repeated 10 times for each ligand. See supplementary data for more details.

The aforementioned was repeated using the rat intestinal maltase as the protein template instead of human intestinal maltase.

CHAPTER IV
CONCLUSION

In summary, two new series of bioconjugates 1) quercitylcinnamate derivatives and 2) quercitylcinnamamide derivatives were prepared from *trans*-cinnamic acid derivatives and natural carbasugar, (+)-*proto*-quercitol.

Out of fifteen quercitylcinnamates, six derivatives including **2.6ER**, **2.6ES**, **2.7ER**, **2.7ES**, **2.8ER** and **2.8ES** inhibited rat intestinal maltase and sucrase 4-6 times, which were more potent than their corresponding cinnamic analogues. Notably, **2.6ER** was the most potent inhibitor against maltase and sucrase with IC_{50} values of 5.31 and 43.65 μM, respectively. Of interest, its inhibitory potency toward maltase was 6 times greater than its parent, caffeic acid (IC_{50} = 34.69 μM, **2.6**), while its radical scavenging (SC_{50} 0.11 mM) was comparable to that of commercial antioxidant BHA (SC_{50} 0.10 mM). Moreover, an investigation on mechanism underlying inhibitory effect of **2.6ER** showed that it blocked maltase and sucrase functions by mixed inhibition manner.

Among the prepared sixteen quercitylcinnamamide analogues, **2.6AR**, **2.6AS**, **2.7AR**, **2.7AS**, **2.8AR** and **2.8AS**, were considered as potent α-glucosidase inhibitors from rat intestine with IC_{50} value in the range of 0.41-269.45 μM, which are 1.2-208 times greater than that of starting cinnamic acid derivatives. Of the prepared compounds, **2.8AS** was the highest potent for against maltase with an IC_{50} value of 0.41 μM, which had potency similar to antidiabetic drug, acarbose and voglibose (IC_{50} = 1.5, 0.25 μM, respectively). Moreover, the DPPH radical scavenging (SC_{50} = 0.07 mM) was found to be in the same range with BHA. In addition, an investigation on mechanism suggested in non-competitive manner, which was considered as the first synthetic non-competitive inhibitor for α-glucosidase in rat small intestine for maltase. The combination between **2.8AS** and acarbose significantly increased the inhibitory activity rather than the individual use suggesting the strong synergistic effect.

Computational analysis using AUTODOCK 4.0 and Fpocket programs discovered new allosteric sites on maltase and also revealed that **2.8AS** binds to the enzyme in a different pocket site (allosteric site) from acarbose. Thus, the combination between **2.8AS** and acarbose could be used as a new drug for the treatment of type II DM patients.

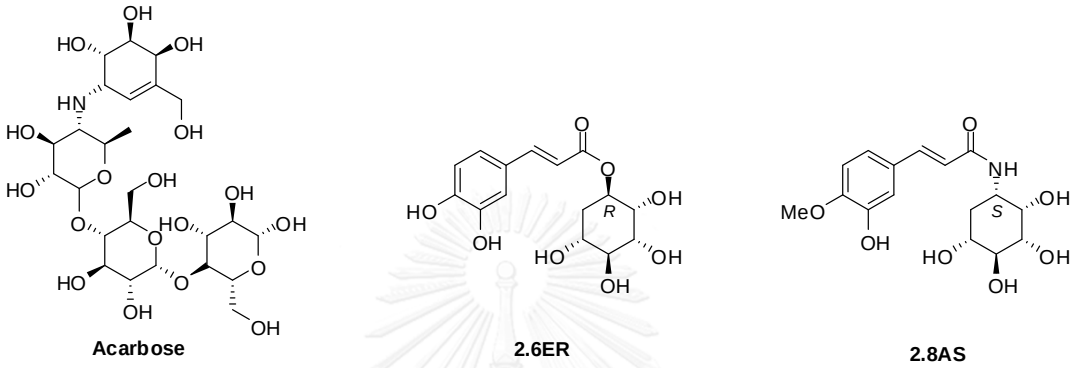

Figure 4.1 Structure of acarbose, **2.6ER** and **2.8AS**.

CHAPTER V

HYPERVALENT IODINE(III)-PROMOTED METAL-FREE S–H ACTIVATION: AN APPROACH FOR THE CONSTRUCTION OF S–N AND S–C BONDS

5.1 C–N Bond formation via the O–H activation of *N*-heterocycle.

5.1.1 Introduction on cyclic amidine and their derivatives

Amino-substituted nitrogenous heterocycles are pharmaceutically interesting scaffold in medicinal chemistry due to their broad spectrum of biological activities. Generic structures of those compounds are shown in Scheme 5.1 in which the amino group is attached to various heterocycles such as pyrimidine, pyridine and quinazoline.

Typically, the synthesis of heterocyclic amidine starts from their heterocyclic amide which is mostly commercially available (Scheme 5.1A). Activation of the tautomerizable hydroxy group into the corresponding halide followed by S_NAr substitution of nitrogen nucleophile [65-67] or Buchwald–Hartwig Pd-mediated coupling [68-70] reaction led to target amidines (Scheme 5.1A). The main drawback of this route is the halogenation step which is often performed under harsh and acidic conditions with reagents such as $SOCl_2$, $POCl_3$, and PCl_5.

Recently, Mansour and co-workers have developed the utilization of the highly active phosphonium salts, benzotriazol-1-yloxytris-(dimethylamino) phosphonium hexafluorophosphate (BOP) as activator for one pot amination reaction [71] (Scheme 5.1B). Even though this reaction is mild convenient and highly functional group compatible, the activator is very expensive. In addition, the reaction itself is poorly atom-economical while generating a carcinogenic byproduct (HMPA). Therefore, a more practical transformation is necessary for process improvement.

In recent work, Wacharasindhu and co-workers [72] attempted to perform O–H activation on 4-hydroxyquinazoline (**5.1**) using inexpensive and less toxic activator, the Mukaiyama's reagent (2-chloro-1-methyl-pyridinium iodide), in the hope that it will generate target amidine. However, the N–H activation occurred and gave the 3-

alkylquinazolin-4-ones in one-pot in good yield (Scheme 5.1C). Therefore, in this work we aim to search for a new activator for the C–N bond formation in the *N*-hetero cyclic amide having greener property in comparison with previous woks (Scheme 5.1D).

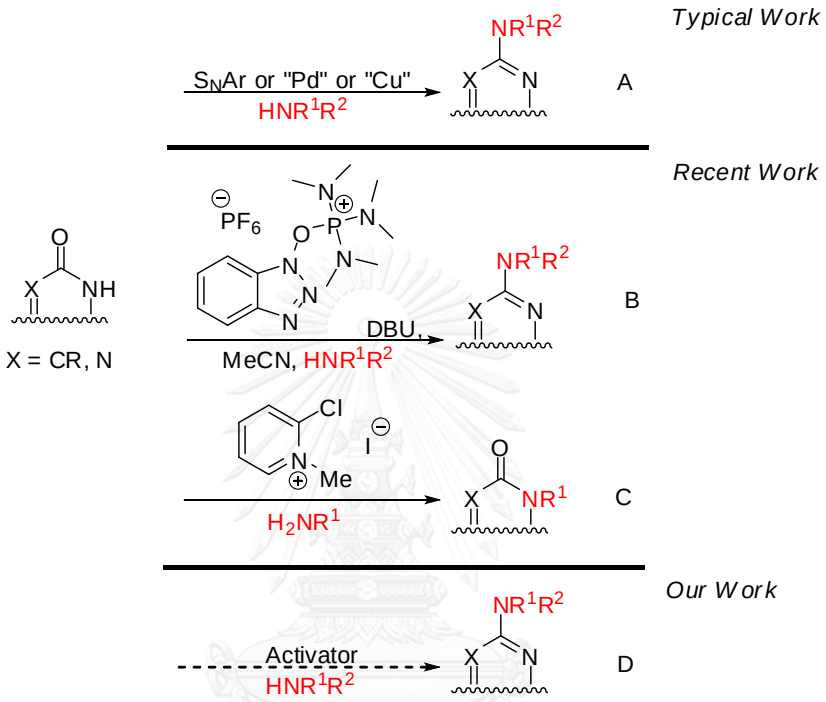

Scheme 5.1 Reaction of *N*-heterocycles with activating agents.

5.1.2 Activation via tosylation reaction

In this work, we planned to conduct the tosylation reaction at the oxygen atom on cyclic amidine, which should lead us to the cyclic amidine via S_NAr reaction with the corresponding amine as seen in Scheme 5.2.

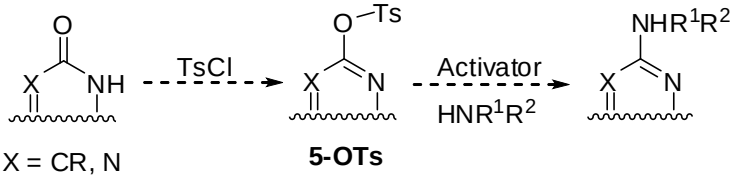

Scheme 5.2 Scheming plan for C–N bond formation of *N*-heterocycles via tosylated adduct.

Based on our plan, we attempted to synthesize *O*-tosylated product (**5-OTs**) via the reaction between **5.1** and tosyl chloride. Surprisingly, the expected *O*-tosylated product **5-OTs** was not observed and we only isolated *N*-tosylated product (**5.2**) as the sole product. The structure of compound **5.2** was confirmed by H NMR spectroscopy, showing the unusual high filed of proton at H-C2 position (8.78 ppm) [73]. This perhaps is caused by the loss of aromaticity at ring B. To extend the scope of this reaction, unhindered primary amines such as *n*-butylamine and benzylamine (Table 5.1, entries 1-2), were reacted with *N*-tosylated quinazoline **5.2**. These reactions proceeded to provide the 3-substituted-quinazolin-4-ones (**5.3**) in good yields (Table 5.1, entries 1-2), whereas cyclohexylamine, aniline and 4-bromoaniline, gave no reaction (Table 5.1, entries 3-5).

Table 5.1 Preparation of 3-substituted-quinazolin-4-ones (**5.3**) from *N*-tosylated adduct (**5.2**).

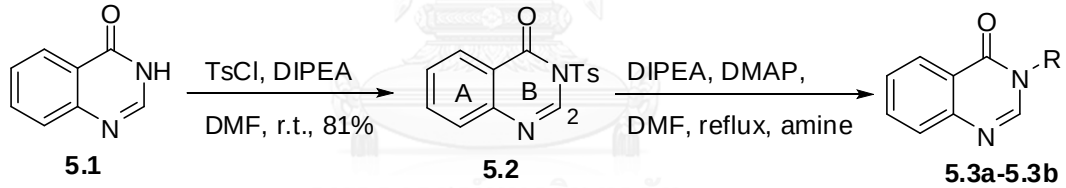

5.1 **5.2** **5.3a-5.3b**

Entry	Amine	Product (yield %)[a]
1	*n*-butylamine	**5.3a** (82)
2	benzylamine	**5.3b** (76)
3	cyclohexylamine	No reaction
4	aniline	No reaction
5	4-bromoaniline	No reaction

[a]Isolated yield

A plausible mechanism of the formation of 3-substituted-quinazolin-4-ones as described in Scheme 5.3. Initially, after the formation of **5.2**, the nitrogen nucleophile will attack the carbonyl group followed by the ring-opening reaction to give the

corresponding imine intermediate (**5.5**). Finally, the nucleophilic attack from amide followed by ring aromatization led to the isolated product (**5.3**). Unfortunately, during our investigation, Poura and co-worker reported the same observation [74].

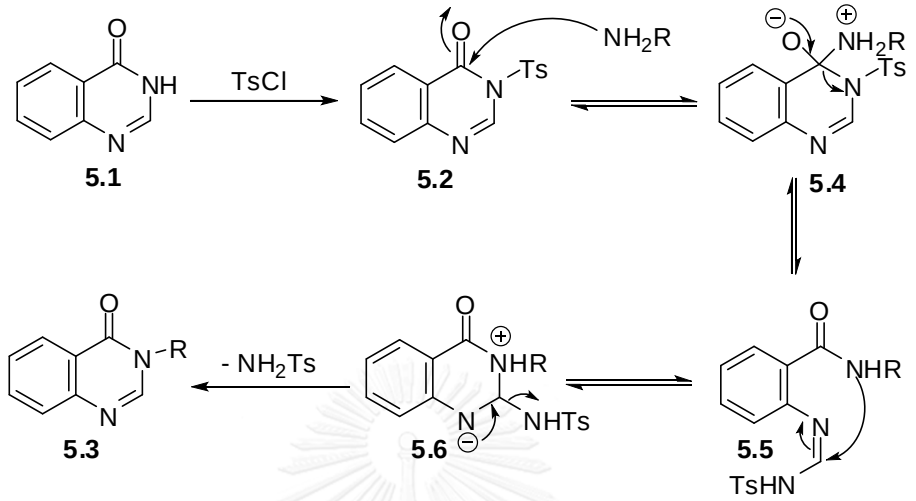

Scheme 5.3 Mechanism of formation of 3-substituted-quinazolin-4-ones (**5.3**).

To avoid N–H tosylation, we changed the starting material from 4-hydroxyquinazoline (**5.1**) to 2-hydroxypyridine (**5.7**) and 4-hydroxypyridine (**5.8**) and the results were demonstrated in Table 5.2. The tosylation of **5.7** and **5.8** gave the desired *O*-tosylated product (**5.7Ts** and **5.8Ts**, respectively) in good yields. However, any attempts to perform the S_NAr reaction with **5.7Ts** and **5.8Ts** were unsuccessful, giving no reaction in all cases. Increasing temperature, changing solvents and adding several activators (DABCO, HOBt and DMAP) could not push the reaction effectively forward and only staring materials were recovered after quenching the reaction.

Table 5.2 Results of the activator, solvent and temperature screening for the amination reaction.

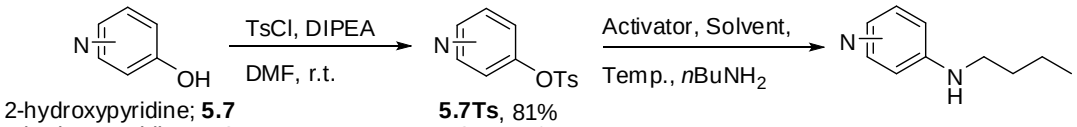

2-hydroxypyridine; **5.7**
4-hydroxypyridine; **5.8**

5.7Ts, 81%
5.8Ts, 74%

Entry	Starting material	Activator	Solvent	Temp.	Yield (%)
1	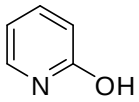	DABCO, HOBt	DMF	rt	No reaction
2		DABCO, HOBt	Toluene	rt	No reaction
3		DABCO, HOBt	MeCN	rt	No reaction
4		DIPEA, DMAP	DMF	reflux	No reaction
5		DIPEA, DMAP	Toluene	reflux	No reaction
6	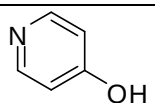	DABCO, HOBt	DMF	rt	No reaction
7		DABCO, HOBt	Toluene	rt	No reaction
8		DABCO, HOBt	MeCN	rt	No reaction
9		DIPEA, DMAP	DMF	reflux	No reaction
10		DIPEA, DMAP	Toluene	reflux	No reaction

5.1.3 Hypervalent iodine(III) activation

In recent years, there have been numerous reports on using hypervalent iodine(III) to oxidize the phenolic group [75-78]. Therefore, in this section we planned to use hypervalent iodine(III) as an activator for the C–N bond formation. Among hypervalent iodine reagents, we chose (diacetoxy)iodo benzene (DIB) (**5.9**) for further examination because of low cost, less toxic and wide availability of such reagent.

The predicted mechanism for the formation of aminoquinazoline derivatives (**5.12**) as described in Scheme 5.4. We hope that anion of **5.10** would undergo ligand exchange with DIB, leading to the formation of *O*-iodide intermediate **5.11**. Then, **5.11** will react with amine via S_NAr reaction followed by elimination of iodine(III) to give aminoquinazoline **5.12** as the desired product.

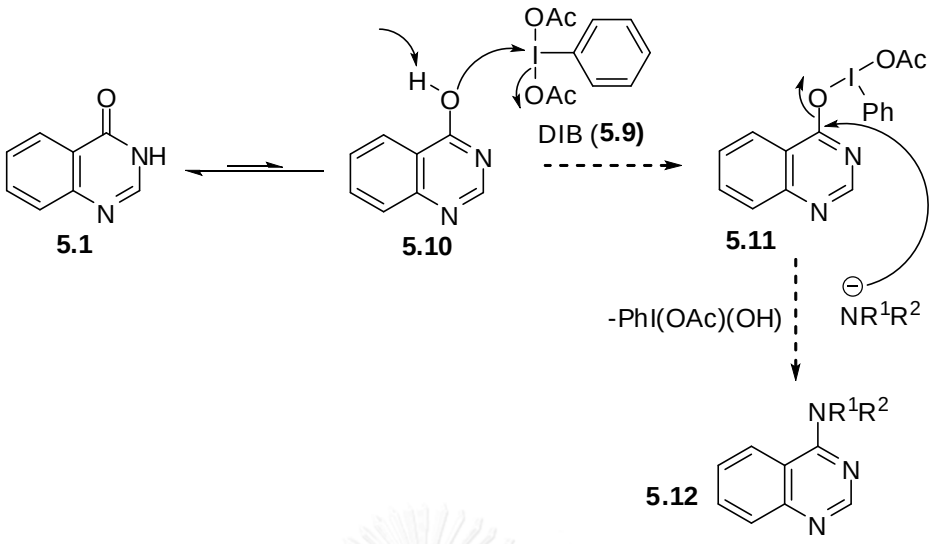

Scheme 5.4 An anticipated mechanism for the C-N bond formation via hypervalent iodine(III)-mediation.

To prove our hypothesis, we reacted various heterocycles (**5.1** or **5.7** or **5.8**) with DIB and *n*-butylamine as nucleophile in the presence of DBU as base in acetonitrile (MeCN) or *N*,*N*-dimethylformamide (DMF) as solvent. Unfortunately, the reaction was unsuccessful and only staring materials were recovered after quenching the reaction (Scheme 5.5).

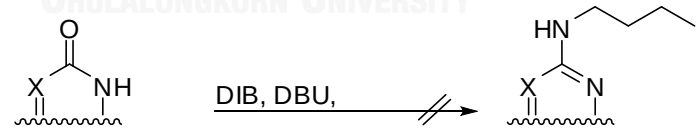

X = CR, N

4-hydroxyquinazoline; **5.1**
2-hydroxypyridine; **5.7**
4-hydroxypyridine; **5.8**

Scheme 5.5 Reaction of *N*-heterocycle (**5.1** or **5.7** or **5.8**) with (diacetoxy)iodo benzene.

5.1.4 S–H activation

Based on the previous results, we found that C–N bond formation via the O–H activation of *N*-heterocycles did not give a desired amidine product. Therefore, we changed the reacting center from O–H group to S–H group because the sulfur atom on *N*-heterocycles and iodine atom on hypervalent iodine(III) should be suitable for each other based on hard-soft acid base theory. Therefore, we planned to convert cyclic amide to the corresponding thiol and performed S_NAr reaction using DIB as seen in Scheme 5.6.

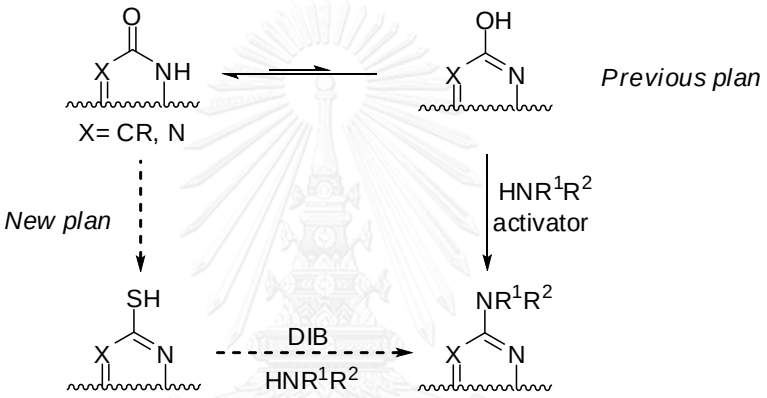

Scheme 5.6 Previous plan and new plan for synthesis of amino heterocycle.

Initially, we treated 2-mercaptopyridine (**5.13**) with DIB in the presence of *n*-butylamine as a nucleophile (Table 5.3). Incidentally, we isolated sulfenamide **5.13a** (45-53% yields) instead of the expected amidine **5.15**. Moreover, other unhindered primary amines such as benzylamine and cyclohexylamine (Table 5.3, entries 3-4) successfully reacted with **5.13** to give the sulfenamide **5.13b**-**5.13c** in moderate yields. In addition, 4-mercaptopyridine (**5.14**) was also used instead of **5.13** and reacted with unhindered primary amines (*n*-butylamine and benzylamine) leading to the desired corresponding sulfenamide **5.14a** and **5.14b** in moderate yields (Table 5.3, entries 5-6)

Table 5.3 Synthesis of sulfenamide derivatives from 2- or 4-mercaptopyridine with DIB in MeCN.

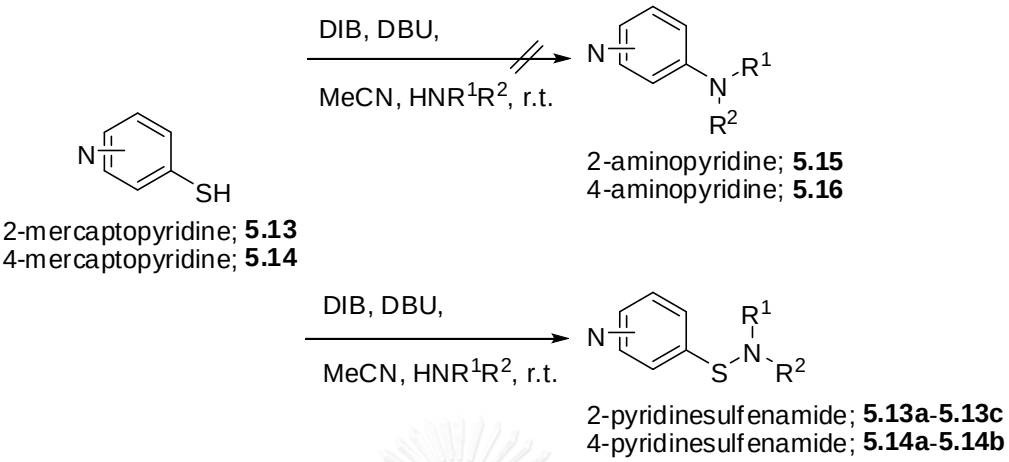

Entry	Starting material	Amine	Product (yield %)[a]
1	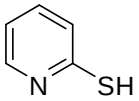	*n*-butylamine	5.13a (53)
2[b]		*n*-butylamine	**5.13a** (45)
3		benzylamine	**5.13b** (52)
4		cyclohexylamine	**5.13c** (40)
5	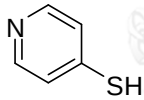	*n*-butylamine	**5.14a** (31)
6		benzylamine	**5.14b** (39)

[a]Isolated yield

[b]Reflux condition

To confirm a structure of compound **5.17a**, we compared the ^{13}C NMR spectrum with *N*-butyl-pyridin-2-yl-amine **5.15a** (Figure 5.4) in the reported literature. ^{13}C NMR data of **5.17a** showed a signal of C1 at δ_C 52.5 ppm as seen in Figure 5.5, but in amidine **5.15a**, it showed a more downfield of C1 at δ_C 42.2 ppm [79].

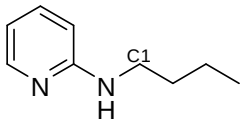

Figure 5.1 Shown a structure of *N*-butyl-pyridin-2-yl-amine (**5.15a**)

This suggested that the high downfield effect from the sulfur atom gave rise to the high chemical shift of **5.17a**. Therefore, the carbon chemical shift at C1 of the sulfenamide series (**5.17a**-**5.17c**, **5.18a**-**5.18b**) displayed the high chemical shifts in a range of δ_C 52.5-58.5 ppm. Moreover, molecular weights of sulfenamides were confirmed by mass spectroscopy (MSESI).

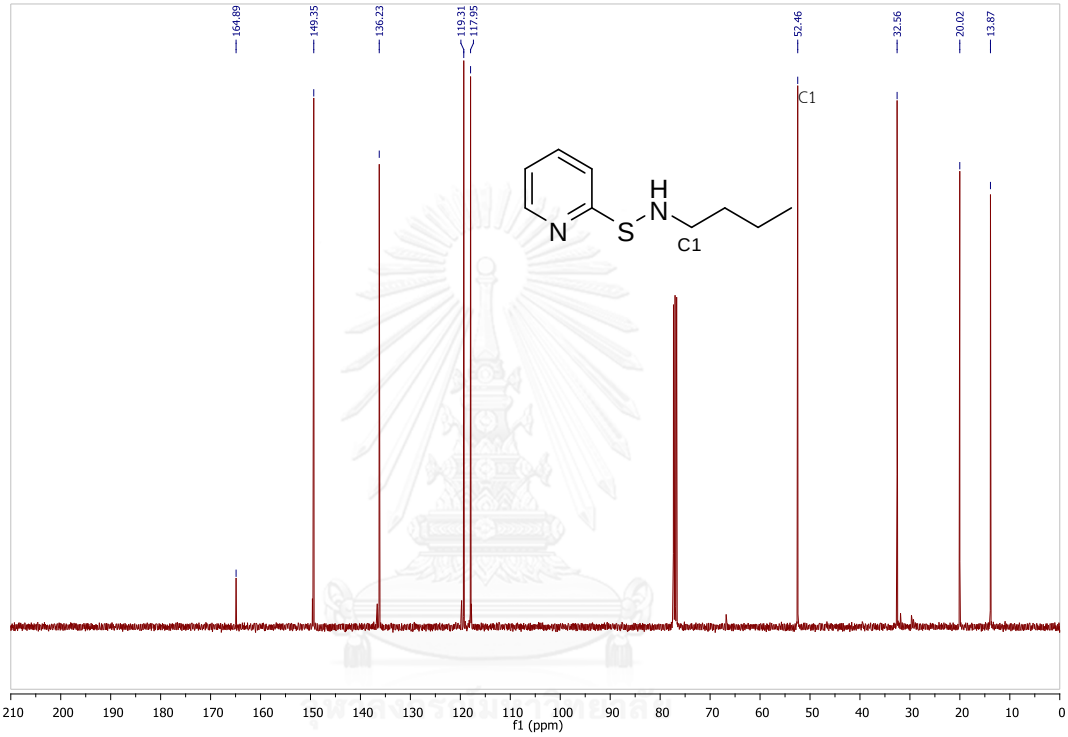

Figure 5.2 ^{13}C NMR chemical shifts in $CDCl_3$ of *N*-butyl-2-pyridinesulfenamide (**5.17a**).

To the best of our knowledge, the use of hypervalent iodine(III) compounds for the preparation of disulfides and sulfenamides are unprecedented. In the next section, we will shift our attention from the synthesis of amidine to disulfide and sulfenamide. The expected result from this work should provide a new metal-free approach for the direct synthesis of disulfides and sulfenamides from the corresponding thiols.

5.2 C–S bond formation via the S-H activation of *N*-heterocycle.

5.2.1 Introduction of organosulfur

Organosulfur compounds containing disulfide or sulfur–nitrogen bonds are important building blocks for a broad range of applications in biological, pharmaceutical, and material sciences. Organosulfur compounds having an S–N bond, on the other hand, are used as biologically active compounds [80-82] and as intermediates in organic synthesis [83-86] and material chemistry [87, 88]. The conventional method for preparing disulfides involves oxidation of thiols by using metal-containing oxidants or catalysts such as Fe, Pb, Ce, Mn, Co, Cr, Cu, or Al [89-94]. Metal-free oxidation methods using halogen (I_2, Br_2), hydrogen peroxide, azo reagents, graphite, sodium nitrite, or Burgess reagent have also been applied (Scheme 5.7a) [95-99].

However, the high toxicity and cost of the reagents, combined with the harsh reaction conditions such as elevated temperature, long reaction time, and risk of over-oxidation represent significant disadvantages. To obtain sulfenamides, disulfides have to be converted into sulfenyl chlorides with chlorine or NCS followed by amination [83, 100, 101]. This method not only requires three synthetic steps but it also involves sulfenyl chlorides, which are very unstable and undergo rapid hydrolysis. Recently, a direct synthesis of sulfenamides from either thiols or disulfides was developed by Taniguchi by using a copper-catalyzed amination reaction [102]. Although this reaction is highly efficient and compatible with many functional groups, metal and elevated temperature are still required in the transformation. Therefore, the development of a metal-free method that can be conducted under mild conditions for the synthesis of dithiols and sulfenamides remains a challenge.

Over the past few decades, hypervalent iodine compounds have been developed as selective reagents for oxidative transformation and construction of carbon–heteroatom and carbon–carbon bonds [103, 104]. Importantly, the environmentally friendly character and commercial availability at reasonable cost make these compounds suitable for synthetic organic reactions. Due to the thiophilic nature of hypervalent iodine reagents, such compounds have recently been shown

to activate sulfur atoms such as thioethers, thioamides, and thioureas [105]. Recently, Patel demonstrated a synthesis of benzimidazoles by using hypervalent iodine(III) reagents such as (diacetoxyiodo)benzene (DIB) to perform intramolecular C–N bond formation between isothiocyanates and amines [106]. To the best of our knowledge, however, no full investigations on the activation of simple thiols by hypervalent iodine reagents have been reported. [107] Therefore, taking clues from this and other works, we sought to exploit the thiophilic properties of hypervalent iodine(III) compounds for the construction of S–N as well as S–C bonds from the disulfides in a one-pot fashion using thiols as starting materials (Scheme 5.7b). This reaction was expected to provide a metal-free approach for the direct synthesis of sulfenamides and aromatic sulfides.

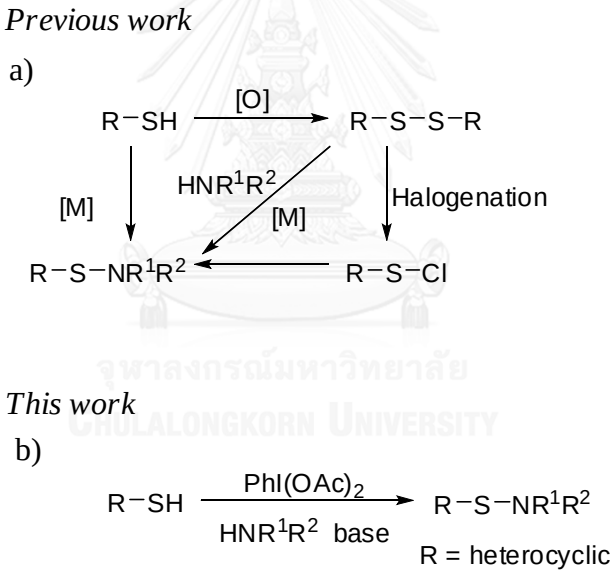

Scheme 5.7 (a) Conventional method for the preparation of disulfides and sulfenamides (b) Utilization of hypervalent iodine reagents for the preparation of sulfenamides.

5.2.2 Results and discussion

5.2.2.1 Synthesis of sulfenamides from thiols (S–N bond)

We explored the use of this hypervalent iodine reagent to synthesize various sulfenamides in a one-pot process. Based on recent reports of using hypervalent iodine(III) reagent to activate the sulfur atom [106], we hypothesized that the reagent could also be used to further activate the disulfide bond. Subsequent nucleophilic attack by a nucleophile such as an amine should generate a sulfenamide. Therefore, we selected three different classes of substrates including cyclohexane (**5.19**), chlorobenzene (**5.20**), and pyridine (**5.13**) thiols for reaction screening using DIB as the oxidant/activator and used *n*-butylamine as a nucleophile in the presence of DIPEA as a base for the neutralization of the acid produced from the reaction (Scheme 5.8). Disappointingly, only disulfides **5.19S** and **5.20S** were isolated as the sole products in 80 and 87% yields, respectively, by conducting the reaction with cyclohexane thiol and 4-methylthiophenol at room temperature overnight. On the other hand, 2-mercaptopyridine (**5.13**) generated a mixture of disulfide **5.13S** and the expected sulfenamide **5.13a** in 33 and 47% yields, respectively. These encouraging results not only show that the reaction could be used to produce heterocyclic sulfenamides in a one-pot synthesis, but they also provide some clues for the reaction mechanism. The disulfide is most likely an intermediate in this transformation.

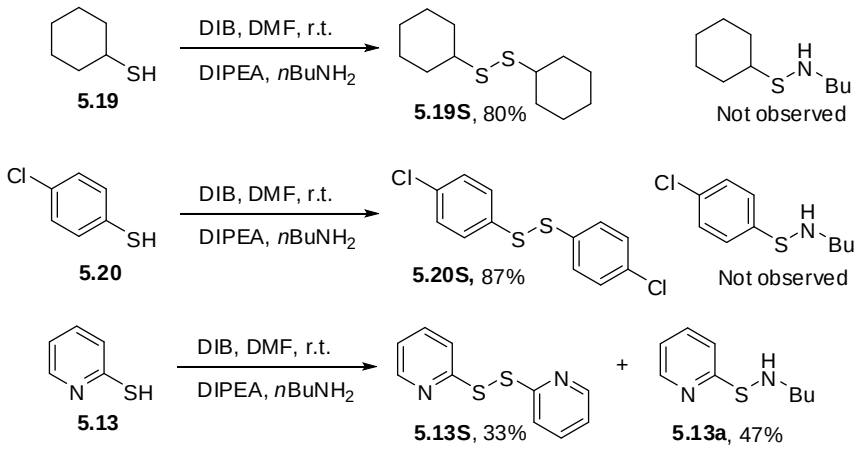

Scheme 5.8 Amination reaction of thiols with DIB reagent

Furthermore the optimization study was performed on 2-mercaptopyridine (**5.13**) with *n*-butylamine and DIB by evaluating various bases, solvents and temperatures (Table 5.4).

Although the reaction is only suitable for the amination of heterocyclic thiols into sulfenamide derivatives, such compounds are valuable building blocks in medicinal chemistry and pharmaceuticals. Sulfenamides containing heterocyclic moieties were reported to show acetylcholine inhibition, insecticidal activities, and antitumor activities among others [108, 109]. We therefore optimized the reaction using 2-mecaptopyridine (**5.13**) with DIB and butylamine (Table 5.4). Substituting the base DIPEA with 1,8-diazabicyclo[5.4.0]-undec-7-ene (DBU) resulted in the exclusive formation of *N*-butylsulfenamide **5.13a** in 82% yield after 4 h without remaining disulfide **5.13S** (entry 1). A short survey of hypervalent iodine(III) reagents showed that DIB is by far the most effective reagent (Table 5.4, entries 2–4). Unlike the method used for the preparation of disulfide, this reaction is solvent-dependent (Table 5.7, entries 5–7). Using MeCN and *N*,*N*-dimethylformamide (DMF) as solvent gave the desired sulfenamide **5.13a** in 53 and 45%yield, respectively. In addition, disulfide **5.13S** was also isolated in 19 and 26% yield, respectively. An attempt to drive the reaction to completion by raising the temperature to 125 °C was made, but lower yields of both the sulfenamide and disulfide products were observed (entry 7). In the absence of DBU, the disulfide was isolated as the major product in 56% yield along with the desired sulfenamide **5.13a** in just 26% yield (entry 8). Changing the base from DBU to DIPEA or K_2CO_3 gave lower yields of the desired sulfenamide **5.13a** (entries 9 and 10). The amount of DIB reagent was crucial in this reaction (entries 11 and 12). When the reaction was performed without DIB, only a small amount of disulfide **5.13S** was obtained (25% yield) with no detectable sulfenamide product. When 0.5 equiv. DIB was used, the sulfenamide was produced in only 25% yield along with the disulfide in 51% yield (entry 12). These results suggested that DIB also facilitated the amination reaction after the oxidation step. However, when an excess amount of DIB (2 equiv.) was added to the reaction mixture (entry 13), the reaction efficiency was similar to that obtained when the reaction was conducted with 0.5 equiv. DIB. We suspected that the amine may have lost its nucleophilicity by

coordination with the excess DIB reagent. Based on these results, we used DIB (1.1 equiv.) as the oxidant/activator and DBU as the base in 2-propanol at room temperature in an open flask as the optimized conditions for further studies (entry 1).

Table 5.4 Optimization of one-pot synthesis of sulfenamide from 2-mercaptopyridine.[a]

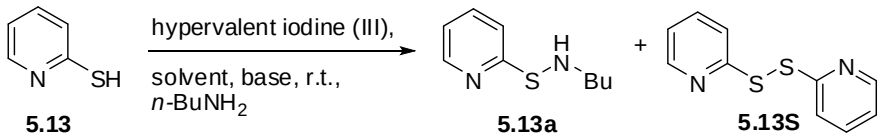

5.13 **5.13a** **5.13S**

Entry	Oxidant (equiv)	Base	Solvent	Yield **5.13a**/**5.13S** (%)[b]
1	$PhI(OCOCH_3)_2$ (1.1)	DBU	*i*PrOH	82:0
2	$PhI(OCOCF_3)_2$ (1.1)	DBU	*i*PrOH	26:67
3	$PhI(OCOtBu)_2$ (1.1)	DBU	*i*PrOH	13:81
4	PhI(OH)(OTs) (1.1)	DBU	*i*PrOH	36:80
5	$PhI(OCOCH_3)_2$ (1.1)	DBU	MeCN	53:19
6	$PhI(OCOCH_3)_2$ (1.1)	DBU	DMF	45:26
7[c]	$PhI(OCOCH_3)_2$ (1.1)	DBU	DMF	5:16
8	$PhI(OCOCH_3)_2$ (1.1)	-	*i*PrOH	25:56
9	$PhI(OCOCH_3)_2$ (1.1)	DIPEA	*i*PrOH	64:25
10	$PhI(OCOCH_3)_2$ (1.1)	K_2CO_3	*i*PrOH	9:79
11	-	DBU	*i*PrOH	0:24
12	$PhI(OCOCH_3)_2$ (0.5)	DBU	*i*PrOH	25:51
13	$PhI(OCOCH_3)_2$ (2.0)	DBU	*i*PrOH	27:57

[a]Reaction conditions: 2-mercaptopyridine (1.0 equiv.), hypervalent iodine(III) (1.1 equiv.), *i*PrOH, 0 °C, 1 min, then base (2.0 equiv.), *n*-butylamine (2.0 equiv.), 0 °C to r.t., 4 h.

[b]Isolated yield after silica gel chromatography.

[c]Reaction heated to reflux.

In development of a new methodology, it is important to demonstrate the compatibility of the method with various substrates. Thus, a panel of amine nucleophiles were subjected to the optimized sulfenylation conditions employing

two heteroaromatic thiols 2- and 4-mercaptopyridines **5.13** and **5.14** (Table 5.5). Without external nucleophile, disulfide **5.13S** was isolated as the sole product in 90% yield in the case of **5.13**. In the presence of simple primary amines such as benzyl and cyclohexylamines, sulfenamides **5.13b** and **5.13c** were obtained in 65 and 54% yield, respectively, along with disulfide **5.13S** in ca. 23% yield. Secondary amines including pyrrolidine, piperidine, and morpholine were acceptable substrates and the corresponding *N*,*N*-dialkyl sulfenamides **5.13d**–**f** were isolated 58–61% yields along with small amounts of **5.13S**. Amine nucleophiles carrying other functional groups such as hydroxy or acetal were also compatible with the reaction conditions, generating the corresponding sulfonamides **5.13g** and **5.13h**, respectively, in 43 and 57% yields. Attempts to improve the formation of sulfenamide by increasing the temperature, nucleophile amount, or reaction time, resulted in insignificant improvements. Unfortunately, the sterically hindered *tert*-butylamine and the less nucleophilic aniline did not act as a nucleophile and only disulfide **5.13S** could be isolated. Similarly, 4-mercaptopyridine (**5.14**) gave the corresponding sulfenamides **5.14a**–**5.14h** in slightly better yields compared with 2-mercaptopyridine (**5.13**).

Although this reaction generally gave only moderate yields when compared with traditional multistep synthesis involving oxidation chlorination and amination, this method can provide a complementary way to prepare sulfenamide derivatives under benign and convenient conditions. With these encouraging results in hand, a panel of commercially available heteroaromatic thiols **5.21**–**5.24** was then examined to demonstrate the generality of this DIB-mediated direct amination reaction (Scheme 5.9); the results are summarized in Table 5.6. It was shown that this new S–N bond-forming reaction is suitable for generating heteroaromatic sulfenamides ranging from monocyclic to bicyclic with good efficiency. The reaction of benzylamine in the presence of DIB and DBU gave the desired *N*-benzylsulfenamides **5.21b**–**5.24b** in good yields of 64–73%. We would like to note that, in comparison with pyridinethiols **5.13**–**5.14**, heterocycles **5.21**–**5.24** underwent complete amination reaction without any disulfide remaining in the reaction. The higher reactivity of these heterocyclic thiols in comparison with pyridine is governed by

increases in the electrophilicity of the sulfur atom, which facilitates nucleophilic substitution by the amines.

Table 5.5 The scope of the reaction with respect to amine nucleophiles in the DIB-mediated direct amination of 2- or 4-mercaptopyridine.[a,b]

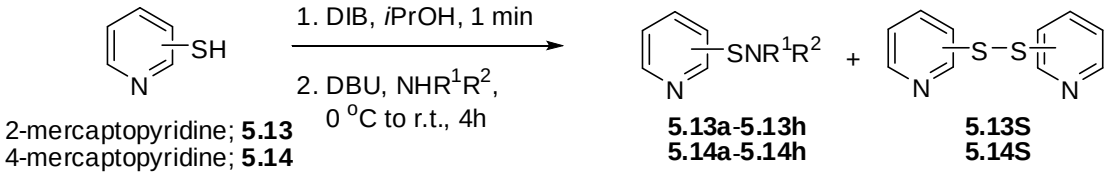

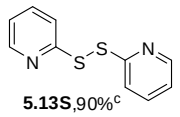
5.13S,90%[c]

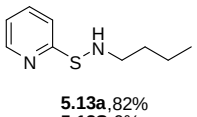
5.13a,82%
5.13S,0%

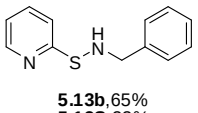
5.13b,65%
5.13S,23%

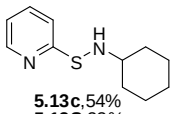
5.13c,54%
5.13S,23%

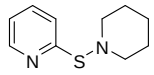
5.13d,61%
5.13S,31%

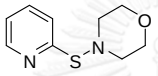
5.13e,59%
5.13S,7%

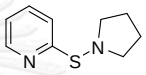
5.13f,60%
5.13S,23%

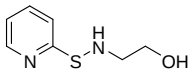
5.13g,43%
5.13S,44%

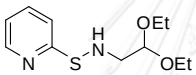
5.13h,57%
5.13S,18%

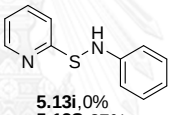
5.13i,0%
5.13S,87%

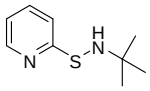
5.13j,0%
5.13S,91%

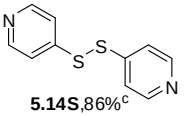
5.14S,86%[c]

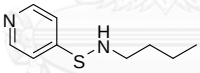
5.14a,77%
5.14S,0%

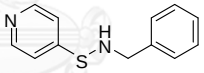
5.14b,51%
5.14S,19%

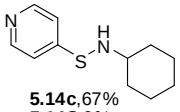
5.14c,67%
5.14S,9%

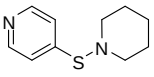
5.14d,63%
5.14S,19%

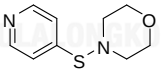
5.14e,64%
5.14S,23%

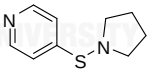
5.14f,68%
5.14S,12%

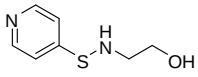
5.14g,57%
5.14S,19%

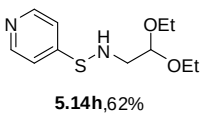
5.14h,62%
5.14S,25%

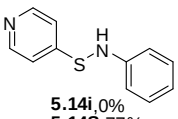
5.14i,0%
5.14S,77%

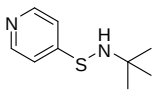
5.14j,0%
5.14S,81%

[a]Reaction conditions: 2- or 4-mercaptopyridine (1.0 equiv.), DIB (1.1 equiv.), *i*PrOH, 0 ℃, 1 min, then DBU (2.0 equiv.), amine (2.0 equiv.), 0 ℃ to r.t., under air, 4 h.

[b]Isolated yield after silica gel chromatography.

[c]Amine and DBU were not added.

Table 5.6 One-pot synthesis of sulfenamide from heterocyclic thiols.[a]

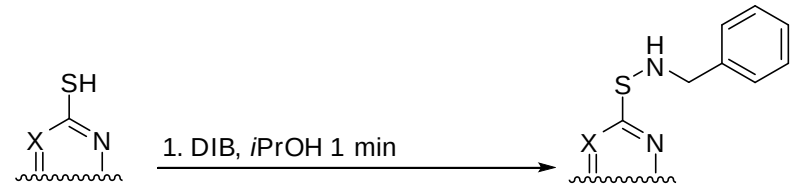

X = C, N, S

5.21-5.24 **5.21b-5.24b**

Entry	Starting material	Product	Yield (%)[b]
1	5.21	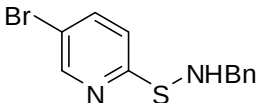	67
2	5.22	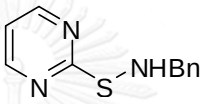	72
3[c]	5.23	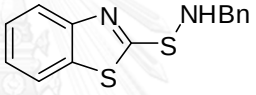	73
4	5.24	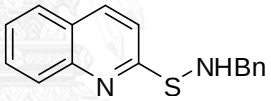	64

[a]Reaction conditions: heteroaromatic thiol (1.0 equiv.), DIB (1.1 equiv.), *i*PrOH, 0 °C, 1 min, then DBU (2.0 equiv.), benzylamine (2.0 equiv.), 0 °C to r.t., 4 h.

[b]Isolated yield after silica gel chromatography.

[c]DMF was used as solvent.

5.2.2.2 S-C bond formation: Direct sulfenylation of indole

In addition to the preparation of sulfenamides, we expanded our discovered methodology to the synthesis of sulfenylindoles. Such compounds represent pharmaceutically and biologically important structures, with their therapeutic value in the treatment of heart disease, allergies, cancer, HIV, and obesity. Traditional approaches for synthesizing this class of compound include sulfenylation of the indole ring by various sulfenylating agents such as sulfenyl halides, *N*-thioimides, and disulfides [110-113]. These approaches require multiple-step transformations because

the starting sulfenating agents are derived from the thiols. We herein report the applicability of the present DIB-mediated sulfenylation reaction for a direct synthesis of sulfenylindole from thiols (Scheme 5.9). In a slight modification of the previous conditions for sulfenamide formation, 4-chlorophenylthiol (**5.20**) was treated with DIB followed by DBU and 1*H*-indole at 120 ℃ under open atmosphere for 12 h. To our delight, thioether **5.25** was obtained in 43% yield along with disulfide **5.20S** in 31% yield.

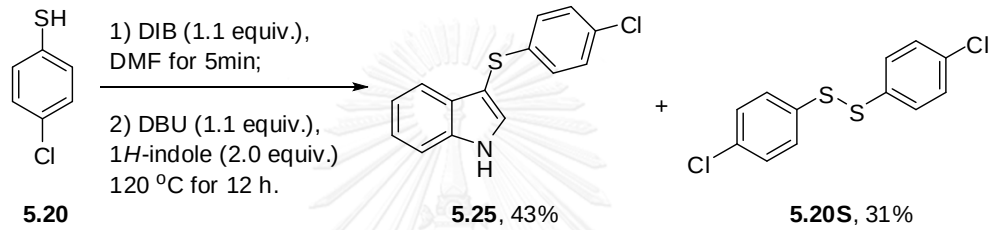

5.20 **5.25**, 43% **5.20S**, 31%

Scheme 5.9 Synthesis of 3-(4-chlorophenylthio)-*1H*-indole.

5.2.3 Proposed mechanism of DIB-mediated sulfenamide formation

A plausible mechanism of the DIB-mediated formation of the disulfides and sulfenamides is shown in Scheme 5.10. Based on previous work on the activation of sulfur by hypervalent iodine reagents [106], we hypothesize that the reaction involves ligand exchange between DIB and thiol, leading to the formation of sulfenyl iodide intermediate **5.26**. A second molecule of thiol then undergoes ligand exchange with 5 to produce the disulfide product. This process is facilitated by the reductive elimination to leave iodobenzene **5.27**, which is a well-known reaction for hypervalent iodine compounds [114]. For the formation of sulfenamide, there are two possible pathways (A and B). In the presence of a strong nucleophile such as amine, a sulfur atom on the disulfide is attacked and expels a sulfide anion, which undergoes further ligand exchange with DIB reagent to again form the reactive key intermediate **5.26** (pathway A). This process makes the leaving group sulfide anion from the starting key intermediate **5.26** and drive the reaction forward. To verify the proposed mechanism, disulfide **5.20S** was treated with *n*-butylamine in the absence

of DIB. Under these conditions, sulfenamide **5.13a** was isolated in 27% yield, supporting the conclusion that the disulfide is an intermediate in this reaction. However, the possibility of direct nucleophilic substitution by the nitrogen amine on the sulfur atom of intermediate **5.26** could not be ruled out (pathway B).

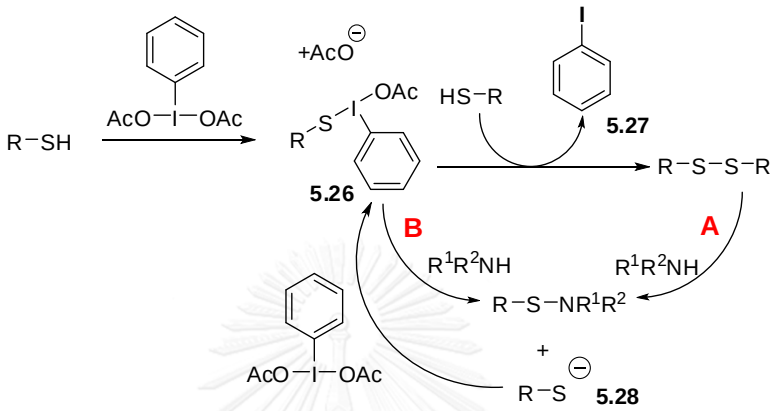

Scheme 5.10 A plausible mechanism of disulfide and sulfenamide formation.

5.3 Experiment

General Remarks: All reagents were purchased from Sigma–Aldrich, Fluka (Switzerland) or Merck (Germany) and used without further purification. All reactions were carried out under air atmosphere. All solvents were used without distillation. MS (ESI) and HRMS (ESI) were obtained with a micrOTOF Bruker mass spectrometer. ^{1}H and ^{13}C NMR spectra were recorded ($CDCl_3$, CD_3OD, and DMSO-d_6 as solvent) at 400 and 100 MHz, respectively, with a Varian Mercury+ 400 NMR or a Bruker (Avance 400) NMR spectrometer using tetramethylsilane (TMS) as internal standard. Chemical shifts are reported in ppm downfield from TMS. Analytical thin-layer chromatography (TLC) was performed on percolated Merck silica gel 60 F254 plates (thick layer, 0.25 mm) and visualized by 254 nm ultraviolet lamp and potassium permanganate as the detecting agent. Column chromatography was performed by using Merck silica gel 60 (70–230 mesh).

General procedure for the synthesis of **5.2**, **5.7Ts**, **5.8Ts**:

A mixture of 4-hydroxyquinazoline (**5.1**) or 2-hydroxypyridine (**5.7**) or 2-hydroxypyridine (**5.8**) (1.0 eq) with 4-toluenesulfonul chloride (TsCl, 1.5 eq) and *N*,*N*'-diisopropylethylamine (DIPEA) (1.5 eq) was stirred at ambient temperature for 12 h. The reaction mixture was washed with water (3×20 mL) and the organic portion was extracted with ethyl aetate (EtOAc) (3×20 mL). The organic layer was washed with saturated aqueous NaCl, followed by dried over Na_2SO_4. After removal of the solvent under reduced pressure, the crude product was purified by silica gel column to afford **5.2Ts**, **5.7Ts**, **5.8Ts** in 81, 85 and 74% yields, respectively.

General procedure for the synthesis of 3-substituted-quinazolin-4-ones (**5.3a**, **5.3b**) (Procedure A):

A mixture of **5.2** (1.0 eq), 4-(dimethylamino)pyridine (DMAP, catalytic amount), *N*,*N*'-diisopropylethylamine (DIPEA, 1.5 eq) and amine (1.5 eq) was stirred in DMF at reflux temperature for 12 h. The reaction mixture was washed with water (3×20 mL) and the organic portion was extracted with ethyl aetate (EtOAc) (3×20 mL). The

organic layer was washed with saturated aqueous NaCl, followed by dried over Na_2SO_4. After removal of the solvent under reduced pressure, the crude product was purified by silica gel column to afford **5.3a** and **5.3b** in 82 and 76% yields, respectively.

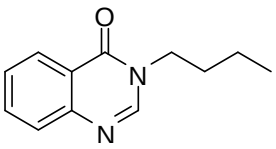

3-butylquinazolin-4(3H)-one (**5.3a**); Synthesized according to procedure A using **5.2** (30.0 mg, 0.100 mmol), DIPEA (35.0 µL, 0.200 mmol), *n*-butylamine (20.2 µL, 0.200 mmol) and DMAP (catalytic amount) in DMF (2 mL) to afford **5.3a** (16.5 mg, 0.082 mmol, 82%). ^{1}H NMR ($CDCl_3$, 400 MHz) δ 8.27 (d, *J* = 8.0 Hz, 1H), 8.03 (s, 1H), 7.72-7.67 (m, 2H), 7.47 (t, *J* = 7.4 Hz, 1H), 3.97 (t, *J* = 7.4 Hz, 2H), 1.85 (brs, 1H), 1.77-1.70 (m, 2H), 1.40-1.36 (m, 2H), 0.93 (t, *J* = 7.4 Hz, 3H).

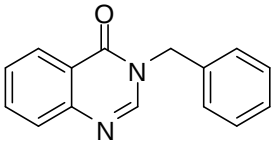

3-benzylquinazolin-4(3H)-one (**5.3b**); Synthesized according to procedure A using **5.2** (27.0 mg, 0.090 mmol), DIPEA (31.5 µL, 0.180 mmol), benzylamine (19.7 µL, 0.180 mmol) and DMAP (catalytic amount) in DMF (2 mL) to afford **5.3b** (16.1 mg, 0.068 mmol, 76%); ^{1}H NMR (CD_3OD, 400 MHz) δ 8.16 (dd, *J* = 8.0, 4.0 H, 1H), 8.05 (s), 1H, 7.75 (t, *J* = 8.0 Hz, 1H), 7.62 (d, *J* = 8,0 Hz, 1H), 7.47 (t, *J* = 8.0 Hz, 1H), 7.27-7.17 (m, 5H), 3.75 (s, 2H).

General procedure for the synthesis of disulfides **5.13S**, **5.14S** (Procedure B):

To a solution of thiol (1.0 equiv.) in *i*PrOH was added DIB (1.0 equiv.) and the solution was stirred at ambient temperature for 5 min. The solvent was removed by rotary evaporation and the crude product was purified by silica gel chromatography.

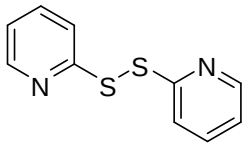

1,2-Di(pyridine-2-yl)disulfane (**5.13S**): [CAS: 2127-03-9]: Synthesized according to procedure B using 2-mercaptopyridine (50.0 mg, 0.450 mmol), DIB (159 mg, 0.495 mmol) in *i*PrOH (4 mL) to afford **5.13S** (44.4 mg, 0.202 mmol, 90%) as a white solid. ^{1}H NMR ($CDCl_3$, 400 MHz): δ = 8.40 (d, *J* = 8.1 Hz, 2H), 7.60–7.49 (m, 4H), 7.04 (m, 2H) ppm. ^{13}C NMR ($CDCl_3$, 100 MHz): δ = 159.0, 149.6, 137.4, 121.1, 119.7 ppm. IR (neat): ν = 3168, 3098, 1604, 1570, 1487, 1438 cm^{-1}.

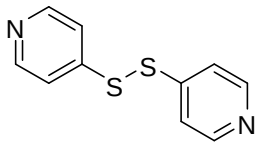

1,2-Di(pyridin-4-yl)disulfane (**5.14S**): [CAS: 2645-22-9]: Synthesized according to procedure B using 4-mercaptopyridine (50.0 mg, 0.450 mmol), DIB [159 mg, 0.495 mmol in *i*PrOH (4 mL)] to afford **5.14S** (42.6 mg, 0.194 mmol, 86%) as a white solid. ^{1}H NMR ($CDCl_3$, 400 MHz): δ = 8.42 (d, *J* = 5.5 Hz, 4H), 7.29 (d, *J* = 5.5 Hz, 4H) ppm. ^{13}C NMR ($CDCl_3$, 100 MHz): δ = 148.9, 145.3, 119.0 ppm. IR (neat) ν = 3032, 3002, 2922, 1568, 1544, 1479, 1405 cm^{-1}.

General procedure for the synthesis of **5.13a**-**h** and **5.14a**-**h** (Procedure C):

A solution of *N*-heterocyclic thiol (1.0 equiv.) in *i*PrOH and DIB (1.1 equiv.) was stirred at 0 °C for 1 min, then DBU (2.0 equiv.) and amine (2.0 equiv.) were added and the mixture was stirred at 0 °C to room temperature for 4 h. The crude product was purified by silica gel column chromatography.

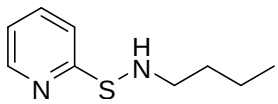

N-Butyl-2-pyridinesulfenamide (**5.13a**): Synthesized according to procedure C using 2-mercaptopyridine (50.0 mg, 0.450 mmol), DIB (159 mg, 0.495 mmol), DBU (134

μL, 0.900 mmol), *n*-butylamine (88.9 μL, 0.900 mmol) in *i*PrOH (4 mL) to afford **5.13a** (73.7 mg, 0.405 mmol, 90%) as a colorless oil. ^{1}H NMR ($CDCl_3$, 400 MHz): δ = 8.36 (d, *J* = 4.0 Hz, 1 H), 7.51 (td, *J* = 8.0, 4.0 Hz, 1 H), 7.26 (d, *J* = 8.0 Hz, 1H), 6.89 (dd, *J* = 8.0, 4.0 Hz, 1H), 3.07 (brs, 1H), 2.92 (m, 2H), 1.50 (m, 2H), 1.30 (m, 2H), 0.85 (t, *J* = 7.3 Hz, 3H) ppm. ^{13}C NMR ($CDCl_3$, 100 MHz): δ = 164.9, 148.1, 135.2, 118.1, 116.8, 52.5, 32.6, 20.0, 13.9 ppm. IR (neat) ν = 3366, 3017, 2957, 2927, 2396, 1708, 1649, 1627, 1578, 1557, 1439, 1422, 1359, 1326 cm^{-1}. HRMS (ESI): m/z calcd. for $[C_9H_{14}N_2S+H]^+$ 183.0956; found 183.0950.

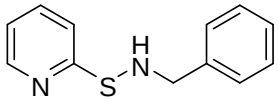

N-Benzyl-2-pyridinesulfenamide (**5.13b**): Synthesized according to procedure C using 2-mercaptopyridine (50.0 mg, 0.450 mmol), DIB (159 mg, 0.495 mmol), DBU (134 μL, 0.900 mmol), benzylamine (98.3 μL, 0.900 mmol) in *i*PrOH (4 mL) to afford **5.13b** (63.2 mg, 0.293 mmol, 65%) as a yellow oil. ^{1}H NMR ($CDCl_3$, 400 MHz): δ = 8.48 (d, *J* = 4.8 Hz, 1H), 7.57 (td, *J* = 8.0, 4.8 Hz, 1H), 7.44–7.27 (m, 6H), 6.89 (dd, *J* = 8.0, 4.8 Hz, 1H), 4.15 (d, *J* = 8.0 Hz, 2H), 3.55 (brs, 1H) ppm. ^{13}C NMR ($CDCl_3$, 100 MHz): δ = 164.0, 149.5, 139.3, 136.3, 128.5, 128.4, 127.6, 119.6, 118.3, 56.7 ppm. IR (neat) ν = 3323, 3059, 3028, 2987, 1599, 1577, 1556, 1500, 1495, 1456, 1416, 1280, 1220 cm^{-1}. HRMS (ESI): m/z calcd. for $[C_{12}H_{12}N_2S-H]^-$ 215.0643; found 215.0637.

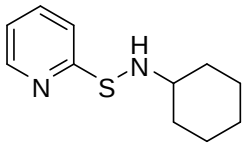

N-Cyclohexyl-2-pyridinesulfenamide (**5.13c**): [CAS: 178735-21-2]: Synthesized according to procedure C using 2-mercaptopyridine (50.0 mg, 0.450 mmol), DIB (159 mg, 0.495 mmol), DBU (134 μL, 0.900 mmol), cyclohexylamine (103 μL, 0.900 mmol) in *i*PrOH (4 mL) to afford **5.13c** (50.5 mg, 0.243 mmol, 54%) as a colorless oil. ^{1}H NMR ($CDCl_3$, 400 MHz): δ = 8.33 (d, *J* = 4.0 Hz, 1H), 7.50 (m, H), 7.36 (d, *J* = 8.0 Hz, 1H), 6.88 (m, 1H), 2.98 (brs, 1H), 2.67 (m, 1H), 1.95 (m, 2H), 1.66 (m, 2H), 1.52 (m, 1H), 1.25–0.99 (m, 5H) ppm. ^{13}C NMR ($CDCl_3$, 100 MHz): δ = 164.9, 148.1, 135.2, 118.1, 116.8,

58.5, 32.6, 24.8, 23.8 ppm. IR (neat) ν = 3342, 3040, 3013, 2937, 2847, 1572, 1552, 1449, 1413, 1367, 1343, 1272, 1258 cm^{-1}. MS (ESI): m/z calcd. for $[C_{11}H_{16}N_2S+H]^+$ 209.11; found 209.11.

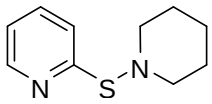

N-Piperidinyl-2-pyridinesulfenamide (**5.13d**): [CAS: 178735-21-2]: Synthesized according to procedure C using 2-mercaptopyridine (50.0 mg, 0.450 mmol), DIB (159 mg, 0.495 mmol), DBU (134 µL, 0.900 mmol), piperidine (62 µL, 0.900 mmol) in *i*PrOH (4 mL) to afford **5.13d** (37.3 mg, 0.192 mmol, 61%) as a colorless oil. ^{1}H NMR ($CDCl_3$, 400 MHz): δ = 8.40 (d, *J* = 4.3 Hz, 1H), 7.58 (td, *J* = 8.1, 1.7 Hz, 1H), 7.48 (d, *J* = 8.1 Hz, 1H), 6.93 (dd, *J* = 6.8, 5.4 Hz, 1H), 3.21–3.10 (m, 4H), 1.68 (dt, *J* = 11.2, 5.8 Hz, 4H), 1.50 (dd, *J* = 11.6, 6.0 Hz, 2H), 1.66 (m, 2H), 1.52 (m, 1H), 1.25–0.99 (m, 5H) ppm. ^{13}C NMR ($CDCl_3$, 100 MHz): δ = 165.8, 149.3, 136.4, 119.1, 118.0, 57.6, 27.4, 23.3 ppm. IR (neat) ν = 3016, 2937, 2857, 2827, 1575, 1555, 1442, 1419, 1363, 1213 cm^{-1}. MS (ESI): m/z calcd. for $[C_{10}H_{14}N_2S+H]^+$ 195.10; found 195.10.

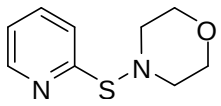

N-Morpholinyl-2-pyridinesulfenamide (**5.13e**): [CAS: 2244-48-6]: Synthesized according to procedure C using 2-mercaptopyridine (50.0 mg, 0.450 mmol), DIB (159 mg, 0.495 mmol), DBU (134 µL, 0.900 mmol), morpholine (77.9 µL, 0.900 mmol) in *i*PrOH (4 mL) to afford **5.13e** (52.1 mg, 0.266 mmol, 59%) as a yellow oil. ^{1}H NMR ($CDCl_3$, 400 MHz): δ = 8.36 (d, *J* = 4.4 Hz, 1H), 7.53 (td, *J* = 8.0, 0.8 Hz, 1H), 7.39 (d, *J* = 8.0 Hz, 1H), 6.91 (m, 1H), 3.71 (m, 4H), 3.17 (m, 4H) ppm. ^{13}C NMR ($CDCl_3$, 100 MHz): δ = 164.2, 149.4, 136.5, 119.6, 118.1, 67.9, 56.2 ppm. IR (neat) ν = 3040, 2953, 2914, 2844, 1569, 1555, 1452, 1412, 1280, 1246 cm^{-1}. MS (ESI): m/z calcd. for $[C_9H_{12}N_2OS+H]^+$ 197.07; found 197.07.

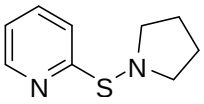

N-Pyrrolidinyl-2-pyridinesulfenamide (**5.13f**): Synthesized according to procedure C using 2-mercaptopyridine (50.0 mg, 0.450 mmol), DIB (159 mg, 0.495 mmol), DBU (134 µL, 0.900 mmol), pyrrolidine (73.9 µL, 0.900 mmol) in *i*PrOH (4 mL) to afford **5.13f** (48.6 mg, 0.270 mmol, 60%) as a colorless oil. ^{1}H NMR (CD_3OD, 400 MHz): δ = 8.21 (d, *J* = 4.4 Hz, 1H), 7.61 (td, *J* = 8.0, 2.0 Hz, 1H), 7.30 (d, *J* = 8.0 Hz, 1H), 6.96 (m, 1H), 3.14 (t, *J* = 6.6 Hz, 4H), 1.86 (m, 4H) ppm. ^{13}C NMR (CD_3OD, 100 MHz): δ = 167.2, 149.9, 138.4, 120.6, 119.1, 56.5, 27.2 ppm. IR (neat) ν = 3016, 2967, 2860, 1572, 1555, 1452, 1412, 1210 cm^{-1}. HRMS (ESI): m/z calcd. for $[C_9H_{12}N_2S+H]^+$ 181.0799; found 181.0786.

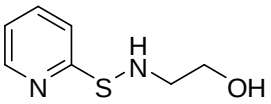

N-(2-Hydroxyethyl)-2-pyridinesulfenamide (**5.13g**): Synthesized according to procedure C using 2-mercaptopyridine (35.0 mg, 0.315 mmol), DIB (111 mg, 0.346 mmol), DBU (94 µL, 0.630 mmol), ethanolamine (38.0 µL, 0.630 mmol) in *i*PrOH (3 mL) to afford **5.13g** (23.0 mg, 0.135 mmol, 43%)) as a colorless oil. ^{1}H NMR (CD_3OD, 400 MHz): δ = 8.35 (d, *J* = 4.6 Hz, 1H), 7.74 (td, *J* = 8.1, 1.7 Hz, 1H), 7.57 (d, *J* = 8.1 Hz, 1H), 7.10 (dd, *J* = 6.8, 5.4 Hz, 1H), 3.68 (t, *J* = 5.6 Hz, 2H), 3.11 (t, *J*= 5.6 Hz, 1H), 3.10 ppm. ^{13}C NMR (CD_3OD, 100 MHz): δ = 167.5, 149.8, 138.4, 120.8, 119.2, 62.2, 55.4 ppm. IR (neat) ν = 3336, 3020, 2947, 2923, 2864, 1575, 1552, 1442, 1412, 1280, 1213 cm^{-1}. HRMS (ESI): m/z calcd. for $[C_7H_{10}N_2OS+H]^+$ 171.0595; found 171.0592.

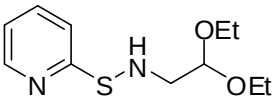

N-(2,2-Diethoxyethyl)-2-pyridinesulfenamide (**5.13h**): Synthesized according to procedure C using 2-mercaptopyridine (50.0 mg, 0.450 mmol), DIB (159 mg, 0.495 mmol), DBU (134 µL, 0.900 mmol), aminoacetaldehyde diethylacetal (131 µL, 0.900 mmol) in *i*PrOH (4 mL) to afford **5.13h** (62.1 mg, 0.257 mmol, 57%) as a yellow oil. ^{1}H NMR (CD_3OD, 400 MHz): δ = 8.22 (d, *J* = 4.4 Hz, 1H), 7.64 (td, *J* = 8.0, 1.6 Hz, 1H), 7.49

(d, *J* = 8.0 Hz, 1H), 6.97 (m, 1H), 4.52 (t, *J* = 5.3 Hz, 1H), 3.62 (m, 2H), 3.46 (m, 2 H), 2.97 (d, *J* = 5.4 Hz, 2H), 1.10 (t, *J* = 5.4 Hz, 6H) ppm. ^{13}C NMR (CD_3OD, 100 MHz): δ = 167.6, 149.8, 138.4, 120.8, 119.2, 103.5, 63.7, 56.0, 15.7 ppm. IR (neat) ν = 3345, 3040, 2970, 2920, 1569, 1552, 1449, 1416, 1373, 1296, 1276, 1236, 1213 cm^{-1}. HRMS (ESI): m/z calcd. for $[C_{11}H_{18}N_2O_2S+Na]^+$ 265.1009; found 265.0987.

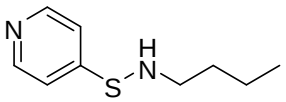

N-Butyl-4-pyridinesulfenamide (**5.14a**): Synthesized according to procedure C using 4-mercaptopyridine (50.0 mg, 0.450 mmol), DIB (159 mg, 0.495 mmol), DBU (134 µL, 0.900 mmol), *n*-butylamine (88.9 µL, 0.900 mmol) in *i*PrOH (4 mL) to afford **5.14a** (63.1 mg, 0.47 mmol, 77%) as a colorless oil. ^{1}H NMR ($CDCl_3$, 400 MHz): δ = 8.33 (d, *J* = 6.1 Hz, 2H), 7.10 (d, *J* = 6.1 Hz, H), 2.92 (m, 1H), 2.66 (brs, 1H), 1.49 (m, 2H), 1.31 (m, 2H), 0.86 (t, *J* = 7.3 Hz, 3H) ppm. ^{13}C NMR ($CDCl_3$, 100 MHz): δ = 154.0, 148.1, 115.6, 51.1, 31.6, 19.0, 12.8 ppm. IR (neat) ν = 3209, 3063, 3026, 3000, 2953, 2920, 2870, 2867, 2442, 2392, 1665, 1575, 1542, 1476, 1436, 1406, 1376, 1366, 1313, 1296, 1213 cm^{-1}. HRMS (ESI): m/z calcd. for $[C_9H_{14}N_2S+H]^+$ 183.0956; found 183.0950.

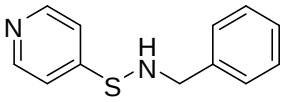

N-Benzyl-4-pyridinesulfenamide (**5.14b**): Synthesized according to procedure C using 4-mercaptopyridine (50.0 mg, 0.450 mmol), DIB (159 mg, 0.495 mmol), DBU (134 µL, 0.900 mmol), benzylamine (98.3 µL, 0.900 mmol) in *i*PrOH (4 mL) to afford **5.14b** (49.6 mg, 0.230 mmol, 51%) as a pale-yellow solid. ^{1}H NMR ($CDCl_3$, 400 MHz): δ = 8.35 (d, *J* = 5.9 Hz, 2H), 7.32–7.23 (m, 5H), 7.13 (d, *J* = 5.9 Hz, 2H), 4.06 (d, *J* = 5.7 Hz, 2H), 3.00 (brs, 1H) ppm. ^{13}C NMR ($CDCl_3$, 100 MHz): δ = 154.3, 149.2, 138.8, 128.7, 128.2, 127.9, 116.7, 56.4 ppm. IR (neat) ν = 3335, 3086, 3063, 3033, 2960, 2445, 2395, 1668, 1572, 1545, 1495, 1479, 1452, 1409, 1353, 1316, 1216 cm^{-1}. HRMS (ESI): m/z calcd. for $[C_{12}H_{12}N_2S+H]^+$ 217.0799; found 217.0793.

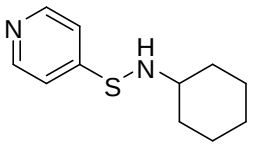

N-Cyclohexyl-4-pyridinesulfenamide (**5.14c**): [CAS: 178735-22-3]: Synthesized according to procedure C using 4-mercaptopyridine (50.0 mg, 0.450 mmol), DIB (159 mg, 0.495 mmol), DBU (134 µL, 0.900 mmol), cyclohexylamine (103 µL, 0.900 mmol) in *i*PrOH (4 mL) to afford **5.14c** (62.7 mg, 0.302 mmol, 67%) as a white solid. ^{1}H NMR ($CDCl_3$, 400 MHz): δ = 8.31 (d, *J* = 6.1 Hz, 2H), 7.14 (d, *J* = 6.1 Hz, 2H), 2.64 (brm, 2H), 1.93 (d, *J* = 11.4 Hz, 2H), 1.67 (d, *J* = 12.4 Hz, 2H), 1.53 (d, *J* = 11.5 Hz, 1H), 1.26–1.00 (m, 5H) ppm. ^{13}C NMR ($CDCl_3$, 100 MHz): δ = 155.7, 149.0, 116.7, 59.6, 33.7, 25.7, 24.8 ppm. IR (neat) ν = 3345, 3066, 3013, 2930, 2860, 2449, 2395, 1715, 1668, 1582, 1542, 1469, 1442, 1409, 1366, 1349, 1316, 1250, 1210 cm^{-1}. MS (ESI): m/z calcd. for $[C_{11}H_{16}N_2S+H]^+$ 209.11; found 209.11.

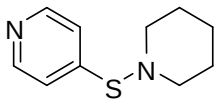

N-Piperidinyl-4-pyridinesulfenamide (**5.14d**): Synthesized according to procedure C using 4-mercaptopyridine (50.0 mg, 0.450 mmol), DIB (159 mg, 0.495 mmol), DBU (134 µL, 0.900 mmol), piperidine (88.9 µL, 0.900 mmol) in *i*PrOH (4 mL) to afford **5.14d** (55.0 mg,0.284 mmol, 63%) as a colorless oil. ^{1}H NMR ($CDCl_3$, 400 MHz): δ = 8.33 (m, 2H), 7.13 (d, *J* = 6.0 Hz, 2H), 2.99 (t, *J* = 6.0 Hz, 4H), 1.63 (m, 4H), 1.44 (m, 2H) ppm. ^{13}C NMR ($CDCl_3$, 100 MHz): δ = 152.5, 148.2, 116.0, 56.6, 26.2, 22.2 ppm. IR (neat) ν = 3070, 3013, 2940, 2850, 2824, 2442, 2389, 1569, 1535, 1476, 1452, 1439, 1402, 1366, 1353, 1309, 1216 cm^{-1}. HRMS (ESI): m/z calcd. for $[C_{10}H_{14}N_2S+H]^+$ 195.0956; found 195.0950.

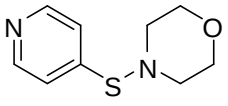

N-Morpholinyl-4-pyridinesulfenamide (**5.14e**): Synthesized according to procedure C using 4-mercaptopyridine (50.0 mg, 0.450 mmol), DIB (159 mg, 0.495 mmol), DBU (134 µL, 0.900 mmol), morpholine (77.9 µL, 0.900 mmol) in *i*PrOH (4 mL) to afford **5.14e** (56.5 mg, 0.288 mmol, 64%) as a yellow oil. ^{1}H NMR ($CDCl_3$, 400 MHz):

δ = 8.36 (d, *J* = 6.1 Hz, 2H), 7.15 (d, *J* = 6.1 Hz, 2H), 3.72 (t, *J* = 4.0 Hz, 4H), 3.02 (t, *J* = 4.0 Hz, 4H) ppm. ^{13}C NMR ($CDCl_3$, 100 MHz): δ = 151.1, 148.4, 116.1, 66.7, 55.2 ppm. IR (neat) ν = 3070, 3020, 2970, 2890, 2429, 2392, 1569, 1542, 1519, 1476, 1449, 1406, 1363, 1313, 1256, 1223cm^{-1}. HRMS (ESI): m/z calcd. for $[C_9H_{12}N_2OS+H]^+$ 197.0749; found 197.0742.

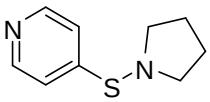

N-Pyrrolidinyl-4-pyridinesulfenamide (**5.14f**): Synthesized according to procedure C using 4-mercaptopyridine (50.0 mg, 0.450 mmol), DIB (159 mg, 0.495 mmol), DBU (134 µL, 0.900 mmol), pyrrolidine (73.9 µL, 0.900 mmol) in *i*PrOH (4 mL) to afford **5.14f** (48.6 mg, 0.270 mmol, 60%) as a colorless oil. ^{1}H NMR (CD_3OD, 400 MHz): δ = 8.21 (d, *J* = 4.4 Hz, 1H), 7.61 (td, *J* = 8.0, 2.0 Hz, 1H), 7.30 (d, *J* = 8.0 Hz, 1H), 6.96 (m, 1H), 3.14 (t, *J* = 6.6 Hz, 4H), 1.86 (m, 4H) ppm. ^{13}C NMR (CD_3OD, 100 MHz): δ = 167.2, 149.9, 138.4, 120.6, 119.1, 56.5, 27.2 ppm. IR (neat) ν = 3016, 2967, 2860, 1572, 1555, 1452, 1412, 1210 cm^{-1}. HRMS (ESI): m/z calcd. for $[C_9H_{12}N_2S+H]^+$ 181.0799; found 181.0786.

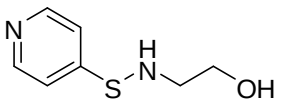

N-(2-Hydroxyethyl)-4-pyridinesulfenamide (**514g**): Synthesized according to procedure C using 4-mercaptopyridine (50.0 mg, 0.450 mmol), DIB (159.0 mg, 0.495 mmol), DBU (134 µL, 0.900 mmol), ethanolamine (54.3 µL, 0.900 mmol) in *i*PrOH (4 mL) to afford **5.14g** (43.7 mg, 0.257 mmol, 57%) as a yellow oil. ^{1}H NMR (CD_3OD, 400 MHz): δ = 8.19 (d, *J* = 6.4 Hz, 2H), 7.25 (d, *J* = 6.4 Hz, 2H), 3.55 (t, *J* = 5.6 Hz, 2H), 2.96 (t, *J* = 5.6 Hz, 2H) ppm. ^{13}C NMR (CD_3OD, 100 MHz): δ = 158.8, 149.2, 118.3, 67.3, 55.0 ppm. IR (neat) ν = 3458, 3405, 3020, 2970, 2927, 2442, 2399, 1751, 1711, 1618, 1575, 1539, 1519, 1479, 1412, 1363, 1220 cm^{-1}. HRMS (ESI): m/z calcd. for $[C_7H_{10}N_2OS+H]^+$ 171.0595; found 171.0592.

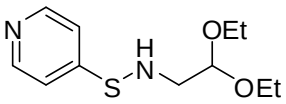

N-(2,2-Diethoxyethyl)-4-pyridinesulfenamide (**5.14h**): Synthesized according to procedure C using 4-mercaptopyridine (100 mg, 0.900 mmol), DIB (318.0 mg, 0.990 mmol), DBU (269 µL, 1.80 mmol), aminoacetaldehyde diethylacetal (262 µL, 1.80 mmol) in *i*PrOH (5 mL) to afford **5.14h** (136 mg, 0.558 mmol, 62%) as a colorless oil. ^{1}H NMR (CD_3OD, 400 MHz): δ = 8.32 (d, *J* = 6.4 Hz, 2 H), 7.35 (d, *J* = 6.4 Hz, 2 H), 4.61 (t, *J* = 5.3 Hz, 1H), 3.72 (m, 2H), 3.57 (m, 2H), 3.07 (d, *J* = 5.3 Hz, 2H), 1.22 (t, *J* = 7.1 Hz, 6H) ppm. ^{13}C NMR (CD_3OD, 100 MHz): δ = 158.8, 149.2, 118.2, 103.5, 63.8, 55.7, 15.7 ppm. IR (neat) ν = 3355, 3013, 2973, 2923, 2485, 2452, 2402, 1661, 1572, 1542, 1479, 1439, 1409, 1376, 1346, 1316, 1300, 1210 cm^{-1}. HRMS (ESI): m/z calcd. for $[C_{11}H_{18}N_2O_2S+H]^+$ 243.1167; found 243.1167.

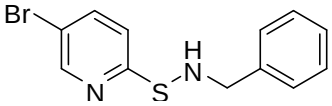

N-Benzyl-5-bromo-2-pyridinesulfenamide (**5.21b**): Synthesized according to procedure C using 5-bromopyridine-2-thiol (50.0 mg, 0.262 mmol), DIB (92.8 mg, 0.288 mmol), DBU (78.4 µL, 0.524 mmol), benzylamine (57.2 µL, 0.524 mmol) in *i*PrOH (3 mL) to afford **5.21b** (51.6 mg, 0.176 mmol, 67%) as a white solid. ^{1}H NMR (CD_3OD, 400 MHz): δ = 8.32 (s, H), 7.72 (dd, *J* = 8.0, 4.0 Hz, 1H), 7.34 (d, *J* = 8.0 Hz, H), 7.23–7.12 (m, 5H), 4.00 (s, 2H) ppm. ^{13}C NMR (CD_3OD, 100 MHz): δ = 166.2, 150.8, 140.9, 140.5, 129.5, 129.4, 128.4, 120.9, 116.6, 57.1 ppm. IR (neat) ν = 3261, 3066, 3023, 2918, 1700, 1601, 1555, 1533, 1499, 1444, 1342 cm^{-1}. HRMS (ESI): m/z calcd. for $[C_{12}H_{11}BrN_2S+H]^+$ 294.9921; found 294.9905.

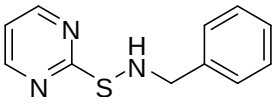

N-Benzyl-2-pyrimidinesulfenamide (**5.22b**): Synthesized according to procedure C using 2-pyrimidinethiol (50.0 mg, 0.446 mmol), DIB (158 mg, 0.490 mmol), DBU (133 µL, 0.892 mmol), benzylamine (97.4 µL, 0.892 mmol) in *i*PrOH (4 mL) to afford **5.22b** (69.7 mg, 0.321 mmol, 72%) as a yellow solid. ^{1}H NMR ($CDCl_3$,

400 MHz): δ = 8.52 (d, *J* = 4.8 Hz, 2H), 7.37–7.17 (m, 5H), 6.92 (t, *J* = 4.6 Hz, 1H), 4.14 (s, 2H), 3.56 (brs, 1H) ppm. ^{13}C NMR ($CDCl_3$, 100 MHz): δ = 175.9, 157.4, 139.2, 128.5, 128.4, 127.5, 116.8, 56.3 ppm. IR (neat) ν = 3325, 3056, 3020, 2927, 2402, 1612, 1588, 1562, 1545, 1489, 1449, 1416, 1376, 1290, 1223, 1193 cm^{-1}. HRMS (ESI): m/z calcd. for $[C_{11}H_{11}N_3S+H]^+$ 218.0745; found 218.0752.

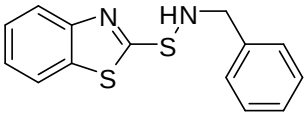

N-Benzyl-2-benzothiazolsulfenamide (**5.23b**): [CAS: 26773-69-3]: Synthesized according to procedure C using 2-Mercaptobenzothiazole (50.0 mg, 0.299 mmol), DIB (106.0 mg, 0.329 mmol), DBU (89.4 µL, 0.598 mmol), benzylamine (65.3 µL, 0.598 mmol) in DMF (3 mL) to afford **5.23b** (59.4 mg, 0.218 mmol, 73%) as a white yellow solid. ^{1}H NMR (CD_3OD, 400 MHz): δ = 7.73–7.73 (m, 2H), 7.35–7.17 (m, 7H), 4.19 (d, *J* = 8.0 Hz, 2H), 3.49 (t, *J* = 8.0 Hz, 1H) ppm. ^{13}C NMR (CD_3OD, 100 MHz): δ = 177.2, 154.8, 138.5, 135.1, 128.7, 128.4, 128.0, 126.0, 123.8, 121.7, 121.1, 57.1 ppm. IR (neat) ν = 3345, 3176, 3063, 3016, 2973, 2392, 1492, 1456, 1429, 1353, 1309, 1273, 1220 cm^{-1}. MS (ESI): m/z calcd. for $[C_{14}H_{12}N_2S+H]^+$ 273.00; found 273.05.

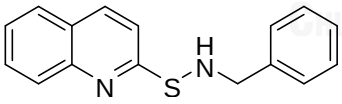

N-Benzyl-2-quinolinesulfenamide (**5.24b**): Synthesized according to procedure C using 2-quinolinethiol (60.0 mg, 0.372 mmol), DIB (132.0 mg, 0.409 mmol) in *i*PrOH (4 mL) to afford **5.24b** (63.4 mg, 0.238 mmol, 64%) as a yellow solid. ^{1}H NMR ($CDCl_3$, 400 MHz): δ = 7.91 (d, *J* = 8.6 Hz, 2H), 7.67 (d, *J* = 8.6 Hz, 1H), 7.60 (t, *J* = 7.6 Hz, 1H), 7.41–7.16 (m, 7H), 4.15 (d, *J* = 5.2 Hz, 2H), 3.68 (brs, 1H) ppm. ^{13}C NMR ($CDCl_3$, 100 MHz): δ = 163.9, 148.3, 136.0, 129.9, 128.6, 128.5, 128.1, 127.8, 127.6, 125.4, 117.0, 56.8 ppm. IR (neat) ν = 3276, 3060, 3023, 2920, 1612, 1588, 1555, 1489, 1456, 1419, 1293 cm^{-1}. HRMS (ESI): m/z calcd. for $[C_{16}H_{14}N_2S+H]^+$ 267.0956; found 267.0954.

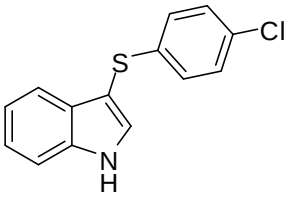

3-(4-Chlorophenylthio)-1H-indole (**5.25**): A solution of 4-chlorothiophenol (50.0 mg, 0.346 mmol, 1.00 equiv.) and DIB (123 mg, 0.381 mmol, 1.10 equiv.) in DMF (3.50 mL) was stirred at ambient temperature for 5 min. DBU (103 µL, 0.692 mmol, 2.00 equiv.) and 1*H*-indole (81.3 mg, 0.692 mmol, 2.00 equiv.) were added and the mixture was stirred at 120 °C for 12 h. The crude product was purified by silica gel chromatography to afford **5.25** (33.5 mg, 0.149 mmol, 43%) as a colorless oil and **5.20S** (8.41 mg, 0.0294 mmol, 17%). ^{1}H NMR (DMSO-d_6, 400 MHz): δ = 11.74 (s, 1H), 7.79 (d, *J* = 2.7 Hz, 1H), 7.50 (d, *J* = 8.1 Hz, 1H), 7.38 (d, *J* = 7.8 Hz, 1H), 7.30–7.23 (m, 2H), 7.20 (t, *J* = 7.1 Hz, 1H), 7.08 (t, *J* = 7.5 Hz, 1H), 7.04–6.97 (m, 2H) ppm. ^{13}C NMR (DMSO-d_6, 400 MHz): δ = 138.4, 136.7, 132.6, 129.3, 128.7, 128.4, 126.8, 122.2, 120.2, 118.1, 112.4, 98.6 ppm. HRMS (ESI): m/z calcd. for $C_{14}H_{10}ClNS$ 259.0222; found 259.0228..

5.4 Conclusion

We have demonstrated an operationally simple and efficient DIB-mediated one-pot direct methodology for the formation of S–N and S–C bonds from thiols. The reaction proceeds smoothly under mild conditions without exclusion of air or moisture. The corresponding sulfenamides were obtained in fair to good yields. Moreover, the reaction can be used to prepare a representative 3-sulfenylindole directly from indole and thiol. This novel method provides an environment friendly, low cost, and easy to operate alternative synthetic route to sulfenamides and sulfenylindole directly from thiols.

REFERENCES

[1] Shaw, J.E., Sicree, R.A., and Zimmet, P.Z. Global estimates of the prevalence of diabetes for 2010 and 2030. Diabetes Research and Clinical Practice 87(1) (2010): 4-14.

[2] Danaei, G., et al. National, regional, and global trends in fasting plasma glucose and diabetes prevalence since 1980: systematic analysis of health examination surveys and epidemiological studies with 370 country-years and 2.7 million participants. Lancet 378(9785) (2011): 31-40.

[3] Zimmet, P., Alberti, K.G.M.M., and Shaw, J. Global and societal implications of the diabetes epidemic. Nature 414(6865) (2001): 782-787.

[4] Gershell, L. Type 2 diabetes market. Nat Rev Drug Discov 4(5) (2005): 367-368.

[5] Saltiel, A.R. and Kahn, C.R. Insulin signalling and the regulation of glucose and lipid metabolism. Nature 414(6865) (2001): 799-806.

[6] Krentz, A.J. and Bailey, C.J. Oral antidiabetic agents: Current role in type 2 diabetes mellitus. Drugs 65(3) (2005): 385-411.

[7] McCarter, J. and Stephenwithers, G. Mechanisms of enzymatic glycoside hydrolysis. Current Opinion in Structural Biology 4(6) (1994): 885-892.

[8] Morgan, B. Monkey business over. Drug Discovery Today 9(5) (2004): 201-202.

[9] von Itzstein, M. The war against influenza: discovery and development of sialidase inhibitors. Nat Rev Drug Discov 6(12) (2007): 967-974.

[10] Chapel, C., et al. Reduction of the infectivity of hepatitis C virus pseudoparticles by incorporation of misfolded glycoproteins induced by glucosidase inhibitors. Journal of General Virology 88(4) (2007): 1133-1143.

[11] Greimel, P., Spreitz, J., Stütz, A.E., and Wrodnigg, T.M. Iminosugars and relatives as antiviral and potential anti-infective agents. Current topics in medicinal chemistry 3(5) (2003): 513-523.

[12] Butters, T.D., Dwek, R.A., and Platt, F.M. Imino sugar inhibitors for treating the lysosomal glycosphingolipidoses. Glycobiology 15(10) (2005): 43R-52R.

[13] Wrodnigg, T.M., Steiner, A.J., and Ueberbacher, B.J. Natural and synthetic iminosugars as carbohydrate processing enzyme inhibitors for cancer therapy. Anti-Cancer Agents in Medicinal Chemistry 8(1) (2008): 77-85.

[14] Yoon, S.-H. and Robyt, J.F. Addition of maltodextrins to the nonreducing-end of acarbose by reaction of acarbose with cyclomaltohexaose and cyclomaltodextrin glucanyltransferase. Carbohydrate Research 337(6) (2002): 509-516.

[15] Borges de Melo, E., da Silveira Gomes, A., and Carvalho, I. α- and β-Glucosidase inhibitors: chemical structure and biological activity. Tetrahedron 62(44) (2006): 10277-10302.

[16] Gravier-Pelletier, C., Maton, W., Dintinger, T., Tellier, C., and Le Merrer, Y. Synthesis and glycosidase inhibitory activity of aminocyclitols with a C6- or a C7-ring. Tetrahedron 59(44) (2003): 8705-8720.

[17] Yoshikawa, M., et al. Salacinol, potent antidiabetic principle with unique thiosugar sulfonium sulfate structure from the Ayurvedic traditional medicine Salacia reticulata in Sri Lanka and India. Tetrahedron Letters 38(48) (1997): 8367-8370.

[18] Yoshikawa, M., Morikawa, T., Matsuda, H., Tanabe, G., and Muraoka, O. Absolute Stereostructure of Potent α-Glucosidase Inhibitor, Salacinol, with Unique Thiosugar Sulfonium Sulfate Inner Salt Structure from Salacia reticulata. Bioorganic & Medicinal Chemistry 10(5) (2002): 1547-1554.

[19] Yoshikawa, M., Murakami, T., Yashiro, K., and Matsuda, H. Kotalanol, a potent α-glucosidase inhibitor with thiosugar sulfonium sulfate structure, from antidiabetic Ayurvedic medicine Salacia reticulata. Chemical and Pharmaceutical Bulletin 46(8) (1998): 1339-1340.

[20] Nakao, Y., Maki, T., Matsunaga, S., van Soest, R.W.M., and Fusetani, N. Penarolide Sulfates A1 and A2, New α-Glucosidase Inhibitors from a Marine Sponge Penares sp. Tetrahedron 56(46) (2000): 8977-8987.

[21] Taha, M., et al. Synthesis of novel inhibitors of α-glucosidase based on the benzothiazole skeleton containing benzohydrazide moiety and their

molecular docking studies. European Journal of Medicinal Chemistry 92(0) (2015): 387-400.

[22] Balan, K., Perumal, P., Sundarabaalaji, N., and Palvannan, T. Synthesis, molecular modeling and biological evaluation of novel 2-allyl amino 4-methyl sulfanyl butyric acid as α-amylase and α-glucosidase inhibitor. Journal of Molecular Structure 1081(0) (2015): 62-68.

[23] Bocci, V., Zanardi, I., Huijberts, M.S.P., and Travagli, V. Diabetes and chronic oxidative stress. A perspective based on the possible usefulness of ozone therapy. Diabetes & Metabolic Syndrome: Clinical Research & Reviews 5(1) (2011): 45-49.

[24] Brownlee, M. Biochemistry and molecular cell biology of diabetic complications. Nature 414(6865) (2001): 813-820.

[25] Maritim, A.C., Sanders, R.A., and Watkins, J.B. Diabetes, oxidative stress, and antioxidants: A review. Journal of Biochemical and Molecular Toxicology 17(1) (2003): 24-38.

[26] Hermanson, G. 2nd ed. Bioconjugate Techniques. Academic Press: San Diego, CA, 2008.

[27] Hosoda, A., et al. Synthesis of feruloyl-myo-inositols and their inhibitory effects on superoxide generation. Bioorganic & Medicinal Chemistry Letters 10(13) (2000): 1439-1442.

[28] Kumar, S., Narain, U., Tripathi, S., and Misra, K. Syntheses of Curcumin Bioconjugates and Study of Their Antibacterial Activities against β-Lactamase-Producing Microorganisms. Bioconjugate Chemistry 12(4) (2001): 464-469.

[29] Zhu, L., Cao, X., Chen, W., Zhang, G., Sun, D., and Wang, P.G. Syntheses and biological activities of daunorubicin analogs with uncommon sugars. Bioorganic & Medicinal Chemistry 13(23) (2005): 6381-6387.

[30] Kim, S.H., et al. Glucose-containing flavones—their synthesis and antioxidant and neuroprotective activities. Bioorganic & Medicinal Chemistry Letters 19(21) (2009): 6009-6013.

[31] Takeda, Y., et al. Morroniside cinnamic acid conjugate as an anti-inflammatory agent. Bioorganic & Medicinal Chemistry Letters 20(16) (2010): 4855-4857.

[32] Han, C.K., et al. Design and synthesis of highly potent fumagillin analogues from homology modeling for a human MetAP-2. Bioorganic & Medicinal Chemistry Letters 10(1) (2000): 39-43.

[33] Kruger, E.A. and Figg, W.D. TNP-470: an angiogenesis inhibitor in clinical development for cancer. Expert Opinion on Investigational Drugs 9(6) (2000): 1383-1396.

[34] De, P., et al. Design, Synthesis, and Biological Evaluation of New Cinnamic Derivatives as Antituberculosis Agents. Journal of Medicinal Chemistry 54(5) (2011): 1449-1461.

[35] Bian, X., Fan, X., Ke, C., Luan, Y., Zhao, G., and Zeng, A. Synthesis and α-glucosidase inhibitory activity evaluation of N-substituted aminomethyl-β-d-glucopyranosides. Bioorganic & Medicinal Chemistry 21(17) (2013): 5442-5450.

[36] Duchek, J., Adams, D.R., and Hudlicky, T. Chemoenzymatic Synthesis of Inositols, Conduritols, and Cyclitol Analogues. Chemical Reviews 111(7) (2011): 4223-4258.

[37] Behr, J.-B., Chevrier, C., Defoin, A., Tarnus, C., and Streith, J. Asymmetric synthesis of potent glycosidase and very potent α-mannosidase inhibitors: 4-amino-4-deoxy-l-erythrose and 4-amino-4,5-dideoxy-l-ribose. Tetrahedron 59(4) (2003): 543-553.

[38] Wacharasindhu, S., Worawalai, W., Rungprom, W., and Phuwapraisirisan, P. (+)-proto-Quercitol, a natural versatile chiral building block for the synthesis of the α-glucosidase inhibitors, 5-amino-1,2,3,4-cyclohexanetetrols. Tetrahedron Letters 50(19) (2009): 2189-2192.

[39] Delgado, A. Recent Advances in the Chemistry of Aminocyclitols. European Journal of Organic Chemistry 2008(23) (2008): 3893-3906.

[40] Nair, J.J., Rárová, L., Strnad, M., Bastida, J., and van Staden, J. Apoptosis-inducing effects of distichamine and narciprimine, rare alkaloids of the plant

family Amaryllidaceae. Bioorganic & Medicinal Chemistry Letters 22(19) (2012): 6195-6199.

[41] Worawalai, W., Rattanangkool, E., Vanitcha, A., Phuwapraisirisan, P., and Wacharasindhu, S. Concise synthesis of (+)-conduritol F and inositol analogues from naturally available (+)-proto-quercitol and their glucosidase inhibitory activity. Bioorganic & Medicinal Chemistry Letters 22(4) (2012): 1538-1540.

[42] Worawalai, W., Wacharasindhu, S., and Phuwapraisirisan, P. Synthesis of new N-substituted aminoquercitols from naturally available (+)-proto-quercitol and their [small alpha]-glucosidase inhibitory activity. MedChemComm 3(11) (2012): 1466-1470.

[43] Worawalai, W., Wacharasindhu, S., and Phuwapraisirisan, P. Amine-linked diquercitols as new α-glucosidase inhibitors. Bioorganic & Medicinal Chemistry Letters 24(23) (2014): 5530-5533.

[44] Sato, Y., et al. In vitro and in vivo antioxidant properties of chlorogenic acid and caffeic acid. International Journal of Pharmaceutics 403(1–2) (2011): 136-138.

[45] Ma, C., Hattori, M., and Daneshtalab, M. Preparation of chlorogenic acid analogues as pharmaceutical antioxidants. China Patent 102653514 (Sep 5, 2012).

[46] Hunyadi, A., Martins, A., Hsieh, T.-J., Seres, A., and Zupkó, I. Chlorogenic Acid and Rutin Play a Major Role in the <italic>In Vivo</italic> Anti-Diabetic Activity of <italic>Morus alba</italic> Leaf Extract on Type II Diabetic Rats. PLoS ONE 7(11) (2012): e50619.

[47] Schäfer, A. and Högger, P. Oligomeric procyanidins of French maritime pine bark extract (Pycnogenol®) effectively inhibit α-glucosidase. Diabetes Research and Clinical Practice 77(1) (2007): 41-46.

[48] Barham, D. and Trinder, P. An improved colour reagent for the determination of blood glucose by the oxidase system. Analyst 97(1151) (1972): 142-145.

[49] Adisakwattana, S., Chantarasinlapin, P., Thammarat, H., and Yibchok-Anun, S. A series of cinnamic acid derivatives and their inhibitory activity on intestinal alpha-glucosidase. J Enzyme Inhib Med Chem 24(5) (2009): 1194-200.

[50] Rattanangkool, E., Kittikhunnatham, P., Damsud, T., Wacharasindhu, S., and Phuwapraisirisan, P. Quercitylcinnamates, a new series of antidiabetic bioconjugates possessing α-glucosidase inhibition and antioxidant. European Journal of Medicinal Chemistry 66 (2013): 296-304.

[51] Łysek, R., et al. Search for α-glucosidase inhibitors: New N-substituted valienamine and conduramine F-1 derivatives. Bioorganic & Medicinal Chemistry 14(18) (2006): 6255-6282.

[52] Sim, L., et al. New Glucosidase Inhibitors from an Ayurvedic Herbal Treatment for Type 2 Diabetes: Structures and Inhibition of Human Intestinal Maltase-Glucoamylase with Compounds from Salacia reticulata. Biochemistry 49(3) (2009): 443-451.

[53] Stein, R.L. Kinetics of Enzyme Action: Essential Principles for Drug Hunters. Kinetics of Enzyme Action: Essential Principles for Drug Hunters. 2011.

[54] Chou, T.-C. Theoretical Basis, Experimental Design, and Computerized Simulation of Synergism and Antagonism in Drug Combination Studies. Pharmacological Reviews 58(3) (2006): 621-681.

[55] Sim, L., Quezada-Calvillo, R., Sterchi, E.E., Nichols, B.L., and Rose, D.R. Human Intestinal Maltase–Glucoamylase: Crystal Structure of the N-Terminal Catalytic Subunit and Basis of Inhibition and Substrate Specificity. Journal of Molecular Biology 375(3) (2008): 782-792.

[56] Schmidtke, P., Le Guilloux, V., Maupetit, J., and Tufféry, P. fpocket: Online tools for protein ensemble pocket detection and tracking. Nucleic Acids Research 38(SUPPL. 2) (2010): W582-W589.

[57] Le Guilloux, V., Schmidtke, P., and Tuffery, P. Fpocket: An open source platform for ligand pocket detection. BMC Bioinformatics 10 (2009).

[58] Dawidowicz, A.L., Wianowska, D., and Olszowy, M. On practical problems in estimation of antioxidant activity of compounds by DPPH method (Problems in estimation of antioxidant activity). Food Chemistry 131(3) (2012): 1037-1043.

[59] Altschul, S.F., Gish, W., Miller, W., Myers, E.W., and Lipman, D.J. Basic local alignment search tool. Journal of Molecular Biology 215(3) (1990): 403-410.

[60] Biasini, M., et al. SWISS-MODEL: modelling protein tertiary and quaternary structure using evolutionary information. Nucleic Acids Research 42(W1) (2014): W252-W258.

[61] Arnold, K., Bordoli, L., Kopp, J., and Schwede, T. The SWISS-MODEL workspace: a web-based environment for protein structure homology modelling. Bioinformatics 22(2) (2006): 195-201.

[62] Kiefer, F., Arnold, K., Künzli, M., Bordoli, L., and Schwede, T. The SWISS-MODEL Repository and associated resources. Nucleic Acids Research 37(suppl 1) (2009): D387-D392.

[63] Guex, N., Peitsch, M.C., and Schwede, T. Automated comparative protein structure modeling with SWISS-MODEL and Swiss-PdbViewer: A historical perspective. ELECTROPHORESIS 30(S1) (2009): S162-S173.

[64] Frisch, M.J.T., G. W.; Schlegel, H. B.; Gill, P. M. W.; Johnson, B. G.; Robb, M. A.; Cheeseman, J. R.; Keith, T.; Petersson, G. A.; Montgomery, J. A.; Raghavachari, K.; AlLaham, M. A.; Zakrzewski, V. G.; Ortiz, J. V.; Foresman, J. B.; Peng, C. Y.; Ayala, P. Y.; Chen, W.; Wong, M. W.; Andres, J. L.; Replogle, E. S.; Gomperts, R.; Martin, R. L.; Fox, D. J.; Binkley, J. S.; Defrees, D. J.; Baker, J.; Stewart, J. P.; Head Gordon, M.; Gonzalez, C.; Pople, J. A. Gaussian 98 (Revision A11) (2002): Gaussian: Pittsburgh, PA.

[65] VanBrocklin, H.F., et al. Anilinodialkoxyquinazolines: Screening Epidermal Growth Factor Receptor Tyrosine Kinase Inhibitors for Potential Tumor Imaging Probes. Journal of Medicinal Chemistry 48(23) (2005): 7445-7456.

[66] Mishani, E., et al. High-Affinity Epidermal Growth Factor Receptor (EGFR) Irreversible Inhibitors with Diminished Chemical Reactivities as Positron Emission Tomography (PET)-Imaging Agent Candidates of EGFR Overexpressing Tumors. Journal of Medicinal Chemistry 48(16) (2005): 5337-5348.

[67] Domarkas, J., et al. The Combi-Targeting Concept: Synthesis of Stable Nitrosoureas Designed to Inhibit the Epidermal Growth Factor Receptor (EGFR). Journal of Medicinal Chemistry 49(12) (2006): 3544-3552.

[68] Dai, Q., Ran, C., and Harvey, R.G. Synthesis of Adducts of o-Quinone Metabolites of Carcinogenic Polycyclic Aromatic Hydrocarbons with 2'-Deoxyribonucleosides. Organic Letters 7(6) (2005): 999-1002.

[69] Elmquist, C.E., Stover, J.S., Wang, Z., and Rizzo, C.J. Site-Specific Synthesis and Properties of Oligonucleotides Containing C8-Deoxyguanosine Adducts of the Dietary Mutagen IQ. Journal of the American Chemical Society 126(36) (2004): 11189-11201.

[70] Lee, H., Luna, E., Hinz, M., Stezowski, J.J., Kiselyo, A.S., and Harvey, R.G. Synthesis of Oligonucleotide Adducts of the Bay Region Diol Epoxide Metabolites of Carcinogenic Polycyclic Aromatic Hydrocarbons. The Journal of Organic Chemistry 60(17) (1995): 5604-5613.

[71] Wan, Z.-K., Wacharasindhu, S., Levins, C.G., Lin, M., Tabei, K., and Mansour, T.S. The Scope and Mechanism of Phosphonium-Mediated SNAr Reactions in Heterocyclic Amides and Ureas. The Journal of Organic Chemistry 72(26) (2007): 10194-10210.

[72] Punthasee, P., Vanitcha, A., and Wacharasindhu, S. Mukaiyama's reagent promoted C–N bond formation: a new method to synthesize 3-alkylquinazolin-4-ones. Tetrahedron Letters 51(13) (2010): 1713-1716.

[73] Mertens, M.D., Pietsch, M., Schnakenburg, G., and Gütschow, M. Regioselective Sulfonylation and N- to O-Sulfonyl Migration of Quinazolin-4(3H)-ones and Analogous Thienopyrimidin-4(3H)-ones. The Journal of Organic Chemistry 78(18) (2013): 8966-8979.

[74] Špulák, M., Novák, Z., Palát, K., Kuneš, J., Pourová, J., and Pour, M. The unambiguous synthesis and NMR assignment of 4-alkoxy and 3-alkylquinazolines. Tetrahedron 69(6) (2013): 1705-1711.

[75] Miyazawa, E., Sakamoto, T., and Kikugawa, Y. Synthesis of Spirodienones by Intramolecular Ipso-Cyclization of N-Methoxy-(4-halogenophenyl)amides Using

[Hydroxy(tosyloxy)iodo]benzene in Trifluoroethanol. The Journal of Organic Chemistry 68(13) (2003): 5429-5432.

[76] Boto, A., Hernández, D., and Hernández, R. Short and Efficient Synthesis of Chiral Furyl Carbinols from Carbohydrates. Organic Letters 9(9) (2007): 1721-1724.

[77] Souto, J.A., Zian, D., and Muñiz, K. Iodine(III)-Mediated Intermolecular Allylic Amination under Metal-Free Conditions. Journal of the American Chemical Society 134(17) (2012): 7242-7245.

[78] Berkessel, A., Glaubitz, K., and Lex, J. Enantiomerically Pure β-Amino Acids: A Convenient Access to Both Enantiomers of trans-2-Aminocyclohexanecarboxylic Acid. European Journal of Organic Chemistry 2002(17) (2002): 2948-2952.

[79] Okano, K., Tokuyama, H., and Fukuyama, T. Synthesis of Secondary Arylamines through Copper-Mediated Intermolecular Aryl Amination. Organic Letters 5(26) (2003): 4987-4990.

[80] Dukat, M., Mosier, P.D., Kolanos, R., Roth, B.L., and Glennon, R.A. Binding of Serotonin and N1-Benzenesulfonyltryptamine-Related Analogs at Human 5-HT6 Serotonin Receptors: Receptor Modeling Studies. Journal of Medicinal Chemistry 51(3) (2008): 603-611.

[81] Huttunen, K.M., et al. The First Bioreversible Prodrug of Metformin with Improved Lipophilicity and Enhanced Intestinal Absorption. Journal of Medicinal Chemistry 52(14) (2009): 4142-4148.

[82] Lopez, M., et al. Sulfonamide Linked Neoglycoconjugates–A New Class of Inhibitors for Cancer-Associated Carbonic Anhydrases. Journal of Medicinal Chemistry 53(7) (2010): 2913-2926.

[83] Davis, F.A., et al. Chemistry of the sulfur-nitrogen bond. 12. Metal-assisted synthesis of sulfenamide derivatives from aliphatic and aromatic disulfides. The Journal of Organic Chemistry 42(6) (1977): 967-972.

[84] Davis, F.A., Kaminski, J.M., Kluger, E.W., and Freilich, H.S. Chemistry of the sulfur-nitrogen bond. IX. Transmission of electronic effects in N-alkylidenearenesulfenamides, sulfinamides, sulfonamides, and

arenesulfenanilides. Journal of the American Chemical Society 97(24) (1975): 7085-7091.

[85] Matsuo, J.-i., Iida, D., Yamanaka, H., and Mukaiyama, T. N-tert-Butylbenzenesulfenamide-catalyzed oxidation of alcohols to the corresponding carbonyl compounds with N-chlorosuccinimide. Tetrahedron 59(35) (2003): 6739-6750.

[86] Yang, T.-K., et al. Application of New Camphor-Derived Mercapto Chiral Auxiliaries to the Synthesis of Optically Active Primary Amines. The Journal of Organic Chemistry 59(4) (1994): 914-921.

[87] Gradwell, M.H.S. and McGill, W.J. The interaction of sulfenamide accelerators with sulfur, ZNO, and stearic acid in the absence of rubber. Journal of Applied Polymer Science 51(1) (1994): 177-185.

[88] Yoo, J., Kuruvilla, D.J., D'Mello, S.R., Salem, A.K., and Bowden, N.B. New Class of Biodegradable Polymers Formed from Reactions of an Inorganic Functional Group. Macromolecules 45(5) (2012): 2292-2300.

[89] Arisawa, M., Sugata, C., and Yamaguchi, M. Oxidation/reduction interconversion of thiols and disulfides using hydrogen and oxygen catalyzed by a rhodium complex. Tetrahedron Letters 46(36) (2005): 6097-6099.

[90] Dhakshinamoorthy, A., Alvaro, M., and Garcia, H. Aerobic oxidation of thiols to disulfides using iron metal-organic frameworks as solid redox catalysts. Chemical Communications 46(35) (2010): 6476-6478.

[91] Dhakshinamoorthy, A., Navalon, S., Sempere, D., Alvaro, M., and Garcia, H. Aerobic Oxidation of Thiols Catalyzed by Copper Nanoparticles Supported on Diamond Nanoparticles. ChemCatChem 5(1) (2013): 241-246.

[92] Field, L. and Lawson, J.E. Organic Disulfides and Related Substances. I. Oxidation of Thiols to Disulfides with Lead Tetraacetate1. Journal of the American Chemical Society 80(4) (1958): 838-841.

[93] Golchoubian, H. and Hosseinpoor, F. Aerobic oxidation of thiols to disulfides catalyzed by a manganese(III) Schiff-base complex. Catalysis Communications 8(4) (2007): 697-700.

[94] Iranpoor, N., Firouzabadi, H., and Zolfigol, M.A. Dinitrogen Tetroxide Copper Nitrate Complex [Cu(NO3)2.N2O4] As a New Nitrosating Agent for Catalytic Coupling of Thiols via Thionitrite. Synthetic Communications 28(2) (1998): 367-375.

[95] Ali, M.H. and McDermott, M. Oxidation of thiols to disulfides with molecular bromine on hydrated silica gel support. Tetrahedron Letters 43(35) (2002): 6271-6273.

[96] Banfield, S.C., Omori, A.T., Leisch, H., and Hudlicky, T. Unexpected Reactivity of the Burgess Reagent with Thiols: Synthesis of Symmetrical Disulfides. The Journal of Organic Chemistry 72(13) (2007): 4989-4992.

[97] Dreyer, D.R., Jia, H.-P., Todd, A.D., Geng, J., and Bielawski, C.W. Graphite oxide: a selective and highly efficient oxidant of thiols and sulfides. Organic & Biomolecular Chemistry 9(21) (2011): 7292-7295.

[98] Ghorbani-Choghamarani, A., Nikoorazm, M., Goudarziafshar, H., Shokr, A., and Almasi, H. Metal-free oxidative coupling of thiols to disulfides using guanidinium nitrate or nitro urea in the presence of silica sulfuric acid. Journal of Chemical Sciences 123(4) (2011): 453-457.

[99] Oba, M., Tanaka, K., Nishiyama, K., and Ando, W. Aerobic Oxidation of Thiols to Disulfides Catalyzed by Diaryl Tellurides under Photosensitized Conditions. The Journal of Organic Chemistry 76(10) (2011): 4173-4177.

[100] Engqvist, R. and Bergman, J. Synthesis of benzothiopyrano[2,3-b]indol-11-one and benzopyrano[2,3-b]indol-11-one. Tetrahedron 59(48) (2003): 9649-9653.

[101] Correa, A., Tellitu, I., Domínguez, E., and SanMartin, R. Novel Alternative for the N−S Bond Formation and Its Application to the Synthesis of Benzisothiazol-3-ones. Organic Letters 8(21) (2006): 4811-4813.

[102] Taniguchi, N. Copper-Catalyzed Formation of Sulfur–Nitrogen Bonds by Dehydrocoupling of Thiols with Amines. European Journal of Organic Chemistry 2010(14) (2010): 2670-2673.

[103] S. Yusubov, M. and V. Zhdankin, V. Hypervalent Iodine Reagents and Green Chemistry. Current Organic Synthesis 9(2) (2012): 247-272.

[104] Zhdankin, V.V. Organoiodine(V) Reagents in Organic Synthesis. The Journal of Organic Chemistry 76(5) (2011): 1185-1197.

[105] Singh, C.B., Ghosh, H., Murru, S., and Patel, B.K. Hypervalent Iodine(III)-Mediated Regioselective N-Acylation of 1,3-Disubstituted Thioureas. The Journal of Organic Chemistry 73(7) (2008): 2924-2927.

[106] Ghosh, H., Yella, R., Nath, J., and Patel, B.K. Desulfurization Mediated by Hypervalent Iodine(III): A Novel Strategy for the Construction of Heterocycles. European Journal of Organic Chemistry 2008(36) (2008): 6189-6196.

[107] Frei, R. and Waser, J. A Highly Chemoselective and Practical Alkynylation of Thiols. Journal of the American Chemical Society 135(26) (2013): 9620-9623.

[108] Proença, C., et al. Novel sulfenamides as promising acetylcholinesterase inhibitors. Journal of Heterocyclic Chemistry 48(6) (2011): 1287-1294.

[109] Shang, J.-L., et al. Synthesis and evaluation of novel sulfenamides as novel anti Methicillin-resistant Staphylococcus aureus agents. Bioorganic & Medicinal Chemistry Letters 23(3) (2013): 724-727.

[110] Ge, W. and Wei, Y. Iodine-catalyzed oxidative system for 3-sulfenylation of indoles with disulfides using DMSO as oxidant under ambient conditions in dimethyl carbonate. Green Chemistry 14(7) (2012): 2066-2070.

[111] La Regina, G., Gatti, V., Famiglini, V., Piscitelli, F., and Silvestri, R. Venting-while-Heating Microwave-Assisted Synthesis of 3-Arylthioindoles. ACS Combinatorial Science 14(4) (2012): 258-262.

[112] Prasad, C.D., Kumar, S., Sattar, M., Adhikary, A., and Kumar, S. Metal free sulfenylation and bis-sulfenylation of indoles: persulfate mediated synthesis. Organic & Biomolecular Chemistry 11(46) (2013): 8036-8040.

[113] Marcantoni, E., Cipolletti, R., Marsili, L., Menichetti, S., Properzi, R., and Viglianisi, C. An Efficient Catalytic Method for Regioselective Sulfenylation of Electron-Rich Aza-Aromatics at Room Temperature. European Journal of Organic Chemistry 2013(1) (2013): 132-140.

[114] Keshavarz, M. Polymer-supported hypervalent iodine as green oxidant in organic synthesis. Synlett (16) (2011): 2433-2434.

APPENDIX

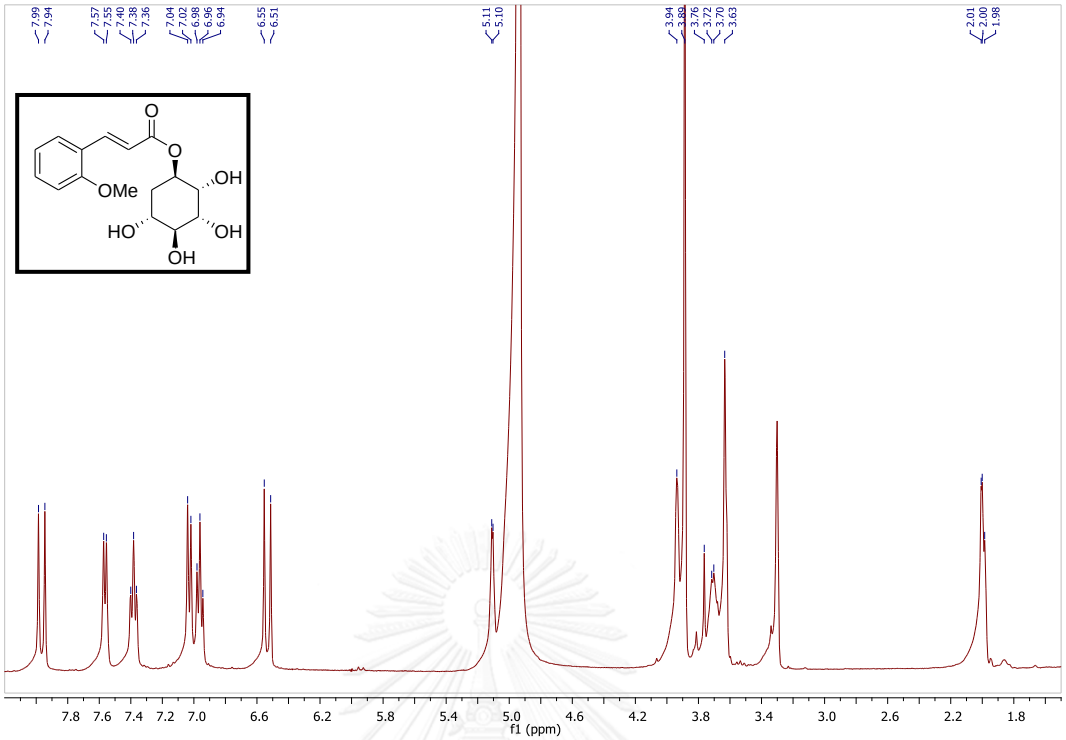

Figure A.1 ^{1}H NMR spectrum of **2.1ER** (CD_3OD)

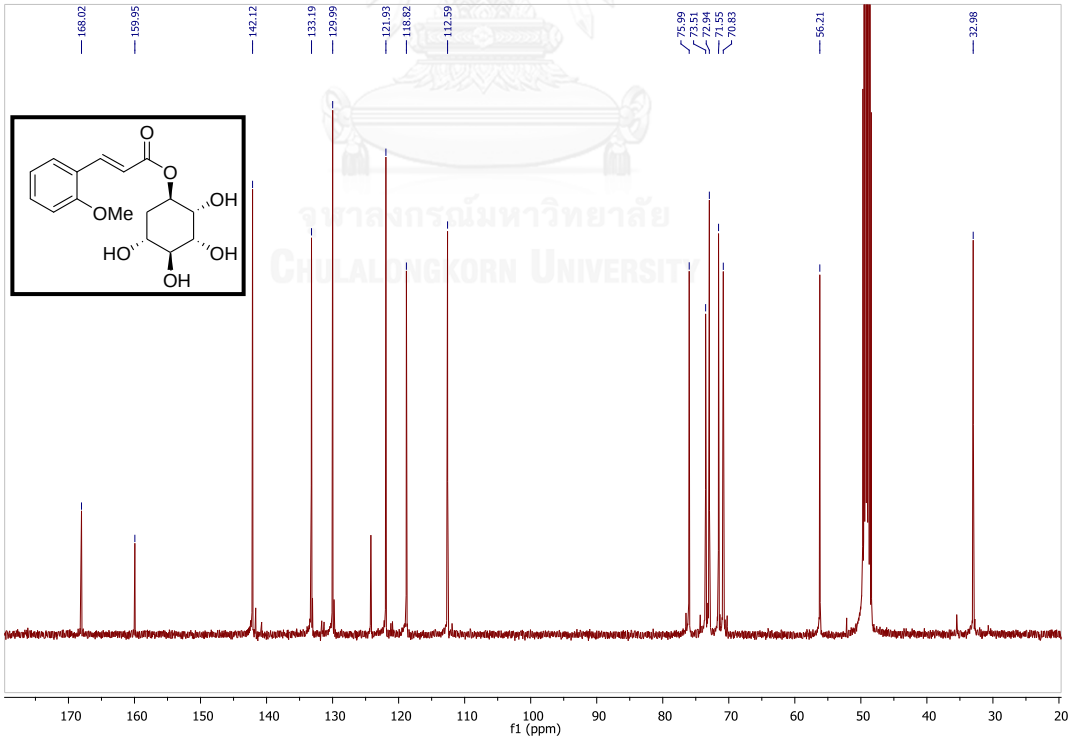

Figure A.2 ^{13}C NMR spectrum of **2.1ER** (CD_3OD)

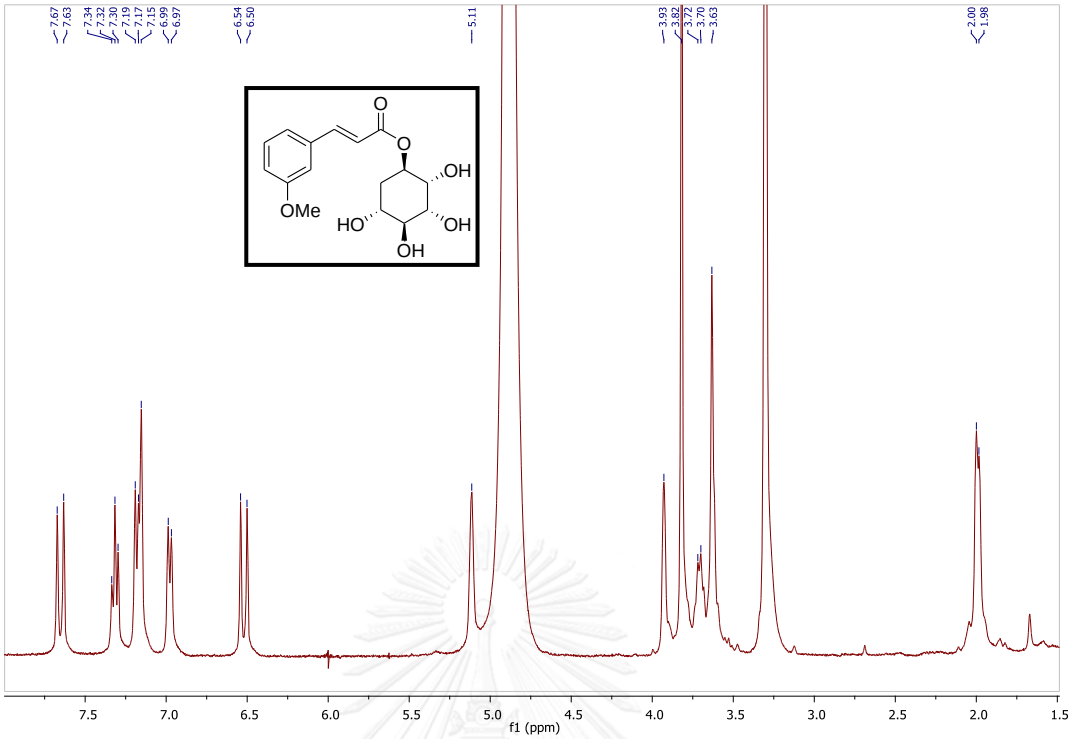

Figure A.3 ^{1}H NMR spectrum of **2.2ER** (CD_3OD)

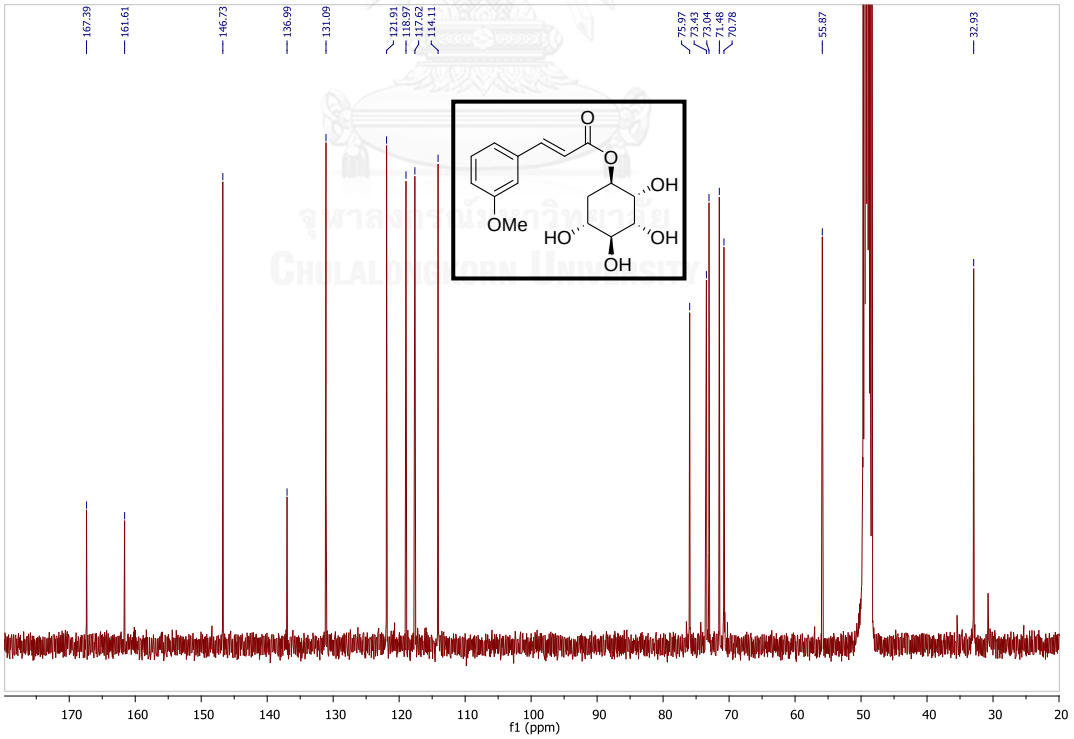

Figure A.4 ^{13}C NMR spectrum of **2.2ER** (CD_3OD)

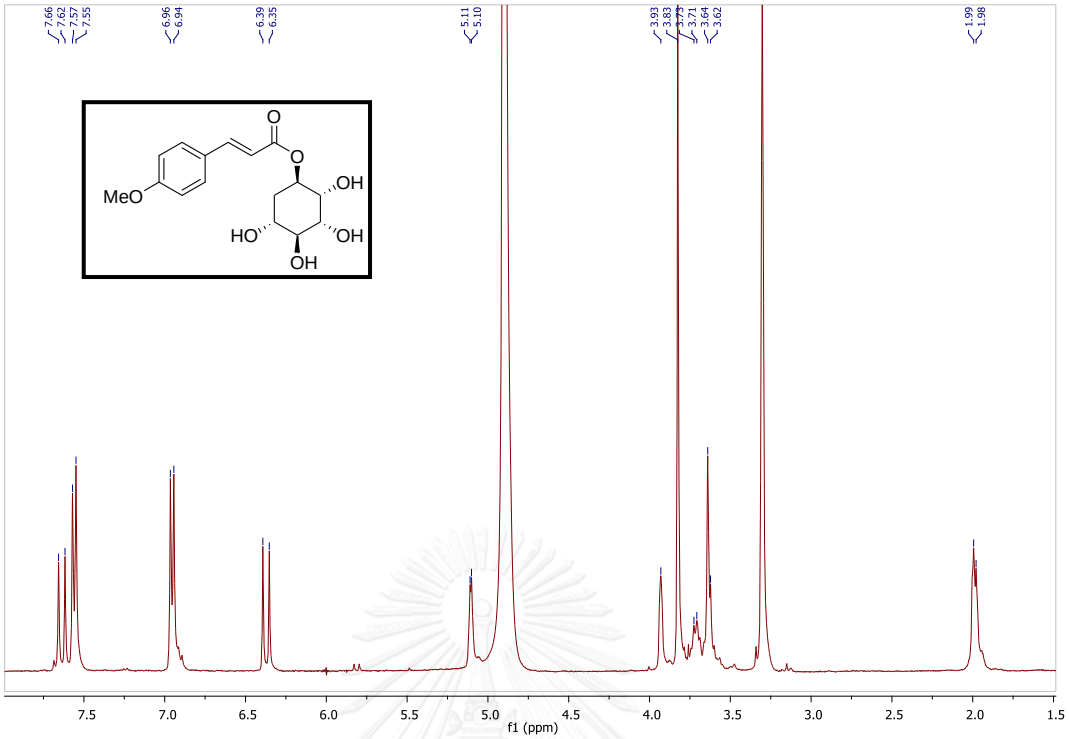

Figure A.5 ^{1}H NMR spectrum of **2.3ER (CD_3OD)**

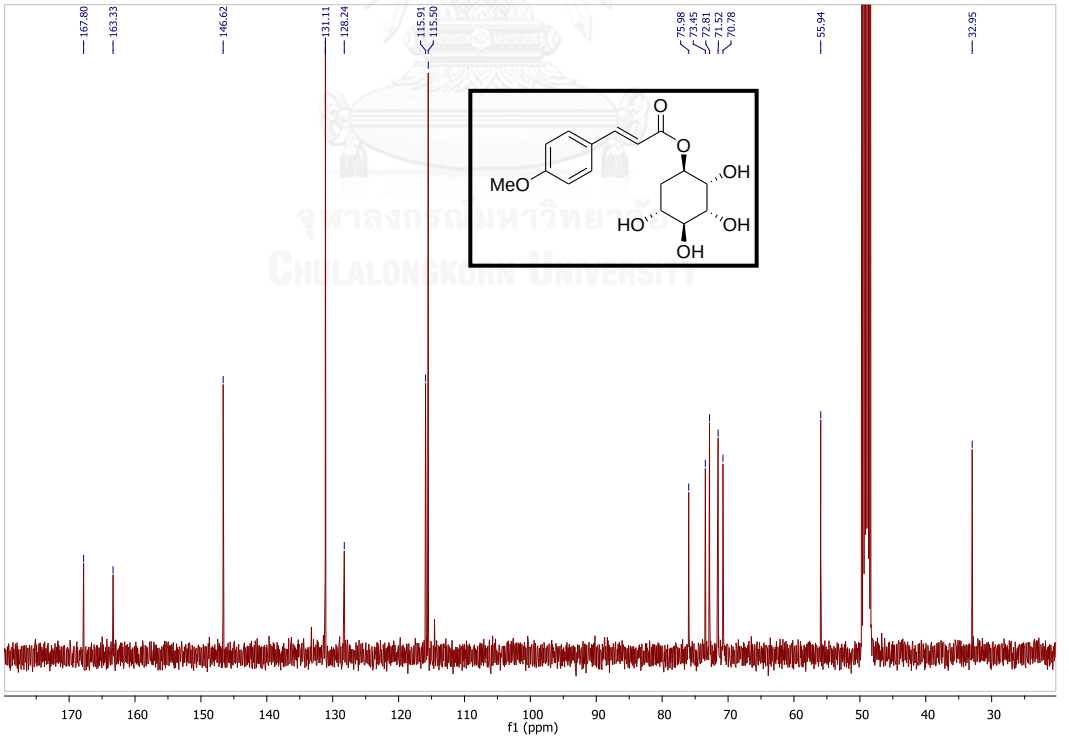

Figure A.6 ^{13}C NMR spectrum of **2.3ER (CD_3OD)**

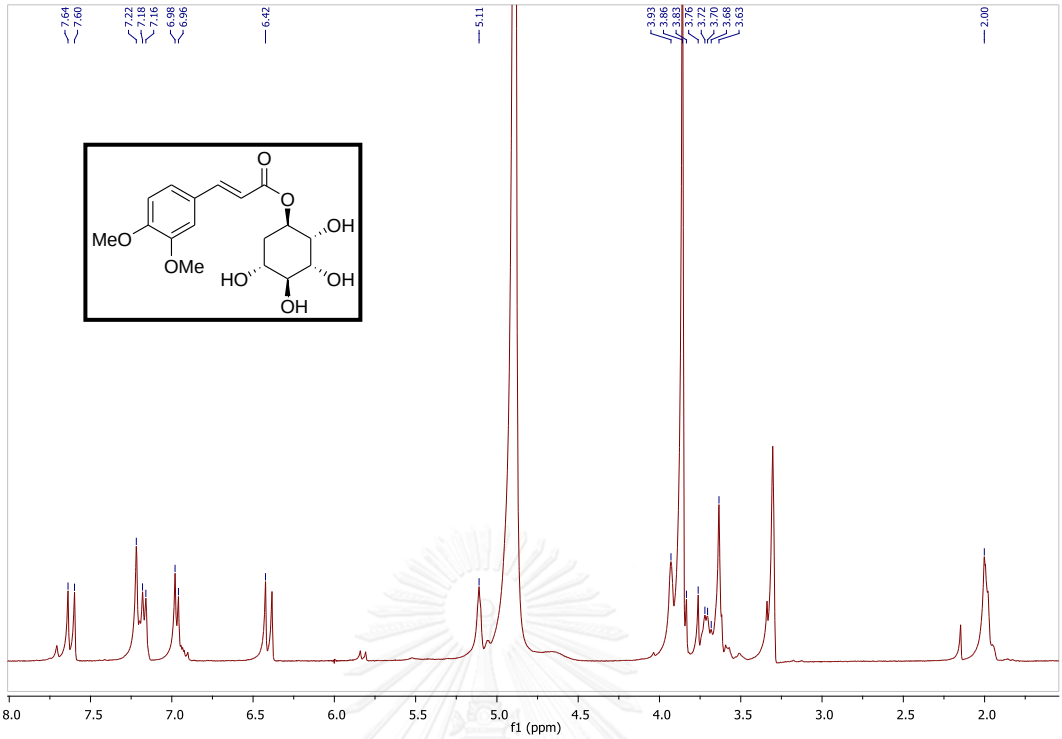

Figure A.7 ^{1}H NMR spectrum of **2.4ER (CD_3OD)**

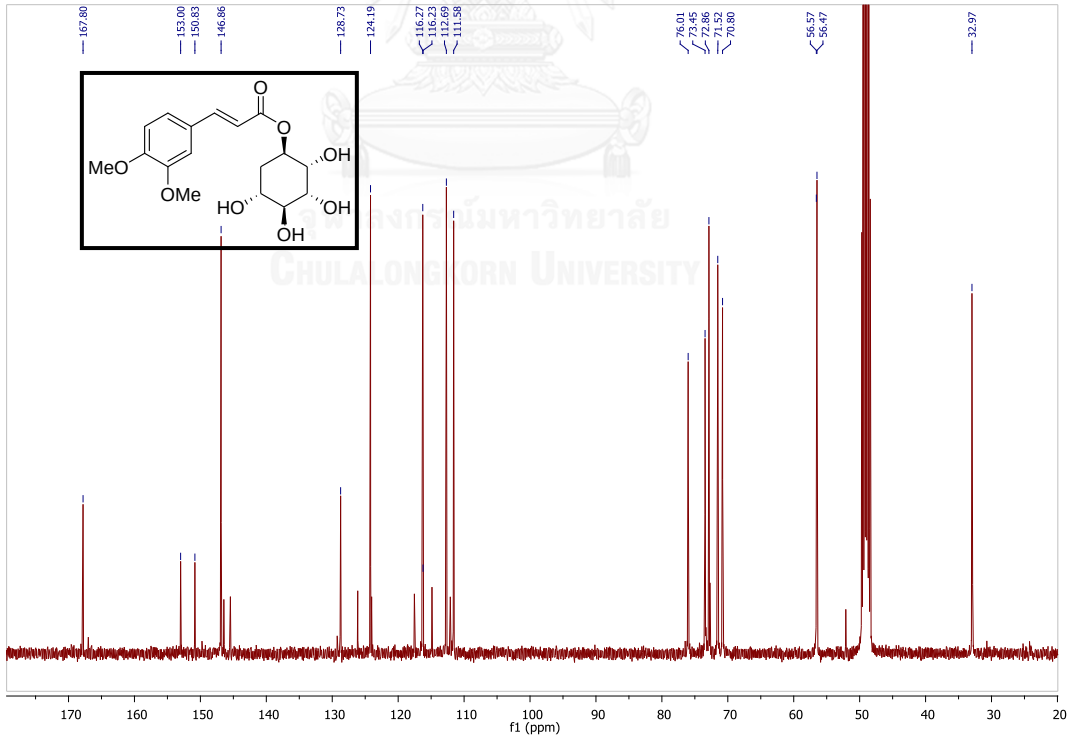

Figure A.8 ^{13}C NMR spectrum of **2.4ER (CD_3OD)**

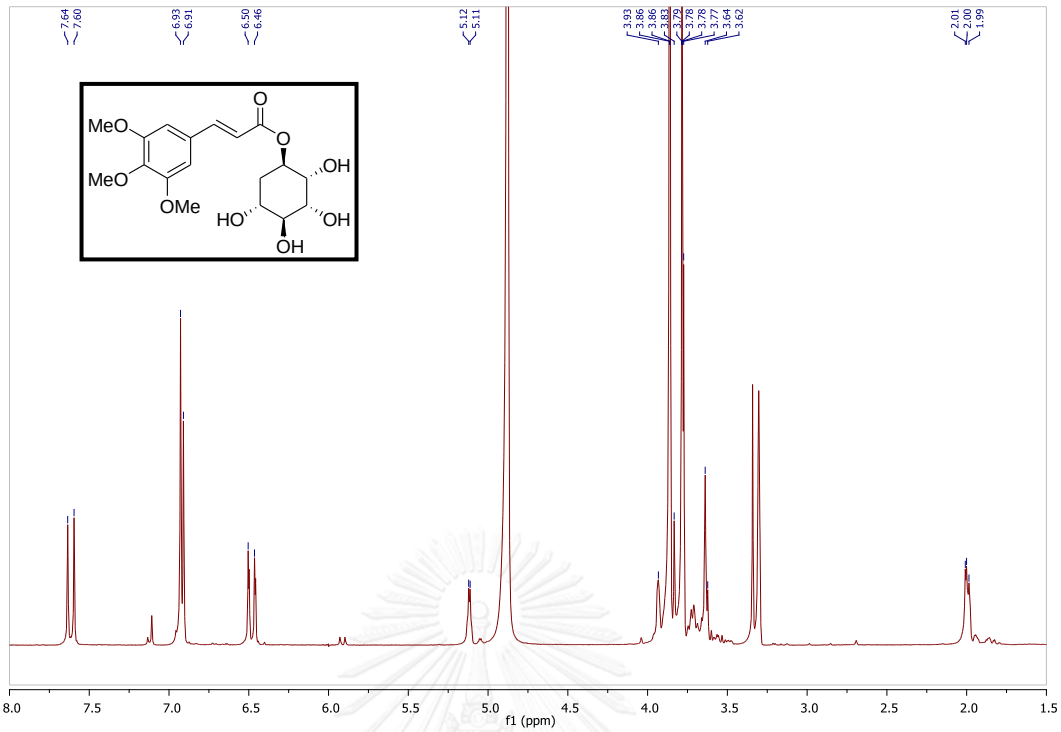

Figure A.9 ^{1}H NMR spectrum of **2.5ER (CD_3OD)**

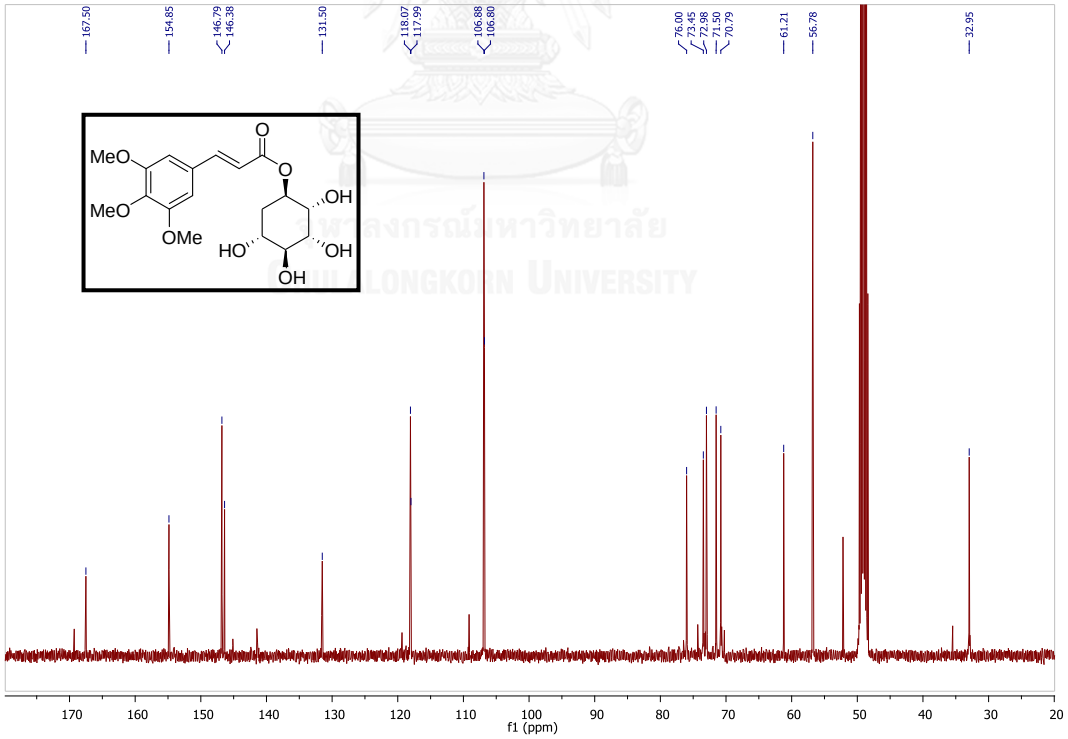

Figure A.10 ^{13}C NMR spectrum of **2.5ER (CD_3OD)**

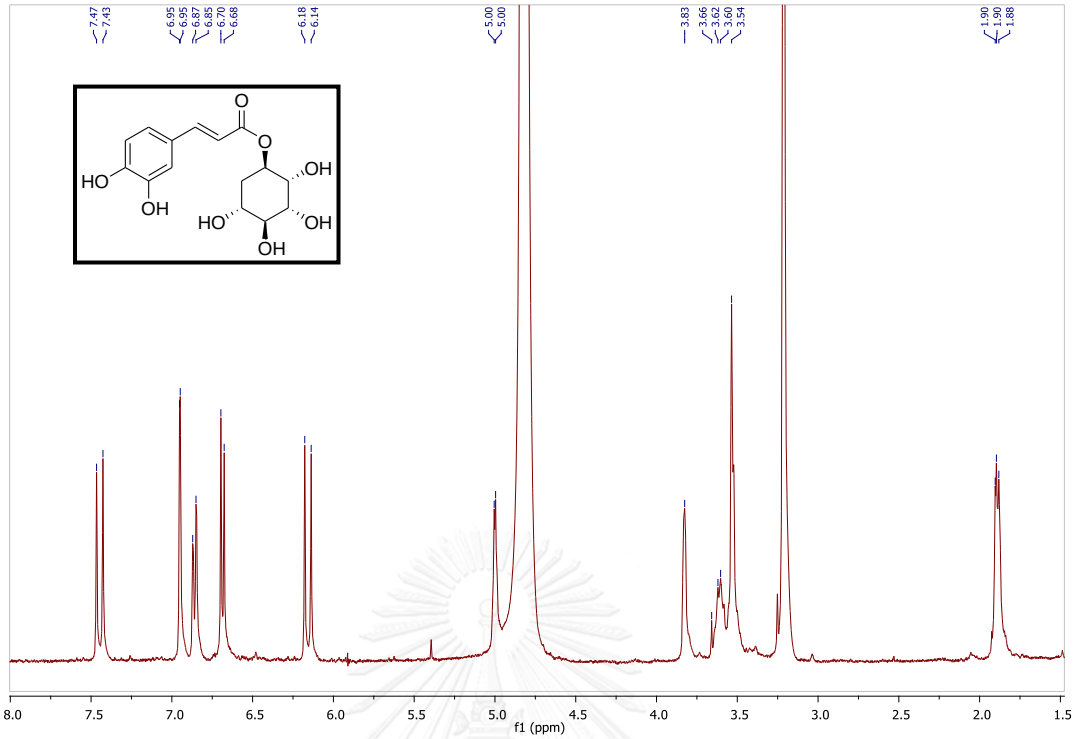

Figure A.11 ^{1}H NMR spectrum of **2.6ER (CD_3OD)**

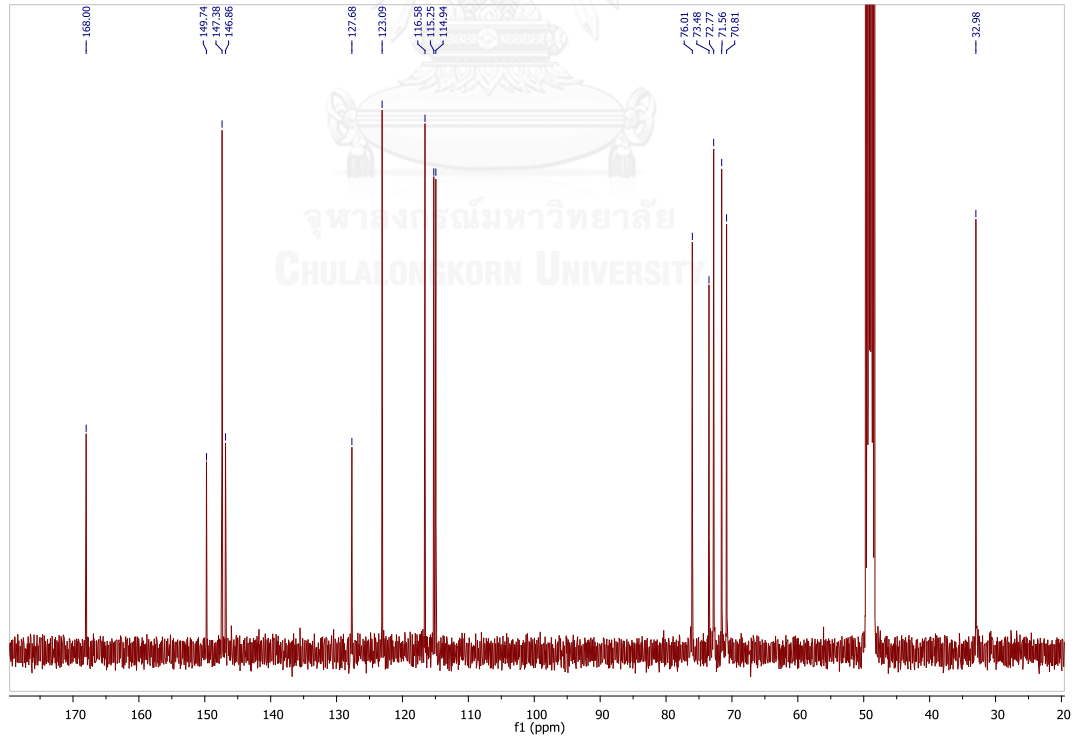

Figure A.12 ^{13}C NMR spectrum of **2.6ER (CD_3OD)**

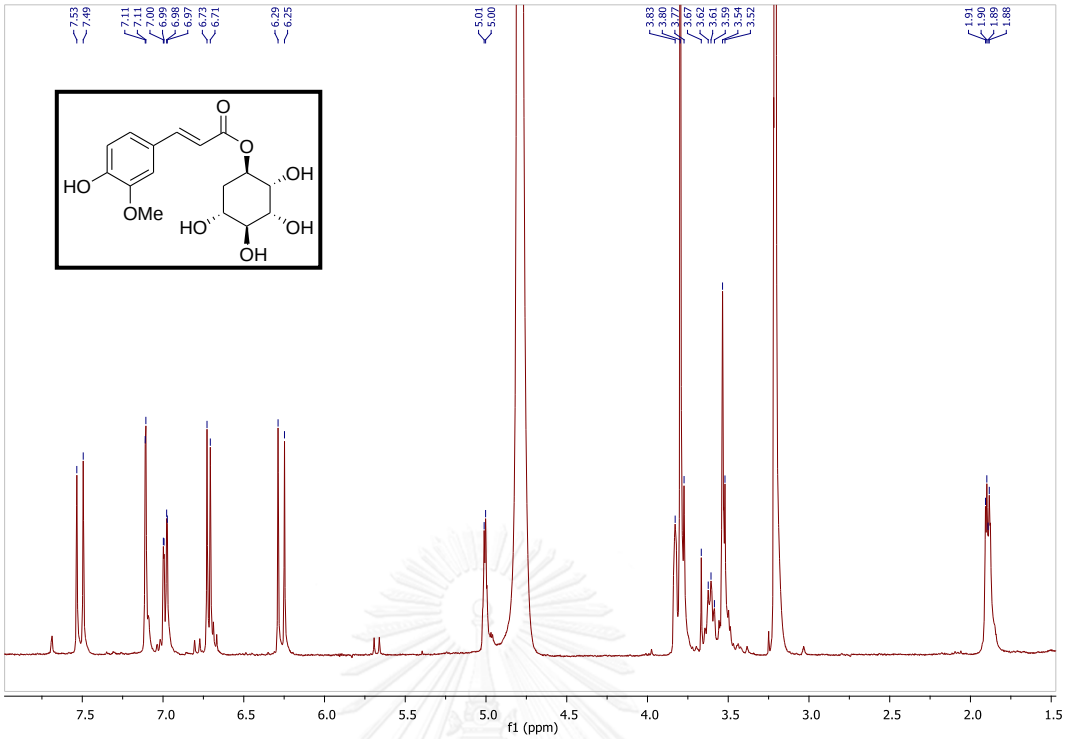

Figure A.13 ^{1}H NMR spectrum of **2.7ER (CD_3OD)**

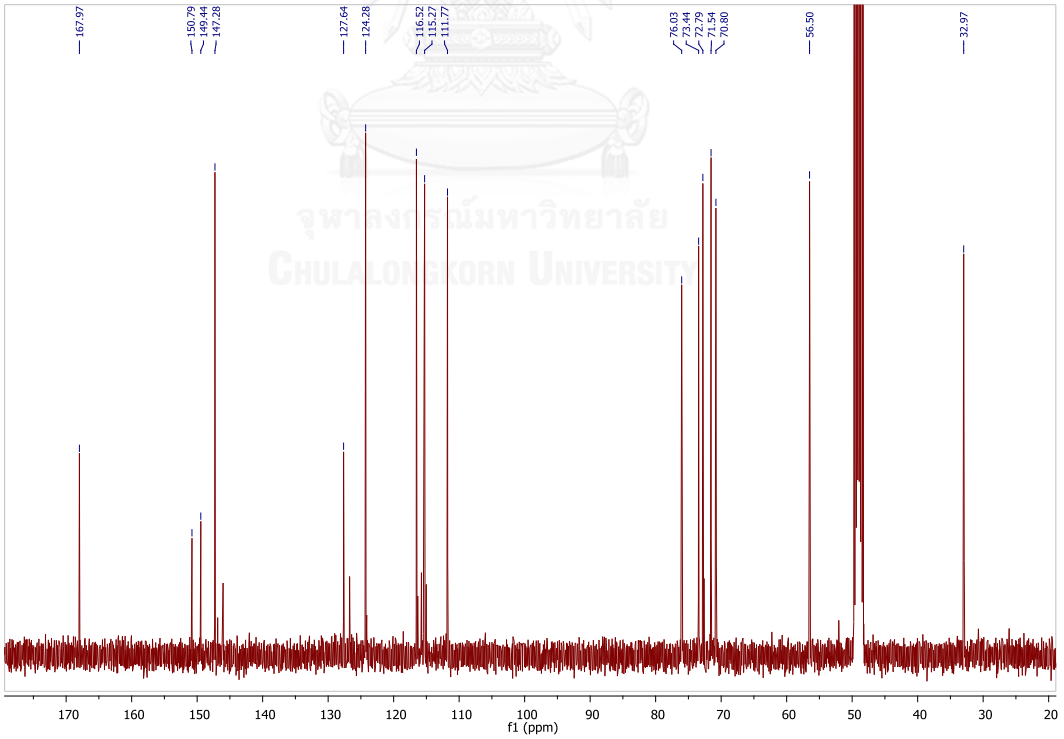

Figure A.14 ^{13}C NMR spectrum of **2.7ER (CD_3OD)**

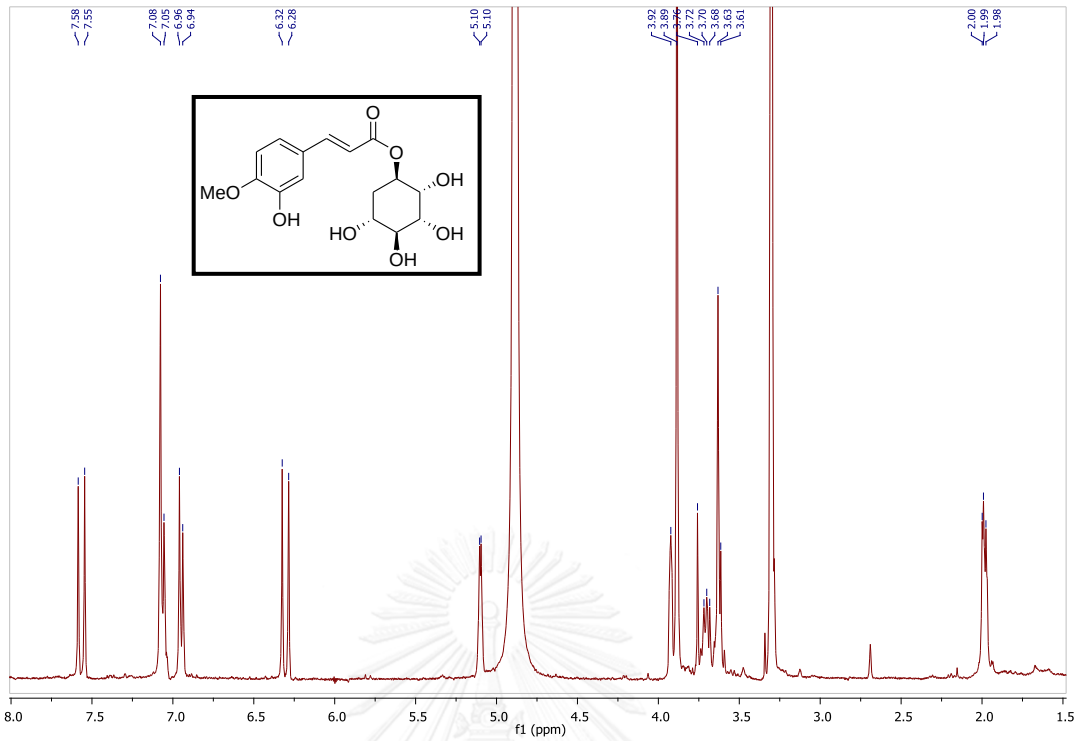

Figure A.15 ^{1}H NMR spectrum of **2.8ER (CD_3OD)**

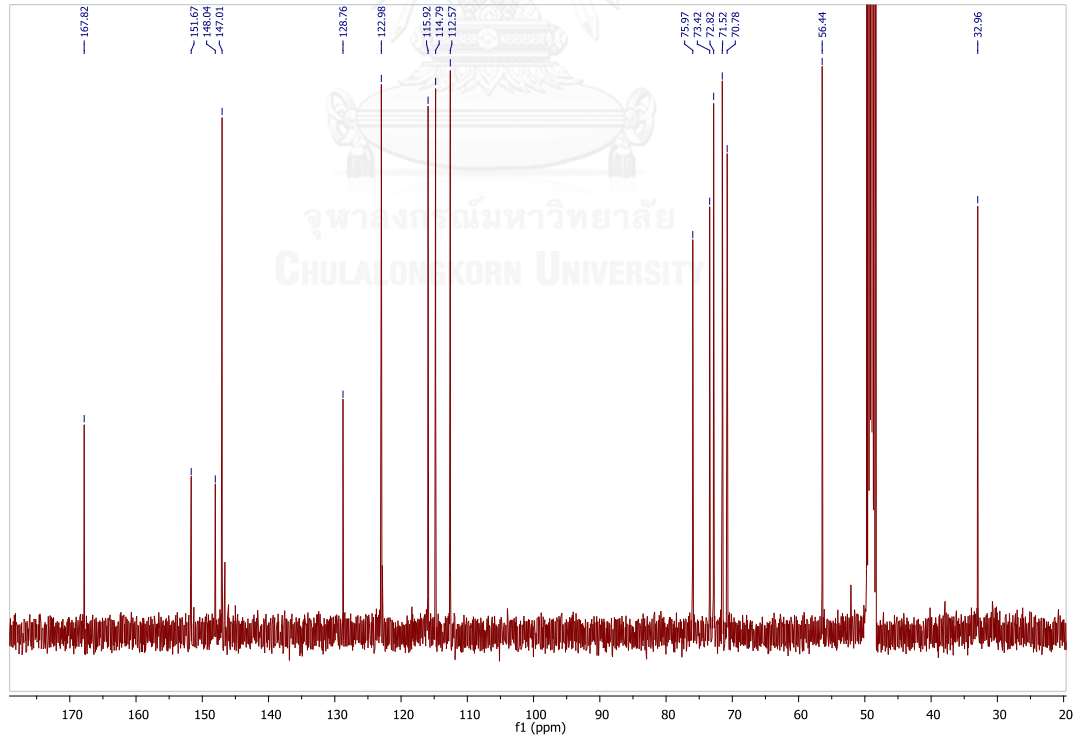

Figure A.16 ^{13}C NMR spectrum of **2.8ER (CD_3OD)**

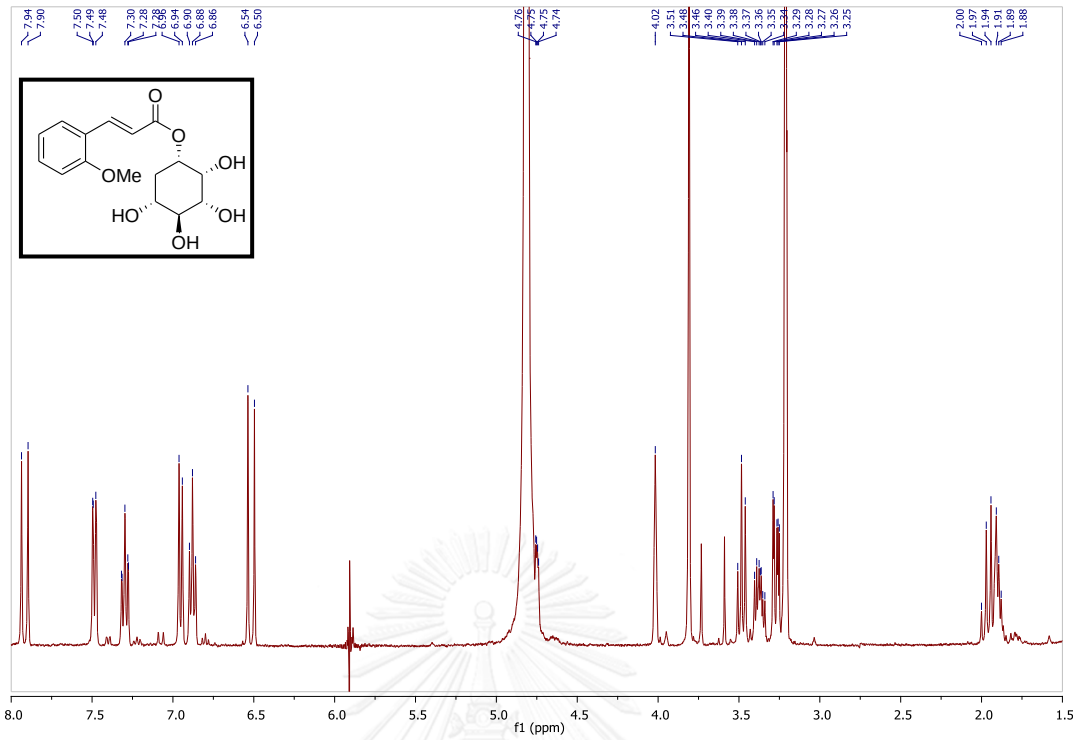

Figure A.17 ^{1}H NMR spectrum of **2.1ES (CD_3OD)**

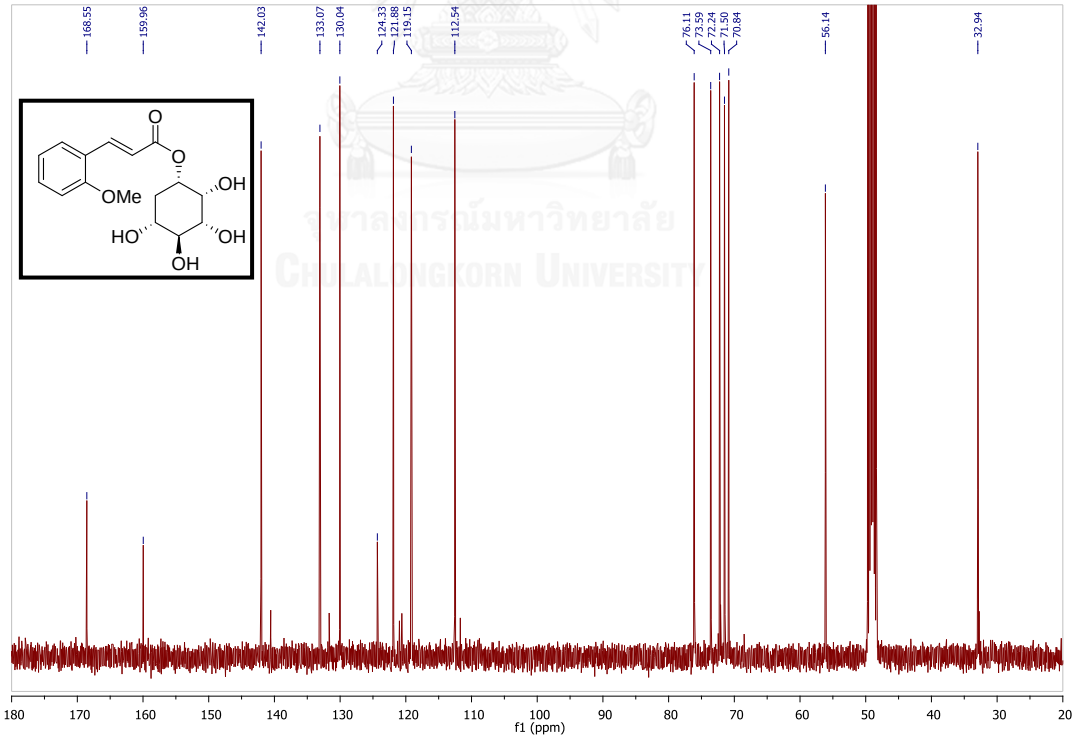

Figure A.18 ^{13}C NMR spectrum of **2.1ES (CD_3OD)**

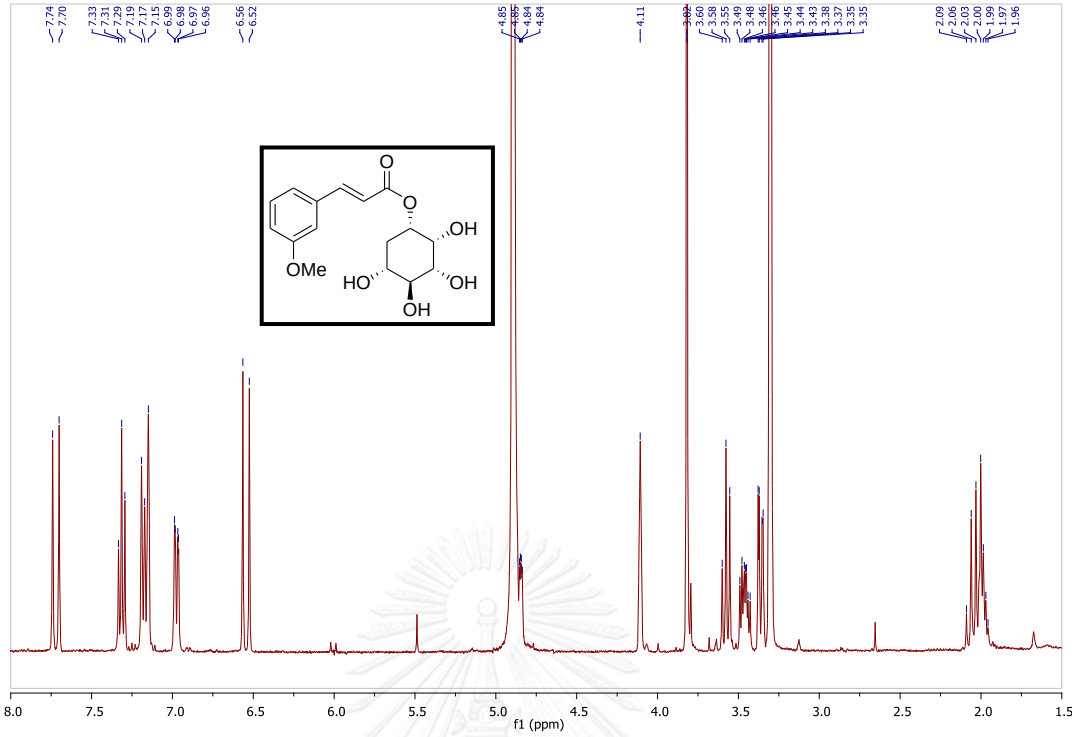

Figure A.19 ^{1}H NMR spectrum of **2.2ES (CD_3OD)**

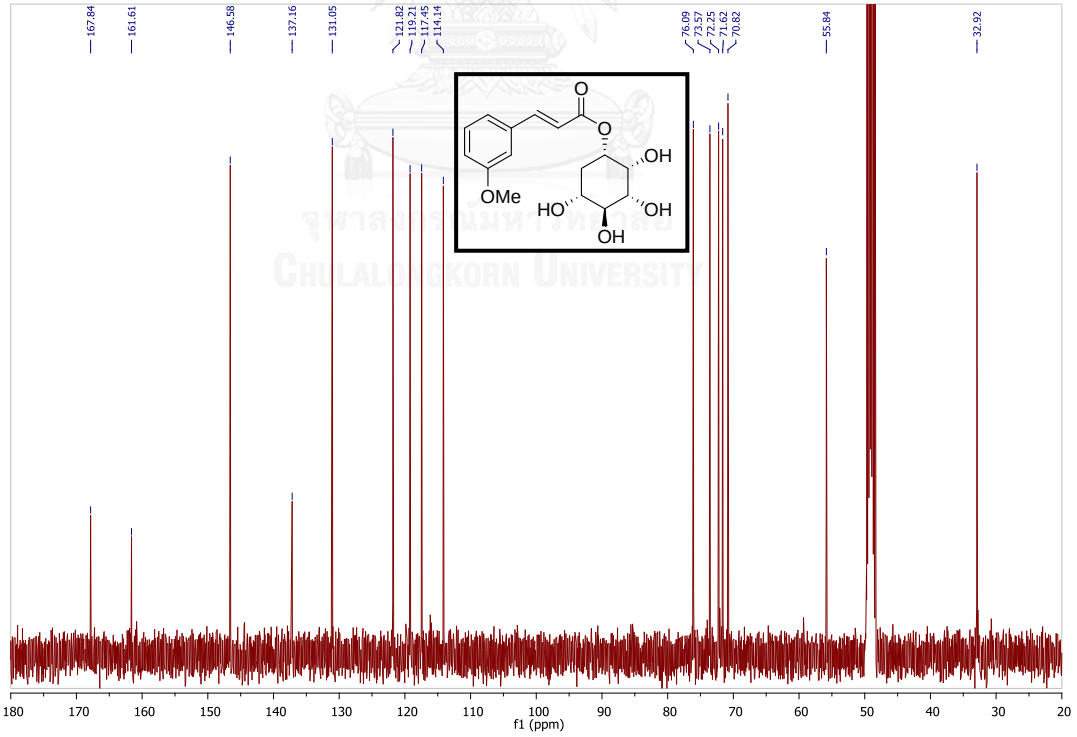

Figure A.20 ^{13}C NMR spectrum of **2.2ES (CD_3OD)**

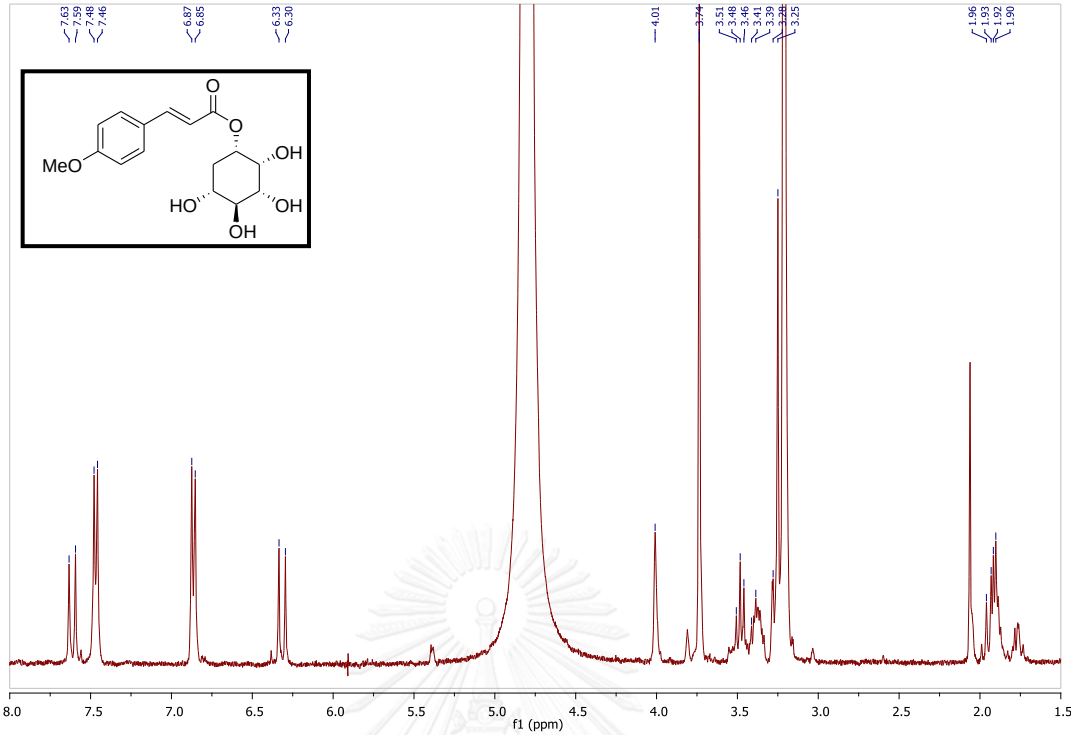

Figure A.21 ^{1}H NMR spectrum of **2.3ES (CD_3OD)**

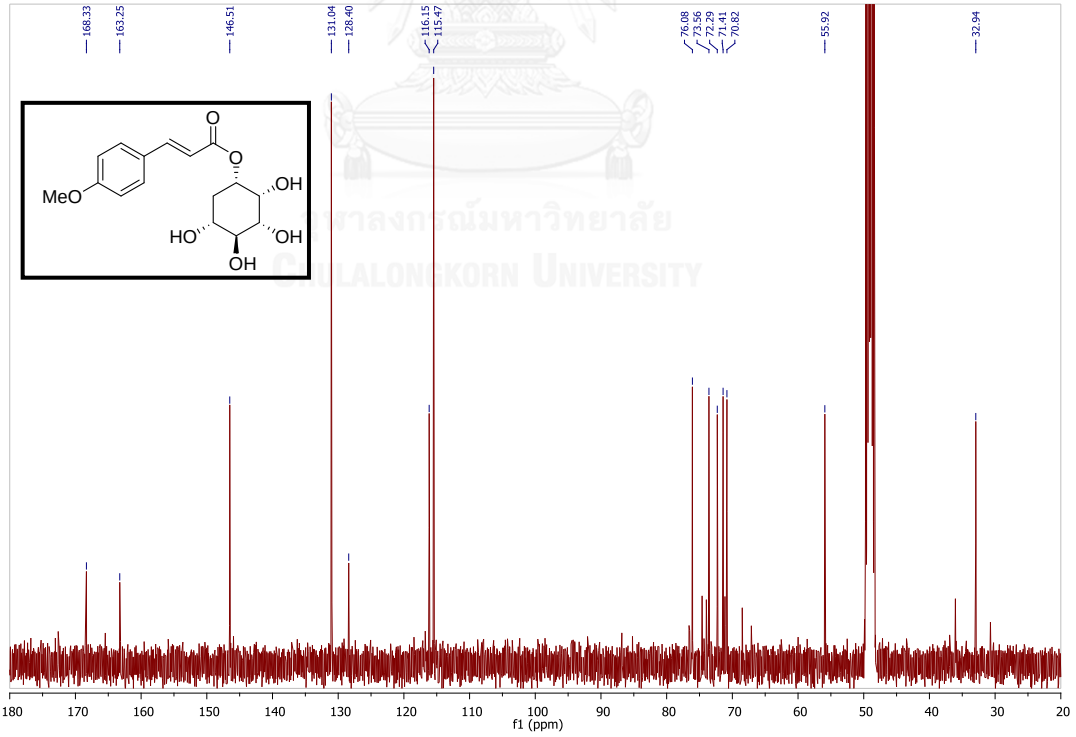

Figure A.22 ^{13}C NMR spectrum of **2.3ES (CD_3OD)**

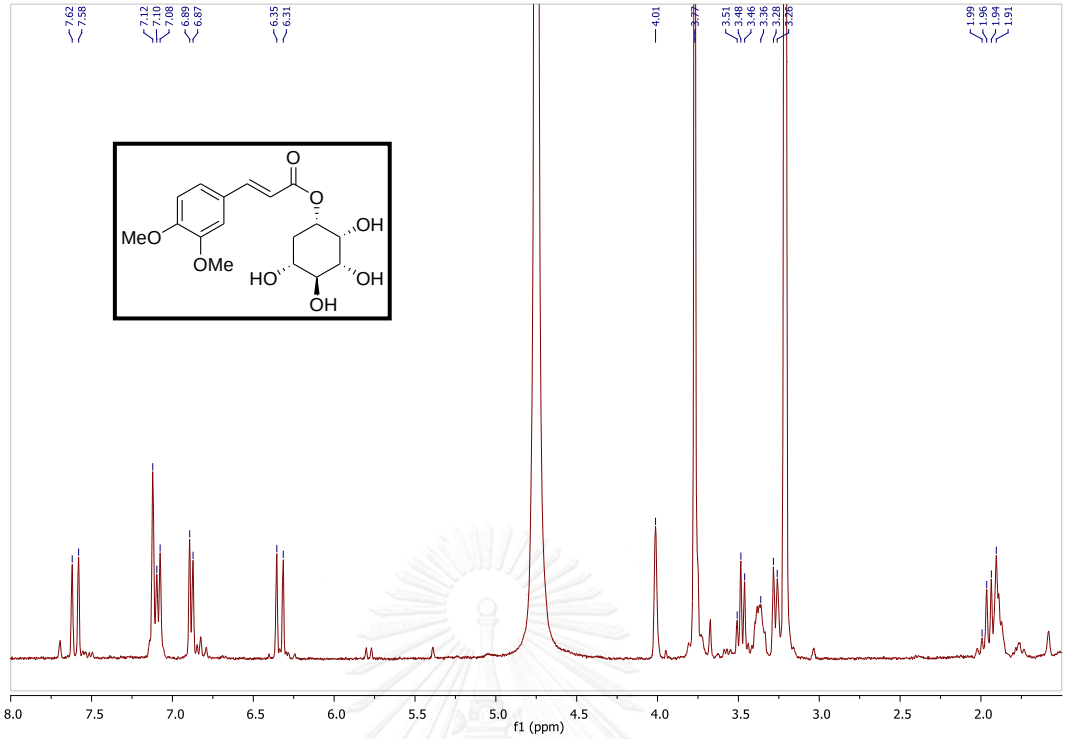

Figure A.23 ^{1}H NMR spectrum of **2.4ES (CD_3OD)**

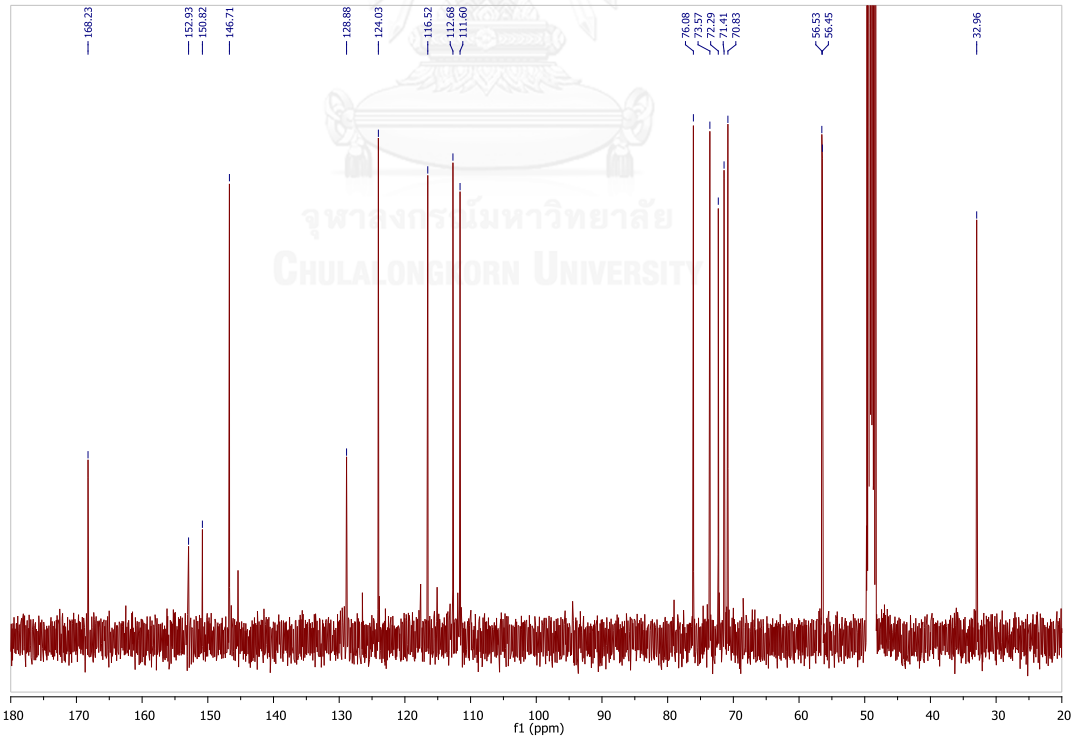

Figure A.24 ^{13}C NMR spectrum of **2.4ES (CD_3OD)**

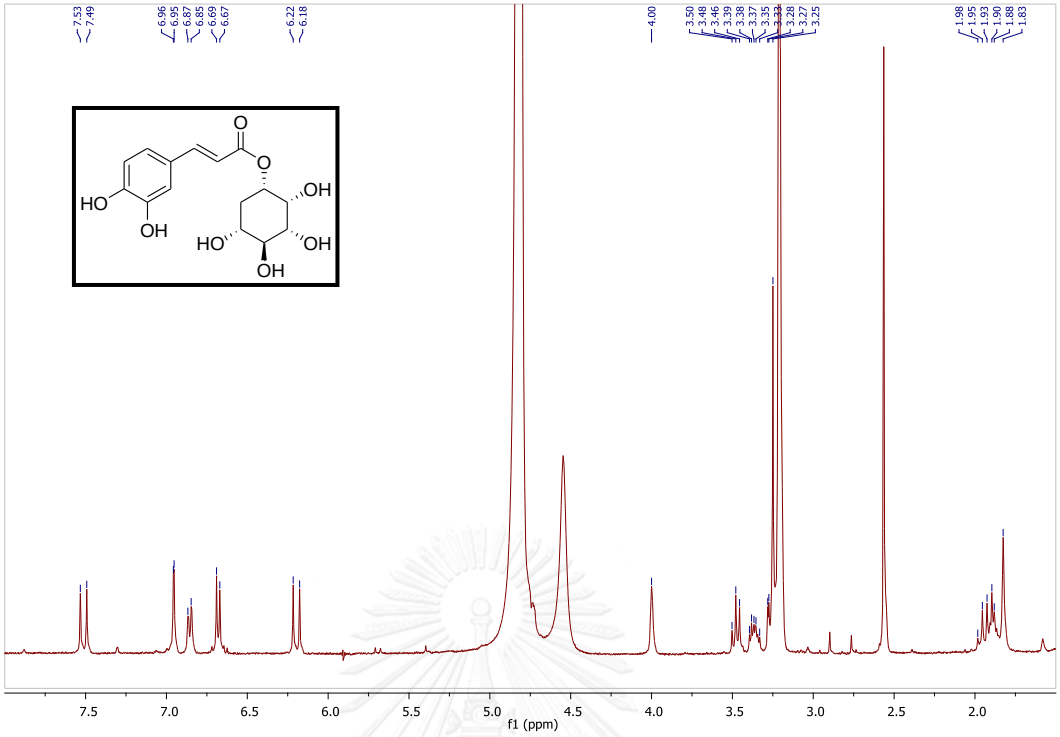

Figure A.25 ^{1}H NMR spectrum of **2.6ES (CD_3OD)**

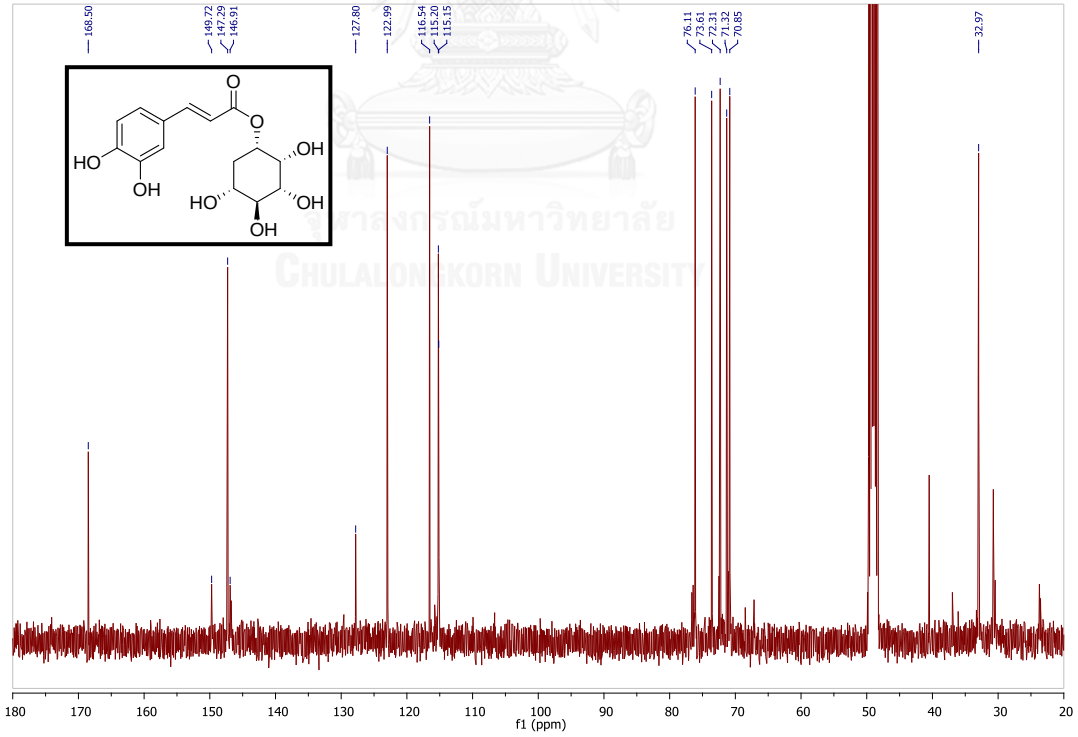

Figure A.26 ^{13}C NMR spectrum of **2.6ES (CD_3OD)**

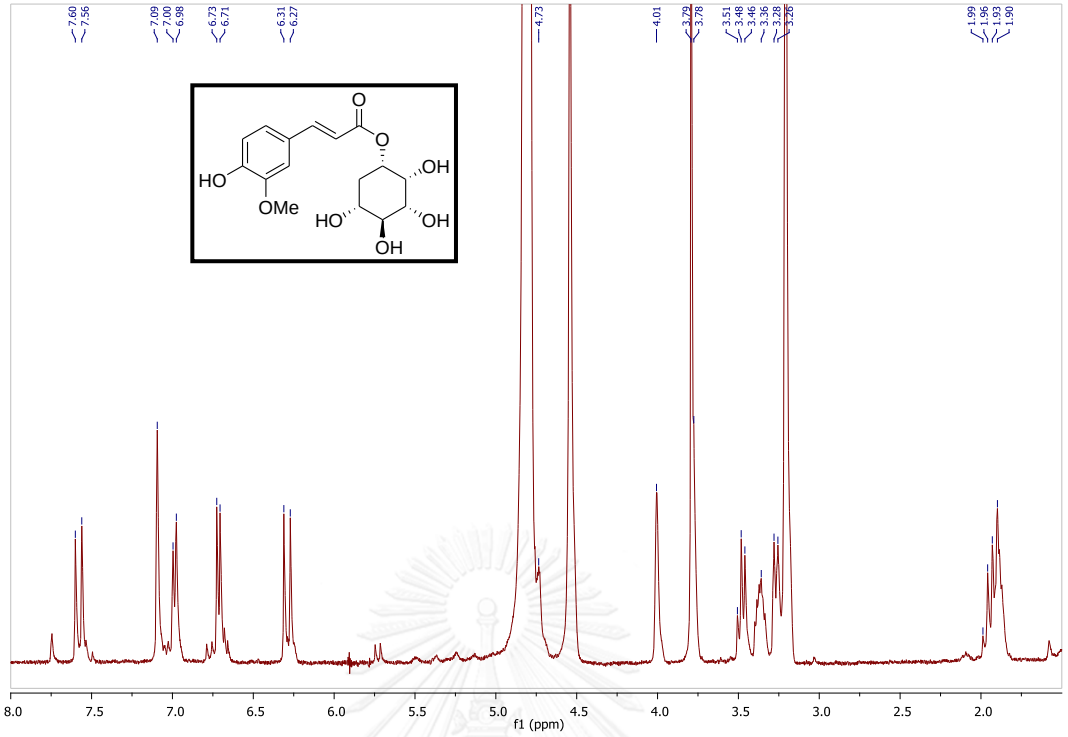

Figure A.27 ^{1}H NMR spectrum of **2.7ES (CD_3OD)**

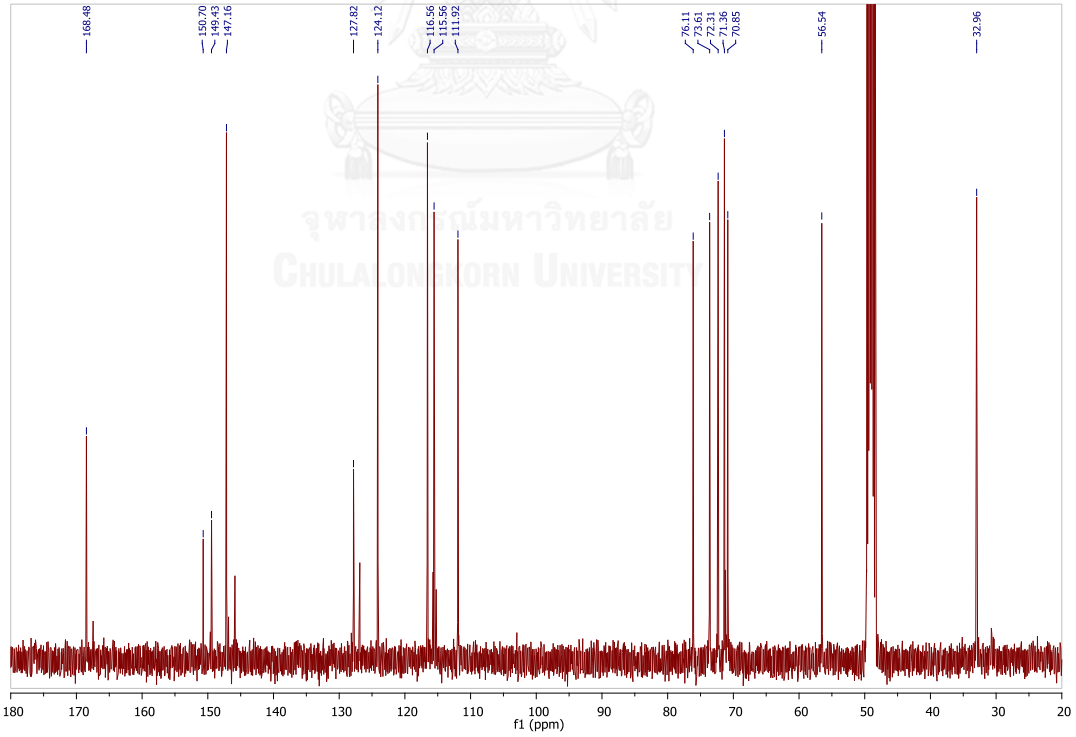

Figure A.28 ^{13}C NMR spectrum of **2.7ES (CD_3OD)**

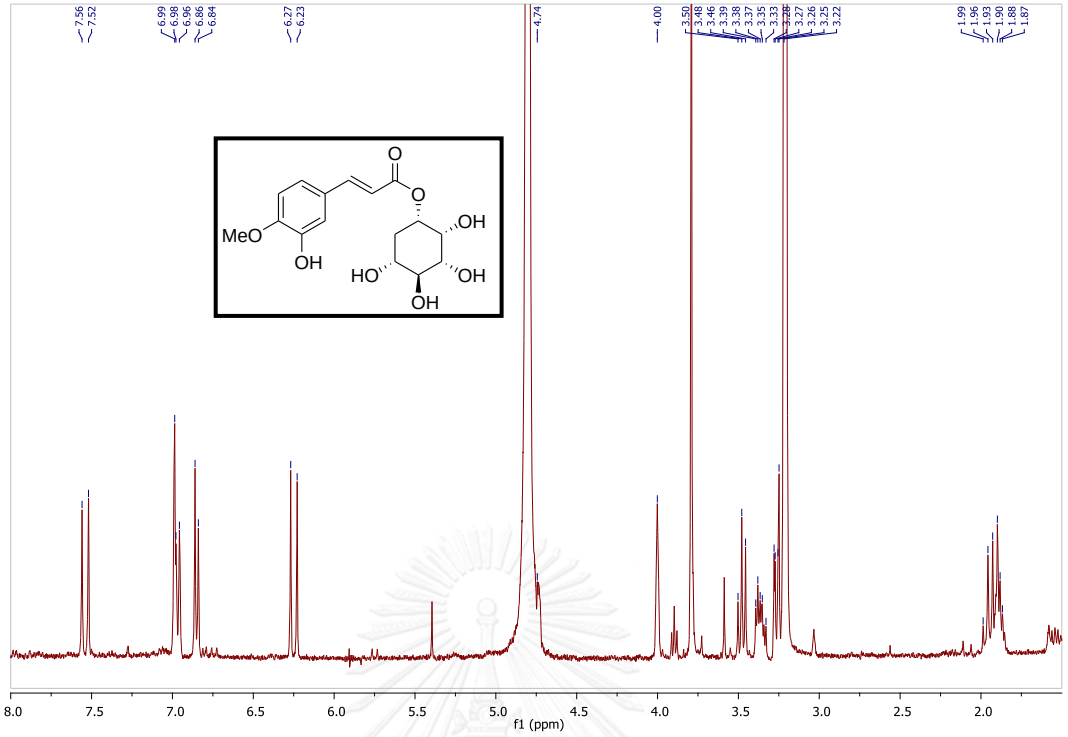

Figure A.29 ^{1}H NMR spectrum of **2.8ES (CD_3OD)**

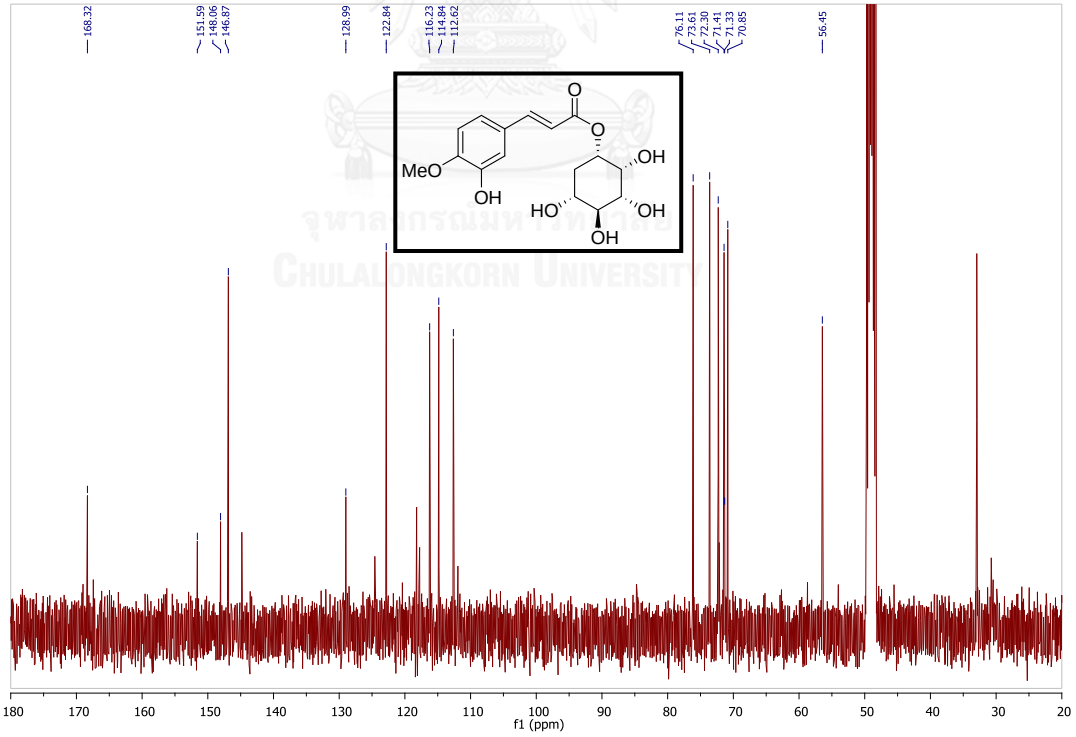

Figure A.30 ^{13}C NMR spectrum of **2.8ES (CD_3OD)**

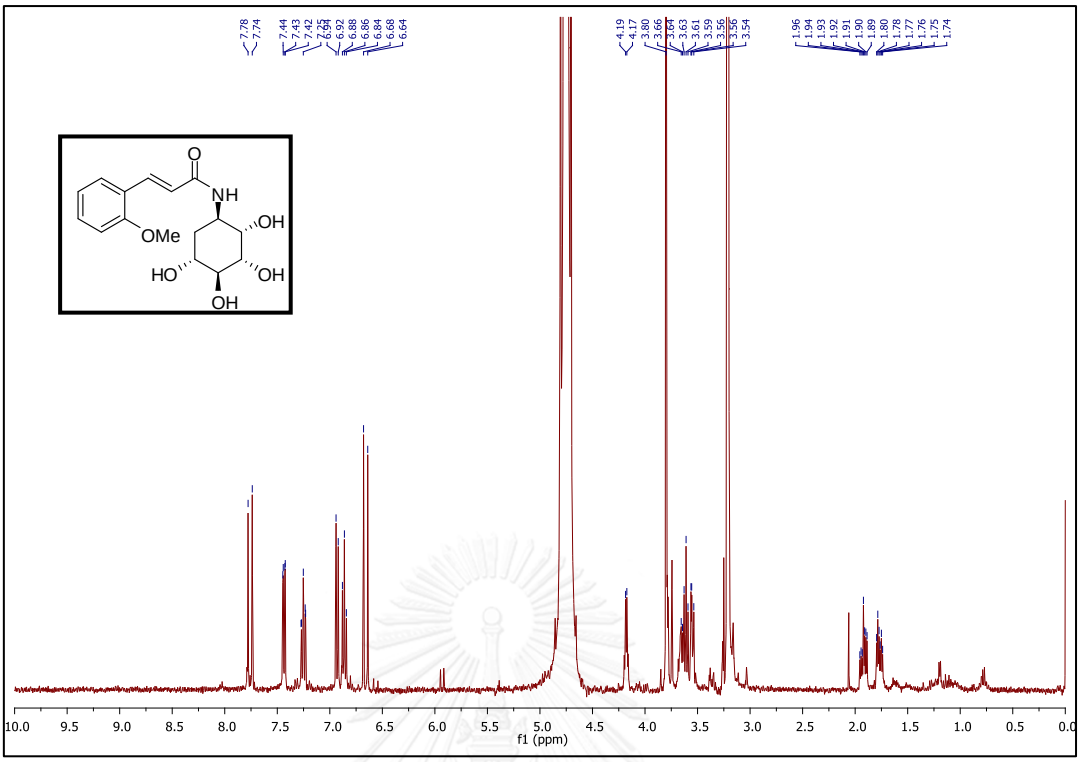

Figure A.31 ^{1}H NMR spectrum of **2.1AR (CD_3OD)**

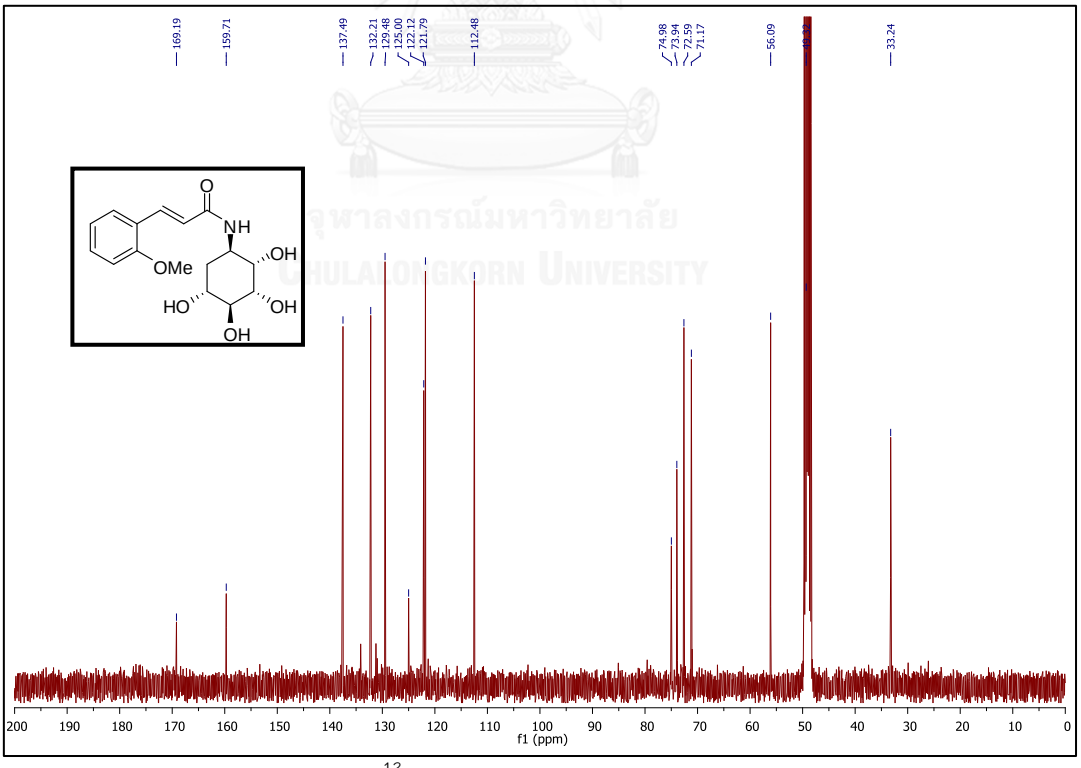

Figure A.32 ^{13}C NMR spectrum of **2.1AR (CD_3OD)**

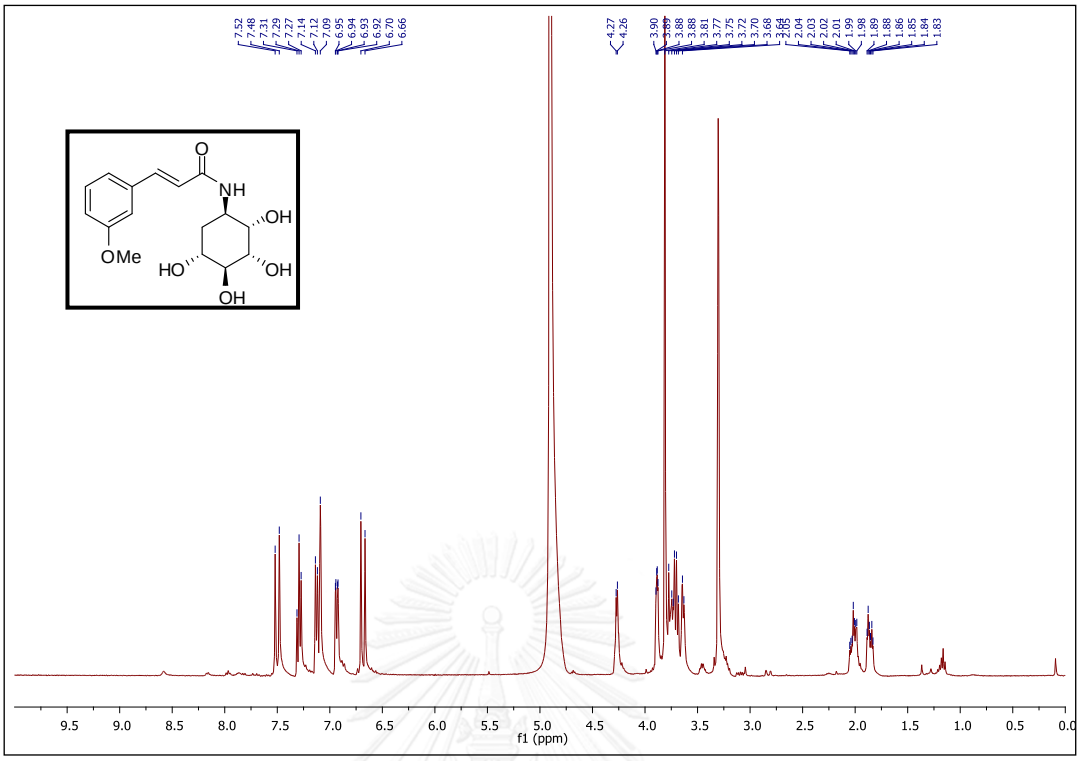

Figure A.33 ^{1}H NMR spectrum of **2.2AR (CD_3OD)**

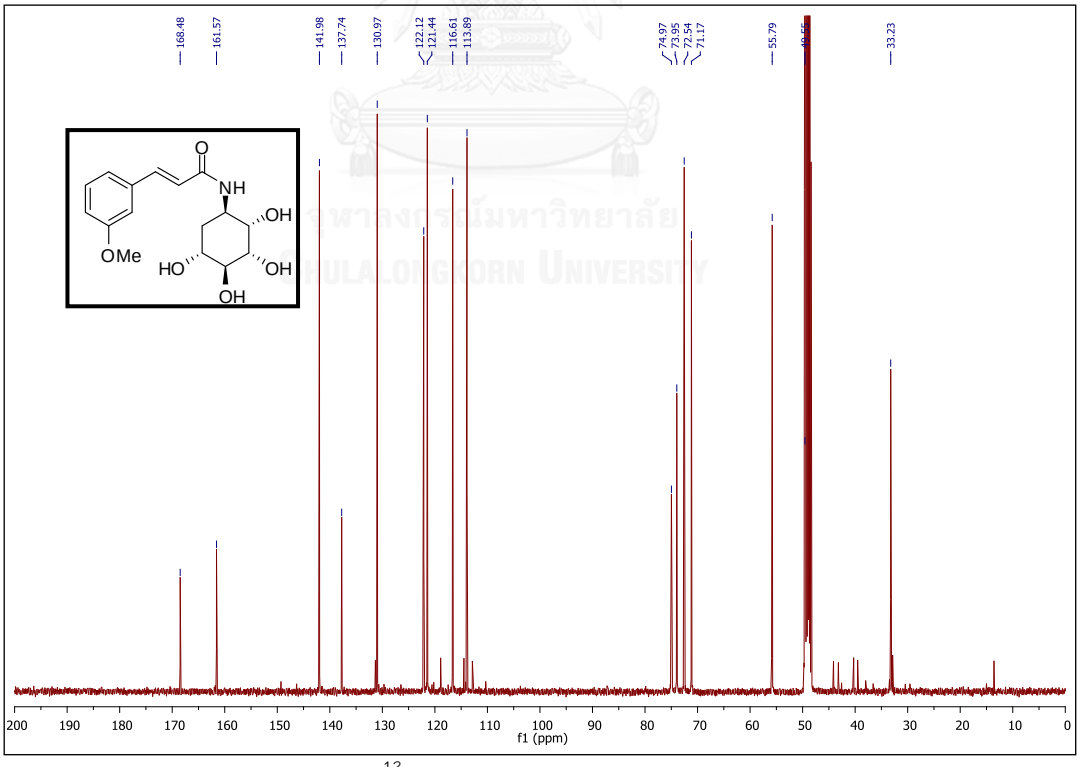

Figure A.34 ^{13}C NMR spectrum of **2.2AR (CD_3OD)**

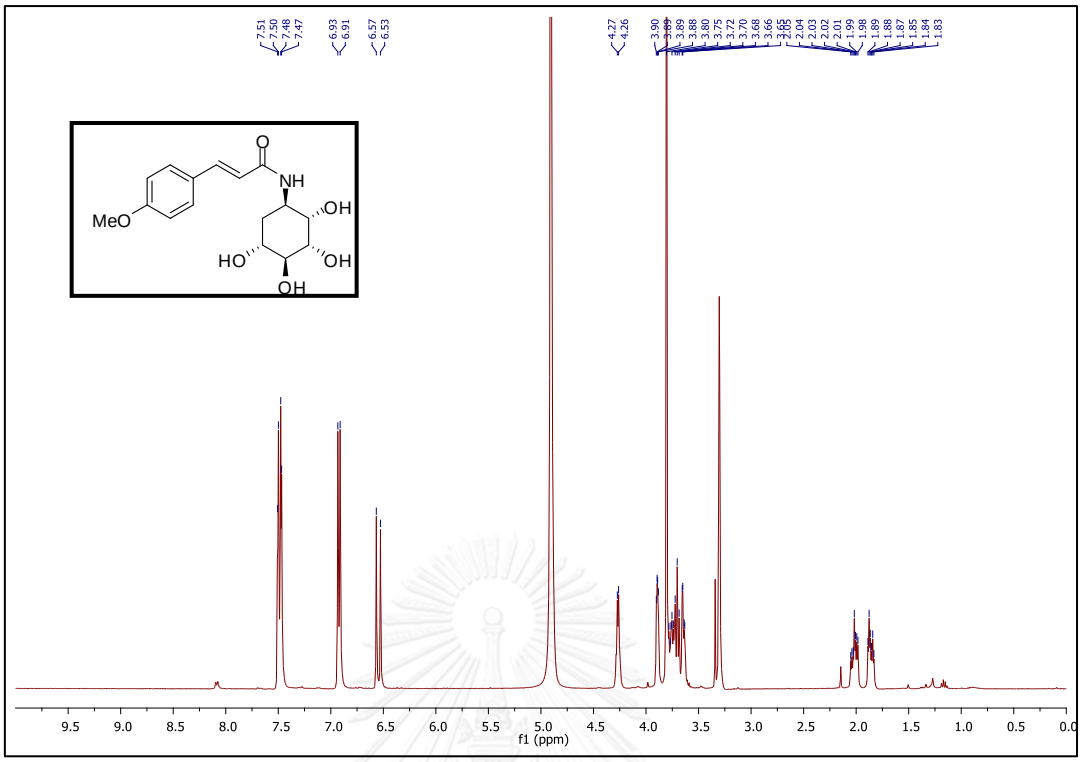

Figure A.35 ^{1}H NMR spectrum of **2.3AR (CD_3OD)**

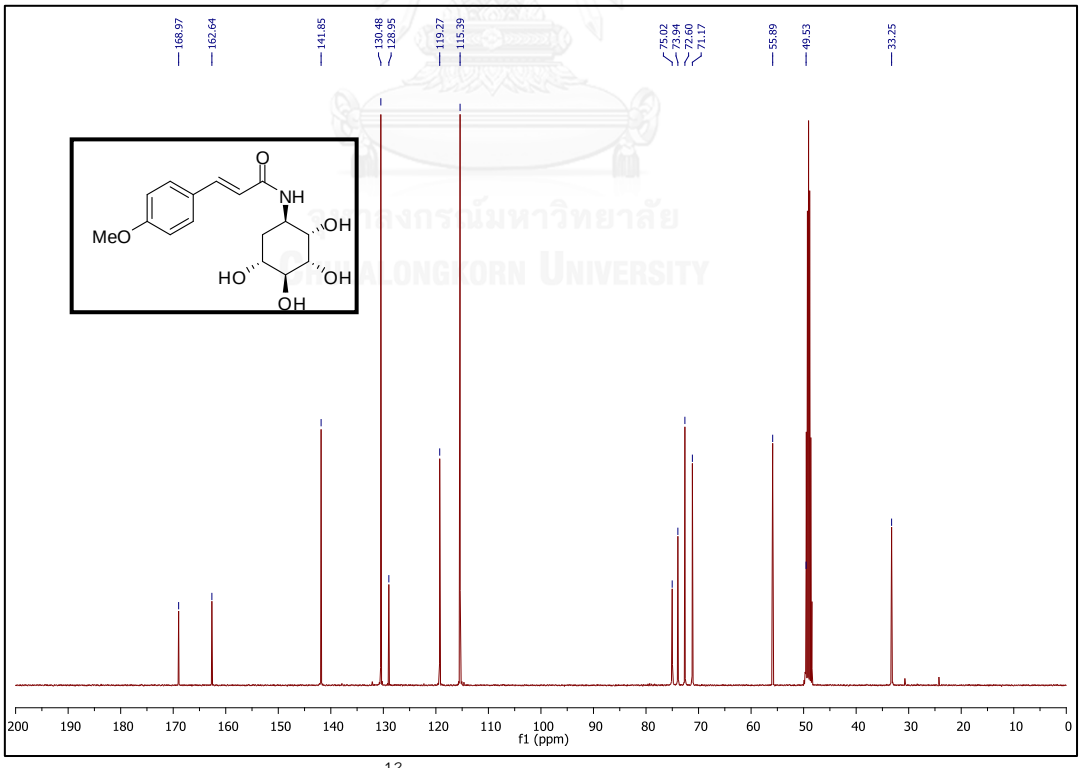

Figure A.36 ^{13}C NMR spectrum of **2.3AR (CD_3OD)**

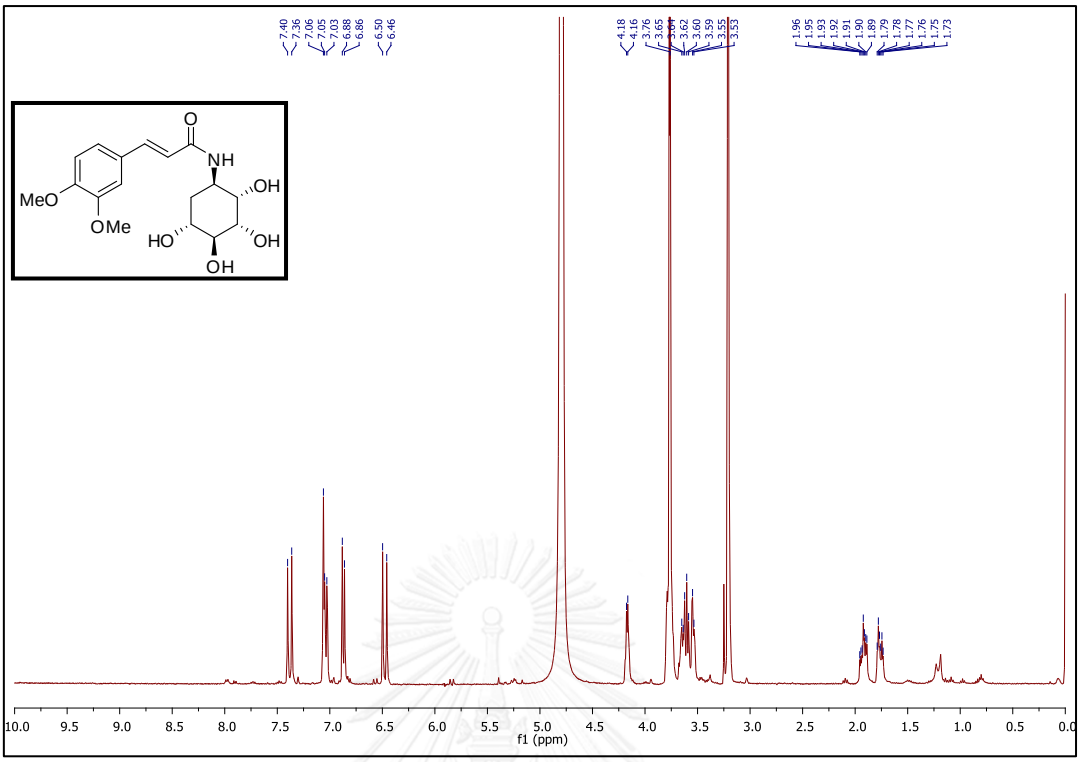

Figure A.37 ^{1}H NMR spectrum of **2.4AR (CD_3OD)**

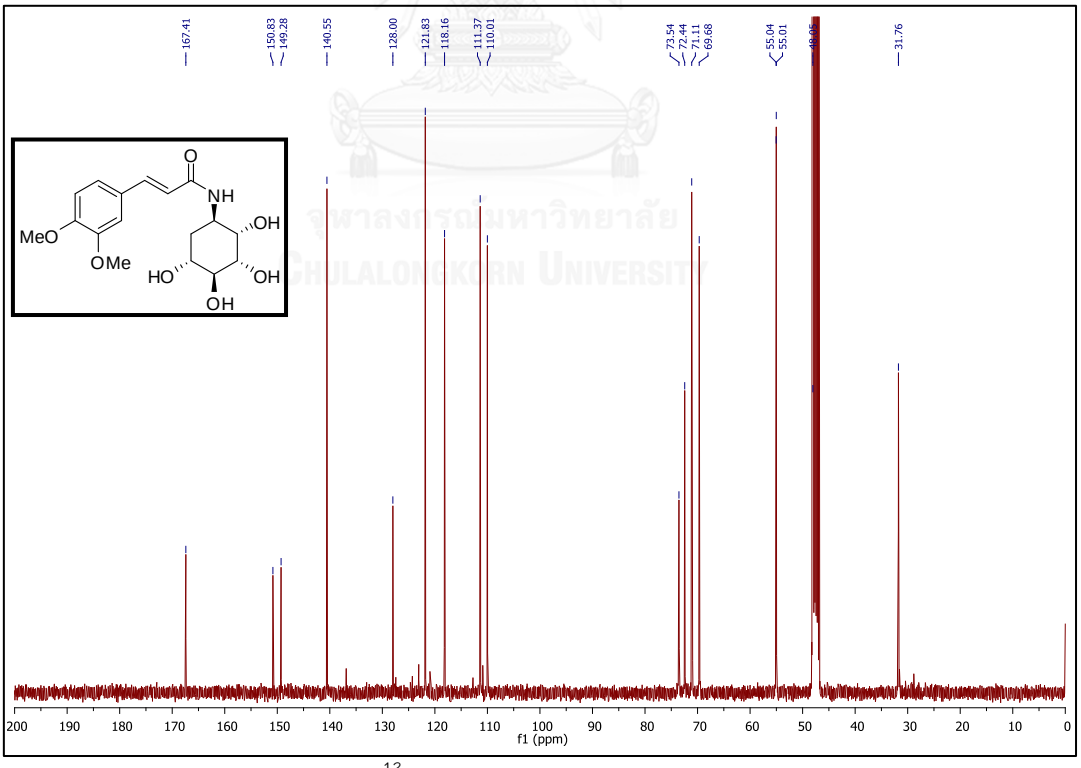

Figure A.38 ^{13}C NMR spectrum of **2.4AR (CD_3OD)**

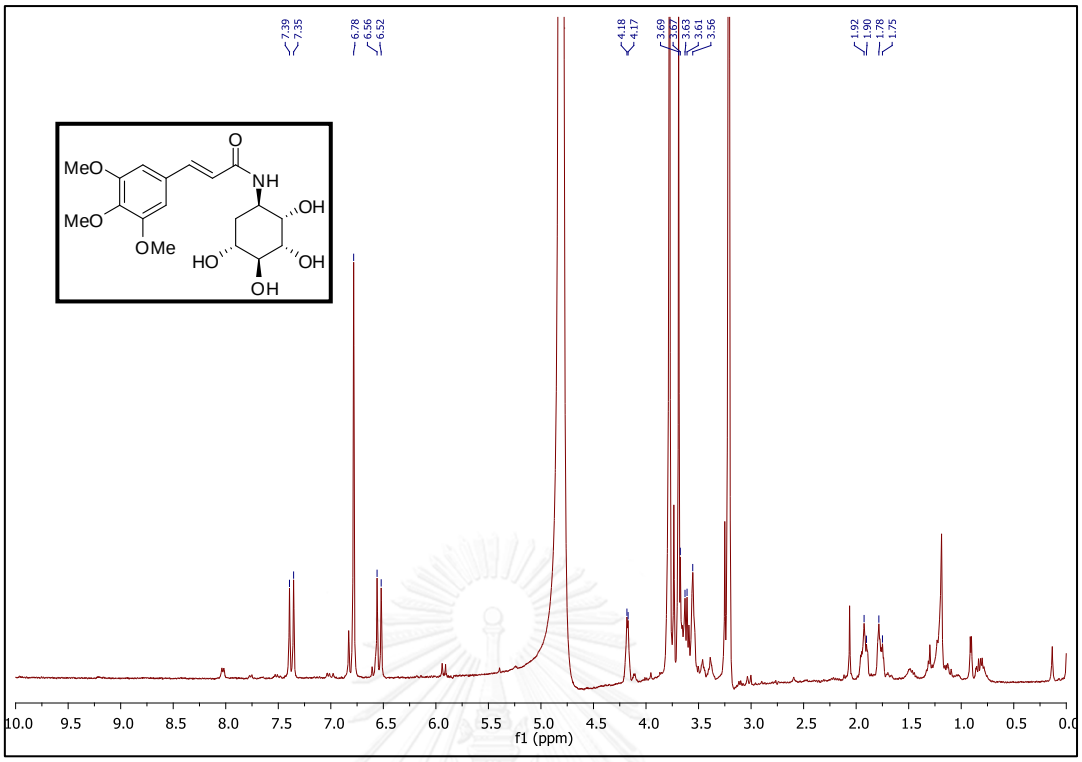

Figure A.39 ^{1}H NMR spectrum of **2.5AR (CD_3OD)**

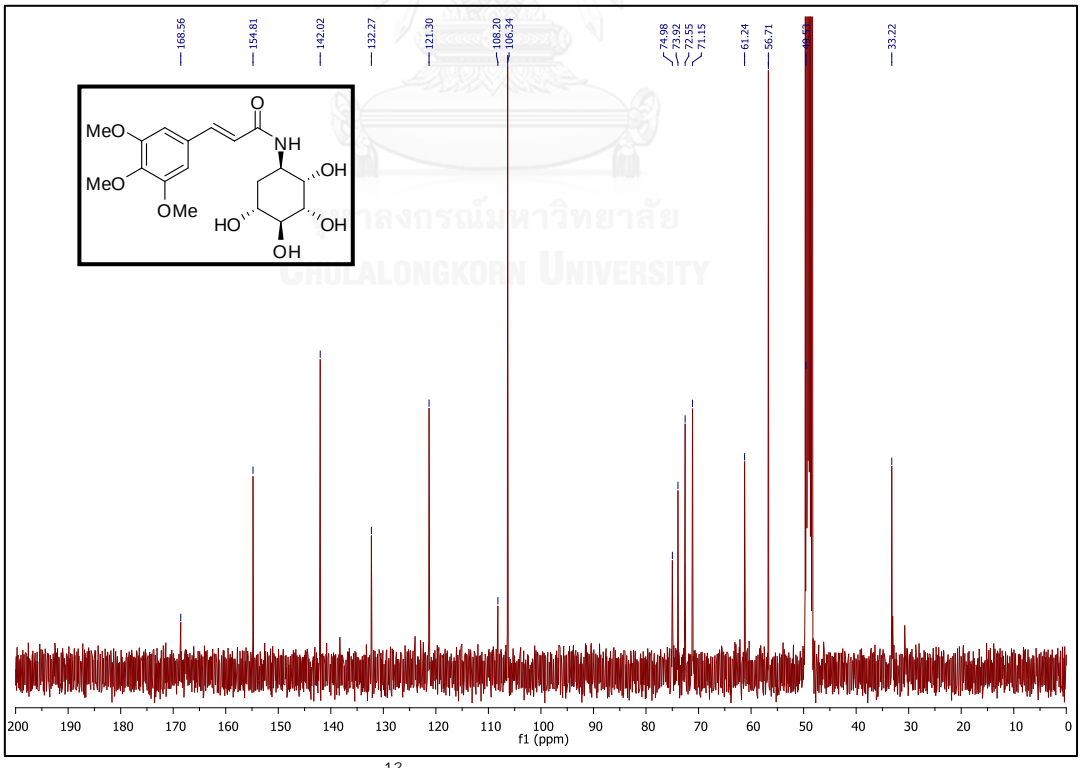

Figure A.40 ^{13}C NMR spectrum of **2.5AR (CD_3OD)**

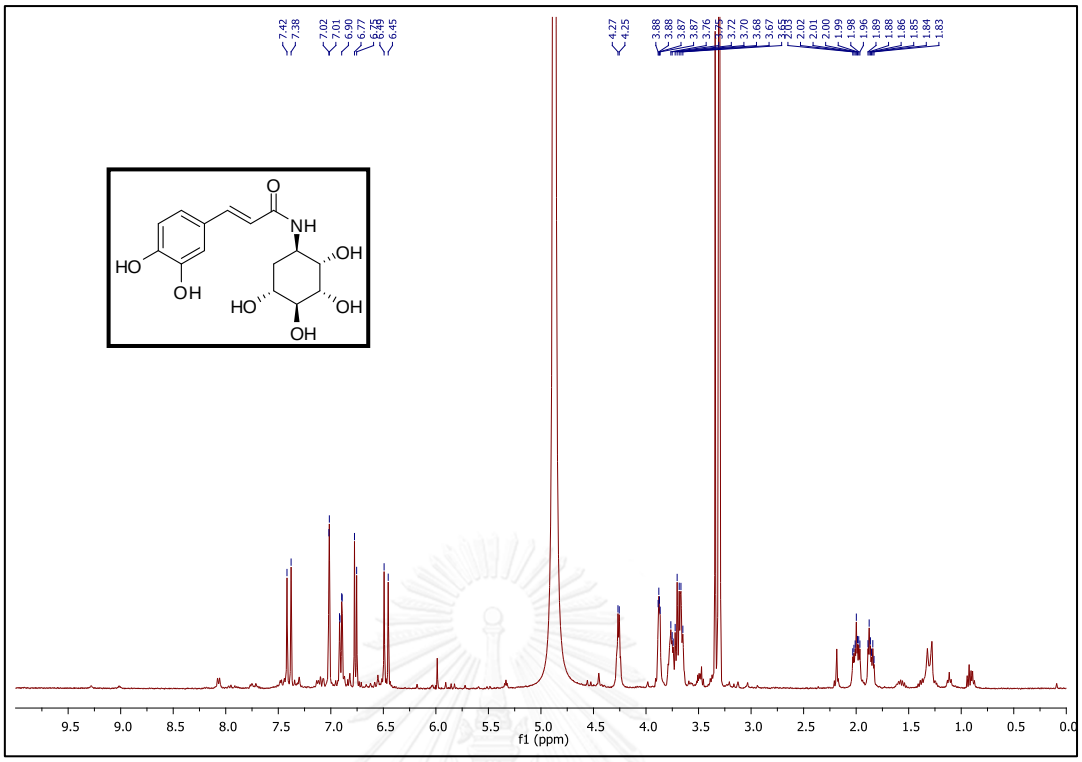

Figure A.41 ^{1}H NMR spectrum of **2.6AR (CD_3OD)**

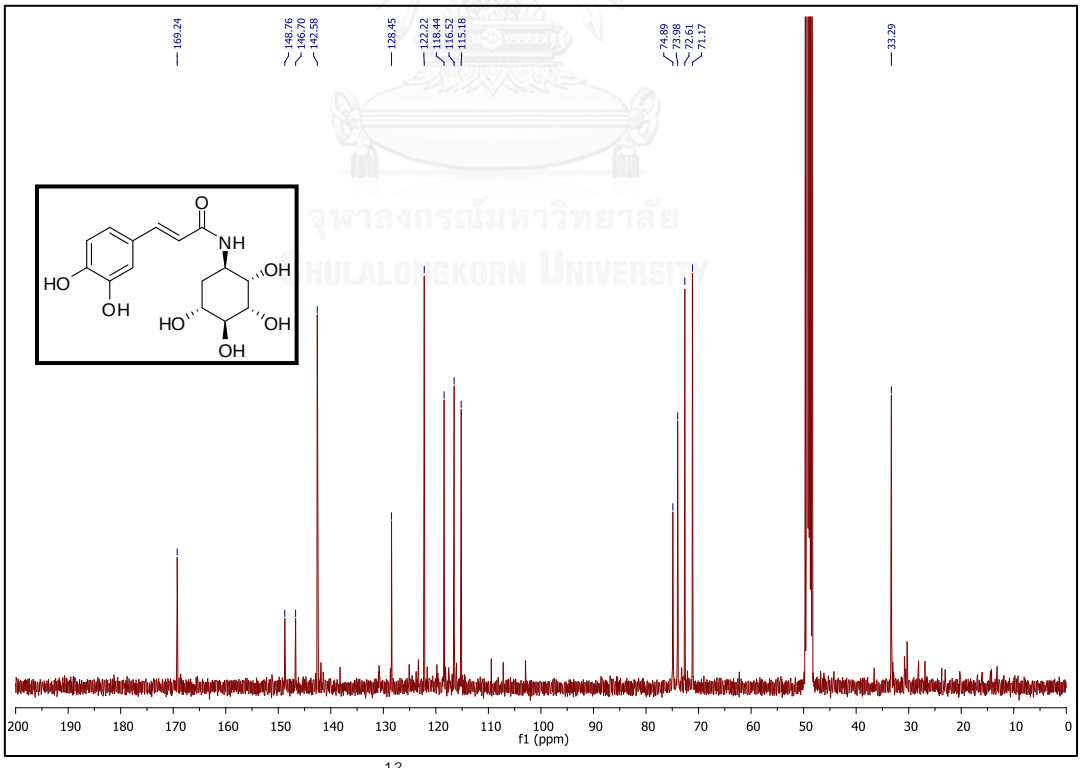

Figure A.42 ^{13}C NMR spectrum of **2.6AR (CD_3OD)**

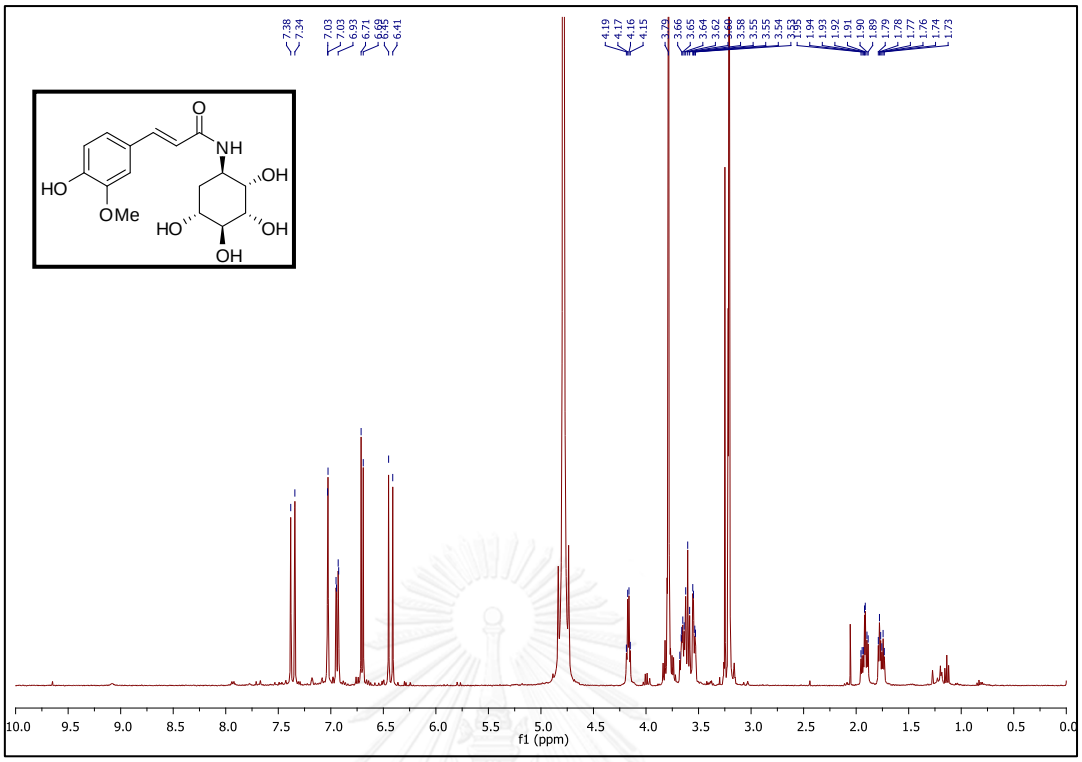

Figure A.43 ^{1}H NMR spectrum of **2.7AR (CD_3OD)**

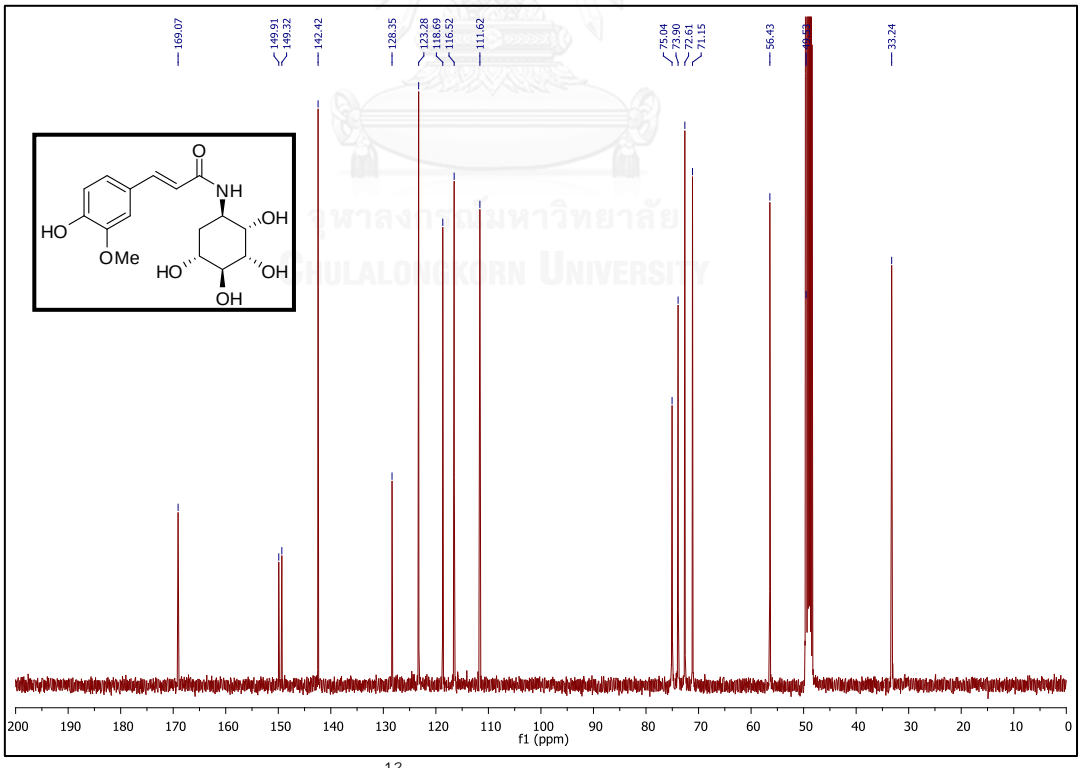

Figure A.44 ^{13}C NMR spectrum of **2.7AR (CD_3OD)**

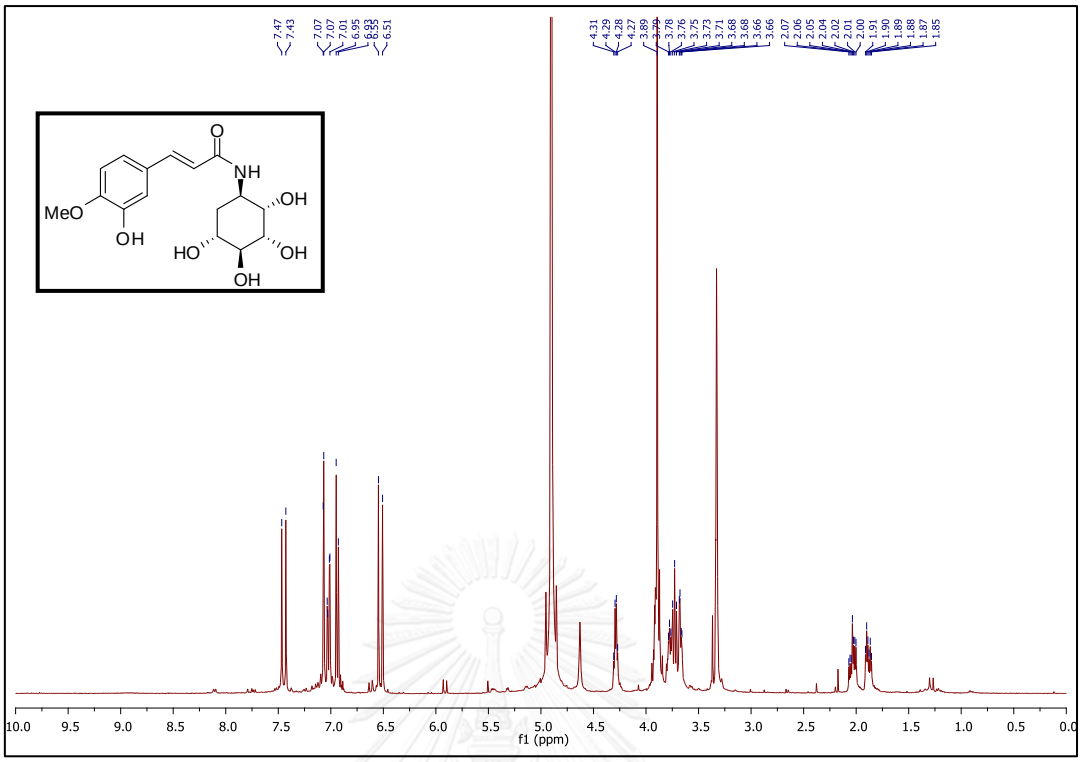

Figure A.45 ^{1}H NMR spectrum of **2.8AR (CD_3OD)**

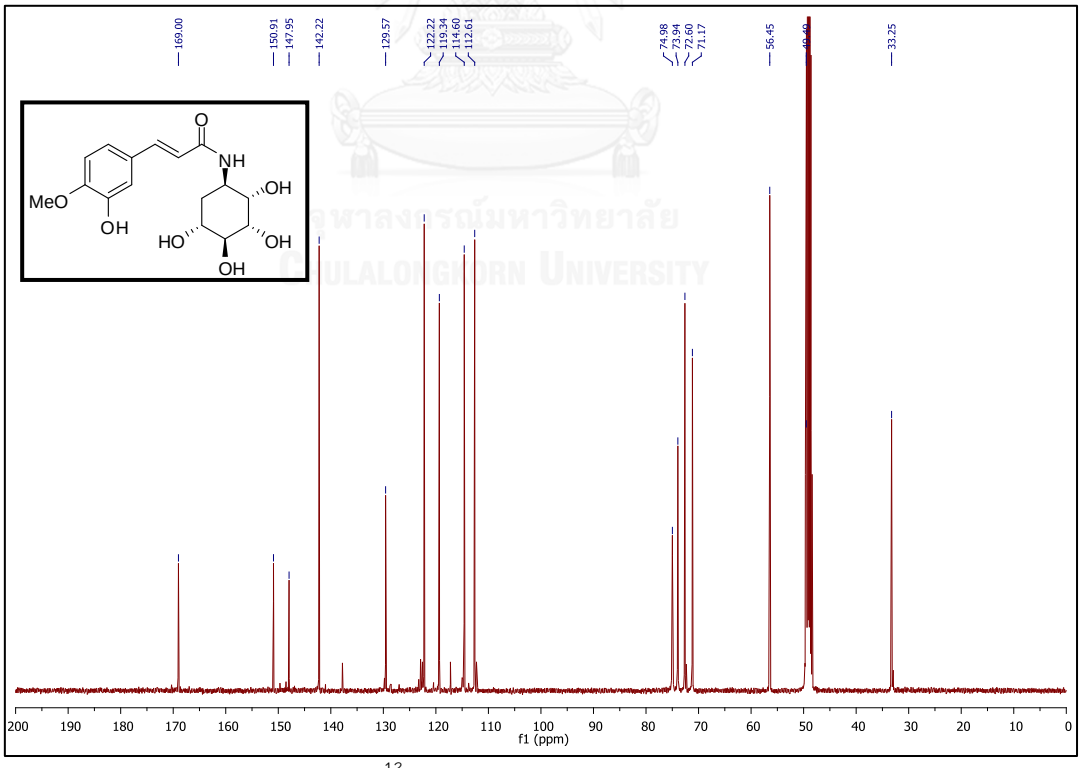

Figure A.46 ^{13}C NMR spectrum of **2.8AR (CD_3OD)**

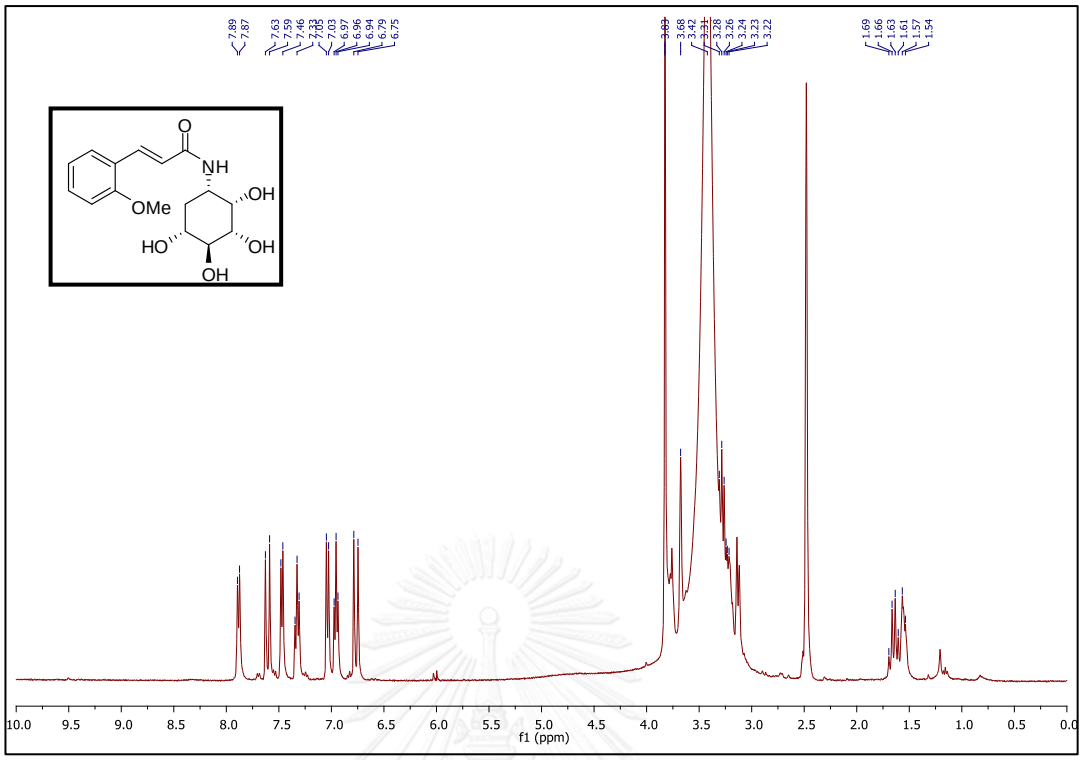

Figure A.47 ^{1}H NMR spectrum of **2.1AS (DMSO-d_6)**

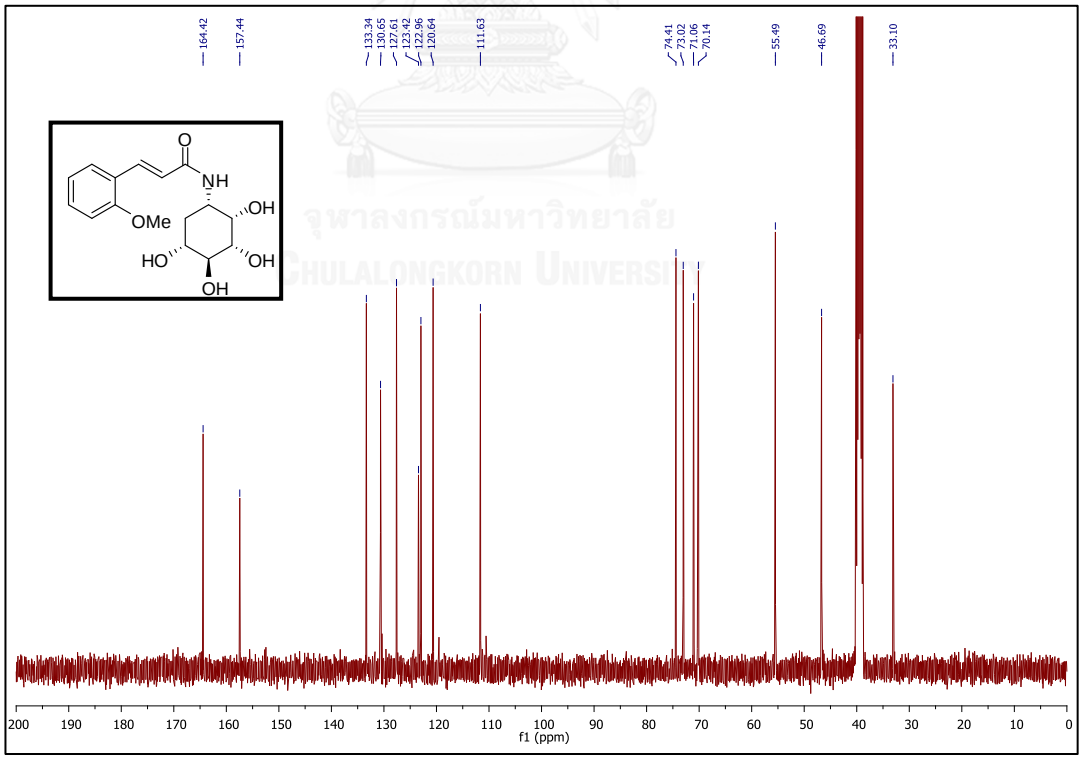

Figure A.48 ^{13}C NMR spectrum of **2.1AS (DMSO-d_6)**

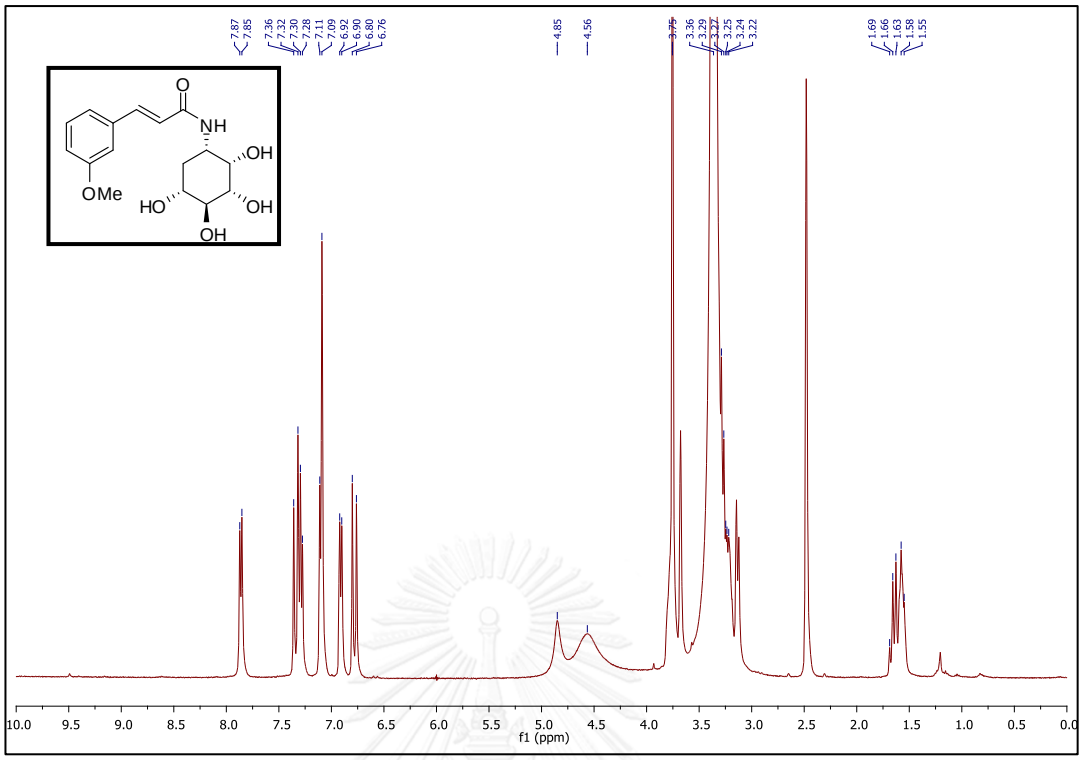

Figure A.49 ^{1}H NMR spectrum of **2.2AS (DMSO-d_6)**

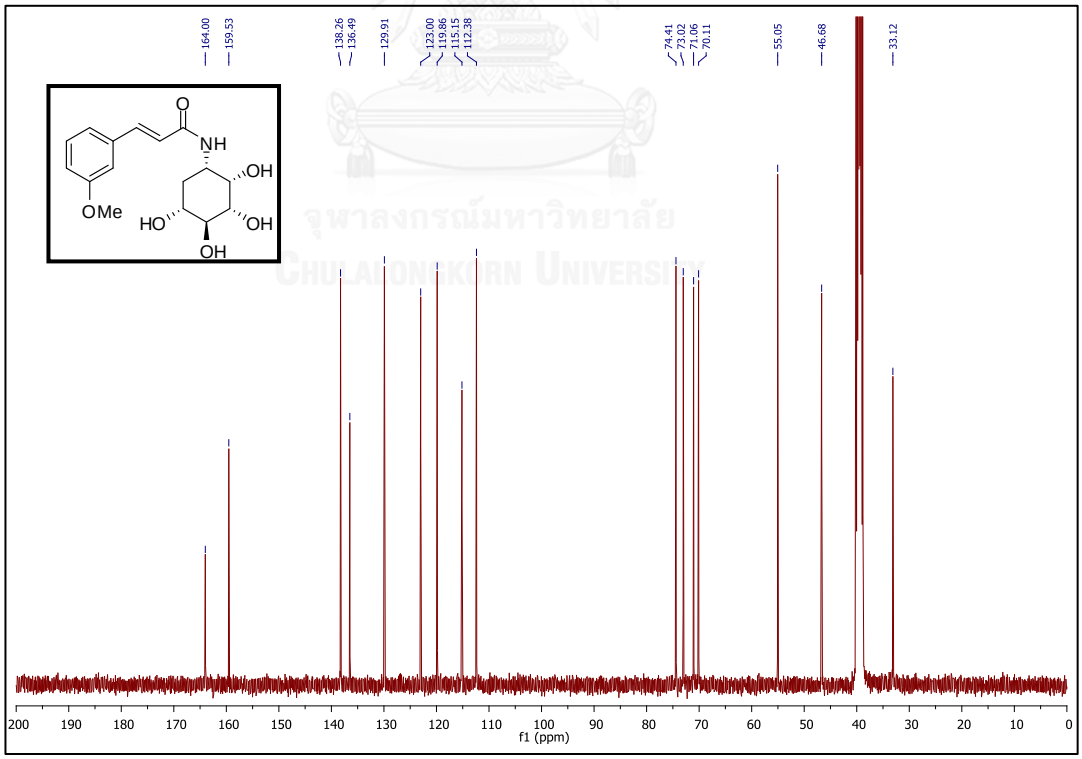

Figure A.50 ^{13}C NMR spectrum of **2.2AS (DMSO-d_6)**

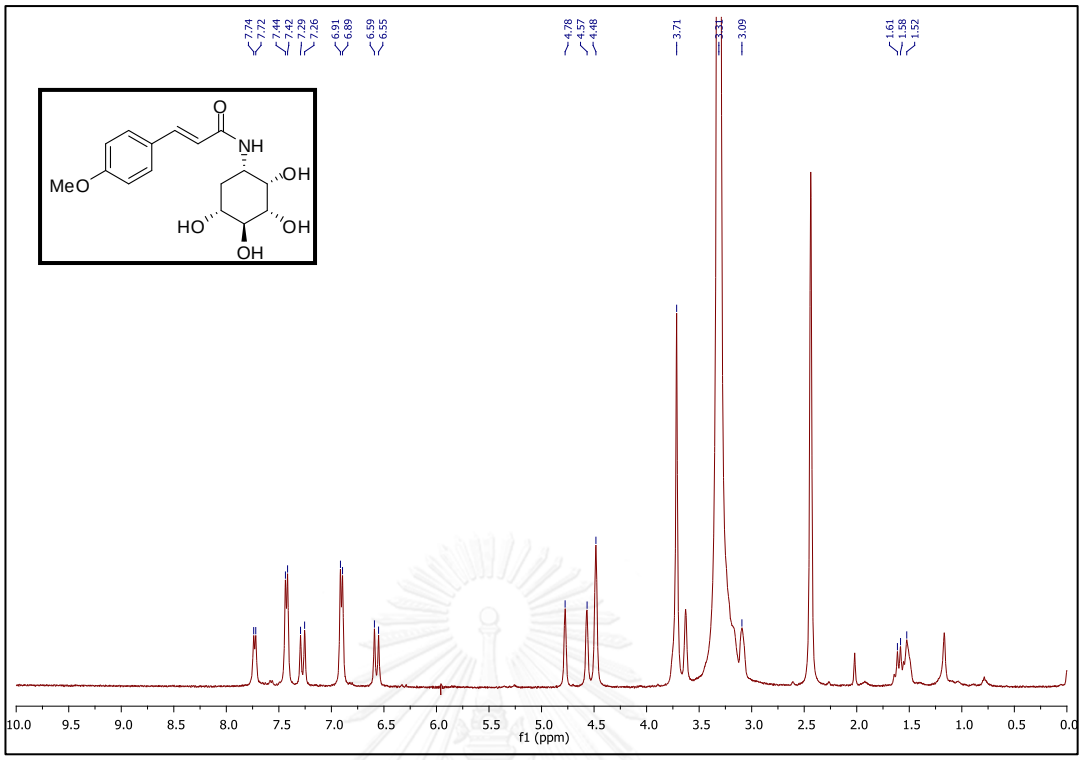

Figure A.51 ^{1}H NMR spectrum of **2.3AS (DMSO-d_6)**

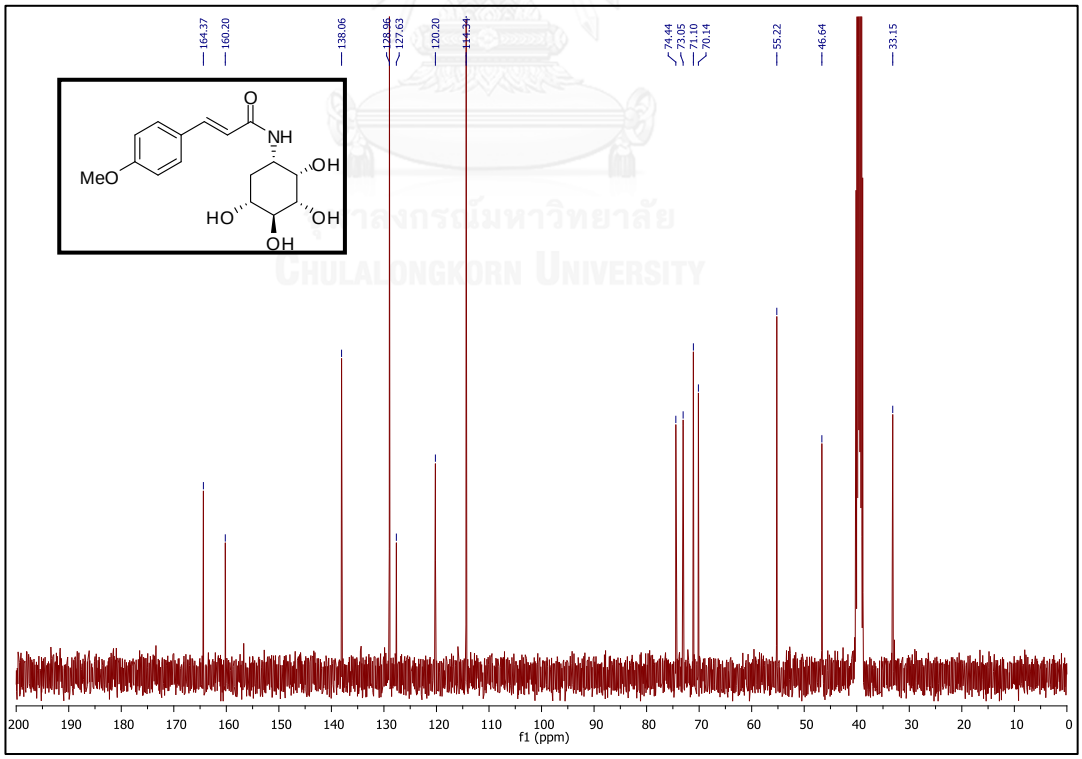

Figure A.52 ^{13}C NMR spectrum of **2.3AS (DMSO-d_6)**

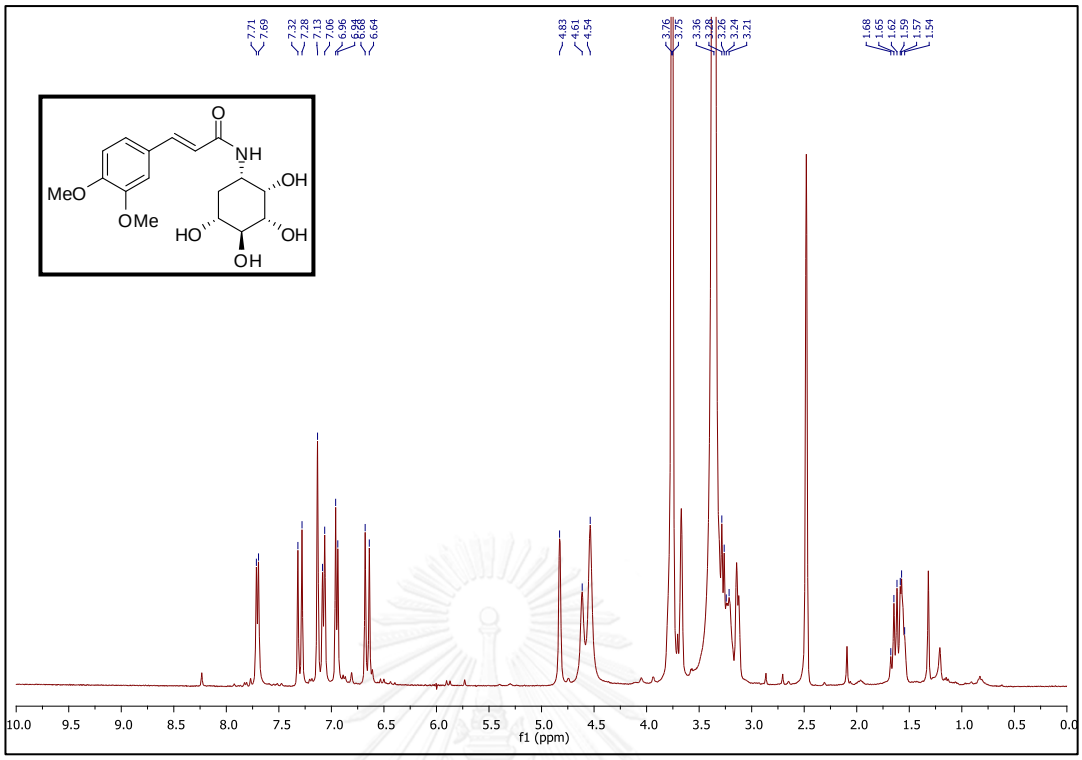

Figure A.53 ^{1}H NMR spectrum of **2.4AS (DMSO-d_6)**

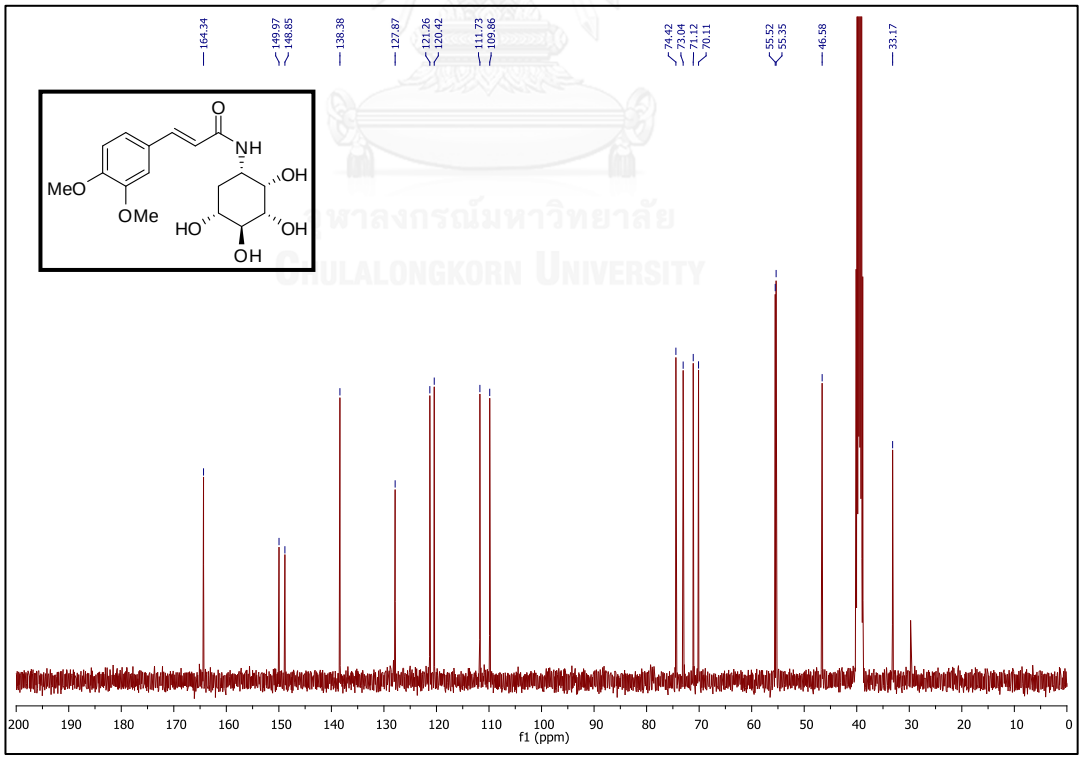

Figure A.54 ^{13}C NMR spectrum of **2.4AS (DMSO-d_6)**

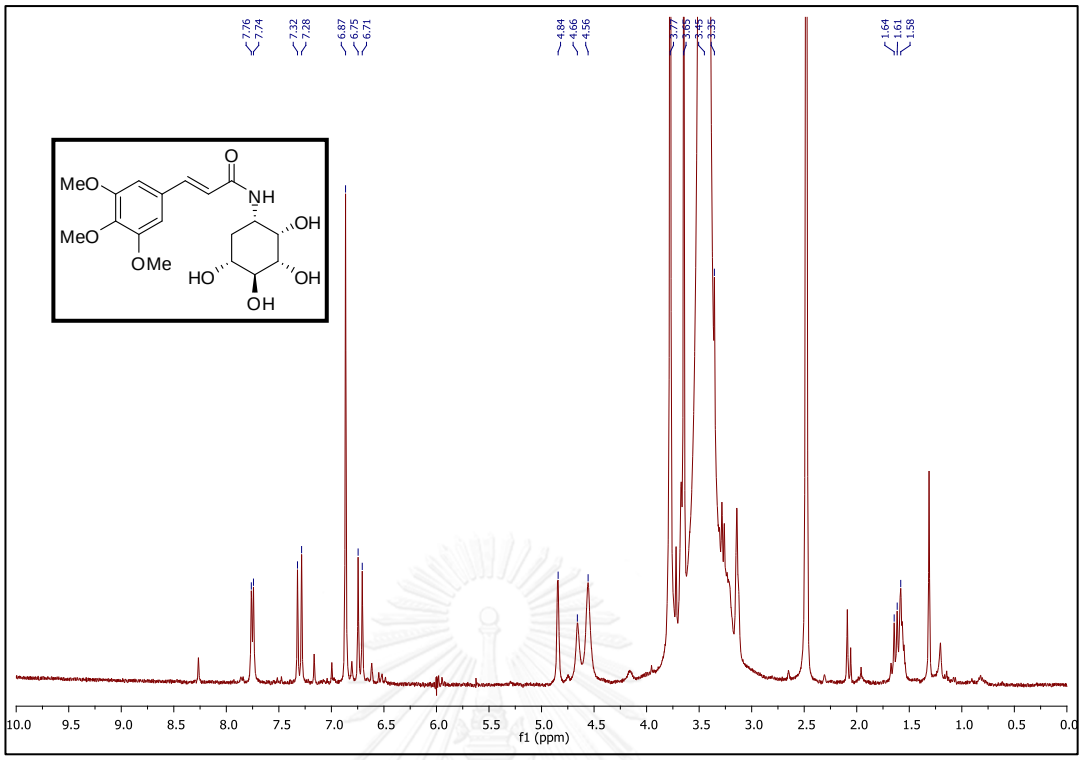

Figure A.55 ^{1}H NMR spectrum of **2.5AS (DMSO-d_6)**

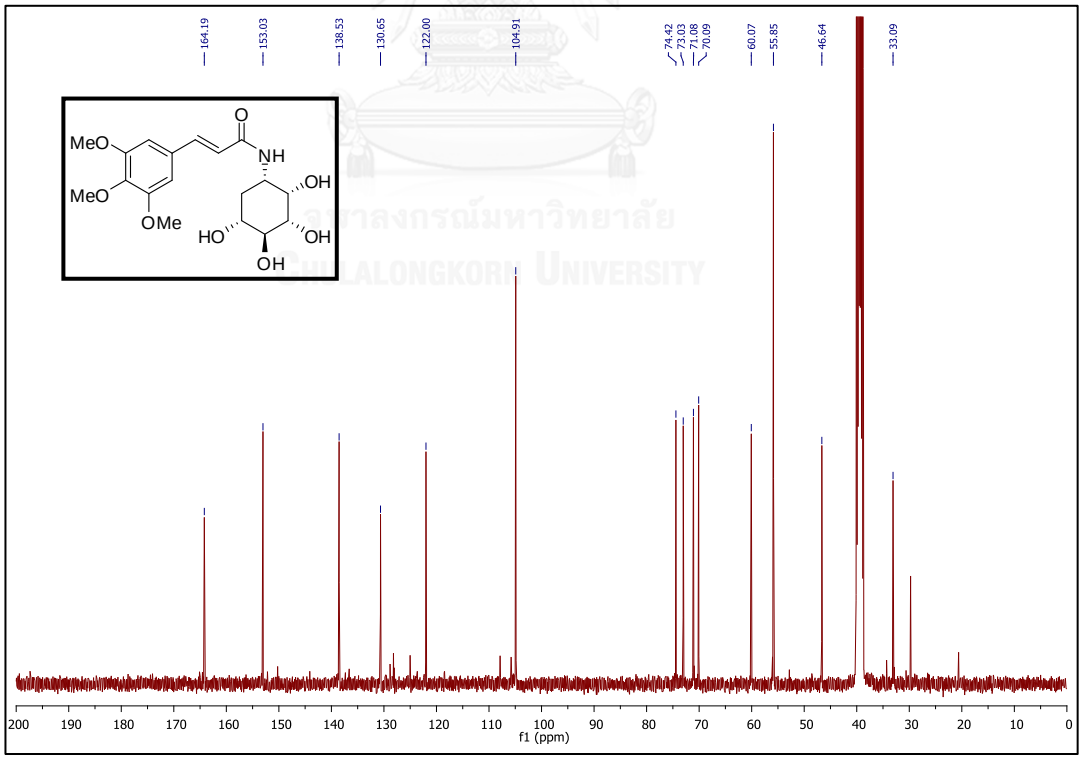

Figure A.56 ^{13}C NMR spectrum of **2.5AS (DMSO-d_6)**

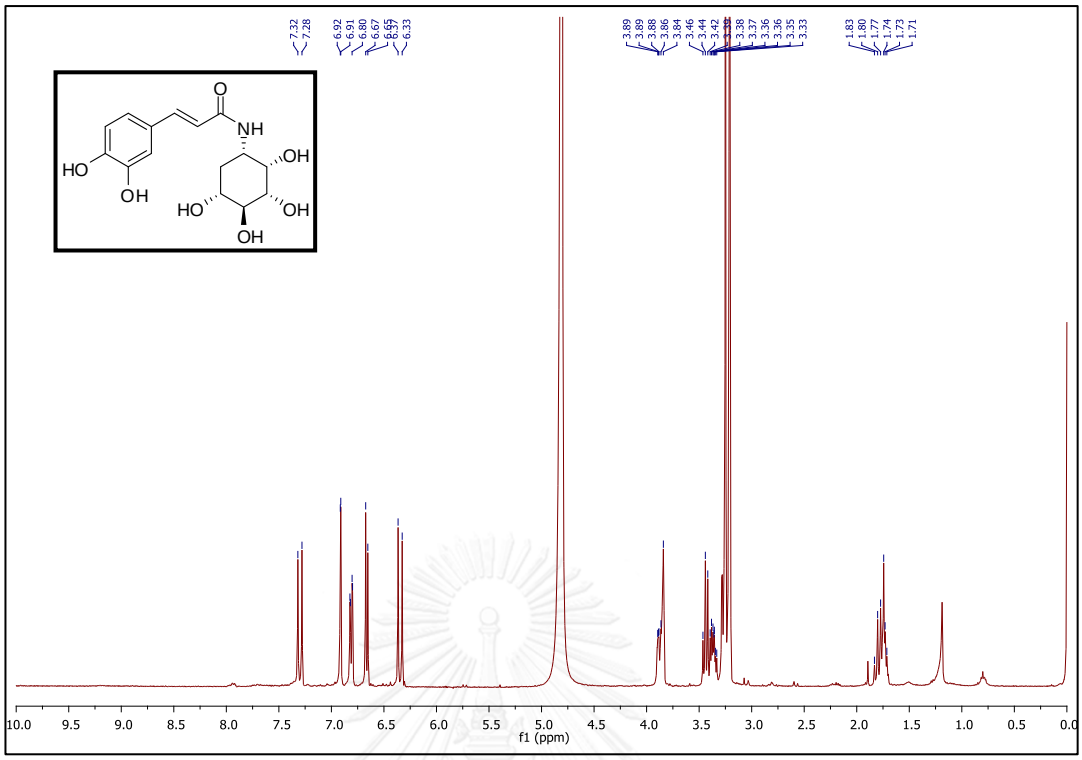

Figure A.57 ^{1}H NMR spectrum of **2.6AS (CD_3OD)**

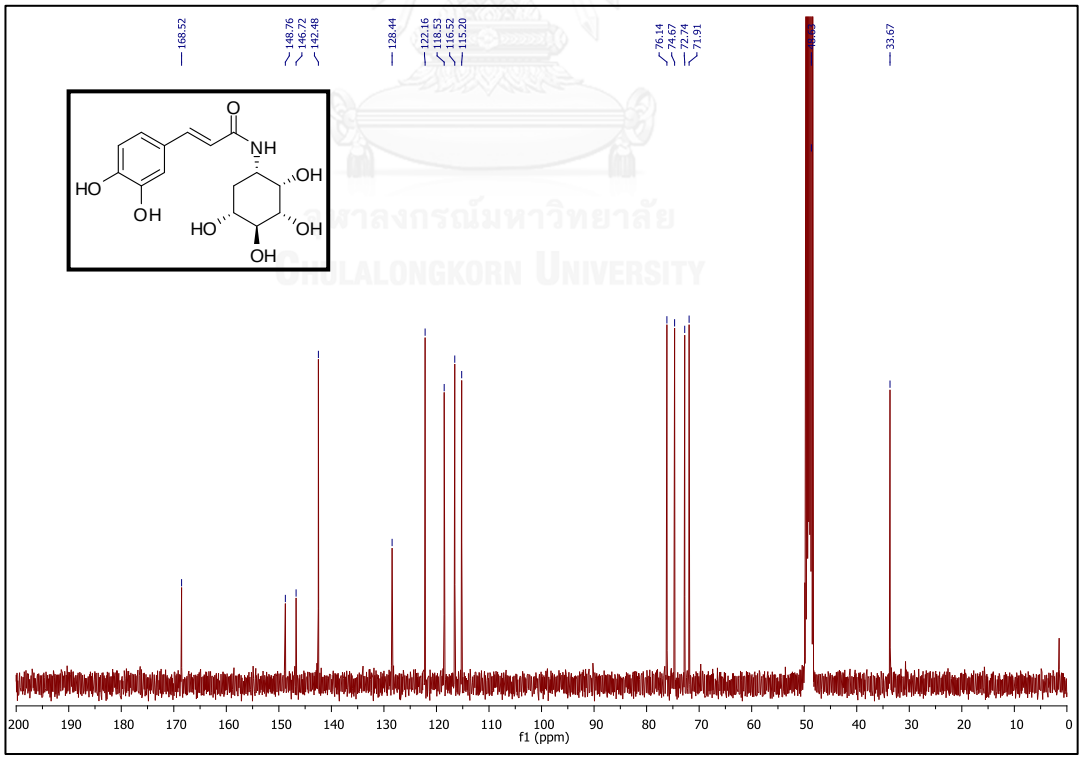

Figure A.58 ^{13}C NMR spectrum of **2.6AS (CD_3OD)**

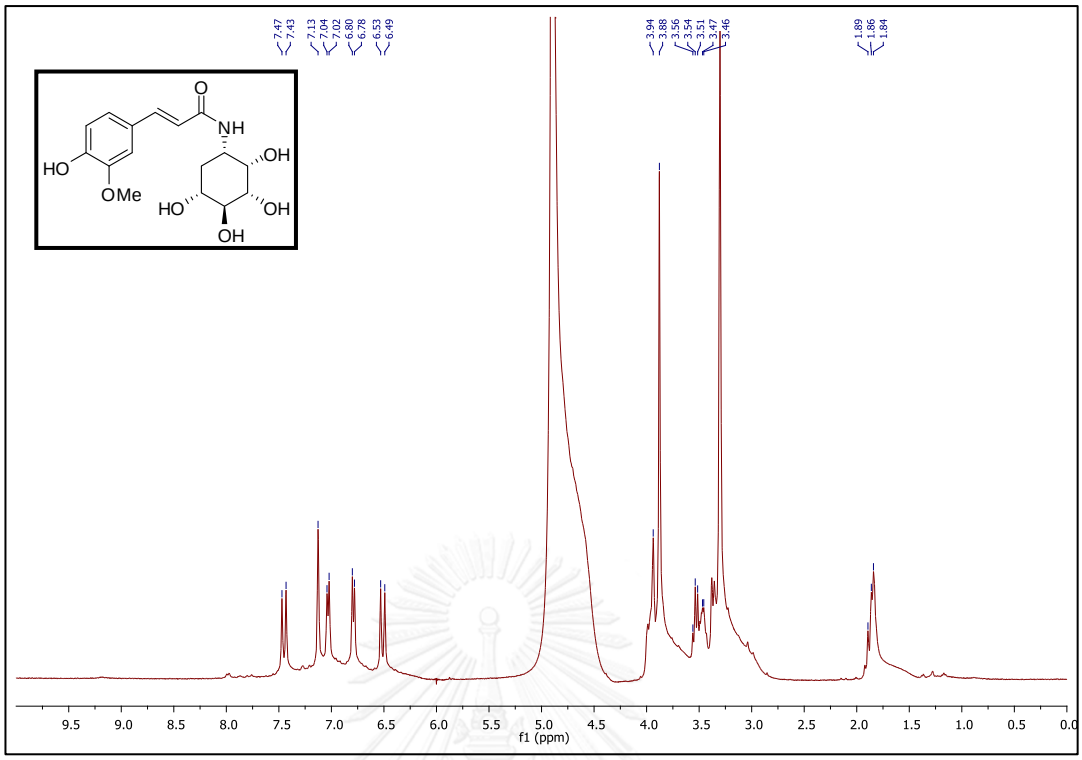

Figure A.59 ^{1}H NMR spectrum of **2.7AS (CD_3OD)**

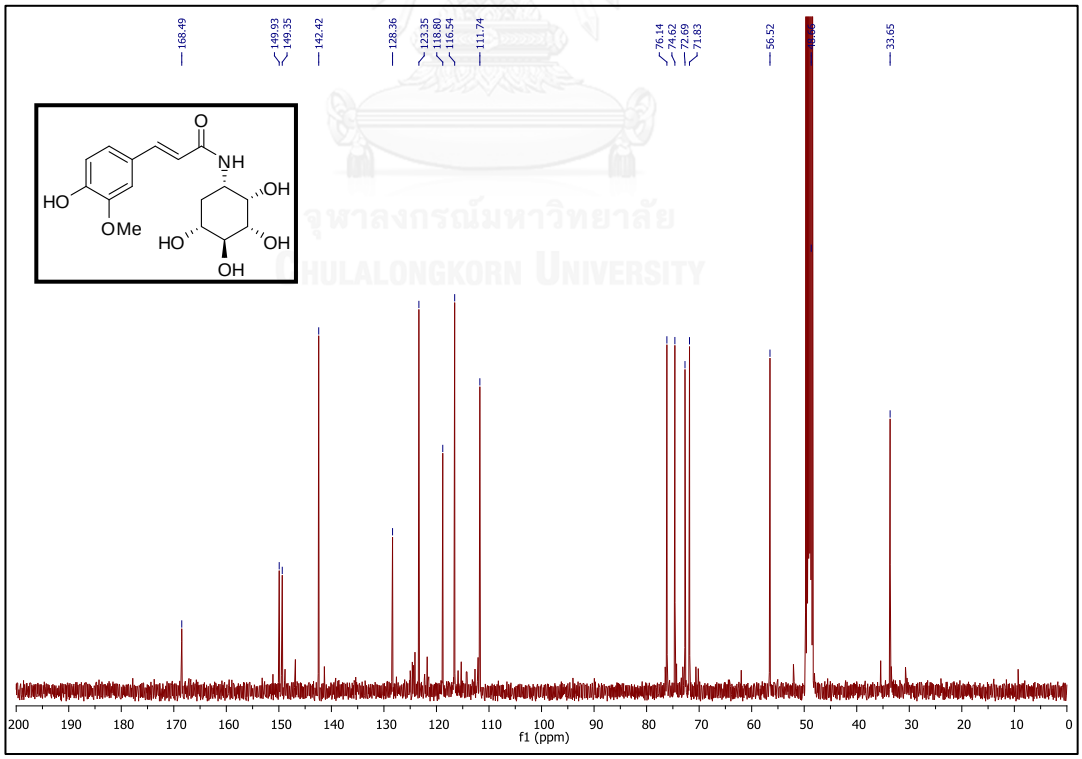

Figure A.60 ^{13}C NMR spectrum of **2.7AS (CD_3OD)**

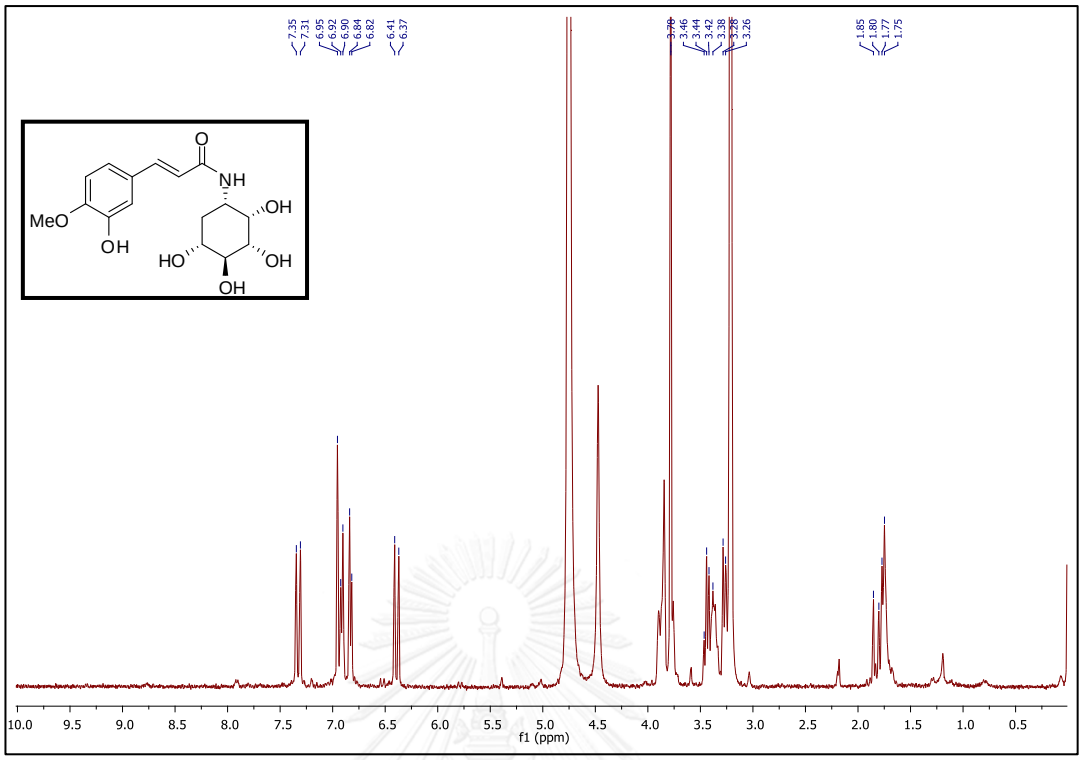

Figure A.61 ^{1}H NMR spectrum of **2.8AS (CD_3OD)**

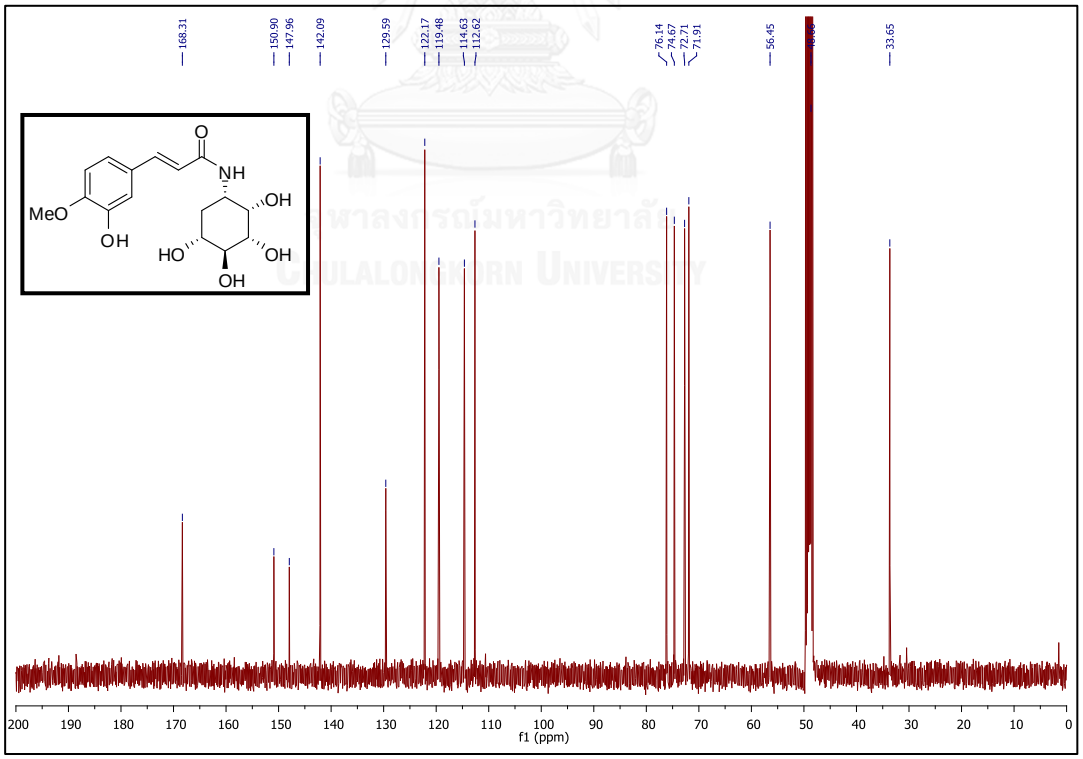

Figure A.62 ^{13}C NMR spectrum of **2.8AS (CD_3OD)**

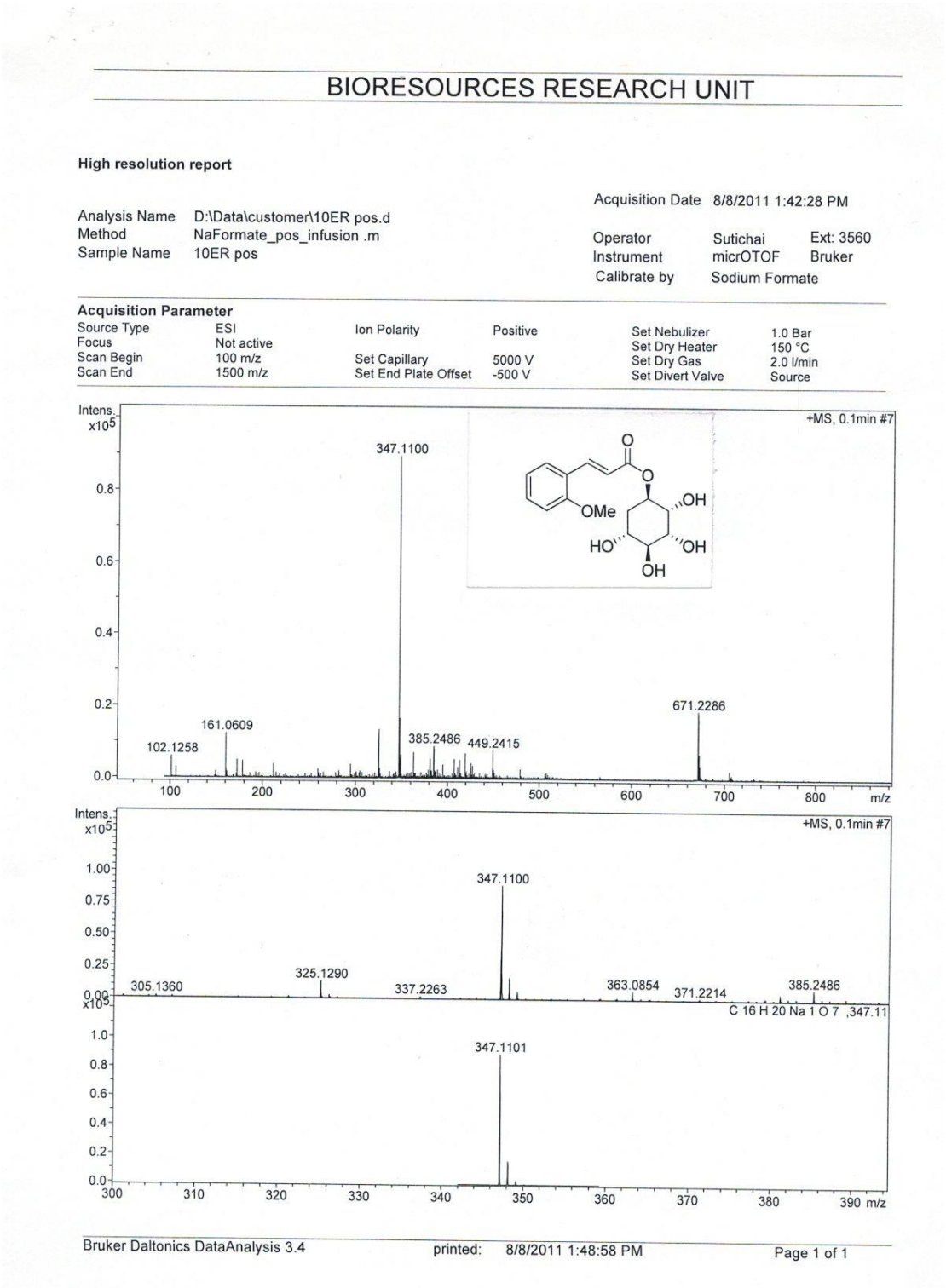

Figure A.63 HRMS of **2.1ER**

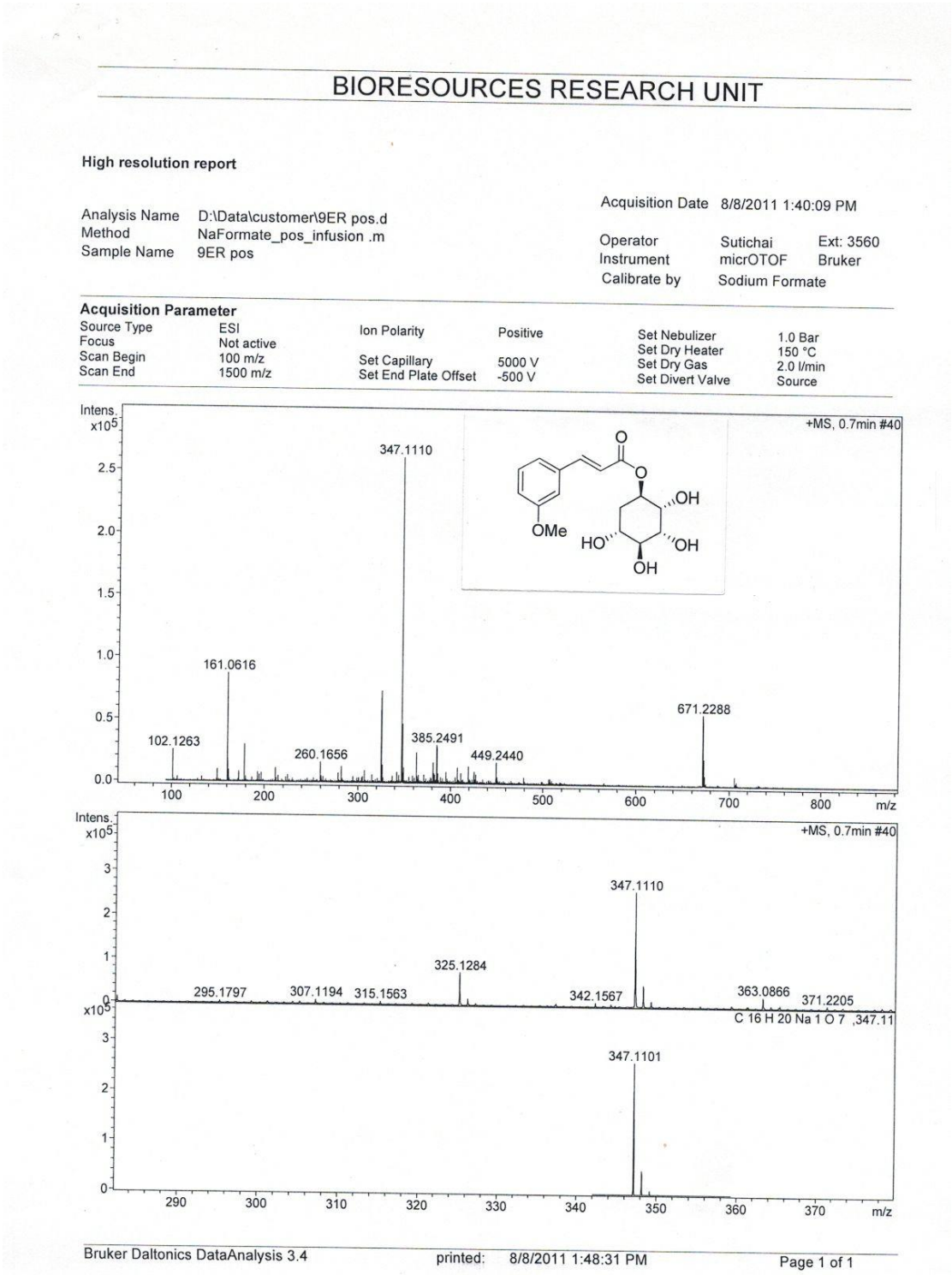

Figure A.64 HRMS of **2.2ER**

BIORESOURCES RESEARCH UNIT

High resolution report

		Acquisition Date	5/23/2011 2:02:43 PM
Analysis Name	D:\Data\customer\5ER.d		
Method	NaFormate_pos_infusion .m	Operator	Sutichai Ext: 3560
Sample Name	5ER	Instrument	micrOTOF Bruker
		Calibrate by	Sodium Formate

Acquisition Parameter

Source Type	ESI	Ion Polarity	Positive	Set Nebulizer	1.0 Bar
Focus	Not active			Set Dry Heater	150 °C
Scan Begin	100 m/z	Set Capillary	5000 V	Set Dry Gas	2.0 l/min
Scan End	1500 m/z	Set End Plate Offset	-500 V	Set Divert Valve	Source

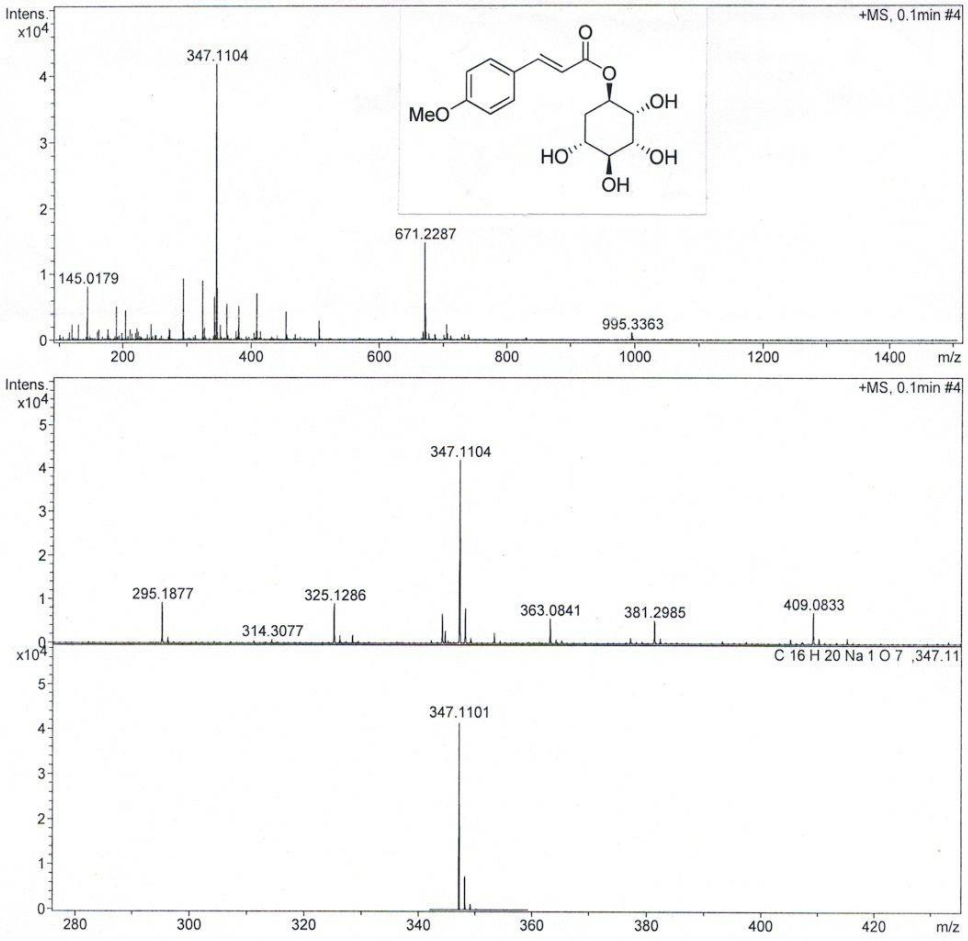

Bruker Daltonics DataAnalysis 3.4 printed: 5/23/2011 2:11:14 PM Page 1 of 1

Figure A.65 HRMS of **2.3ER**

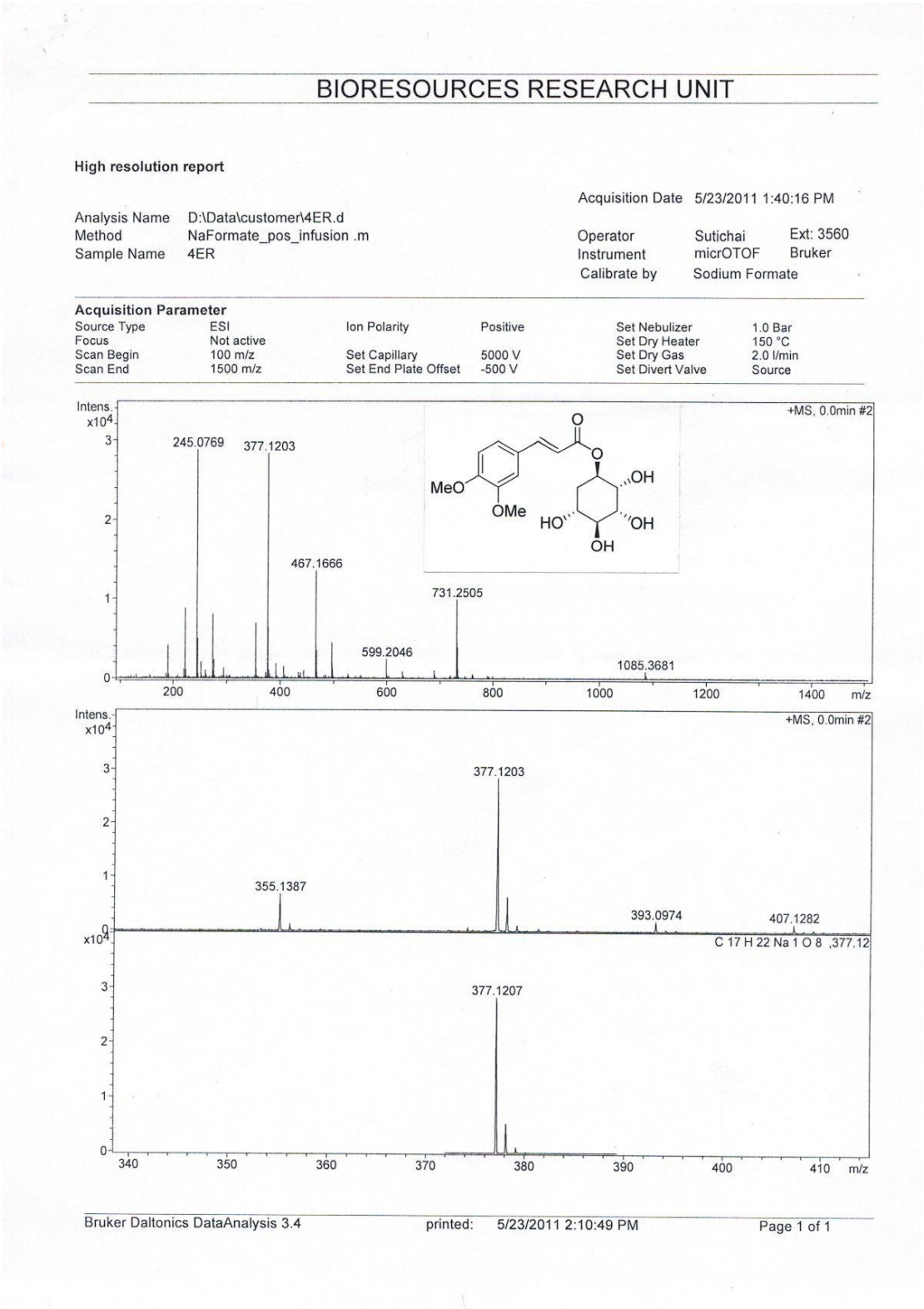

Figure A.66 HRMS of **2.4ER**

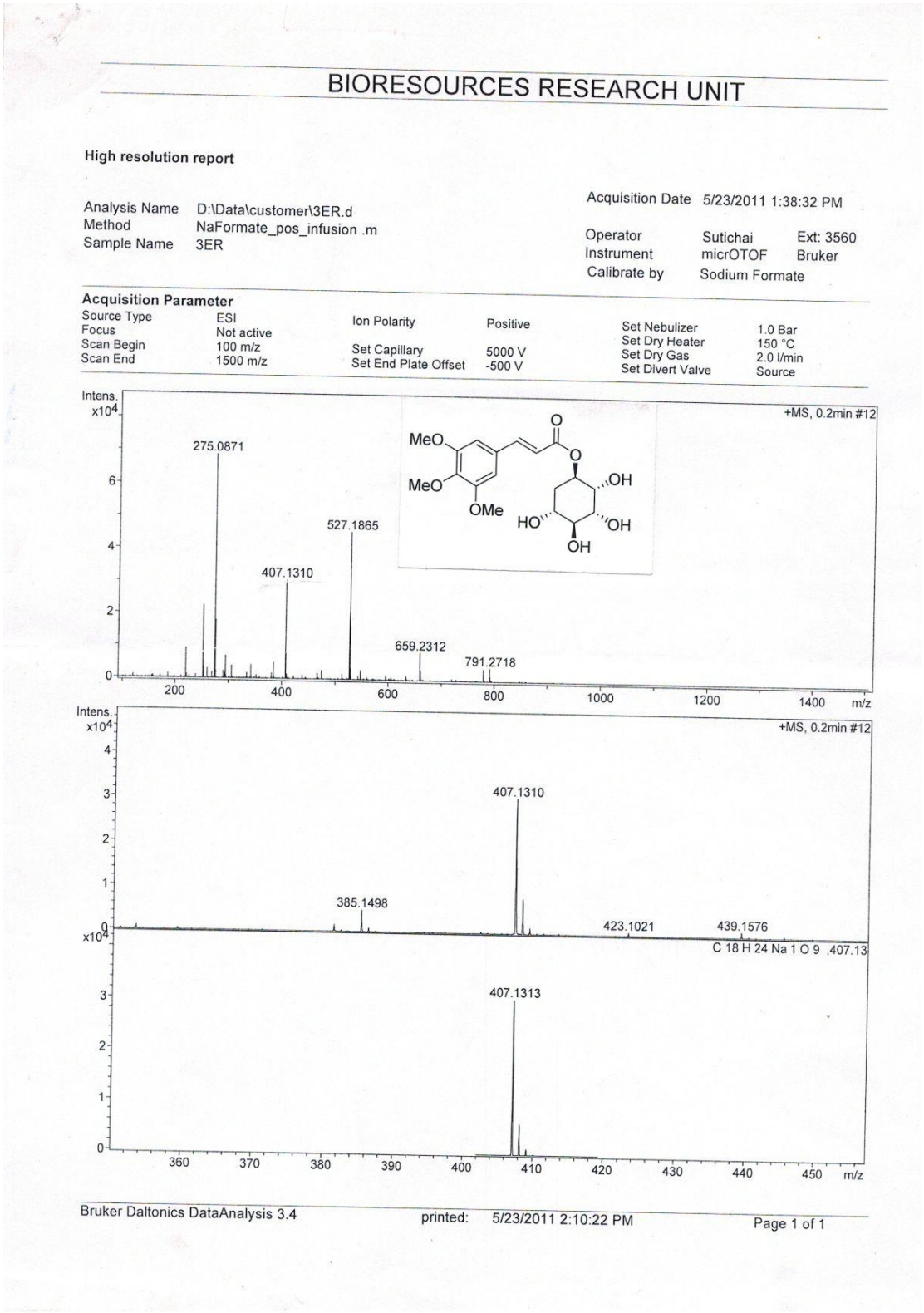

Figure A.67 HRMS of **2.5ER**

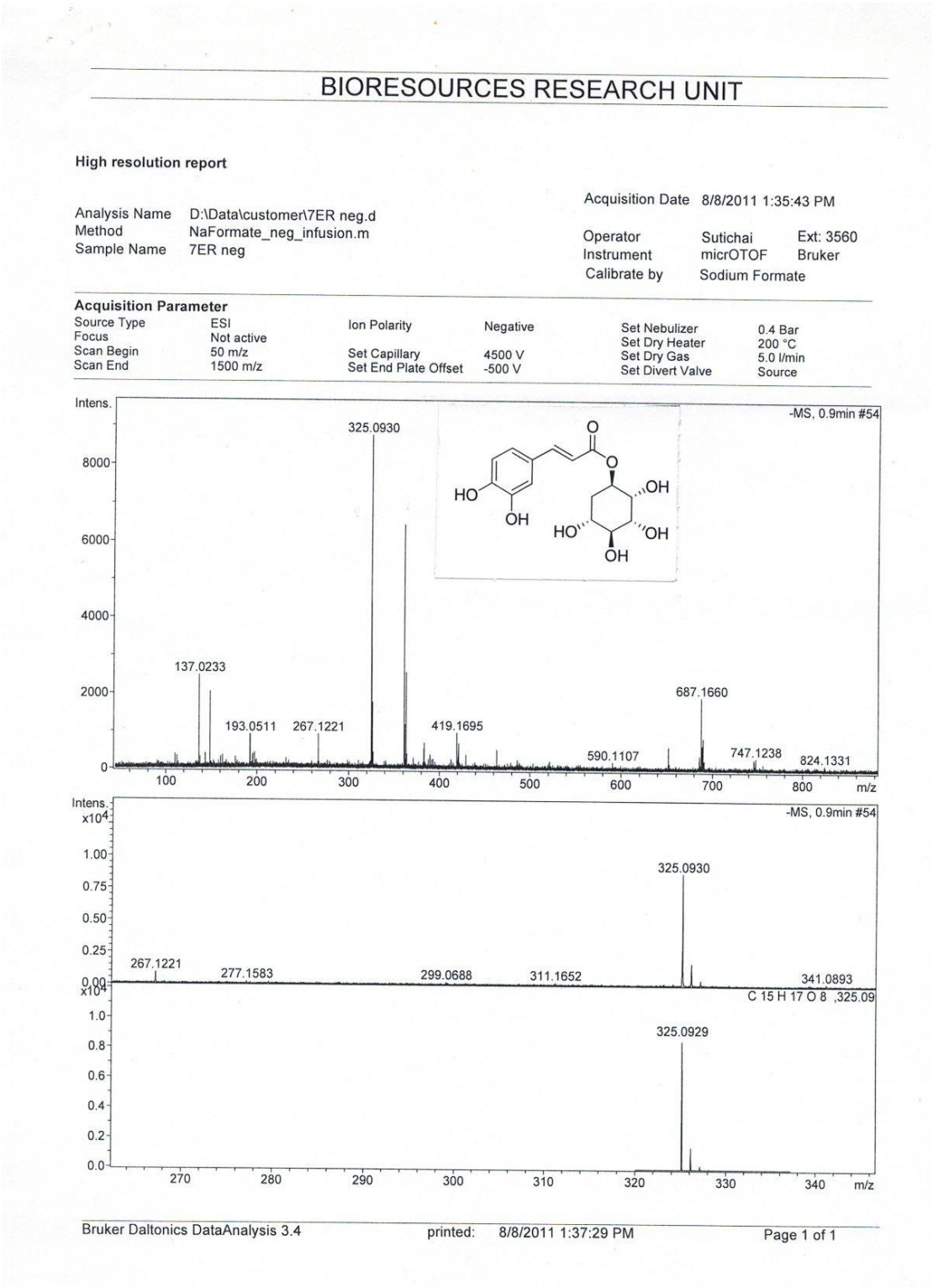

Figure A.68 HRMS of **2.6ER**

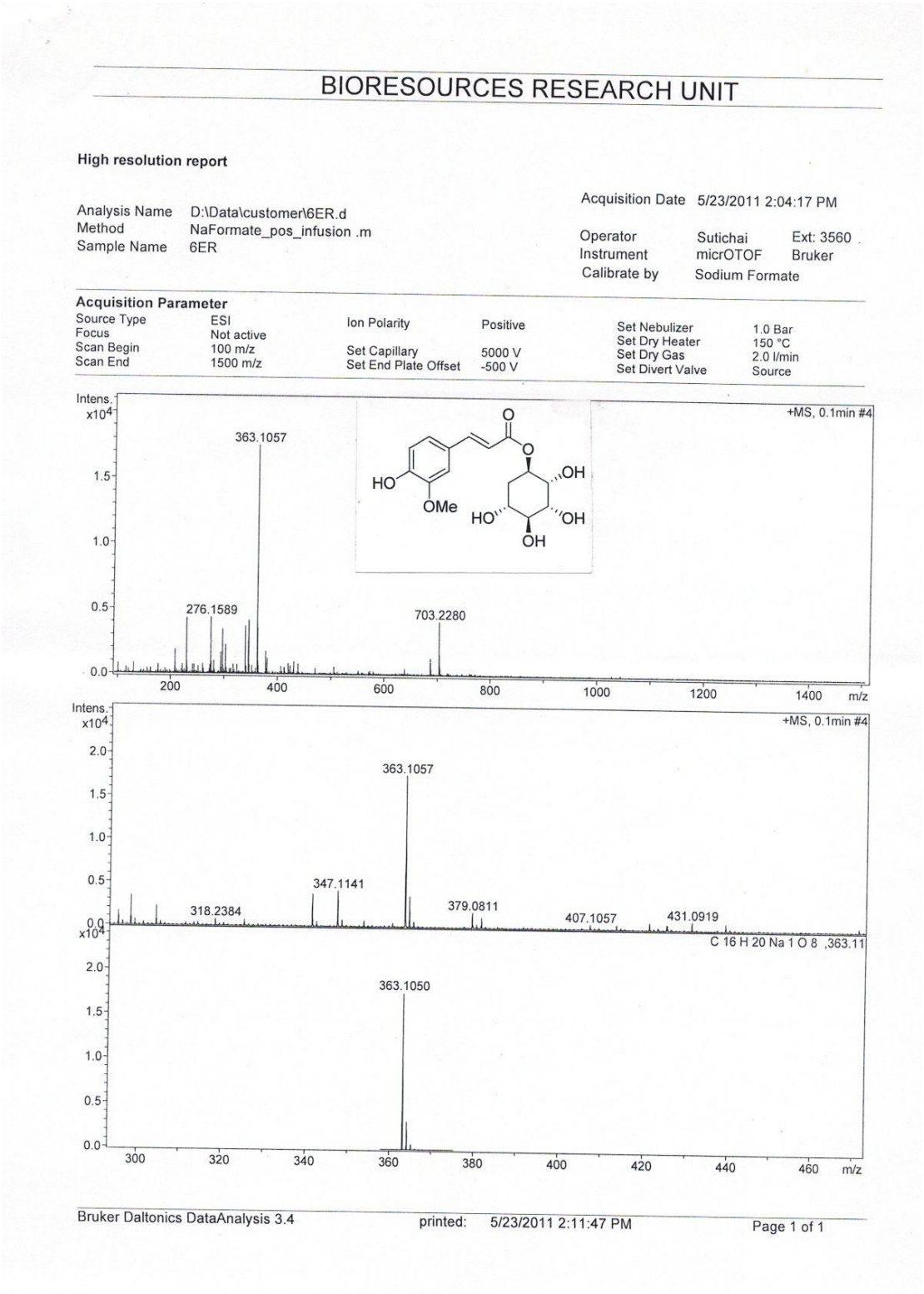

Figure A.69 HRMS of **2.7ER**

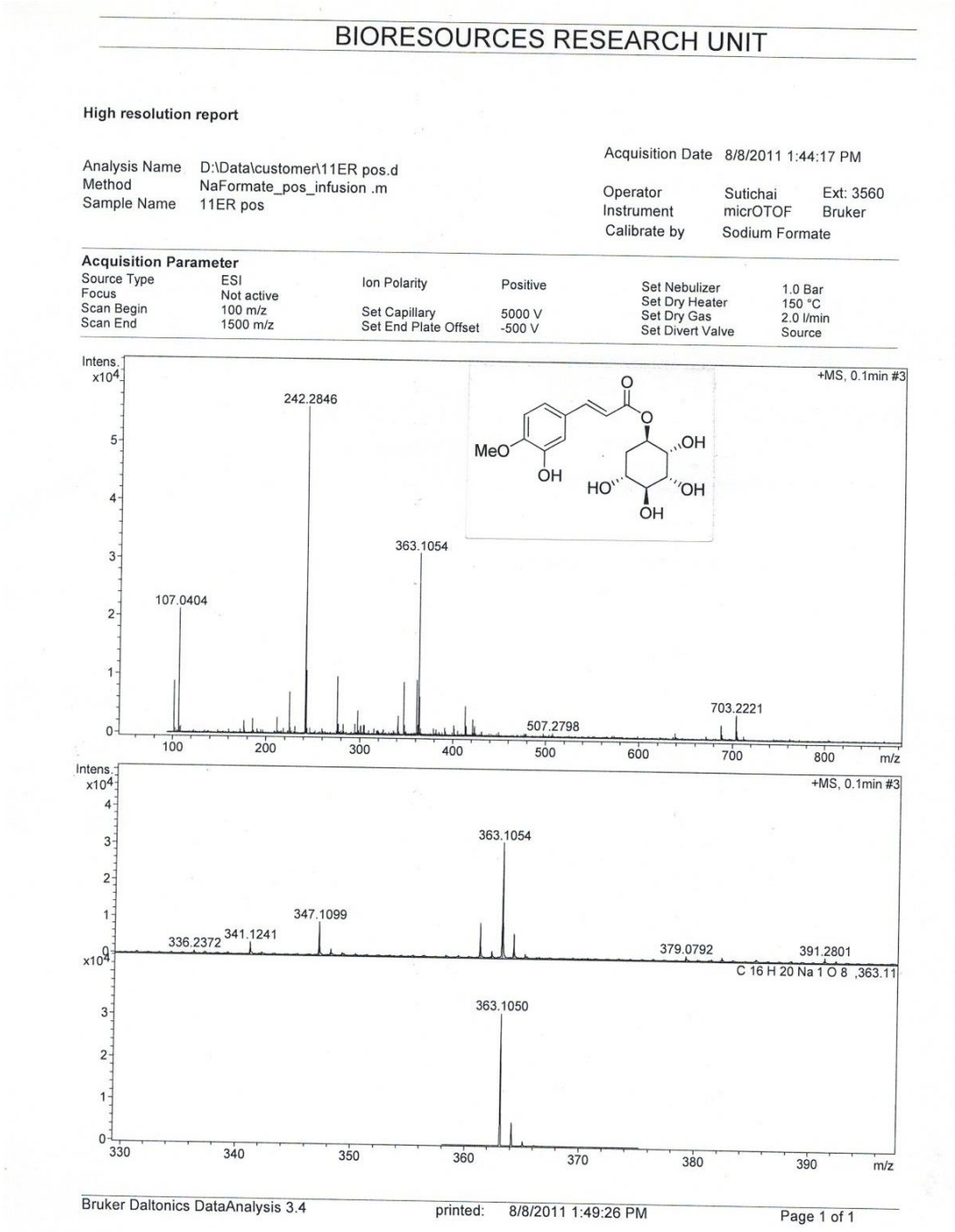

Figure A.70 HRMS of **2.8ER**

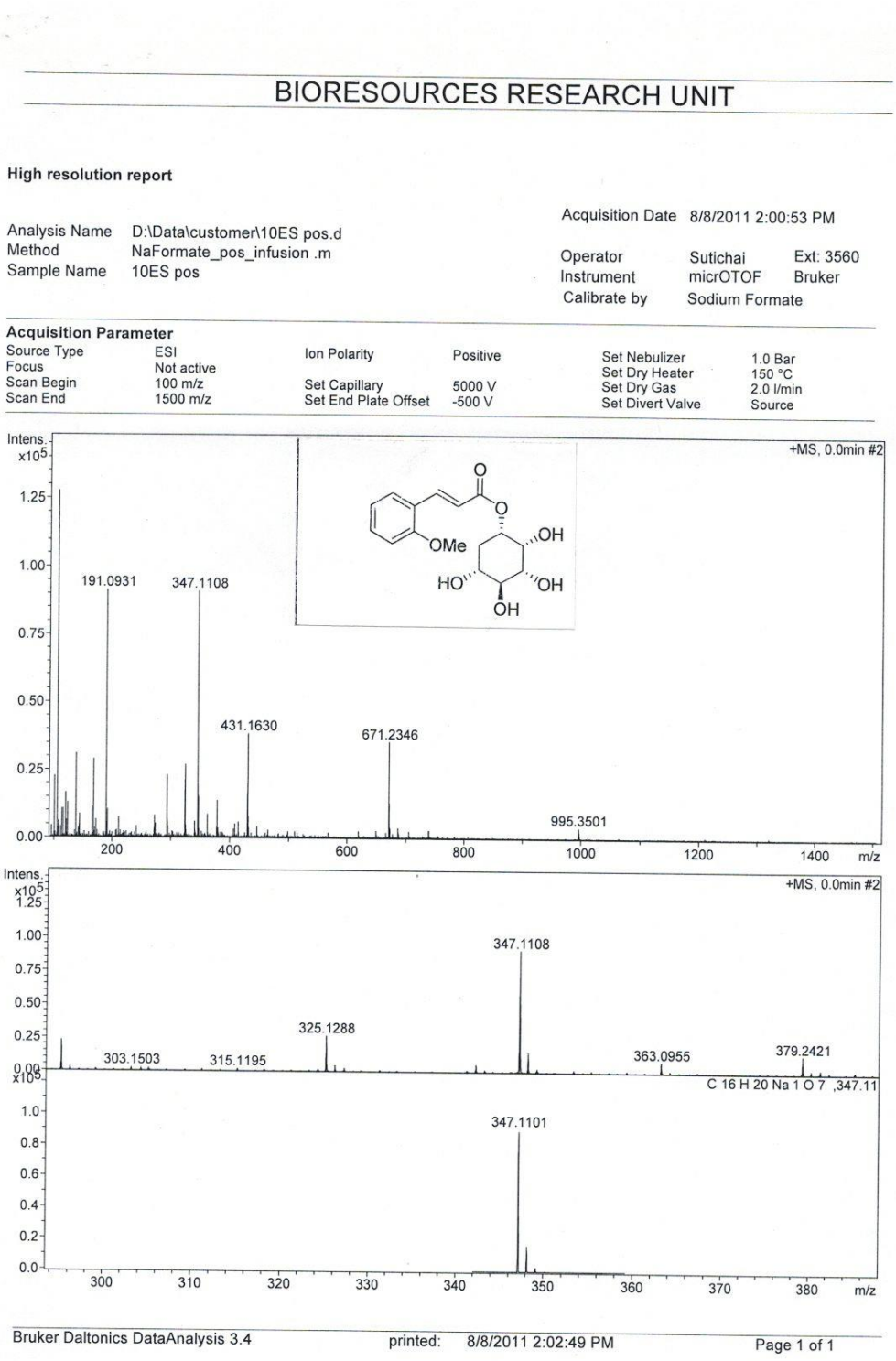

Figure A.71 HRMS of **2.1ES**

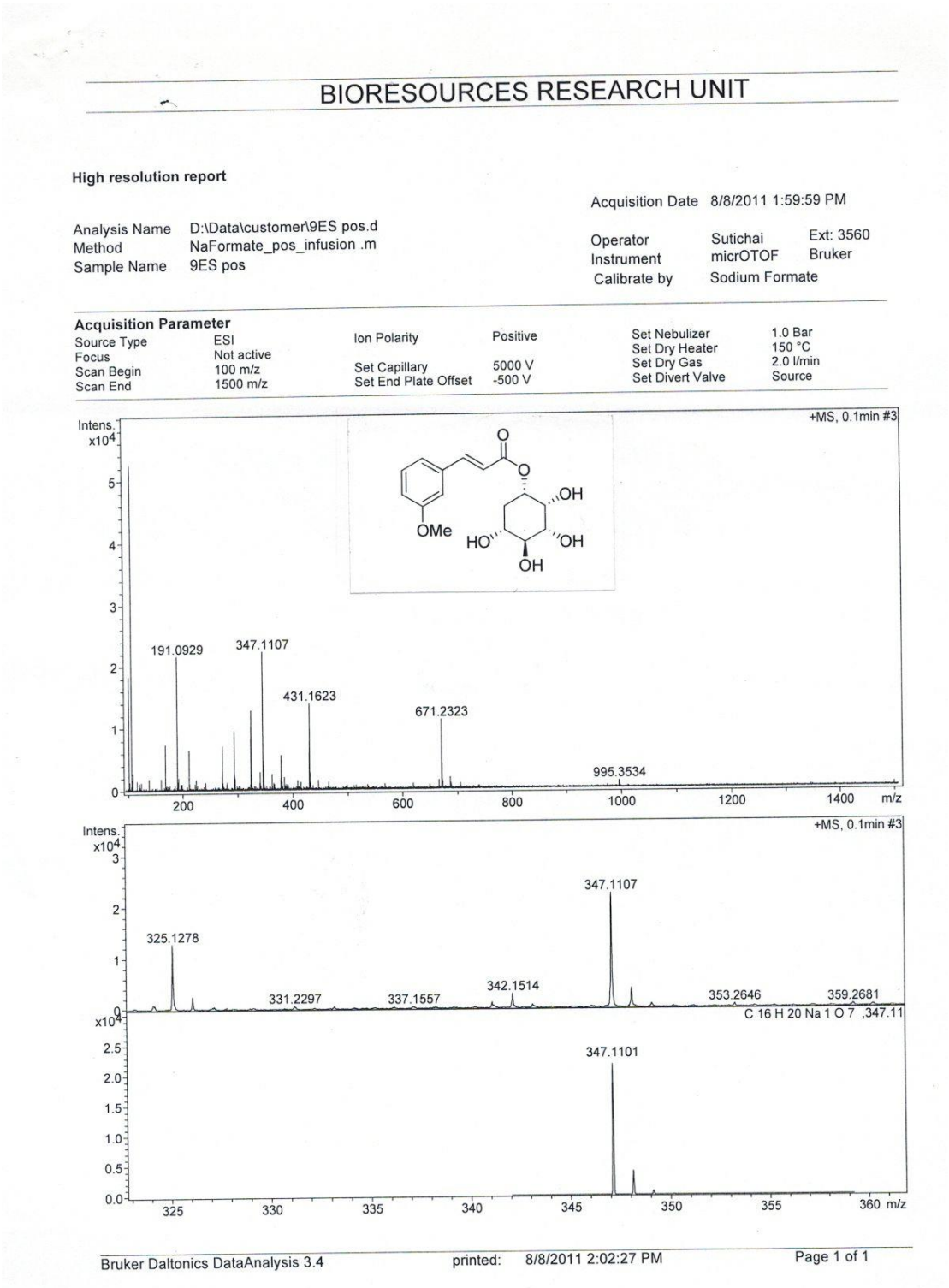

Figure A.72 HRMS of **2.2ES**

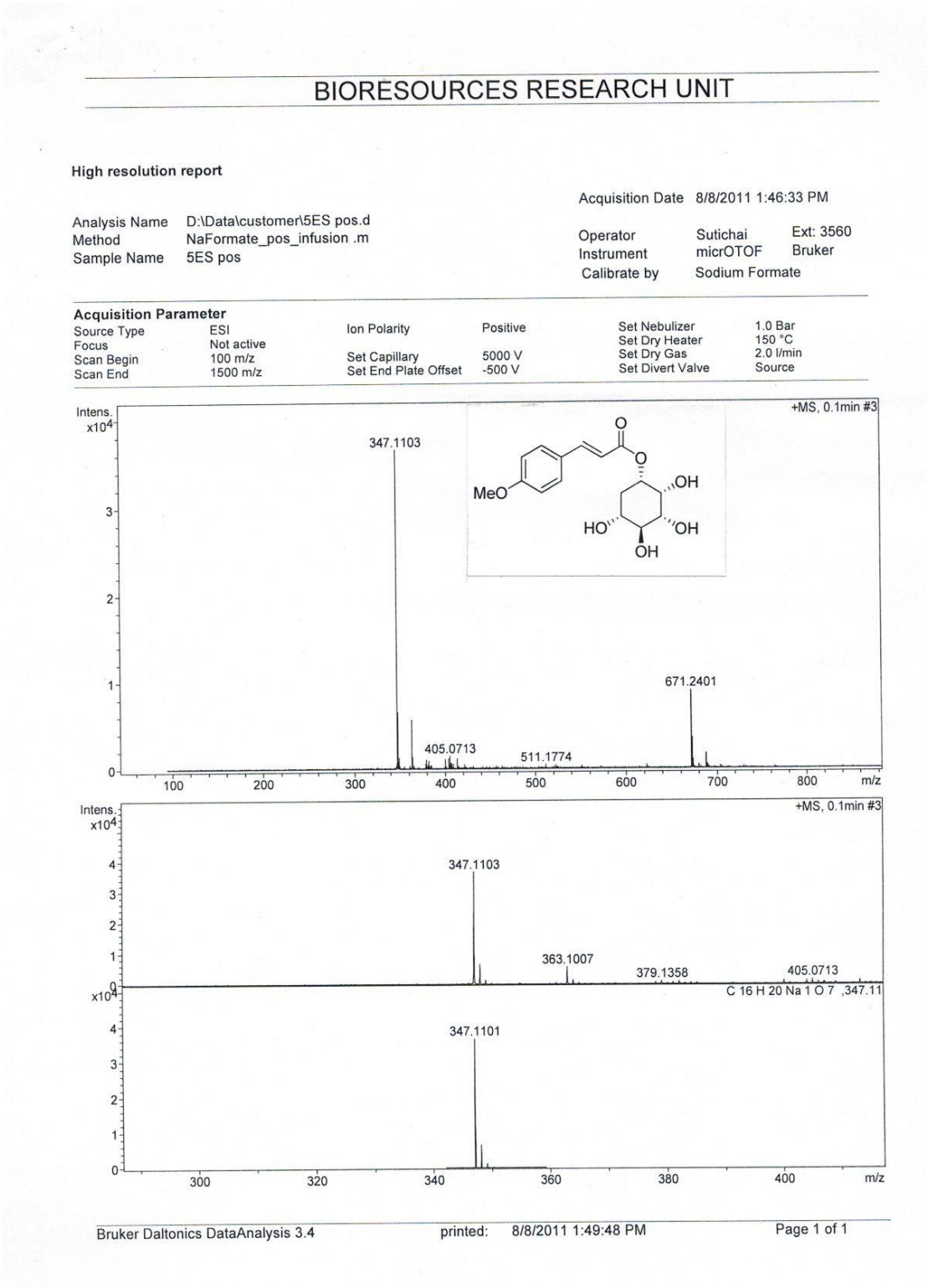

Figure A.73 HRMS of **2.3ES**

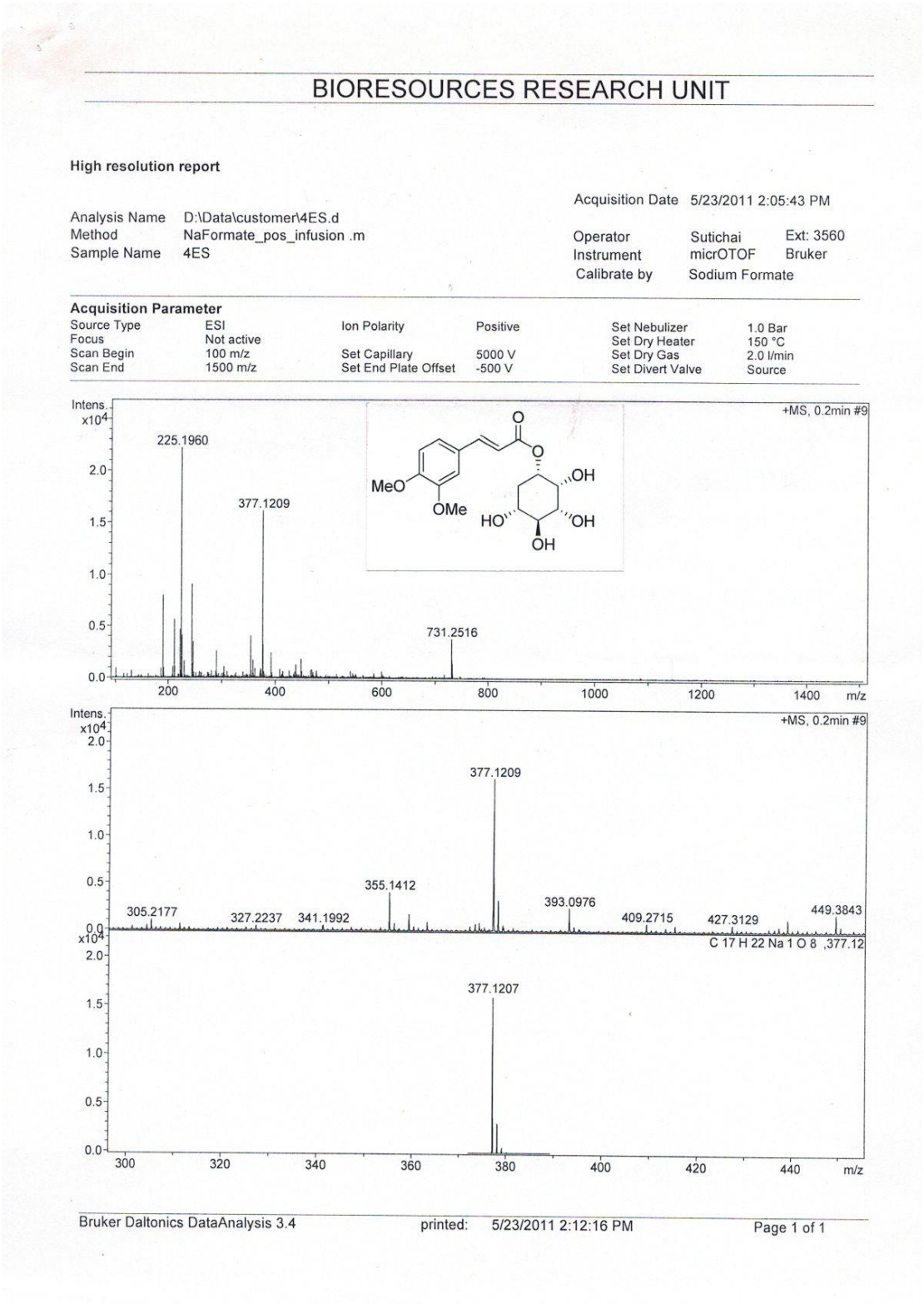

Figure A.74 HRMS of **2.4ES**

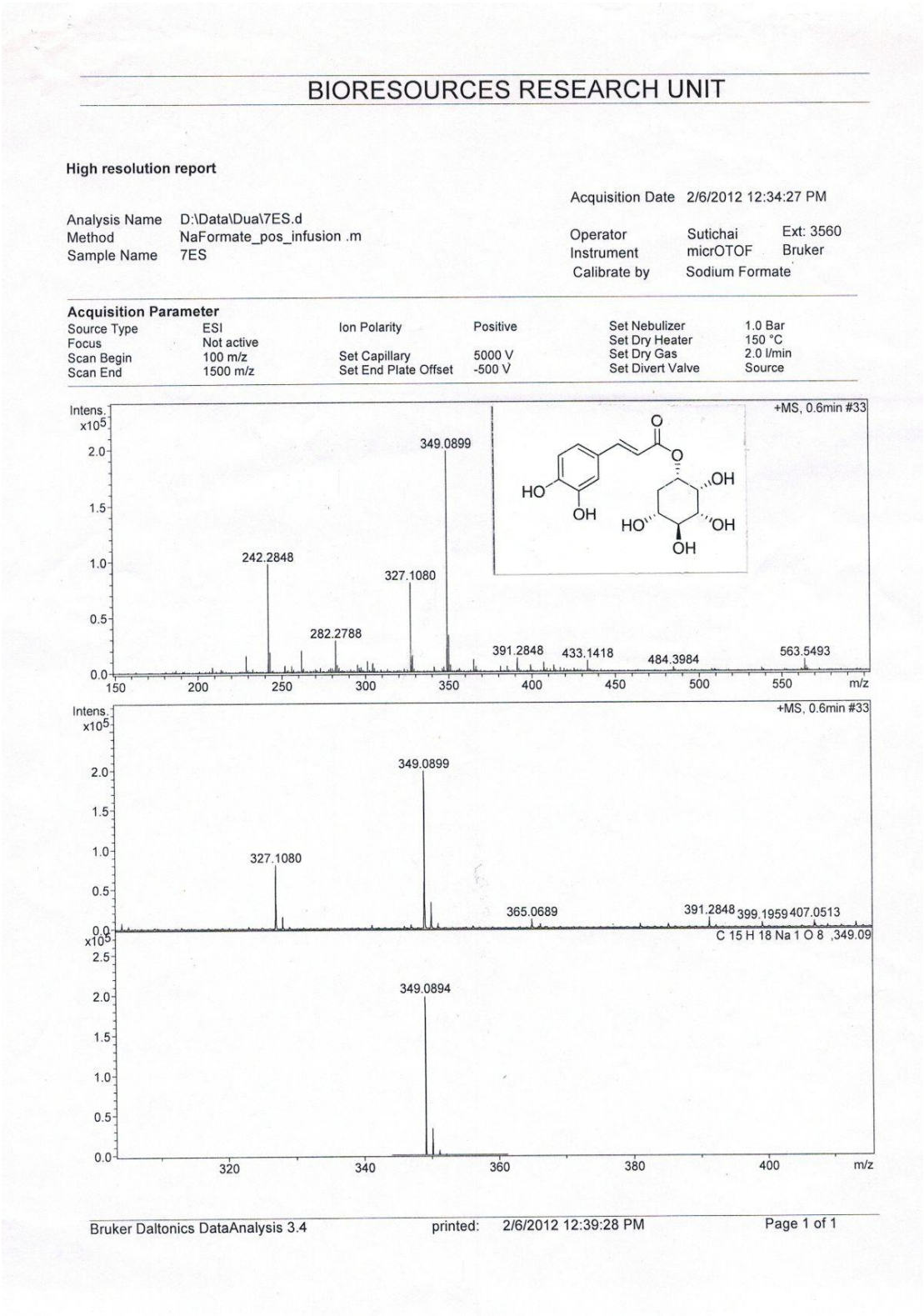

Figure A.75 HRMS of **2.6ES**

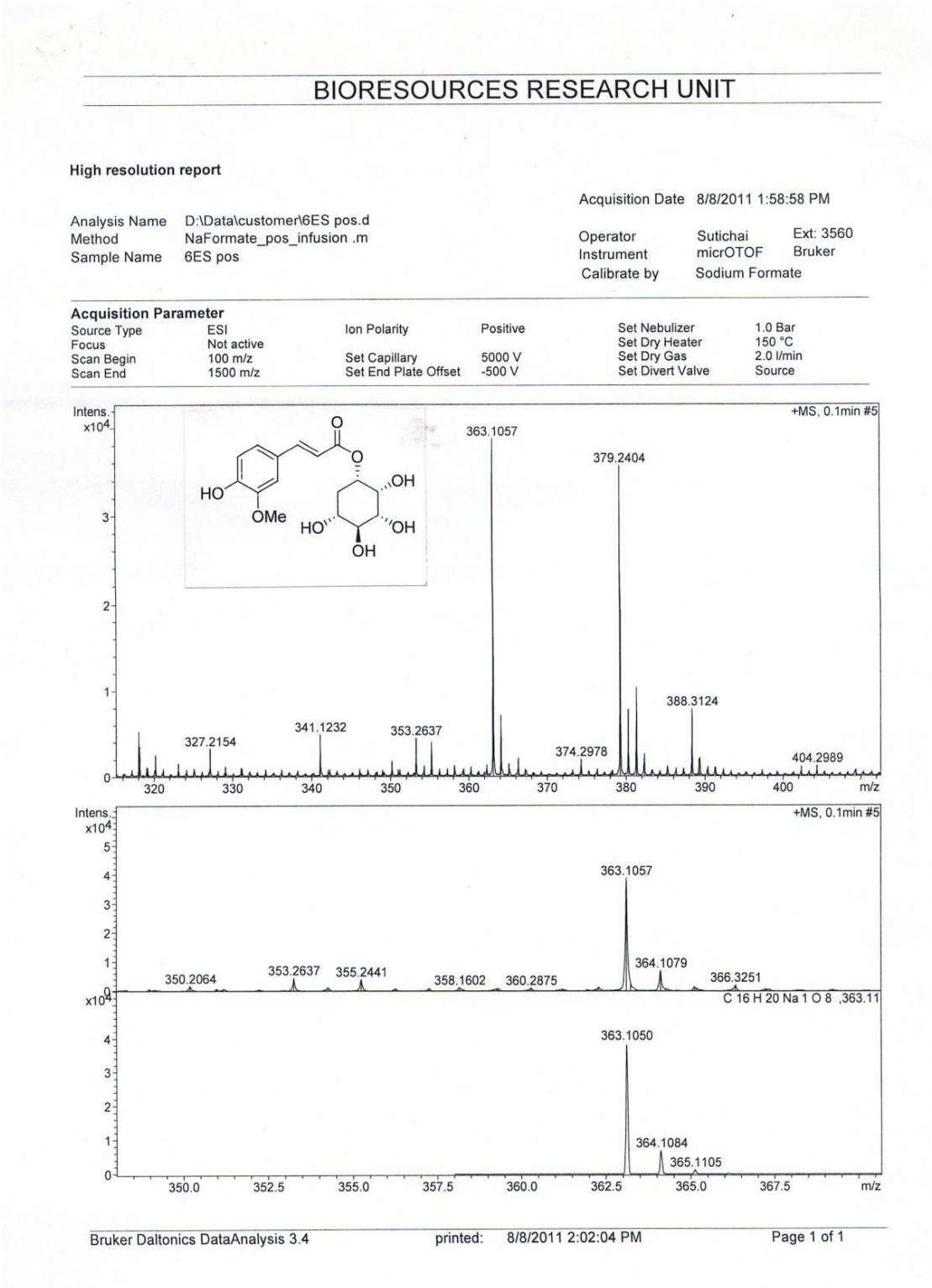

Figure A.76 HRMS of **2.7ES**

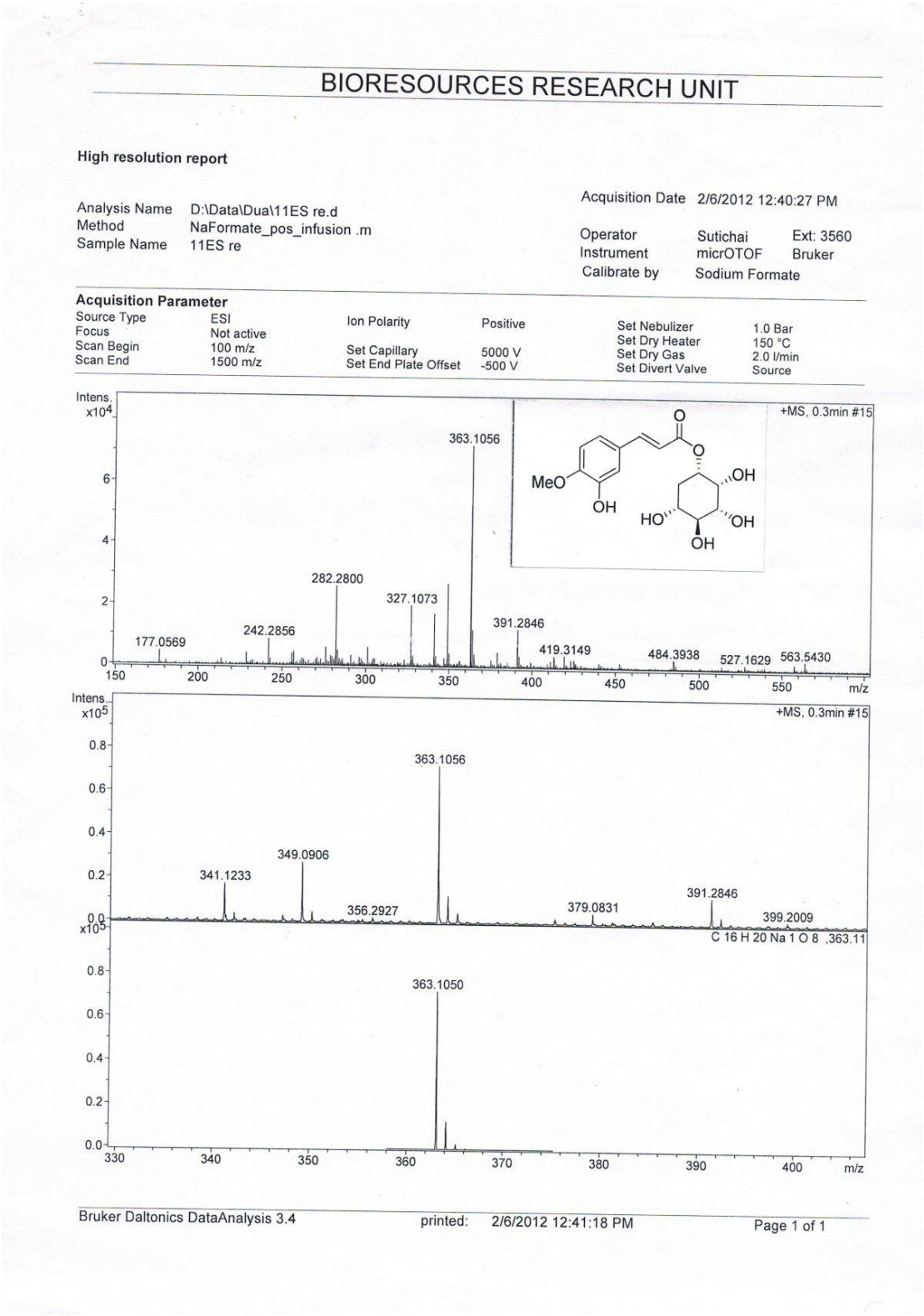

Figure A.77 HRMS of **2.8ES**

BIORESOURCES RESEARCH UNIT

High resolution report

Analysis Name D:\Data\customer\10 AR .d
Method NaFormate_pos_infusion .m
Sample Name 10 AR

Acquisition Date 7/16/2012 1:37:37 PM

Operator Sutichai Ext: 3560
Instrument micrOTOF Bruker
Calibrate by Sodium Formate

Acquisition Parameter

Source Type	ESI	Ion Polarity	Positive	Set Nebulizer	1.0 Bar
Focus	Not active			Set Dry Heater	150 °C
Scan Begin	100 m/z	Set Capillary	5000 V	Set Dry Gas	2.0 l/min
Scan End	1500 m/z	Set End Plate Offset	-500 V	Set Divert Valve	Source

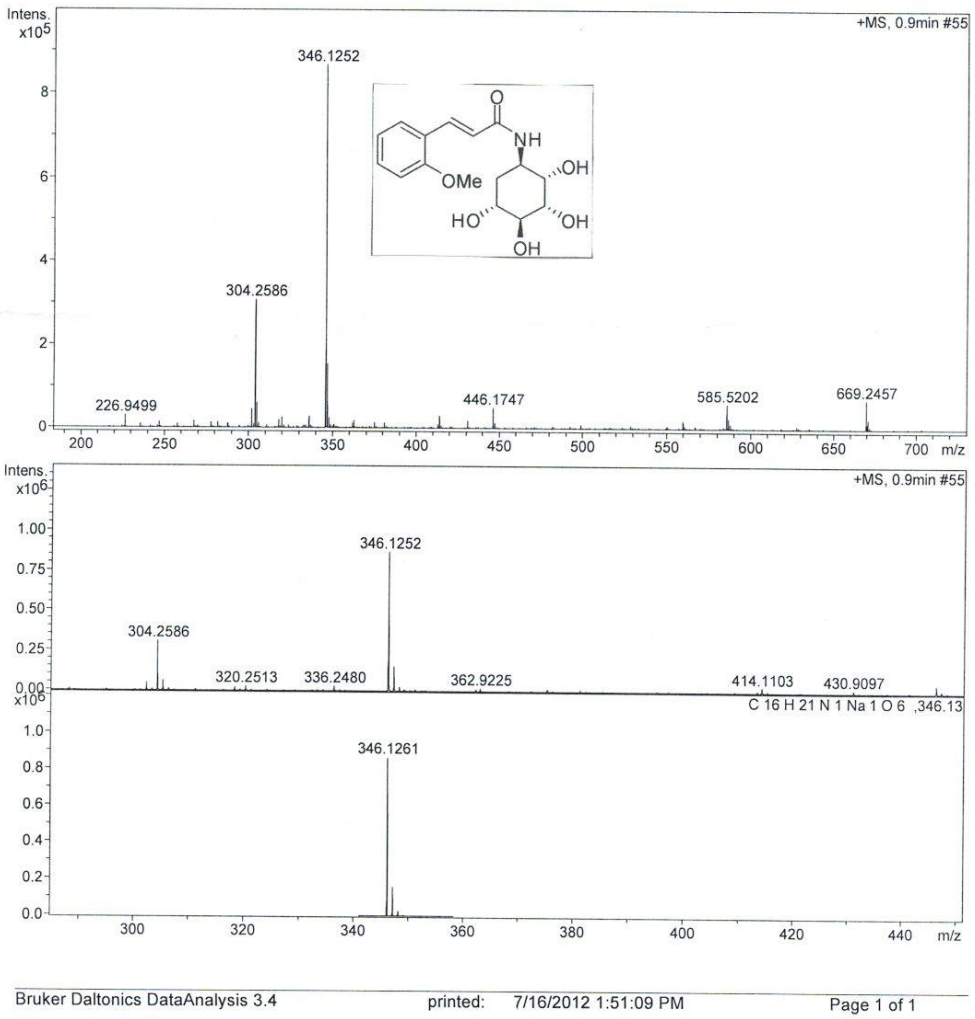

Bruker Daltonics DataAnalysis 3.4 printed: 7/16/2012 1:51:09 PM Page 1 of 1

Figure A.78 HRMS of **2.1AR**

BIORESOURCES RESEARCH UNIT

High resolution report

Analysis Name	D:\Data\customer\9 AR 1.d	Acquisition Date	7/16/2012 1:33:07 PM
Method	NaFormate_pos_infusion .m		
Sample Name	9 AR 1	Operator	Sutichai Ext: 3560
		Instrument	micrOTOF Bruker
		Calibrate by	Sodium Formate

Acquisition Parameter

Source Type	ESI	Ion Polarity	Positive	Set Nebulizer	1.0 Bar
Focus	Not active			Set Dry Heater	150 °C
Scan Begin	100 m/z	Set Capillary	5000 V	Set Dry Gas	2.0 l/min
Scan End	1500 m/z	Set End Plate Offset	-500 V	Set Divert Valve	Source

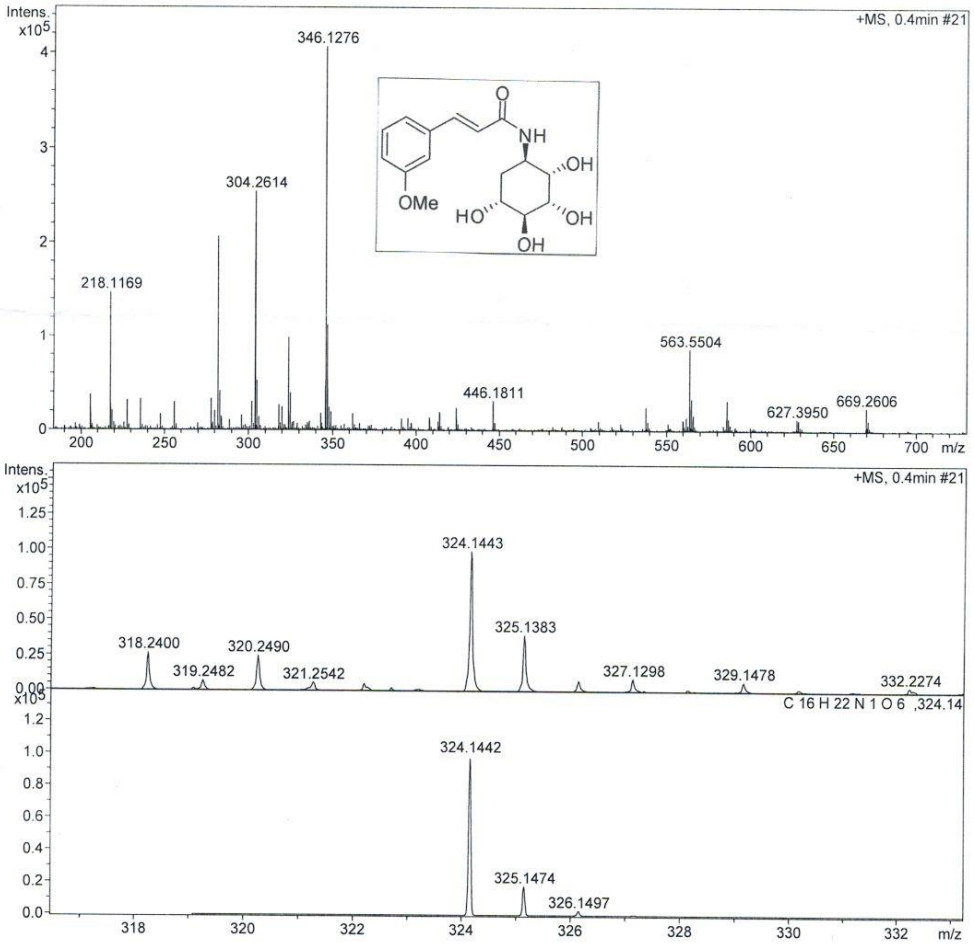

Bruker Daltonics DataAnalysis 3.4 printed: 7/16/2012 1:50:13 PM Page 1 of 1

Figure A.79 HRMS of **2.2AR**

BIORESOURCES RESEARCH UNIT

High resolution report

Acquisition Date 7/16/2012 11:35:08 AM

Analysis Name	D:\Data\customer\5 AR.d	Operator	Sutichai	Ext: 3560
Method	NaFormate_pos_infusion .m	Instrument	micrOTOF	Bruker
Sample Name	5 AR	Calibrate by	Sodium Formate	

Acquisition Parameter

Source Type	ESI	Ion Polarity	Positive	Set Nebulizer	1.0 Bar
Focus	Not active			Set Dry Heater	150 °C
Scan Begin	100 m/z	Set Capillary	5000 V	Set Dry Gas	2.0 l/min
Scan End	1500 m/z	Set End Plate Offset	-500 V	Set Divert Valve	Source

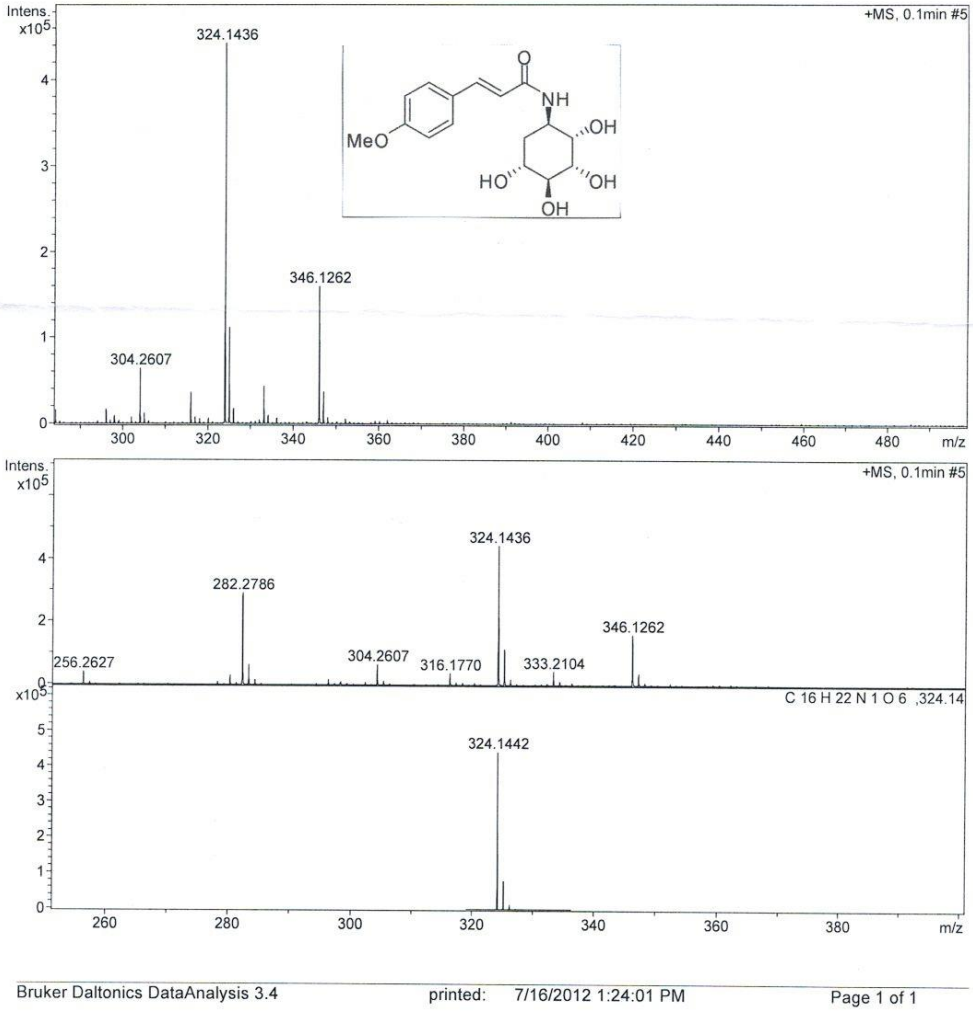

Bruker Daltonics DataAnalysis 3.4 printed: 7/16/2012 1:24:01 PM Page 1 of 1

Figure A.80 HRMS of **2.3AR**

BIORESOURCES RESEARCH UNIT

High resolution report

Analysis Name D:\Data\customer\4 AR.d
Method NaFormate_pos_infusion .m
Sample Name 4 AR

Acquisition Date 7/16/2012 11:33:19 AM

Operator Sutichai Ext: 3560
Instrument micrOTOF Bruker
Calibrate by Sodium Formate

Acquisition Parameter

Source Type	ESI	Ion Polarity	Positive	Set Nebulizer	1.0 Bar
Focus	Not active			Set Dry Heater	150 °C
Scan Begin	100 m/z	Set Capillary	5000 V	Set Dry Gas	2.0 l/min
Scan End	1500 m/z	Set End Plate Offset	-500 V	Set Divert Valve	Source

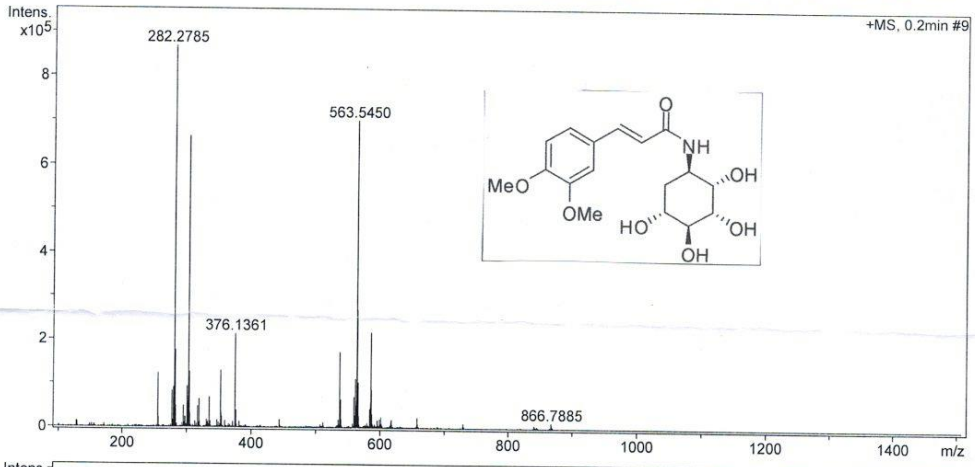

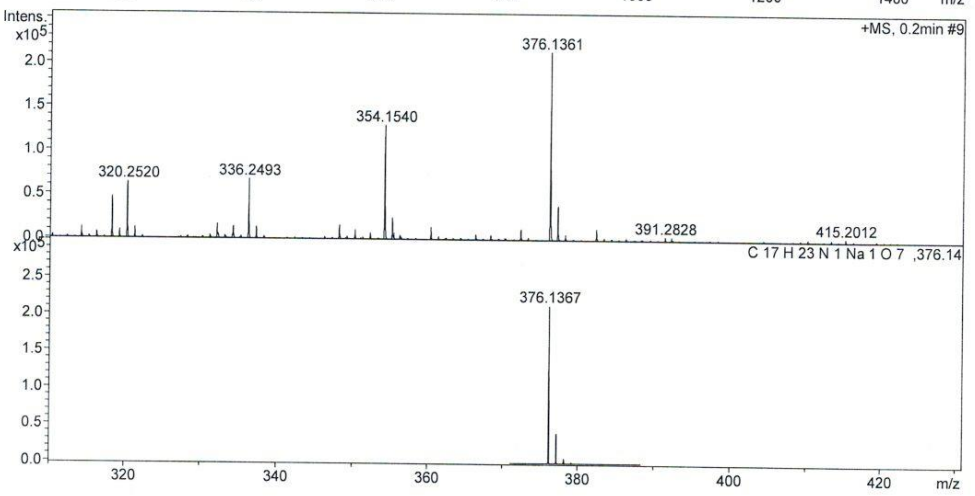

Bruker Daltonics DataAnalysis 3.4 printed: 7/16/2012 1:23:19 PM Page 1 of 1

Figure A.81 HRMS of **2.4AR**

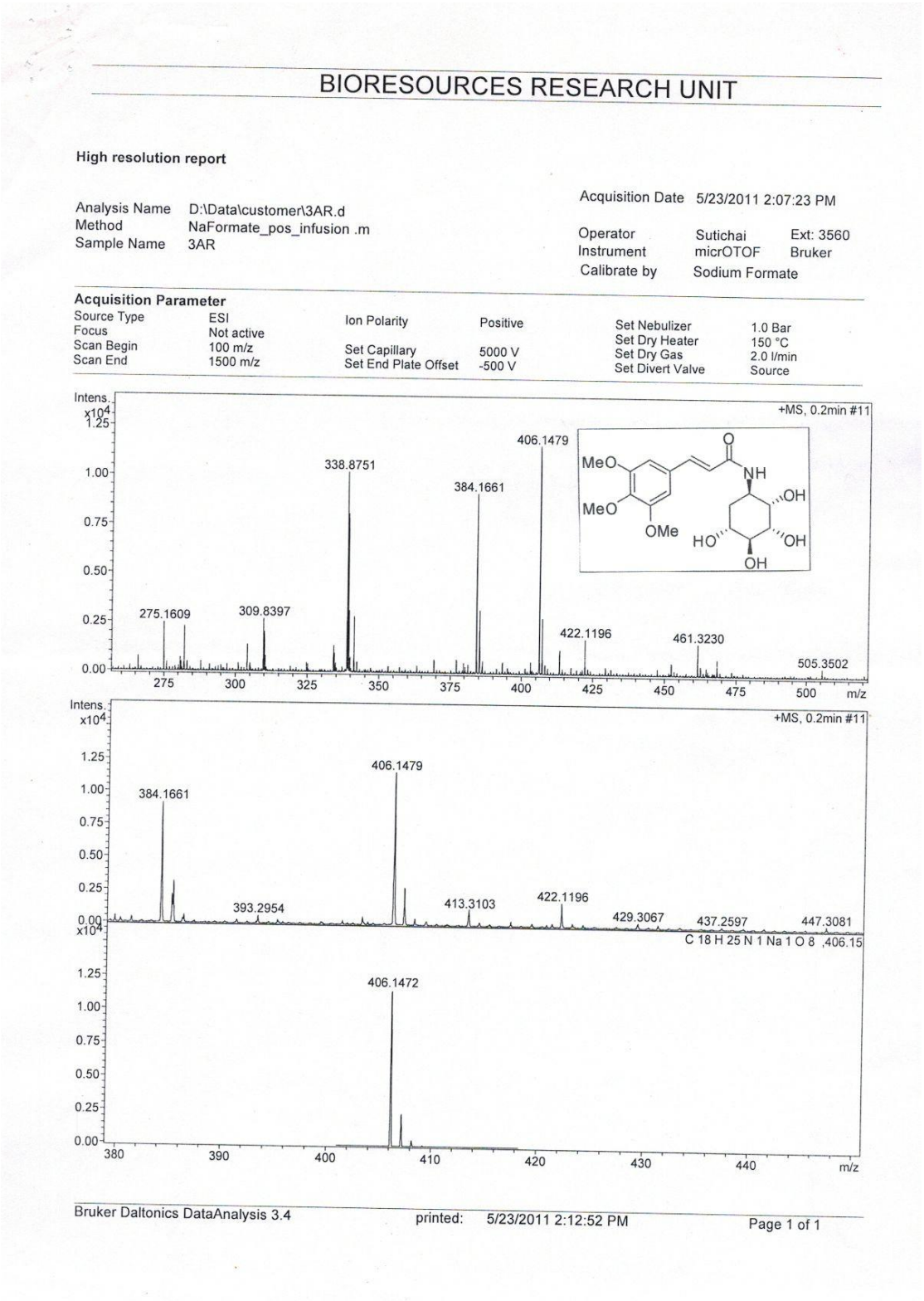

Figure A.82 HRMS of **2.5AR**

BIORESOURCES RESEARCH UNIT

High resolution report

Analysis Name D:\Data\customer\7 AR.d
Method NaFormate_pos_infusion .m
Sample Name 7 AR

Acquisition Date 7/16/2012 1:26:55 PM

Operator Sutichai Ext: 3560
Instrument micrOTOF Bruker
Calibrate by Sodium Formate

Acquisition Parameter

Source Type	ESI	Ion Polarity	Positive	Set Nebulizer	1.0 Bar
Focus	Not active			Set Dry Heater	150 °C
Scan Begin	100 m/z	Set Capillary	5000 V	Set Dry Gas	2.0 l/min
Scan End	1500 m/z	Set End Plate Offset	-500 V	Set Divert Valve	Source

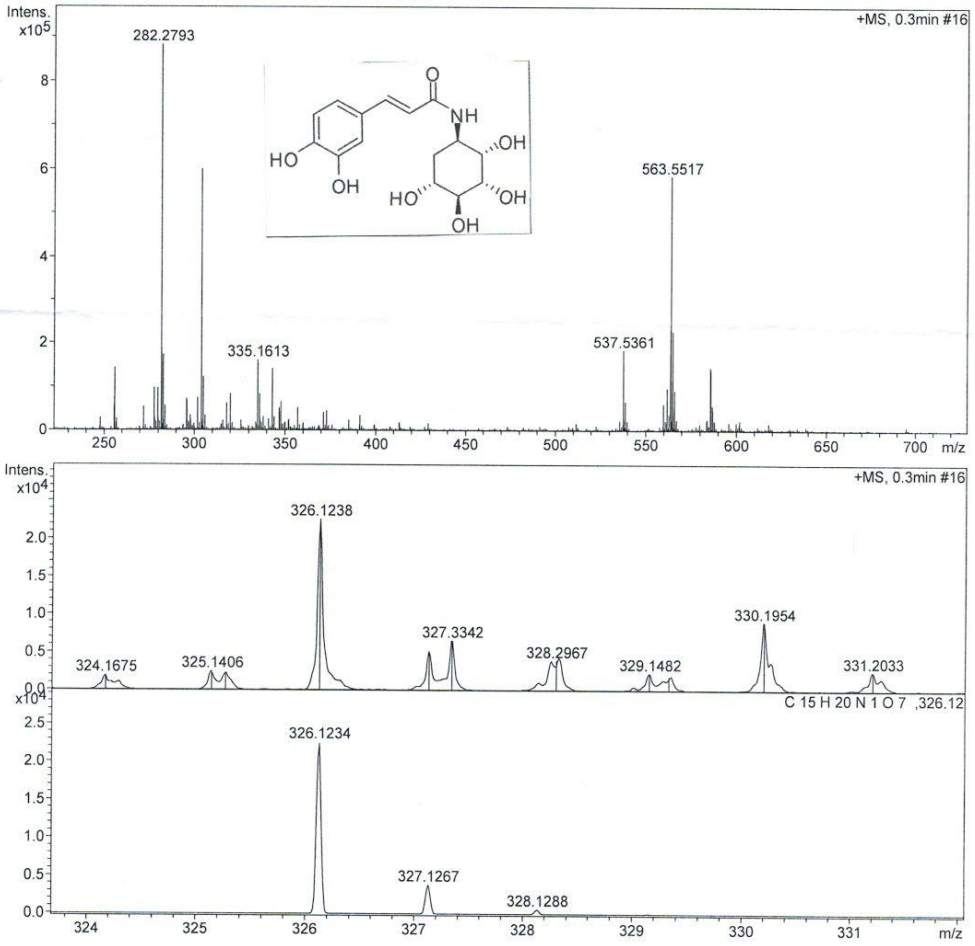

Bruker Daltonics DataAnalysis 3.4 printed: 7/16/2012 1:46:30 PM Page 1 of 1

Figure A.83 HRMS of **2.6AR**

BIORESOURCES RESEARCH UNIT

High resolution report

Analysis Name D:\Data\customer\6 AR.d
Method NaFormate_pos_infusion .m
Sample Name 6 AR

Acquisition Date 7/16/2012 11:36:52 AM

Operator Sutichai Ext: 3560
Instrument micrOTOF Bruker
Calibrate by Sodium Formate

Acquisition Parameter

Source Type	ESI	Ion Polarity	Positive	Set Nebulizer	1.0 Bar
Focus	Not active			Set Dry Heater	150 °C
Scan Begin	100 m/z	Set Capillary	5000 V	Set Dry Gas	2.0 l/min
Scan End	1500 m/z	Set End Plate Offset	-500 V	Set Divert Valve	Source

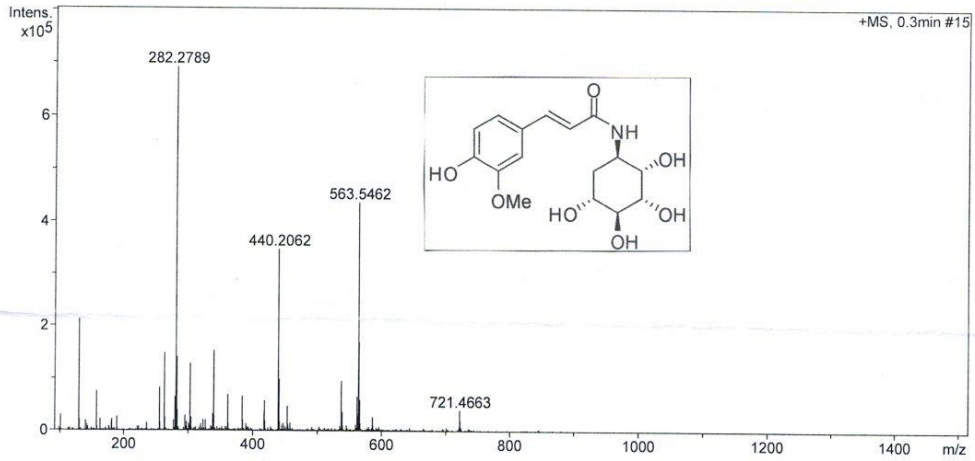

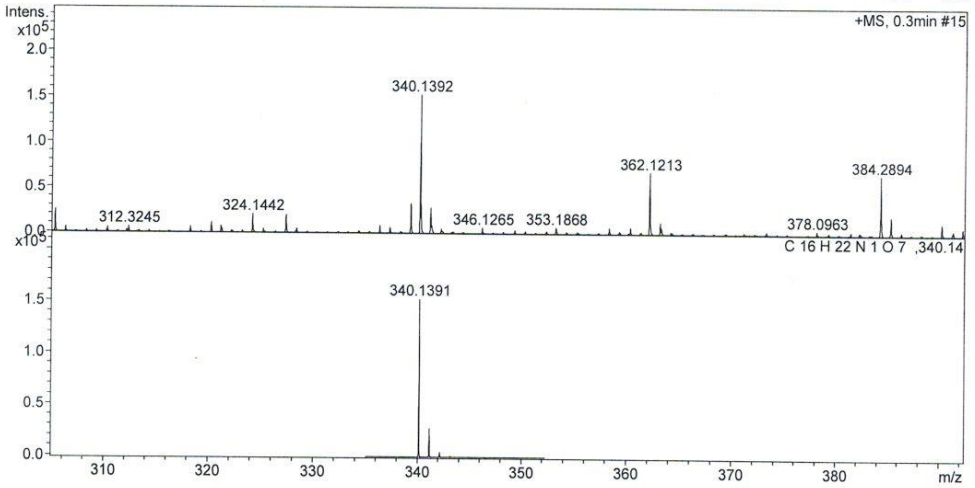

Bruker Daltonics DataAnalysis 3.4 printed: 7/16/2012 1:24:37 PM Page 1 of 1

Figure A.84 HRMS of **2.7AR**

BIORESOURCES RESEARCH UNIT

High resolution report

Analysis Name D:\Data\customer\11 AR 1.d
Method NaFormate_pos_infusion .m
Sample Name 11 AR 1

Acquisition Date 7/16/2012 1:42:36 PM
Operator Sutichai Ext: 3560
Instrument micrOTOF Bruker
Calibrate by Sodium Formate

Acquisition Parameter

Source Type	ESI	Ion Polarity	Positive	Set Nebulizer	1.0 Bar
Focus	Not active			Set Dry Heater	150 °C
Scan Begin	100 m/z	Set Capillary	5000 V	Set Dry Gas	2.0 l/min
Scan End	1500 m/z	Set End Plate Offset	-500 V	Set Divert Valve	Source

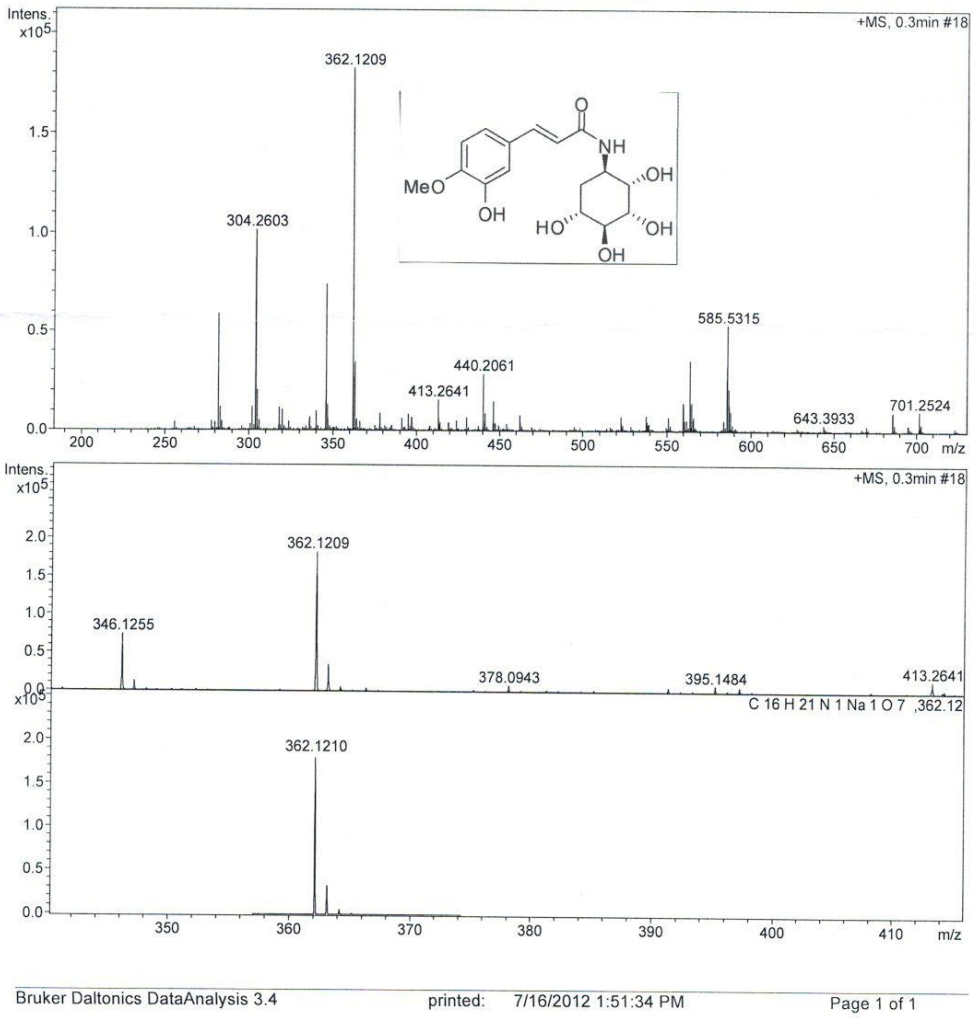

Bruker Daltonics DataAnalysis 3.4 printed: 7/16/2012 1:51:34 PM Page 1 of 1

Figure A.85 HRMS of **2.8AR**

BIORESOURCES RESEARCH UNIT

High resolution report

Acquisition Date 3/19/2012 4:40:34 PM

Analysis Name	D:\Data\customer\10AS.d				
Method	NaFormate_pos_infusion .m			Operator	Sutichai Ext: 3560
Sample Name	10AS			Instrument	micrOTOF Bruker
				Calibrate by	Sodium Formate

Acquisition Parameter

Source Type	ESI	Ion Polarity	Positive	Set Nebulizer	1.0 Bar
Focus	Not active			Set Dry Heater	150 °C
Scan Begin	100 m/z	Set Capillary	5000 V	Set Dry Gas	2.0 l/min
Scan End	1500 m/z	Set End Plate Offset	-500 V	Set Divert Valve	Source

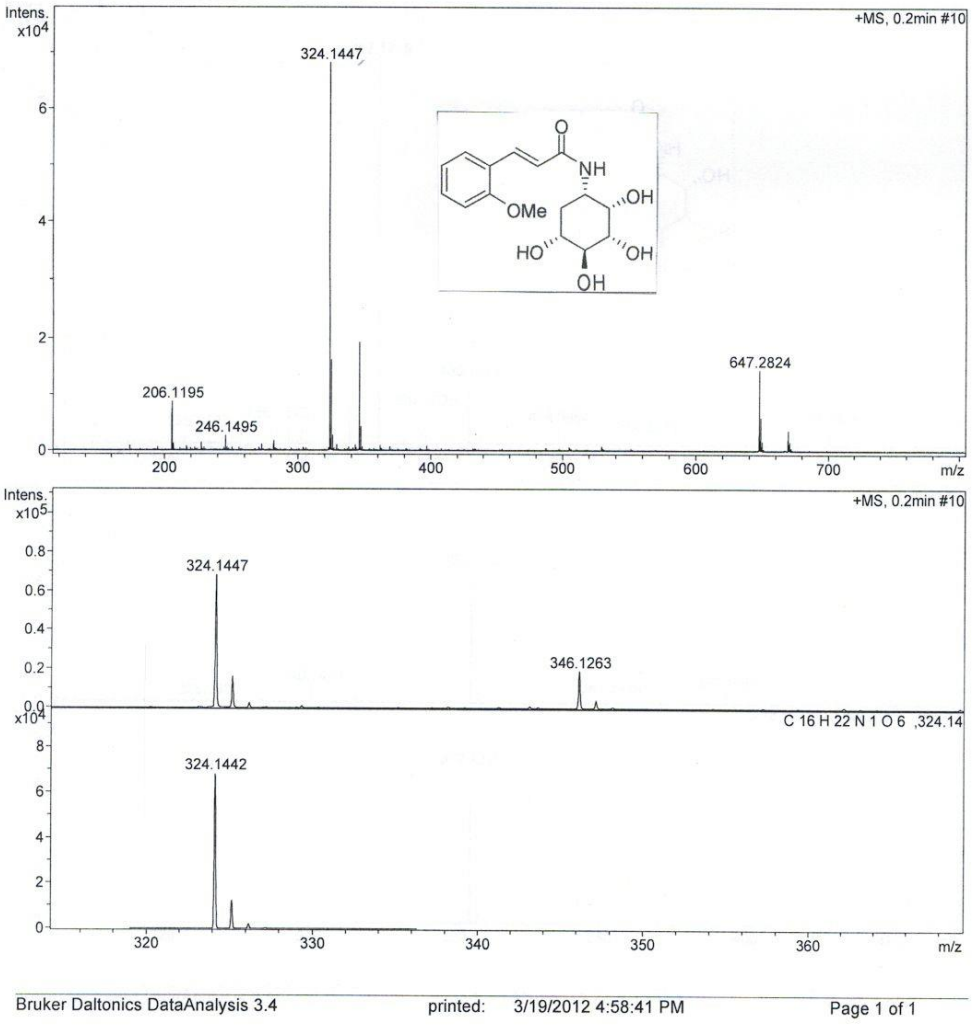

Bruker Daltonics DataAnalysis 3.4 printed: 3/19/2012 4:58:41 PM Page 1 of 1

Figure A.86 HRMS of **2.1AS**

BIORESOURCES RESEARCH UNIT

High resolution report

		Acquisition Date	3/19/2012 4:38:56 PM
Analysis Name	D:\Data\customer\9AS.d		
Method	NaFormate_pos_infusion .m	Operator	Sutichai Ext: 3560
Sample Name	9AS	Instrument	micrOTOF Bruker
		Calibrate by	Sodium Formate

Acquisition Parameter

Source Type	ESI	Ion Polarity	Positive	Set Nebulizer	1.0 Bar
Focus	Not active			Set Dry Heater	150 °C
Scan Begin	100 m/z	Set Capillary	5000 V	Set Dry Gas	2.0 l/min
Scan End	1500 m/z	Set End Plate Offset	-500 V	Set Divert Valve	Source

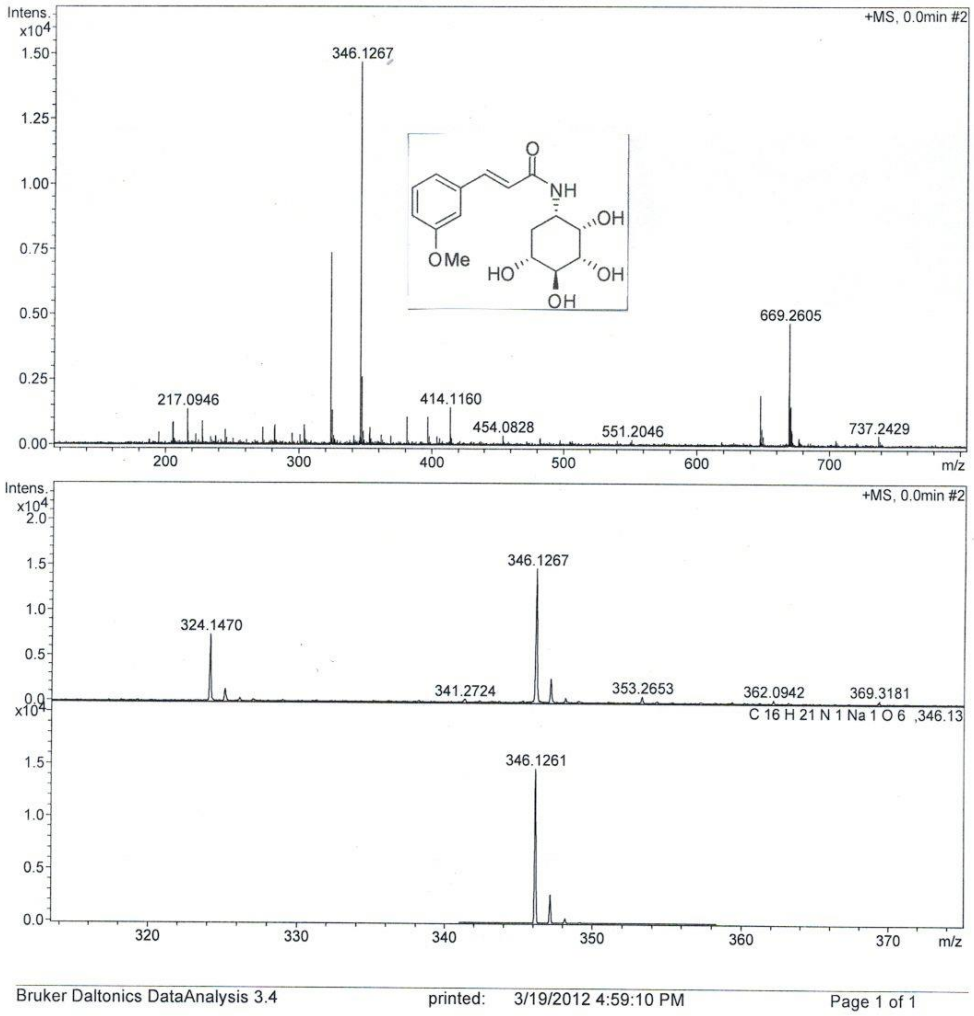

Bruker Daltonics DataAnalysis 3.4 printed: 3/19/2012 4:59:10 PM Page 1 of 1

Figure A.87 HRMS of **2.2AS**

BIORESOURCES RESEARCH UNIT

High resolution report

		Acquisition Date	3/19/2012 4:52:42 PM
Analysis Name	D:\Data\customer\5AS.d		
Method	NaFormate_pos_infusion .m	Operator	Sutichai Ext: 3560
Sample Name	5AS	Instrument	micrOTOF Bruker
		Calibrate by	Sodium Formate

Acquisition Parameter

Source Type	ESI	Ion Polarity	Positive	Set Nebulizer	1.0 Bar
Focus	Not active			Set Dry Heater	150 °C
Scan Begin	100 m/z	Set Capillary	5000 V	Set Dry Gas	2.0 l/min
Scan End	1500 m/z	Set End Plate Offset	-500 V	Set Divert Valve	Source

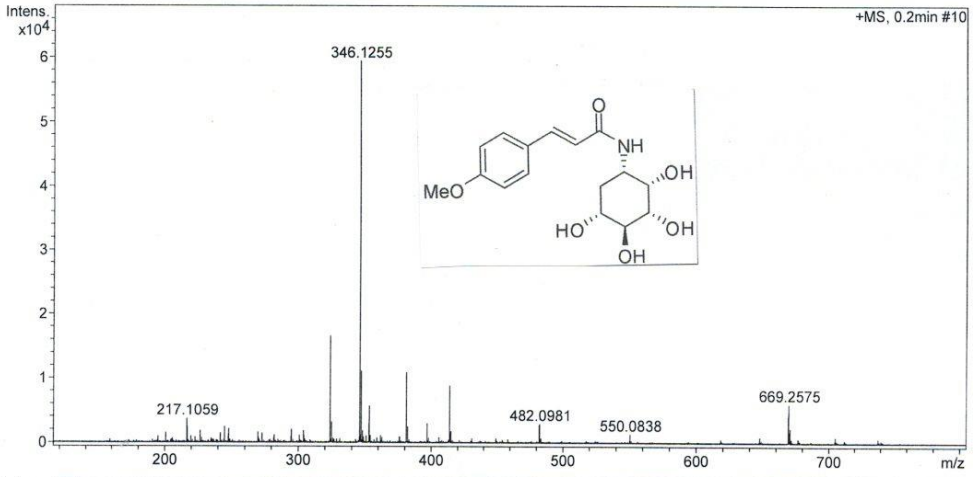

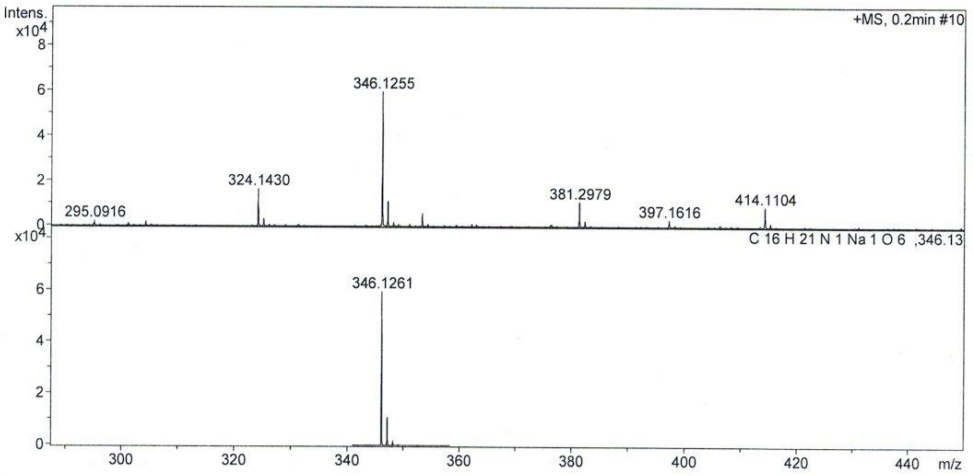

Bruker Daltonics DataAnalysis 3.4 printed: 3/19/2012 4:56:55 PM Page 1 of 1

Figure A.88 HRMS of **2.3AS**

BIORESOURCES RESEARCH UNIT

High resolution report

Acquisition Date 3/19/2012 4:49:14 PM

Analysis Name D:\Data\customer\4AS.d
Method NaFormate_pos_infusion .m
Sample Name 4AS

Operator Sutichai Ext: 3560
Instrument micrOTOF Bruker
Calibrate by Sodium Formate

Acquisition Parameter

Source Type	ESI	Ion Polarity	Positive	Set Nebulizer	1.0 Bar
Focus	Not active			Set Dry Heater	150 °C
Scan Begin	100 m/z	Set Capillary	5000 V	Set Dry Gas	2.0 l/min
Scan End	1500 m/z	Set End Plate Offset	-500 V	Set Divert Valve	Source

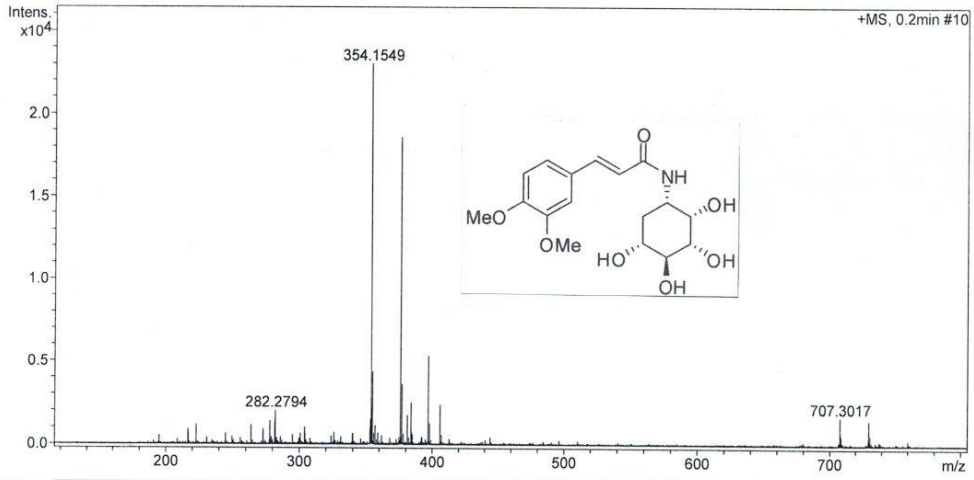

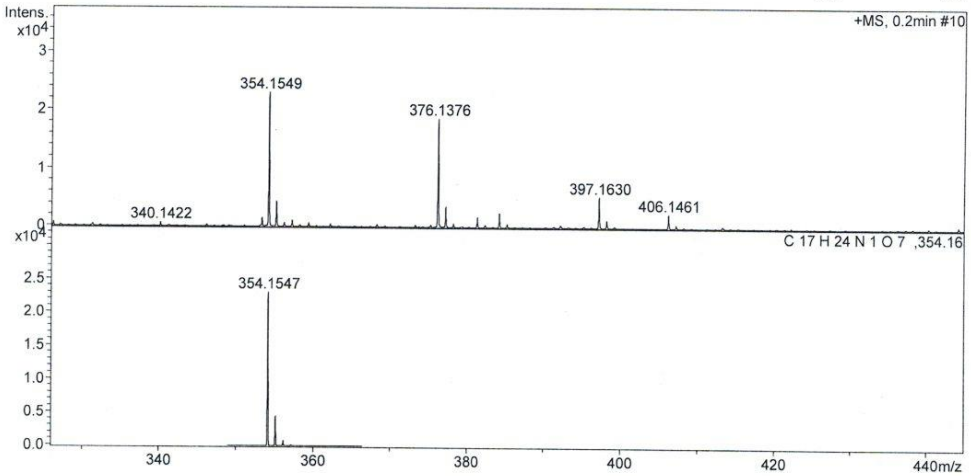

Bruker Daltonics DataAnalysis 3.4 printed: 3/19/2012 4:57:21 PM Page 1 of 1

Figure A.89 HRMS of **2.4AS**

BIORESOURCES RESEARCH UNIT

High resolution report

Acquisition Date 3/19/2012 4:47:30 PM

Analysis Name D:\Data\customer\3AS.d
Method NaFormate_pos_infusion .m
Sample Name 3AS

Operator Sutichai Ext: 3560
Instrument micrOTOF Bruker
Calibrate by Sodium Formate

Acquisition Parameter

Source Type	ESI	Ion Polarity	Positive	Set Nebulizer	1.0 Bar
Focus	Not active			Set Dry Heater	150 °C
Scan Begin	100 m/z	Set Capillary	5000 V	Set Dry Gas	2.0 l/min
Scan End	1500 m/z	Set End Plate Offset	-500 V	Set Divert Valve	Source

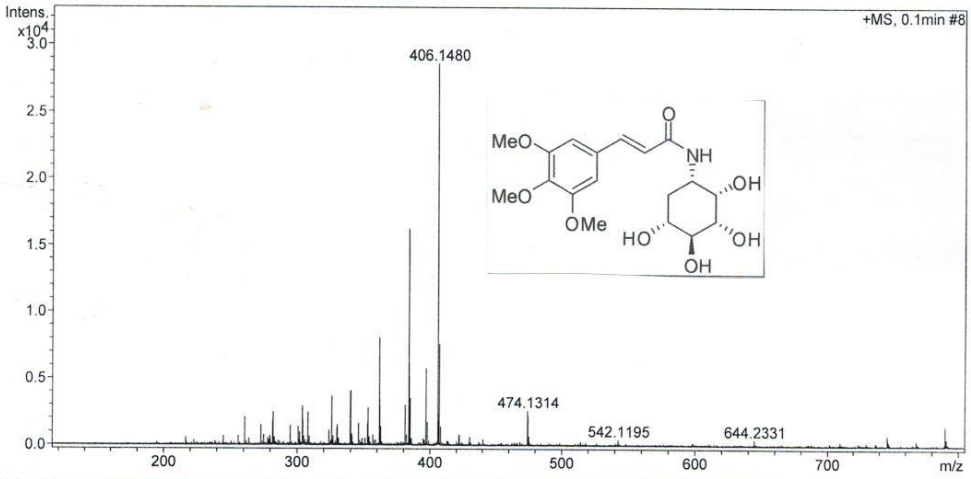

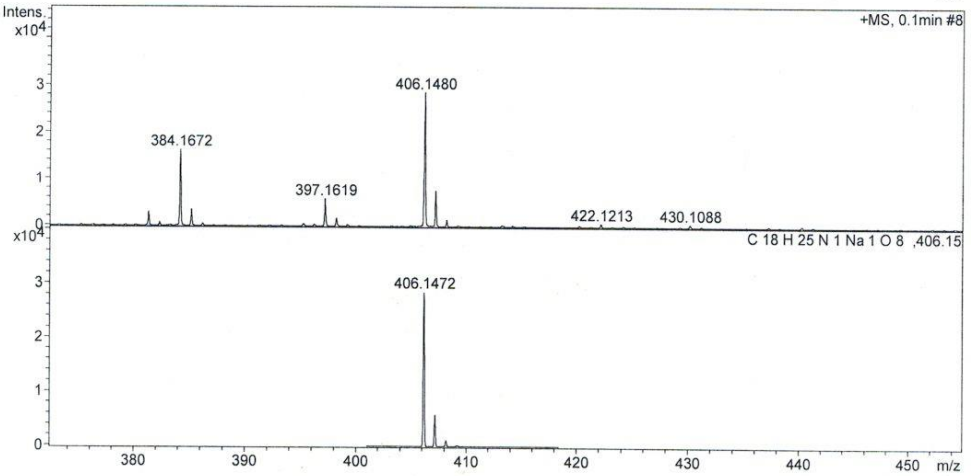

Bruker Daltonics DataAnalysis 3.4 printed: 3/19/2012 4:57:47 PM Page 1 of 1

Figure A.90 HRMS of **2.5AS**

BIORESOURCES RESEARCH UNIT

High resolution report

Analysis Name D:\Data\customer\7AS.d
Method NaFormate_pos_infusion .m
Sample Name 7AS

Acquisition Date 3/19/2012 4:36:59 PM
Operator Sutichai Ext: 3560
Instrument micrOTOF Bruker
Calibrate by Sodium Formate

Acquisition Parameter

Source Type	ESI	Ion Polarity	Positive	Set Nebulizer	1.0 Bar
Focus	Not active			Set Dry Heater	150 °C
Scan Begin	100 m/z	Set Capillary	5000 V	Set Dry Gas	2.0 l/min
Scan End	1500 m/z	Set End Plate Offset	-500 V	Set Divert Valve	Source

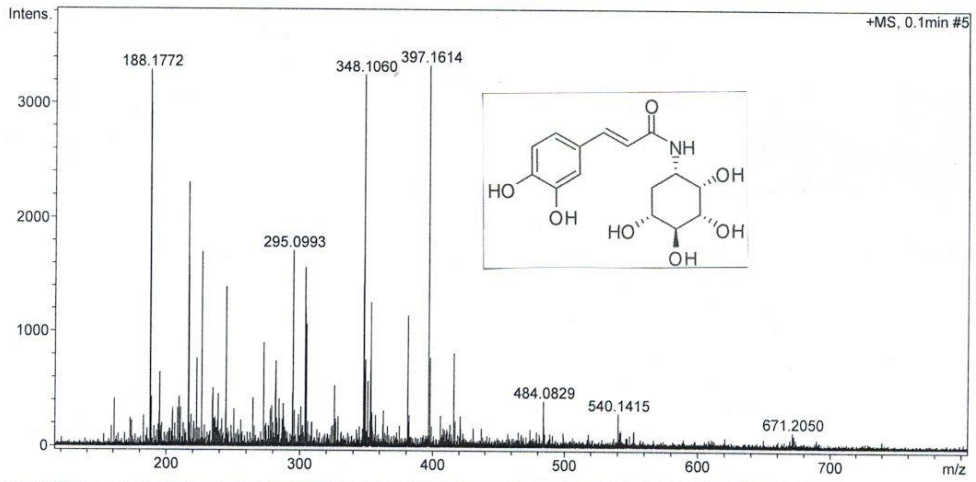

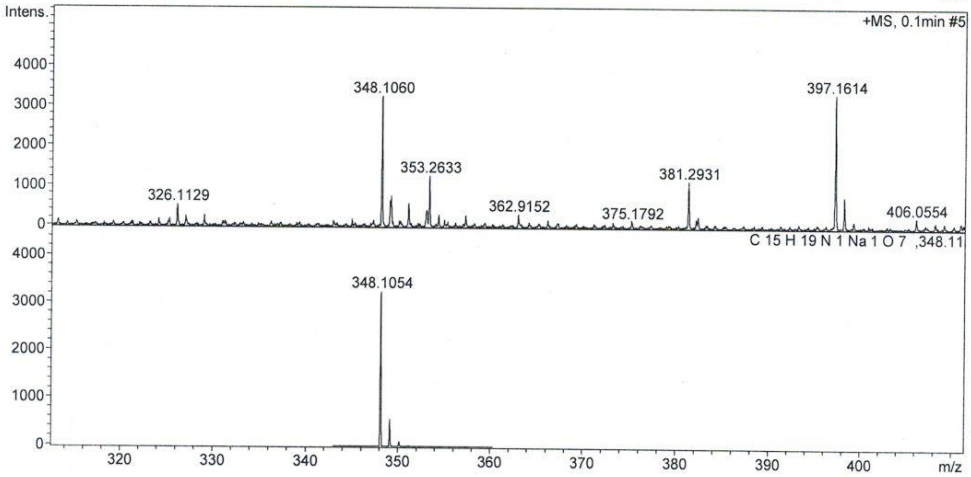

Bruker Daltonics DataAnalysis 3.4 printed: 3/19/2012 4:59:39 PM Page 1 of 1

Figure A.91 HRMS of **2.6AS**

BIORESOURCES RESEARCH UNIT

High resolution report

Acquisition Date 3/19/2012 4:54:25 PM

Analysis Name D:\Data\customer\6AS.d
Method NaFormate_pos_infusion .m
Sample Name 6AS

Operator Sutichai Ext: 3560
Instrument micrOTOF Bruker
Calibrate by Sodium Formate

Acquisition Parameter

Source Type	ESI	Ion Polarity	Positive	Set Nebulizer	1.0 Bar
Focus	Not active			Set Dry Heater	150 °C
Scan Begin	100 m/z	Set Capillary	5000 V	Set Dry Gas	2.0 l/min
Scan End	1500 m/z	Set End Plate Offset	-500 V	Set Divert Valve	Source

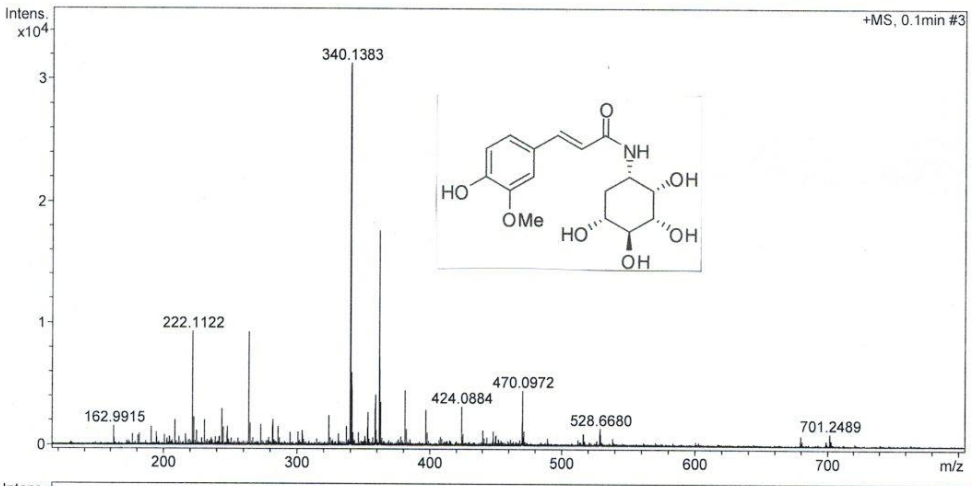

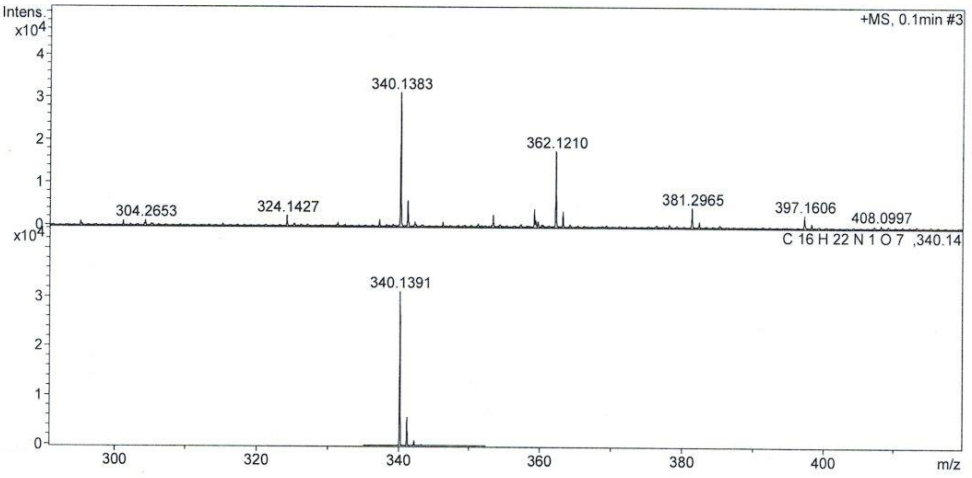

Bruker Daltonics DataAnalysis 3.4 printed: 3/19/2012 4:56:26 PM Page 1 of 1

Figure A.92 HRMS of **2.7AS**

BIORESOURCES RESEARCH UNIT

High resolution report

Analysis Name D:\Data\customer\11AS.d
Method NaFormate_pos_infusion .m
Sample Name 11AS

Acquisition Date 3/19/2012 4:45:46 PM

Operator Sutichai Ext: 3560
Instrument micrOTOF Bruker
Calibrate by Sodium Formate

Acquisition Parameter

Source Type	ESI	Ion Polarity	Positive	Set Nebulizer	1.0 Bar
Focus	Not active			Set Dry Heater	150 °C
Scan Begin	100 m/z	Set Capillary	5000 V	Set Dry Gas	2.0 l/min
Scan End	1500 m/z	Set End Plate Offset	-500 V	Set Divert Valve	Source

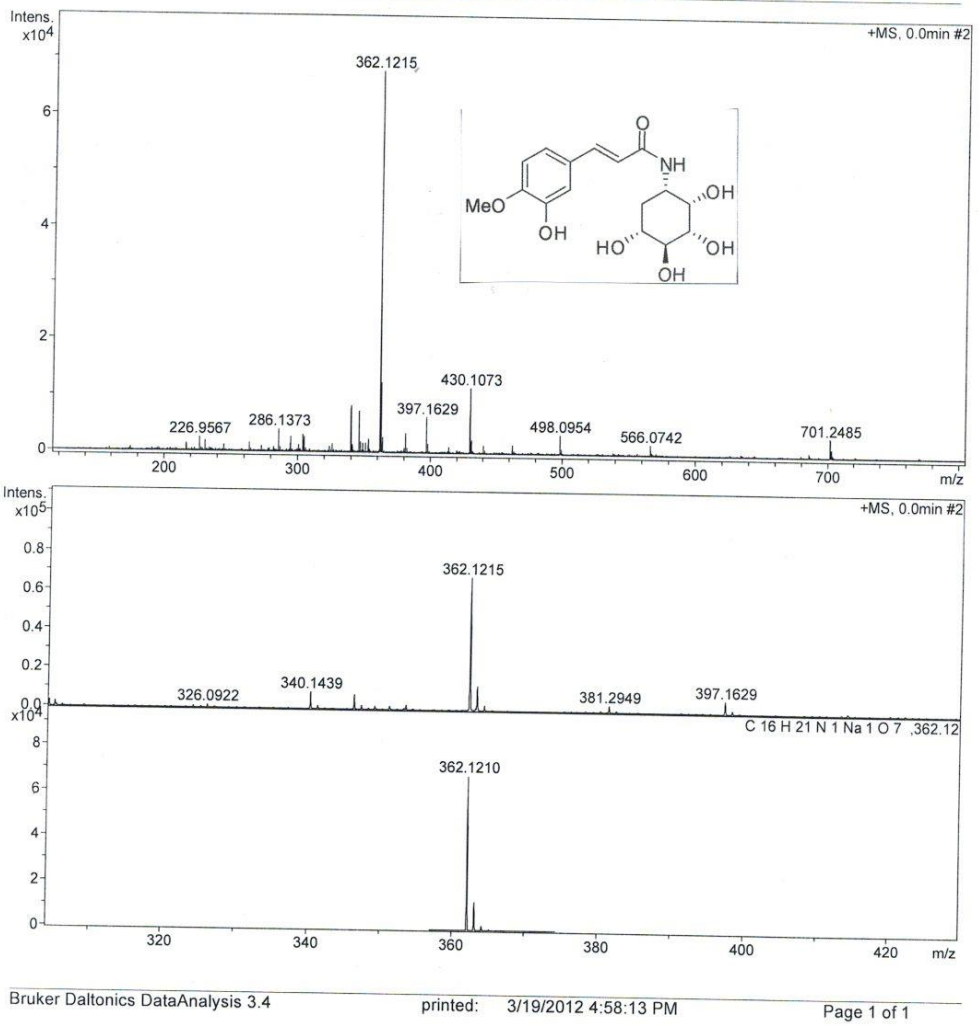

Bruker Daltonics DataAnalysis 3.4 printed: 3/19/2012 4:58:13 PM Page 1 of 1

Figure A.93 HRMS of **2.8AS**

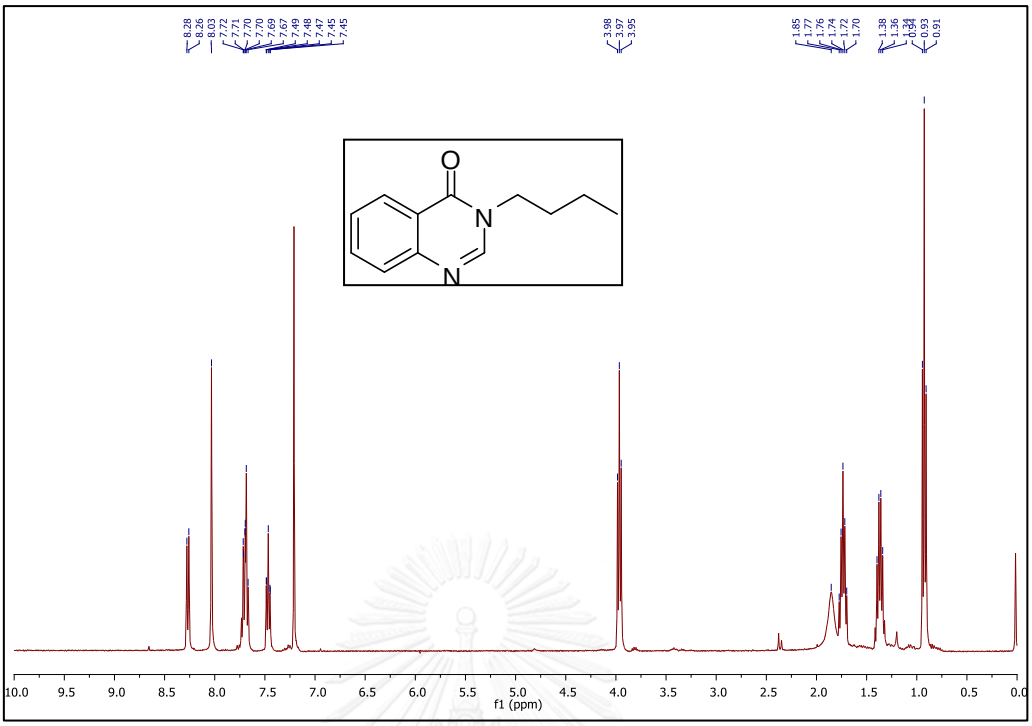

Figure A.94 ^{1}H NMR spectrum of **5.3a** ($CDCl_3$)

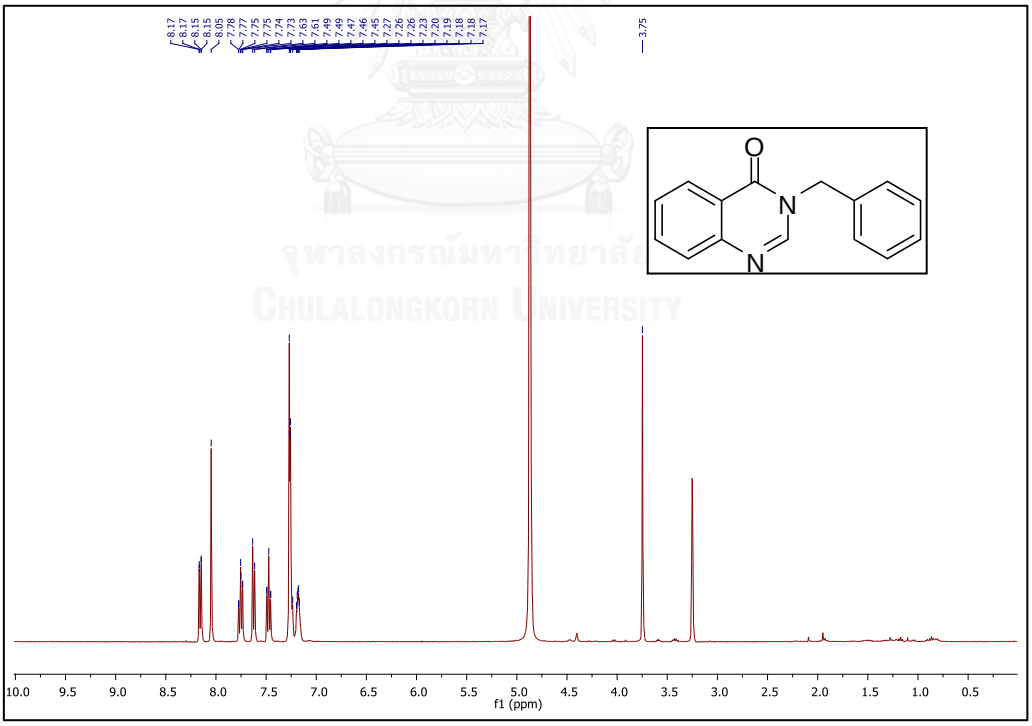

Figure A.95 ^{1}H NMR spectrum of **5.3b** (CD_3OD)

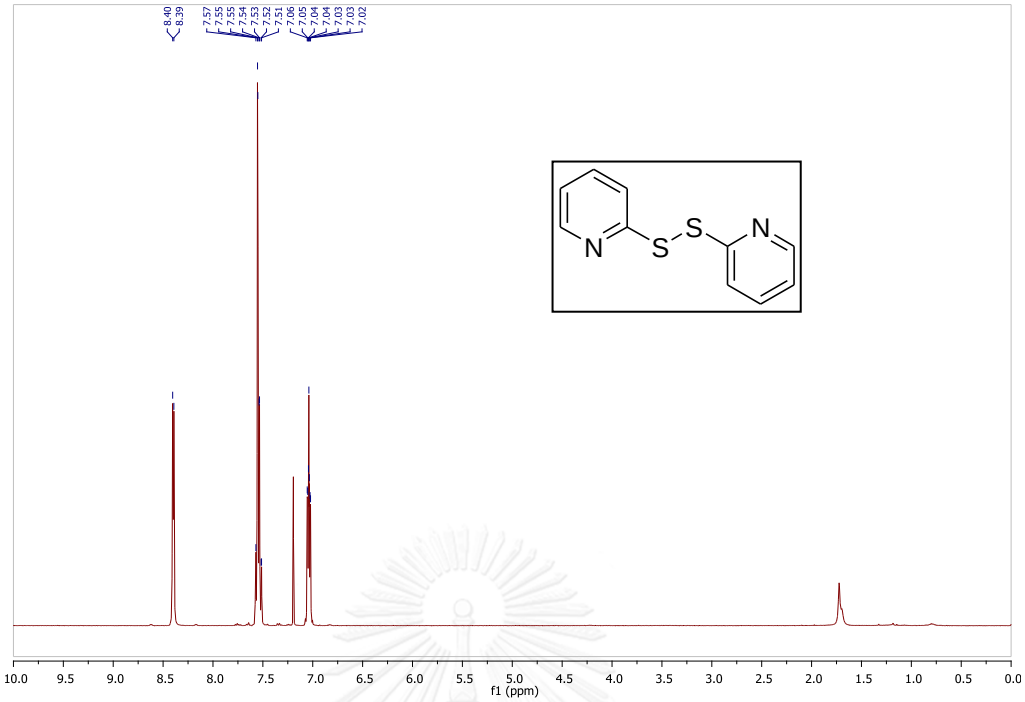

Figure A.96 ^{1}H NMR spectrum of **5.13S ($CDCl_3$)**

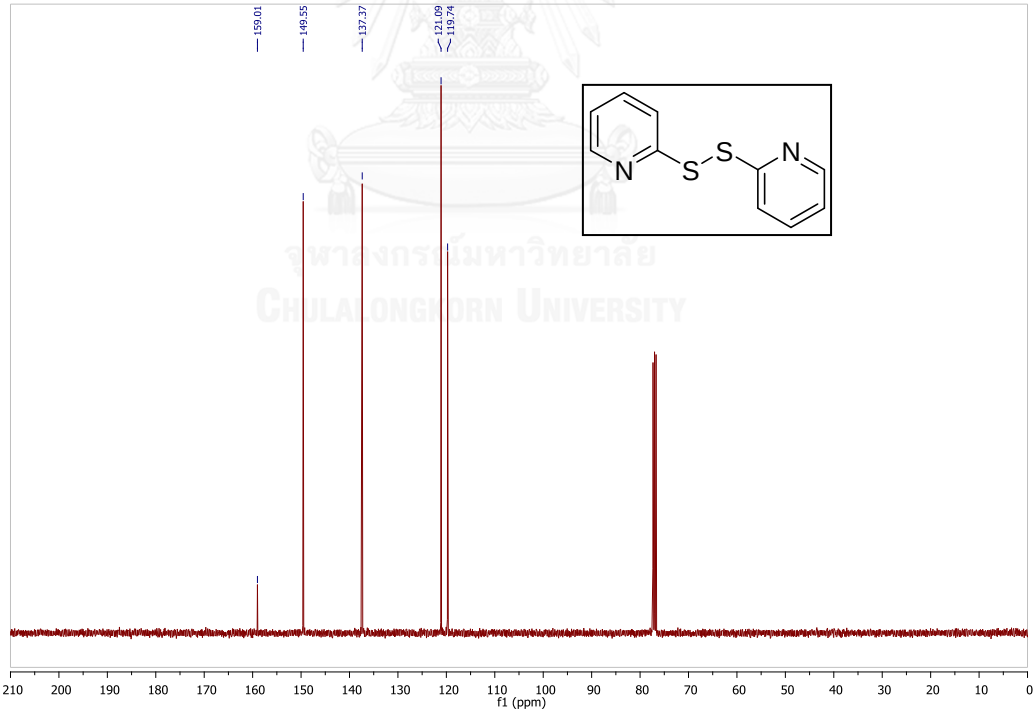

Figure A.97 ^{13}C NMR spectrum of **5.13S ($CDCl_3$)**

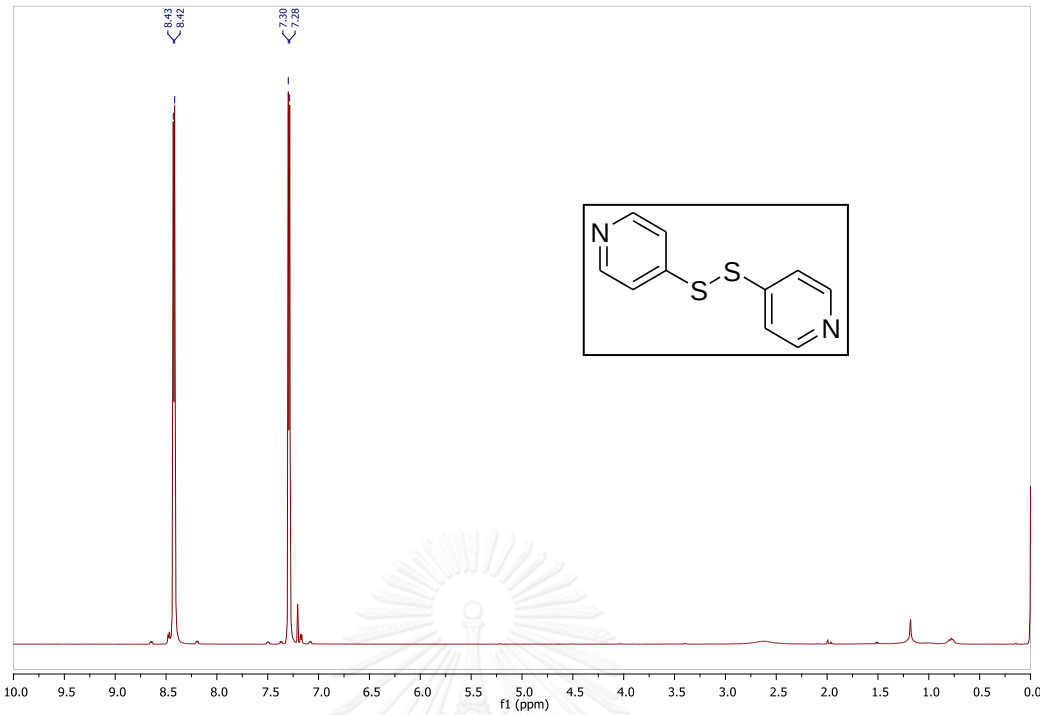

Figure A.98 ^{1}H NMR spectrum of **5.14S ($CDCl_3$)**

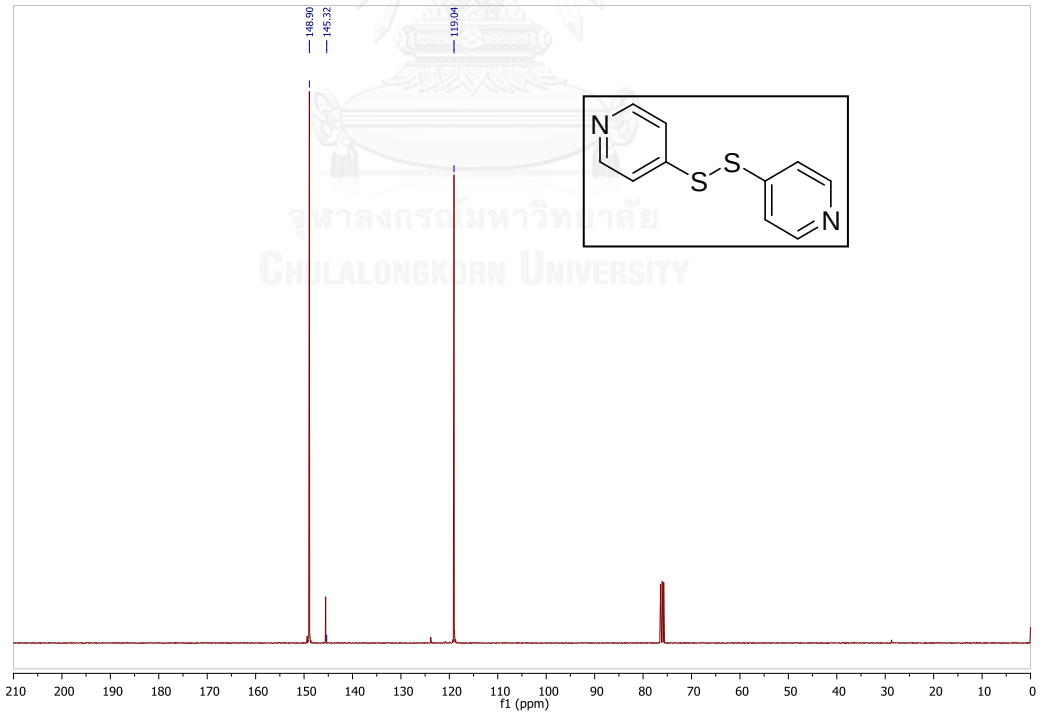

Figure A.99 ^{13}C NMR spectrum of **5.14S ($CDCl_3$)**

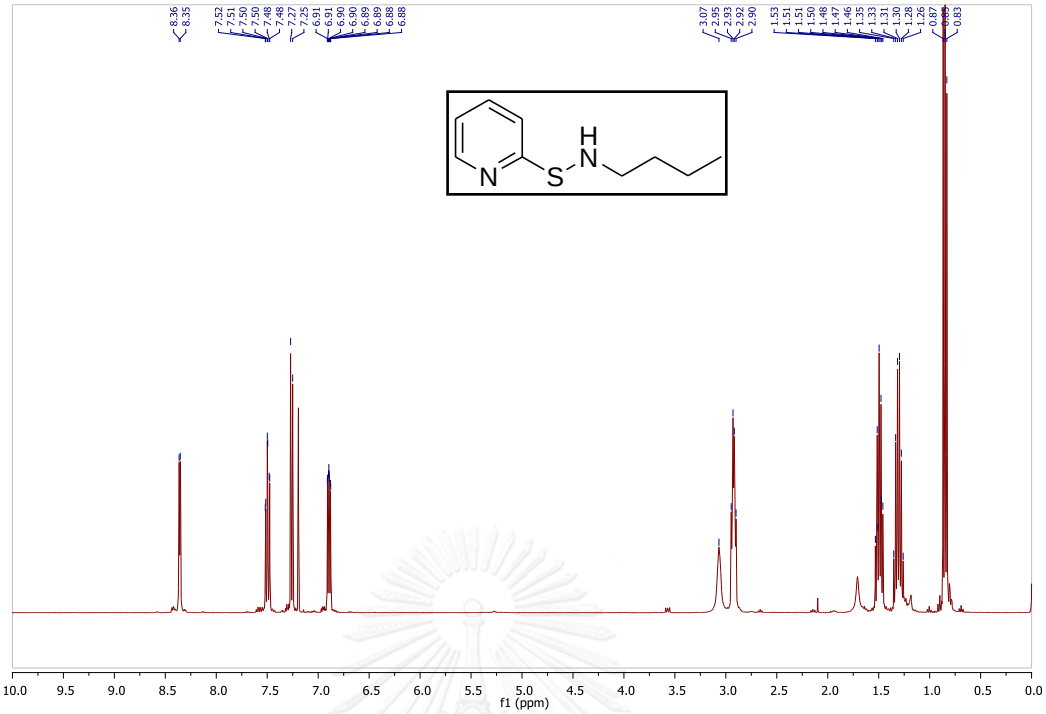

Figure A.100 ^{1}H NMR spectrum of **5.13a** ($CDCl_3$)

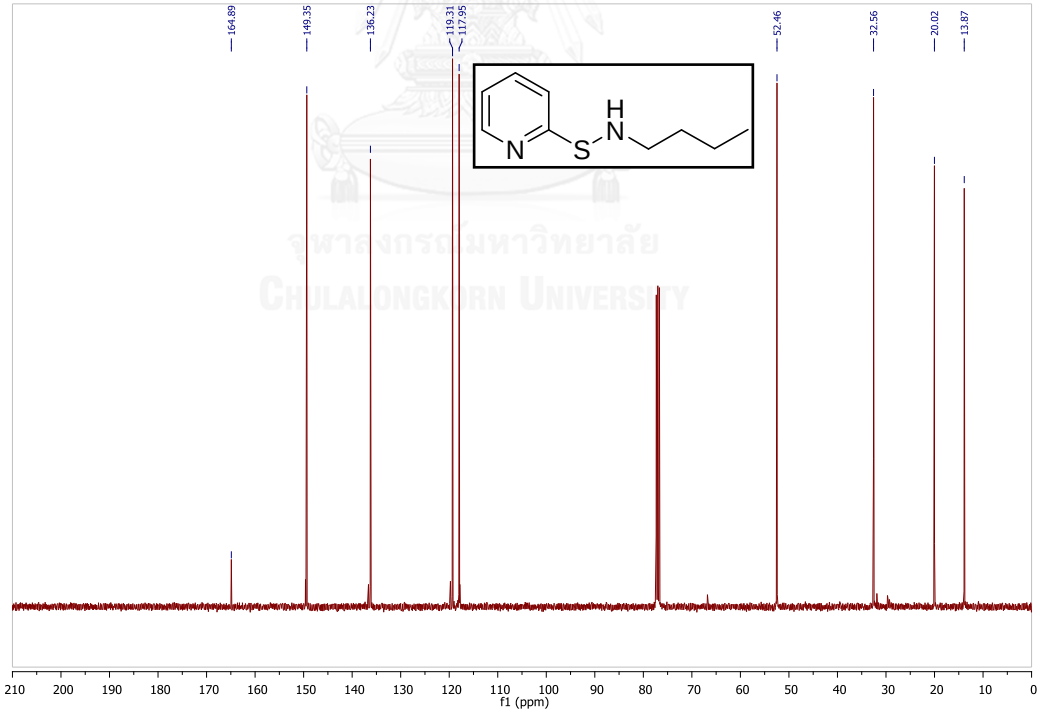

Figure A.101 ^{13}C NMR spectrum of **5.13a** ($CDCl_3$)

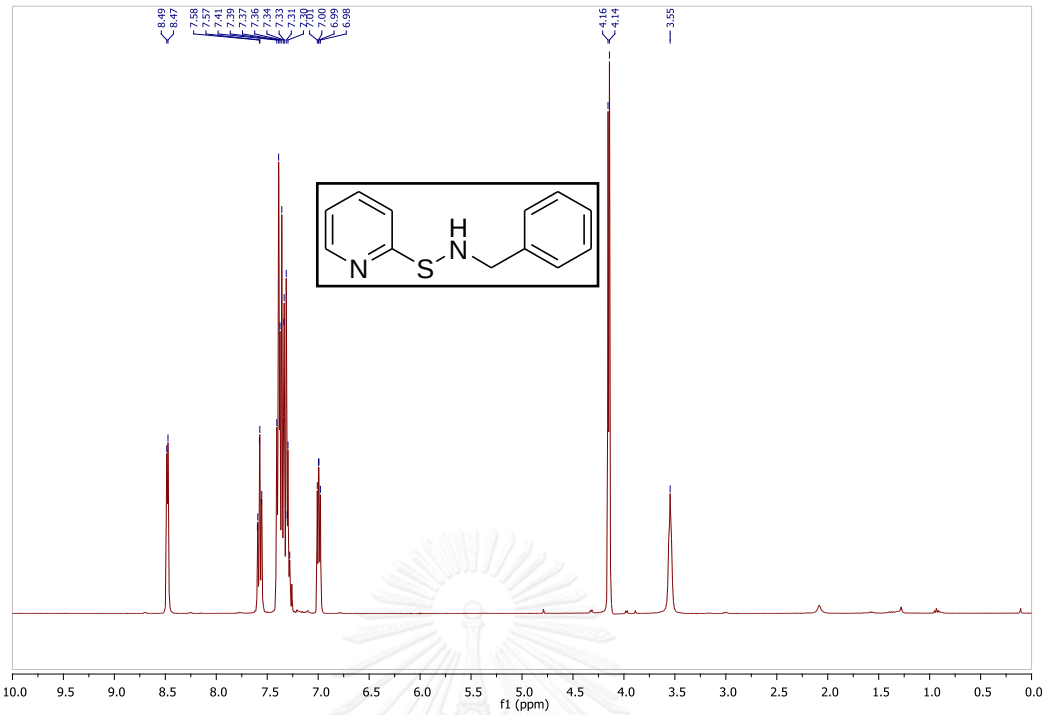

Figure A.102 ^{1}H NMR spectrum of **5.13b** ($CDCl_3$)

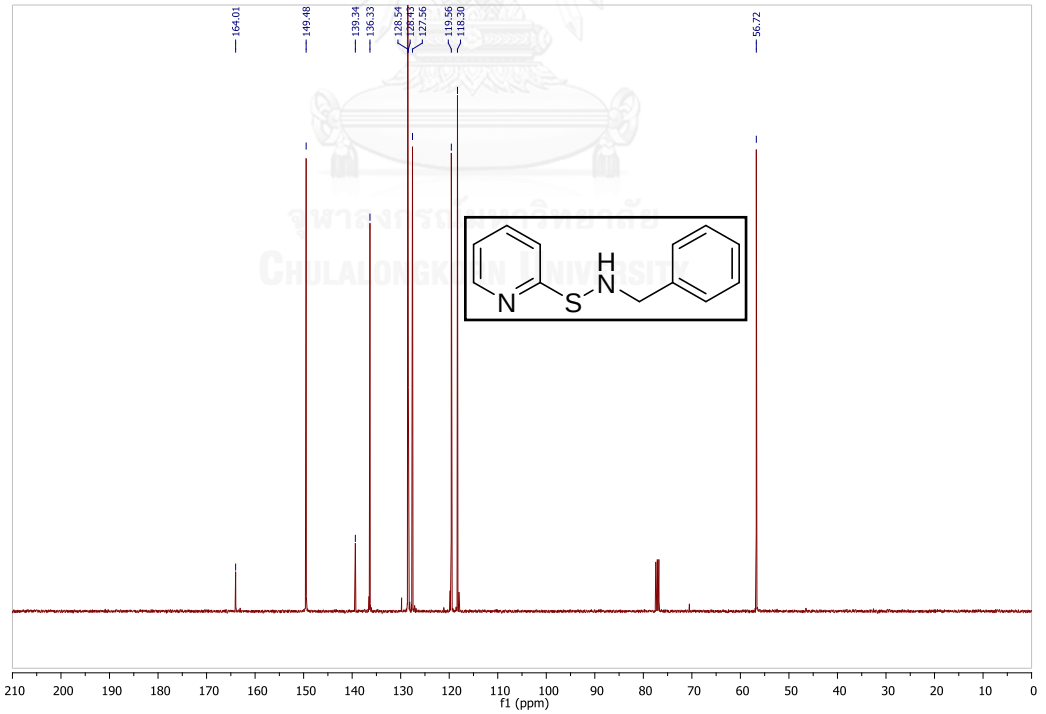

Figure A.103 ^{13}C NMR spectrum of **5.13b** ($CDCl_3$)

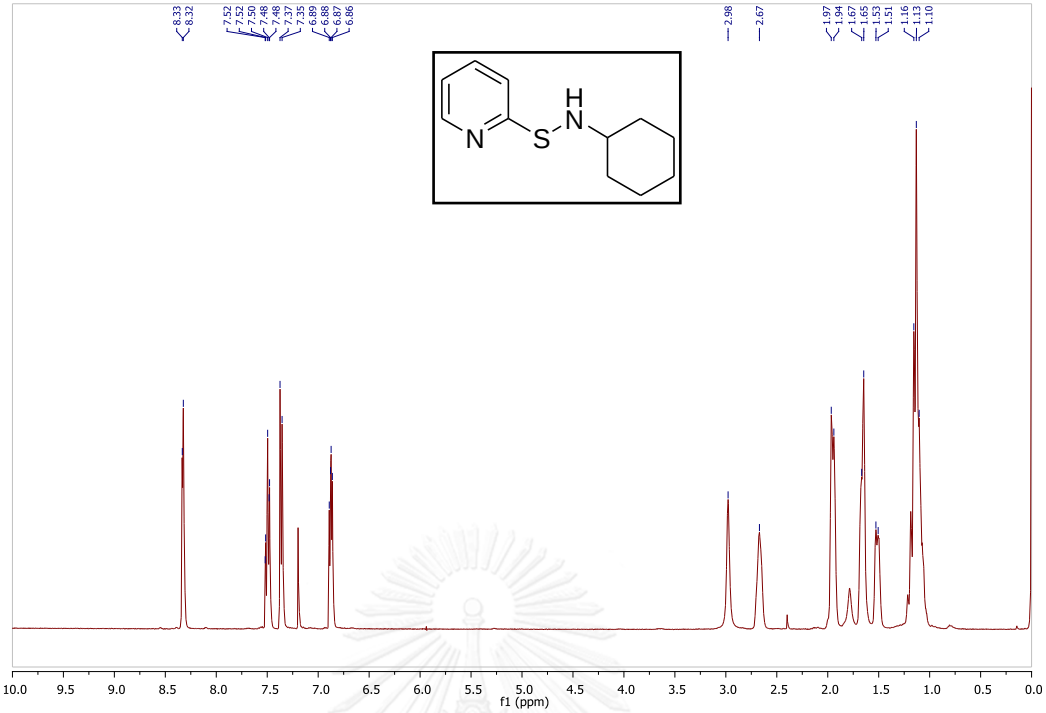

Figure A.104 ^{1}H NMR spectrum of **5.13c** ($CDCl_3$)

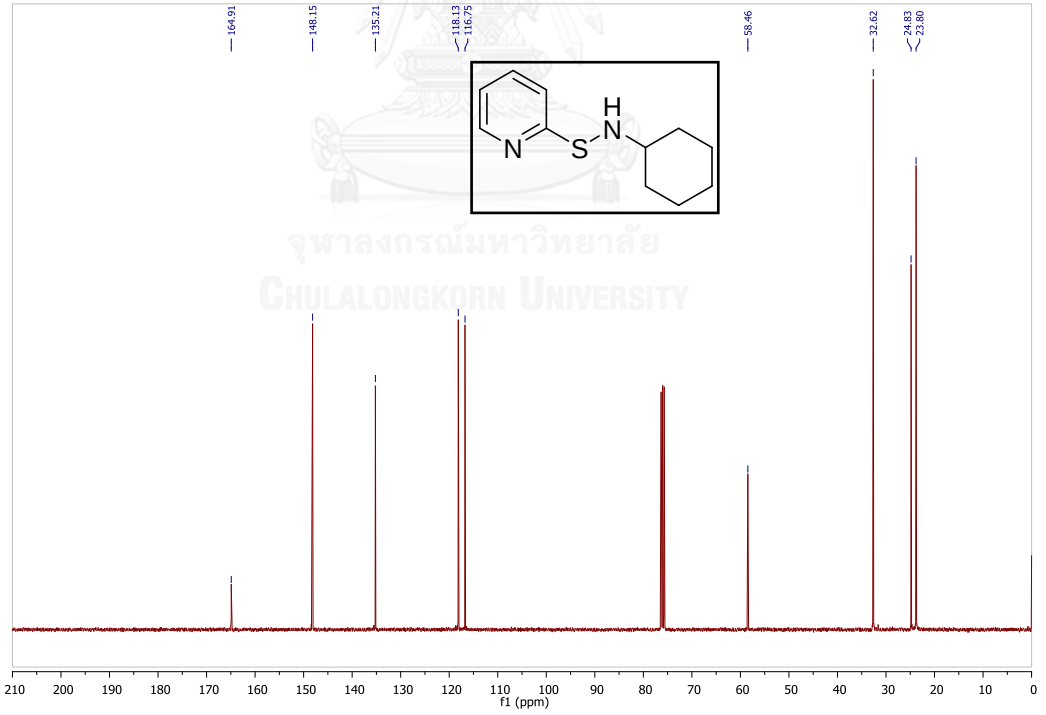

Figure A.105 ^{13}C NMR spectrum of **5.13c** ($CDCl_3$)

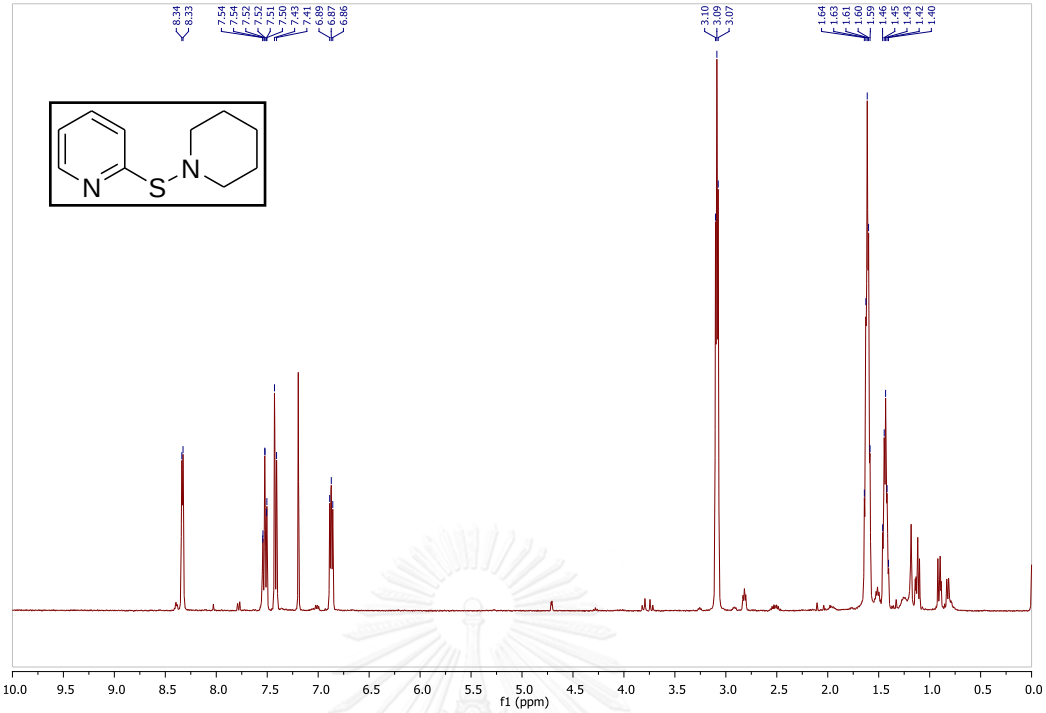

Figure A.106 ^{1}H NMR spectrum of **5.13d** ($CDCl_3$)

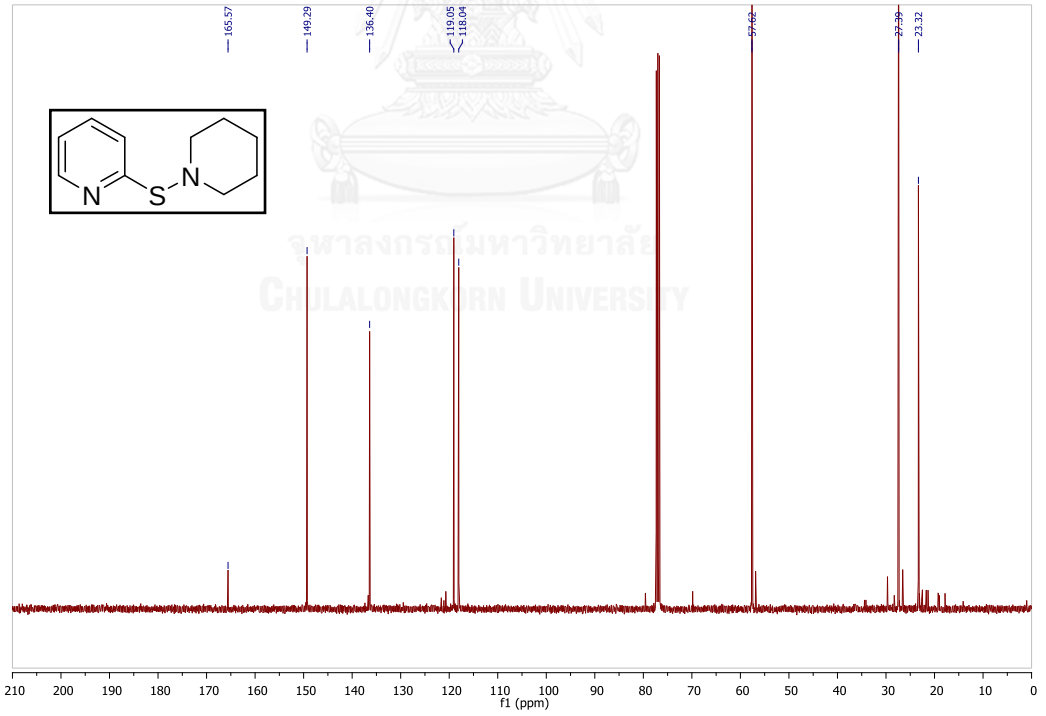

Figure A.107 ^{13}C NMR spectrum of **5.13d** ($CDCl_3$)

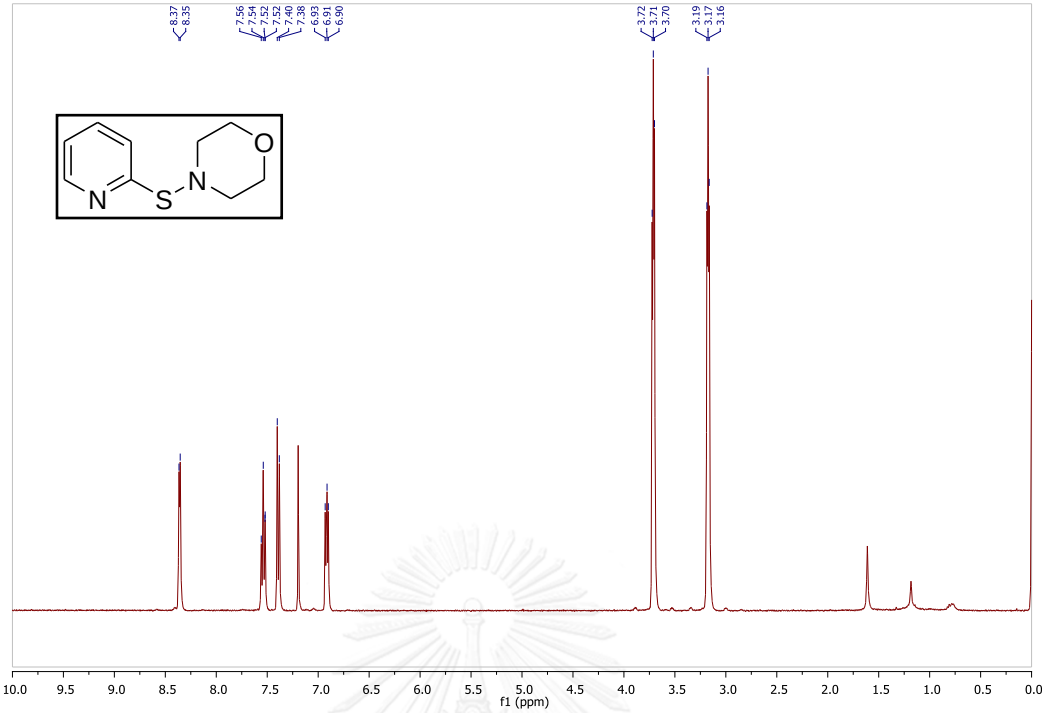

Figure A.108 ^{1}H NMR spectrum of **5.13e** ($CDCl_3$)

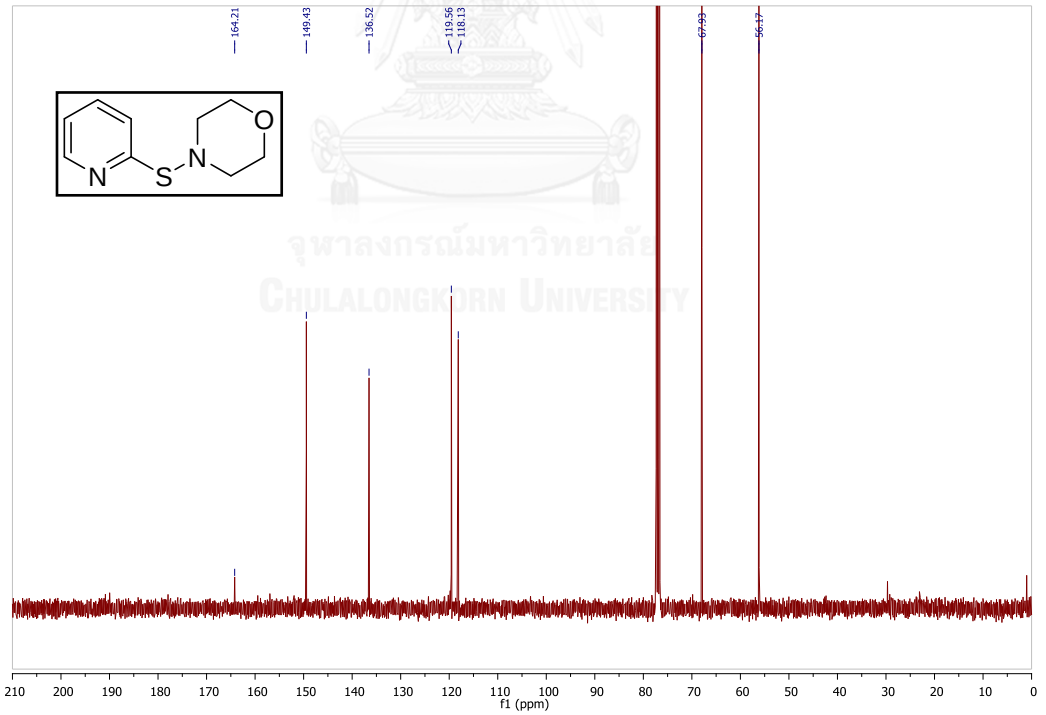

Figure A.109 ^{13}C NMR spectrum of **5.13e** ($CDCl_3$)

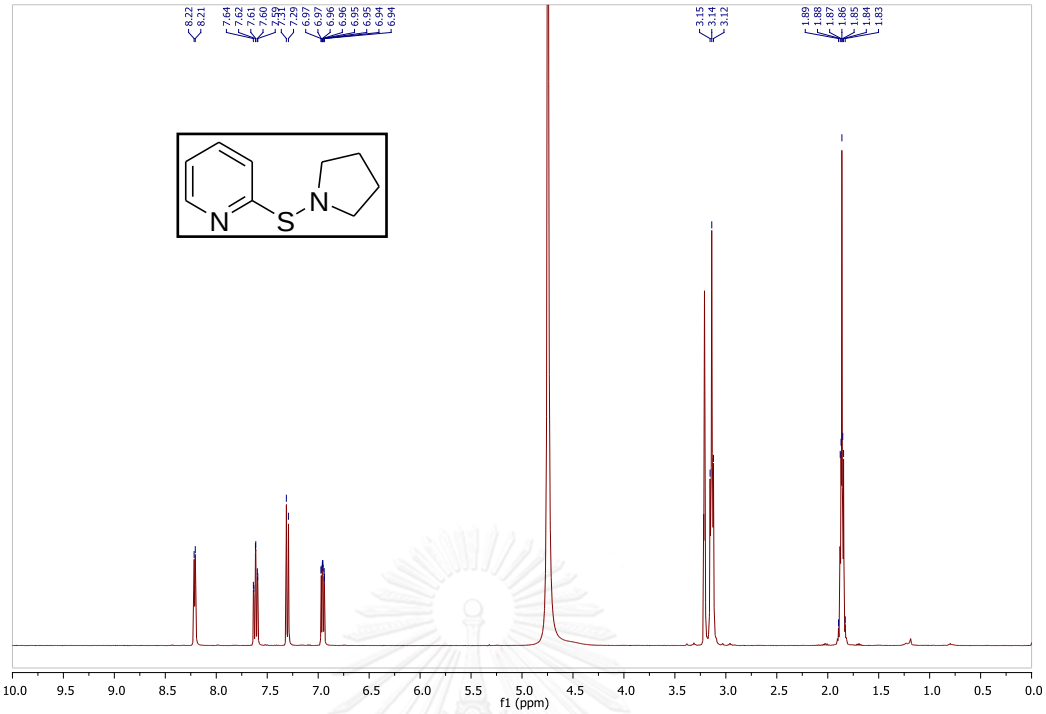

Figure A.110 ^{1}H NMR spectrum of **5.13f** (CD_3OD)

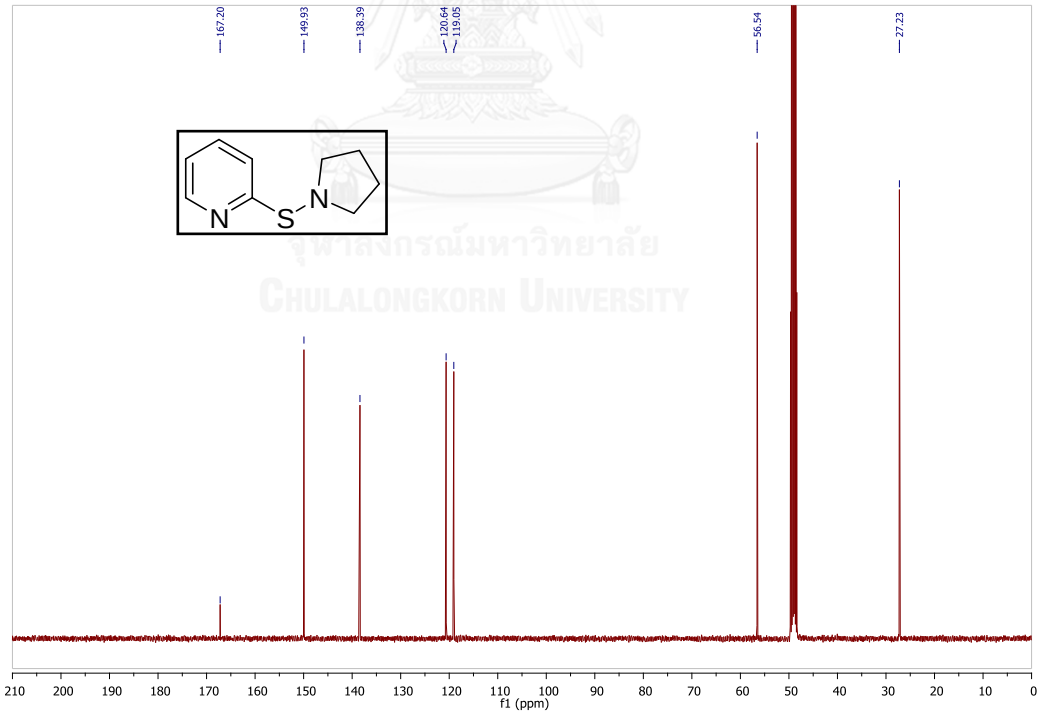

Figure A.111 ^{13}C NMR spectrum of **5.13f** (CD_3OD)

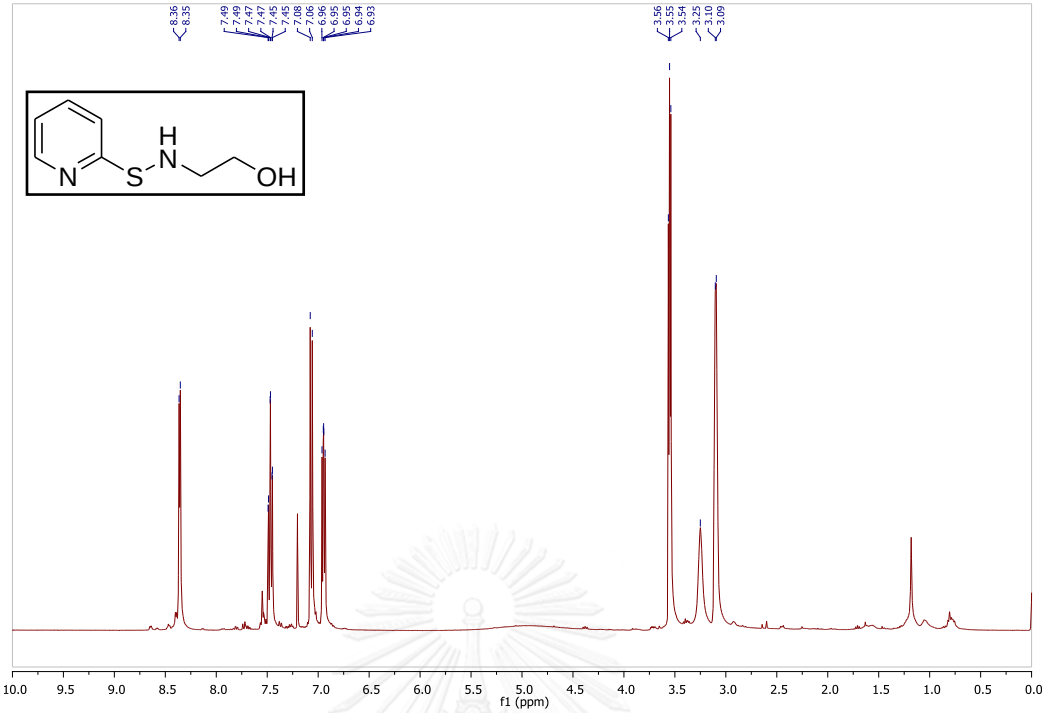

Figure A.112 ^{1}H NMR spectrum of **5.13g** ($CDCl_3$)

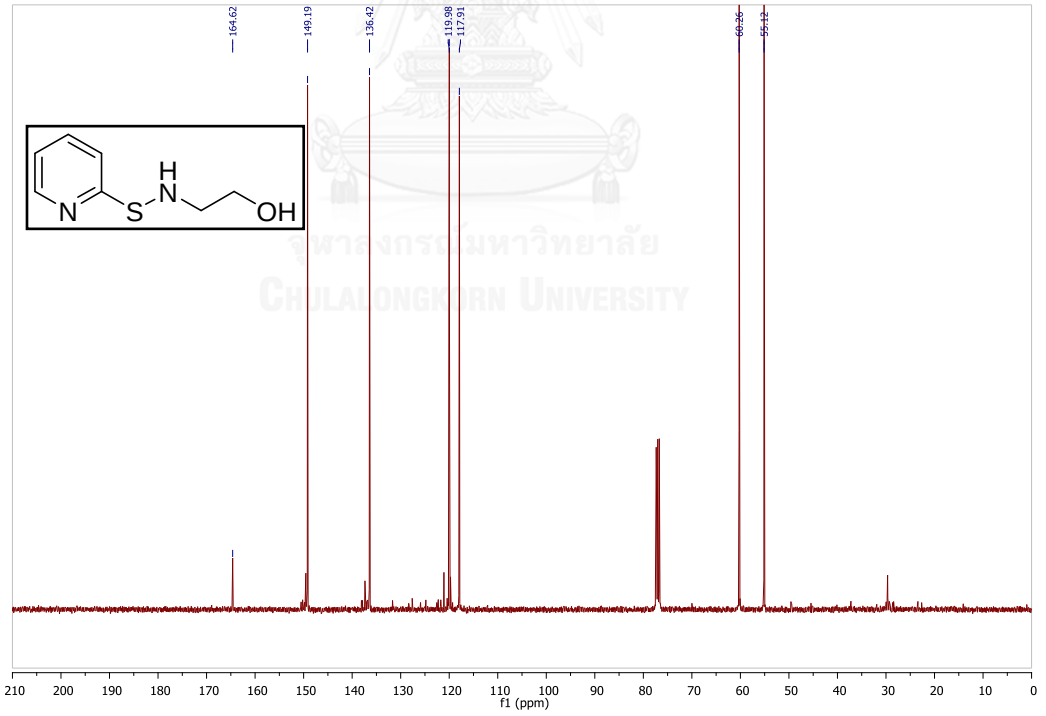

Figure A.113 ^{13}C NMR spectrum of **5.13g** ($CDCl_3$)

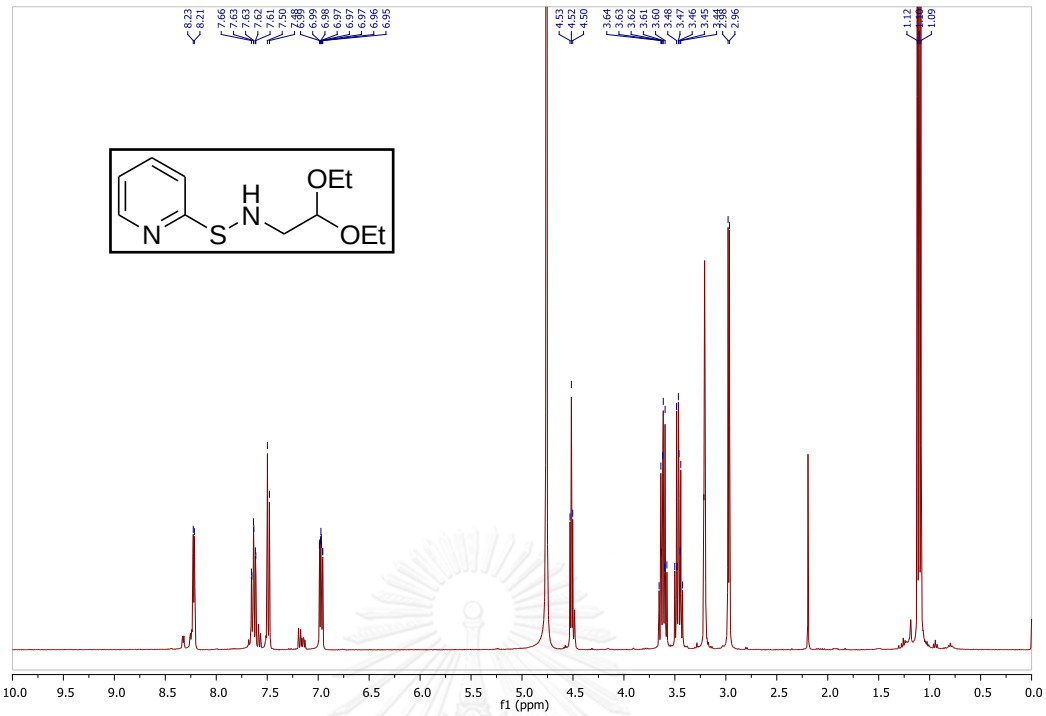

Figure A.114 ^{1}H NMR spectrum of **5.13h** (CD_3OD)

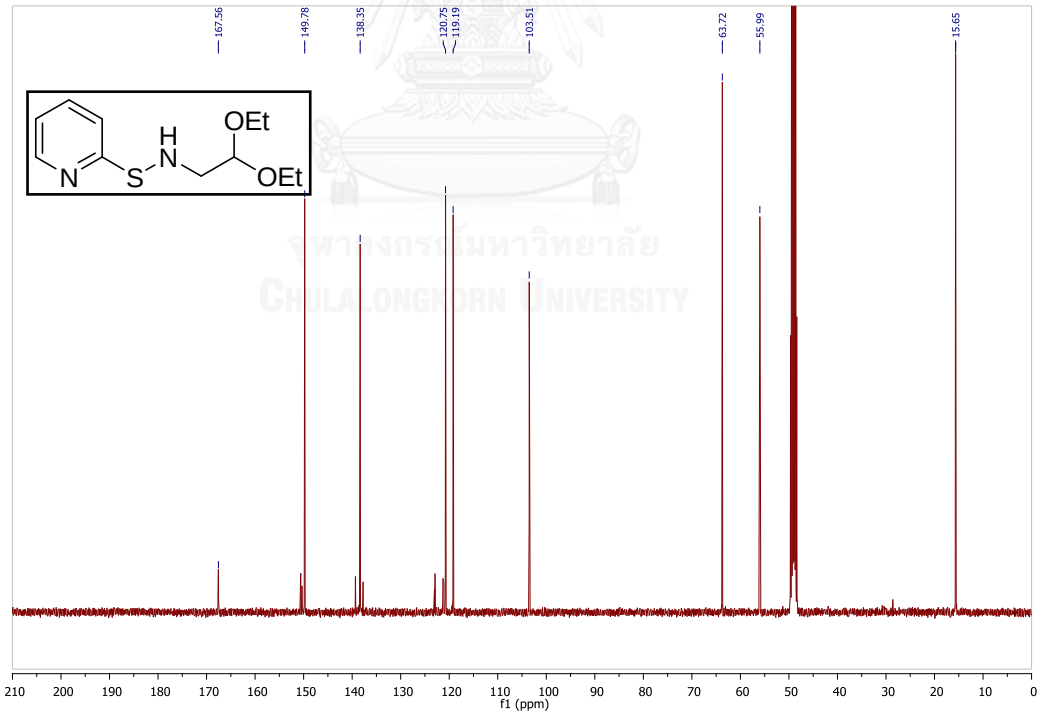

Figure A.115 ^{13}C NMR spectrum of **5.13h** (CD_3OD)

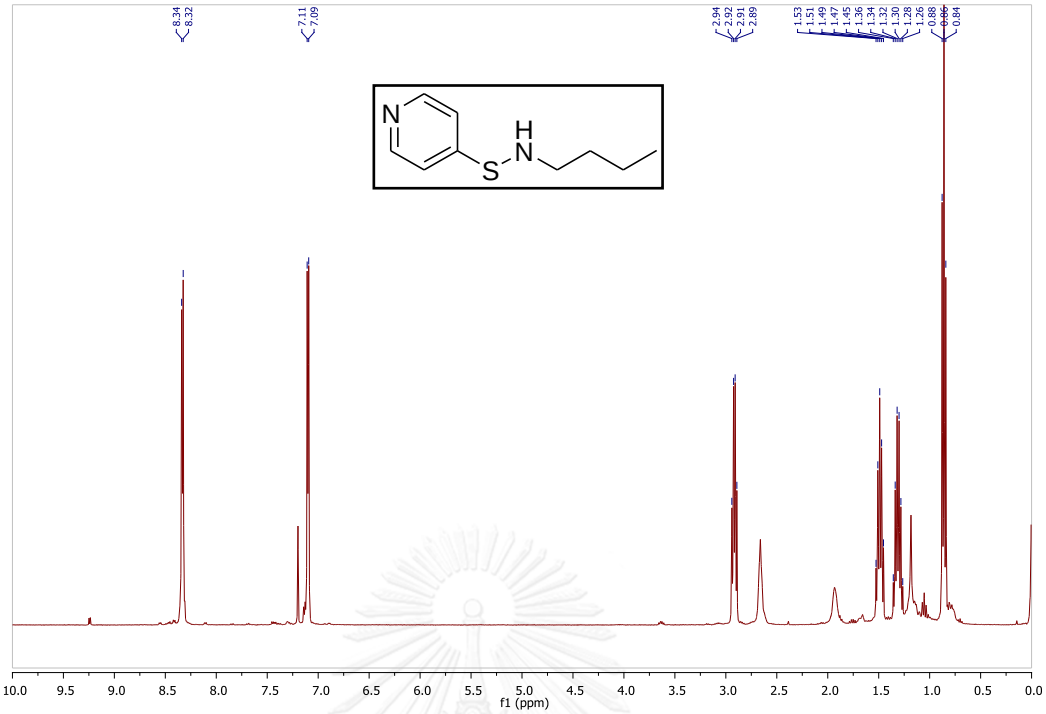

Figure A.116 ^{1}H NMR spectrum of **5.14a** ($CDCl_3$)

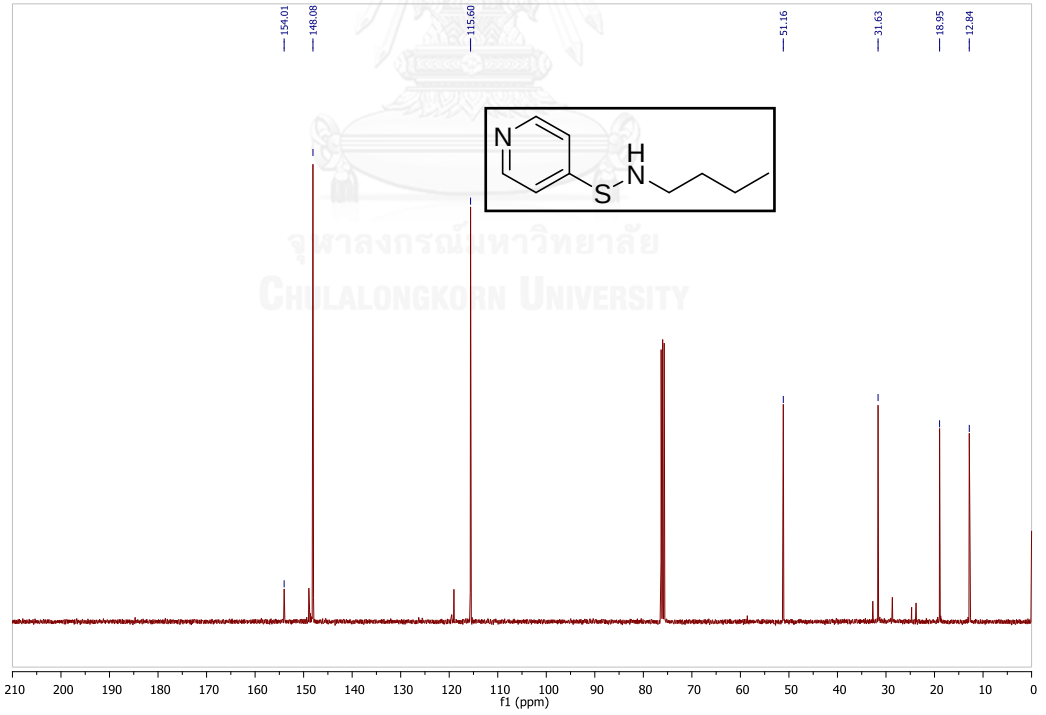

Figure A.117 ^{13}C NMR spectrum of **5.14a** ($CDCl_3$)

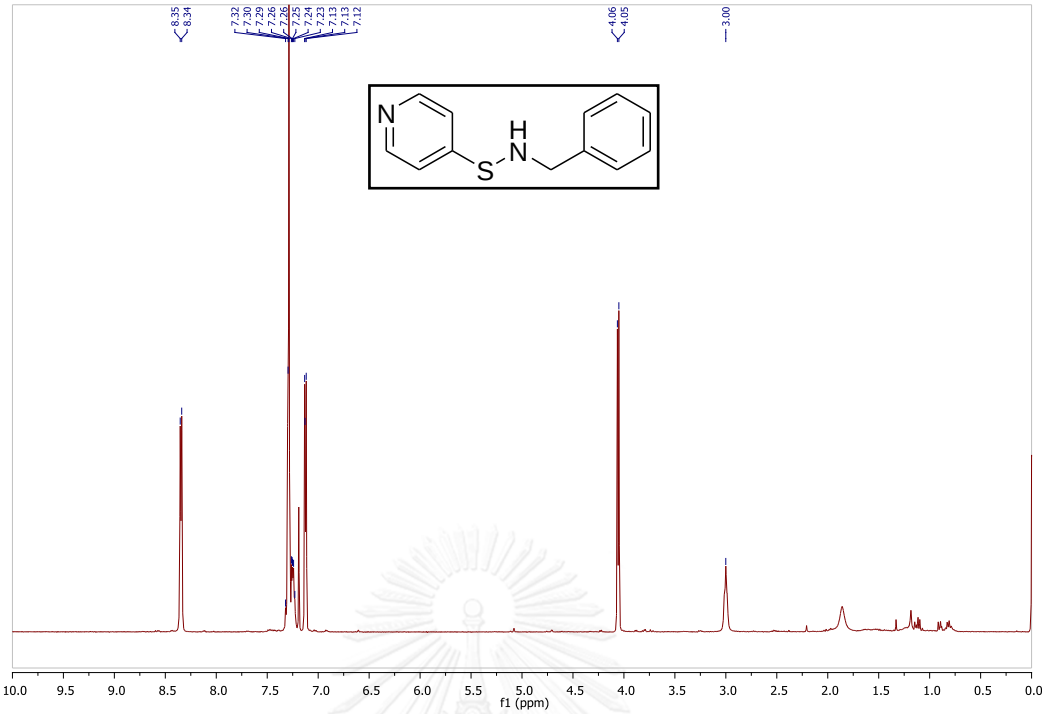

Figure A.118 ^{1}H NMR spectrum of **5.14b** ($CDCl_3$)

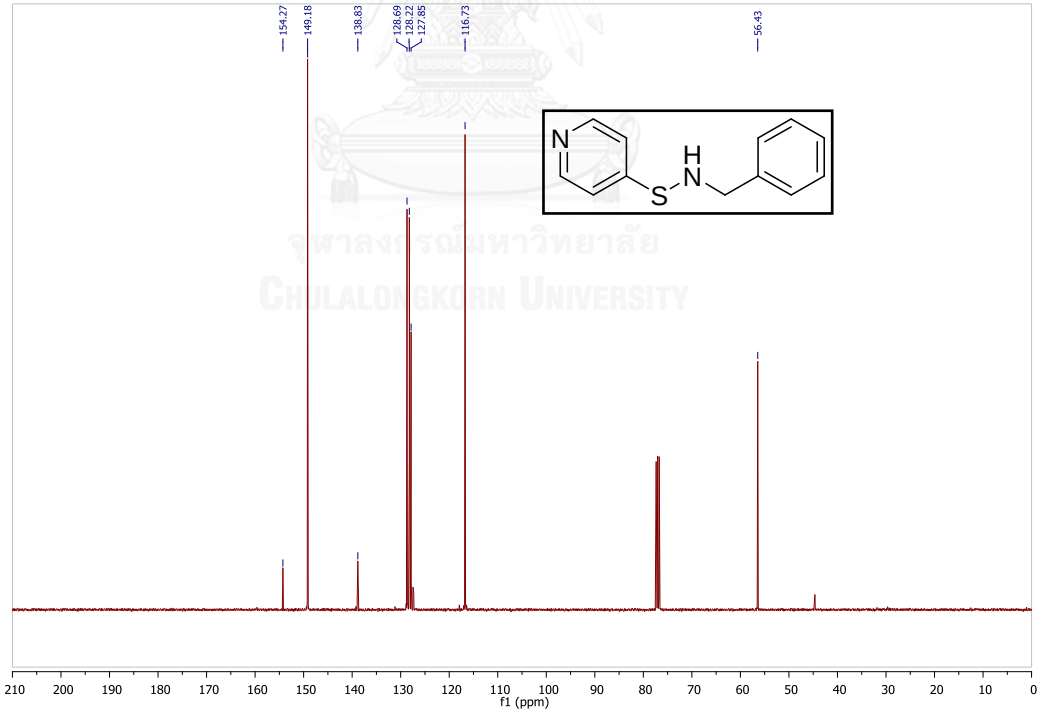

Figure A.119 ^{13}C NMR spectrum of **5.14b** ($CDCl_3$)

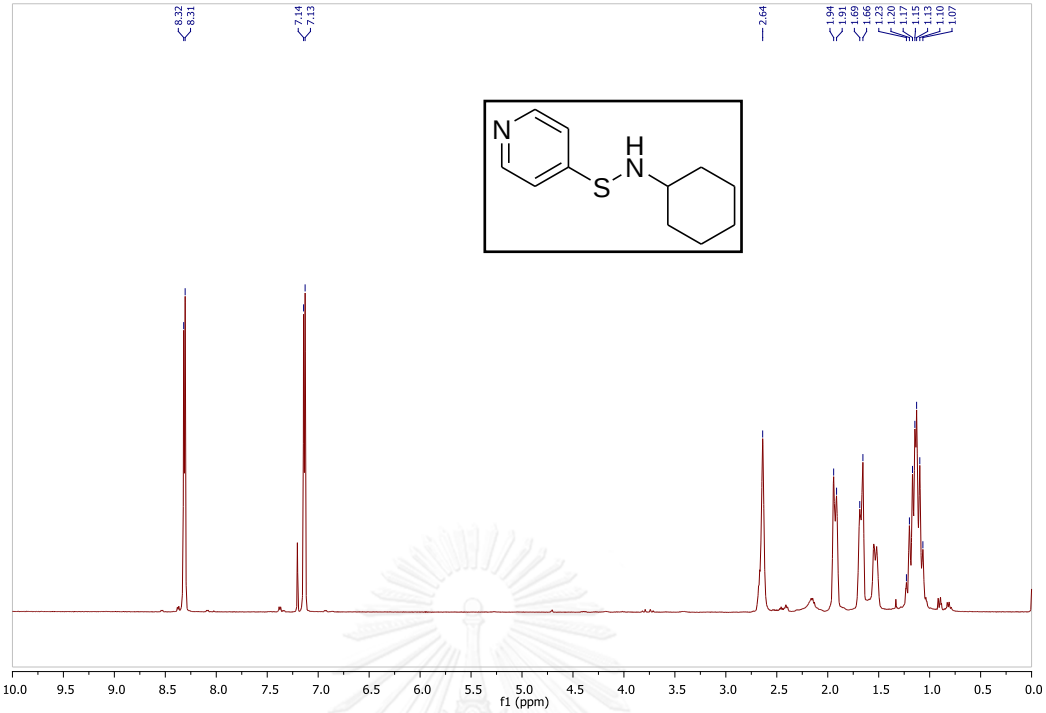

Figure A.120 ^{1}H NMR spectrum of **5.14c** ($CDCl_3$)

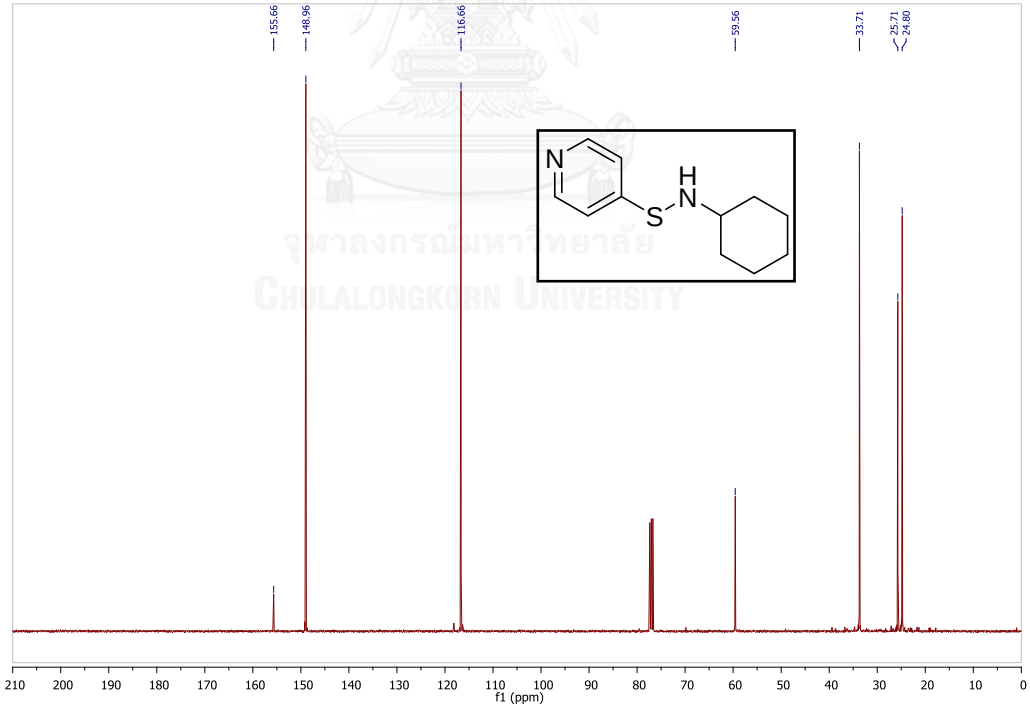

Figure A.121 ^{13}C NMR spectrum of **5.14c** ($CDCl_3$)

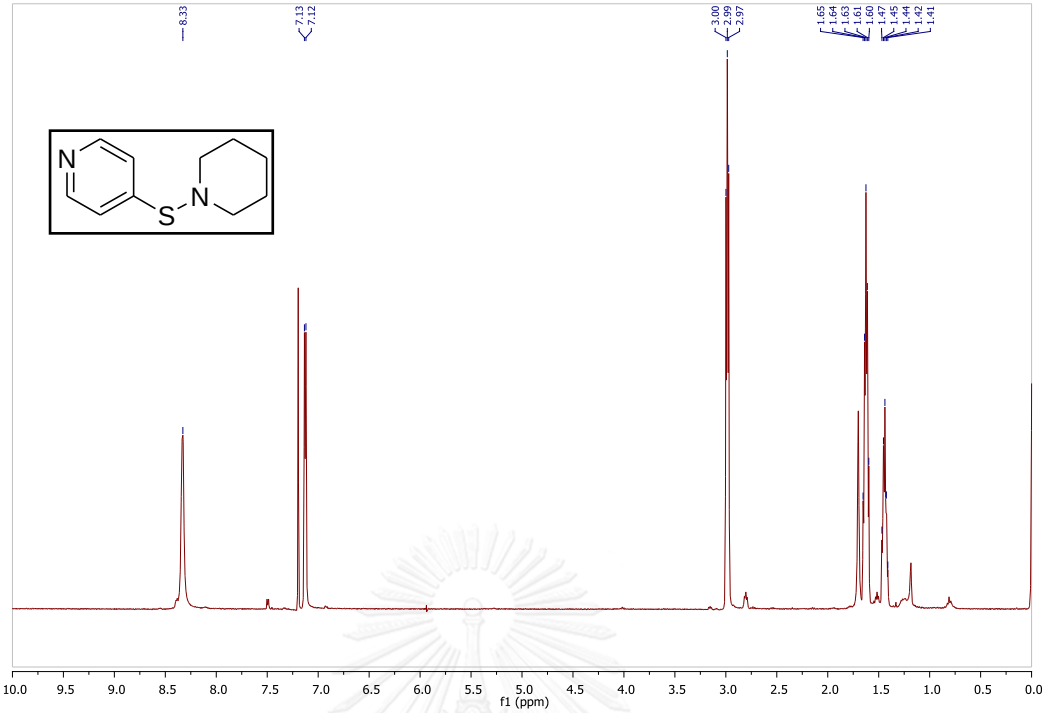

Figure A.122 ^{1}H NMR spectrum of **5.14d** ($CDCl_3$)

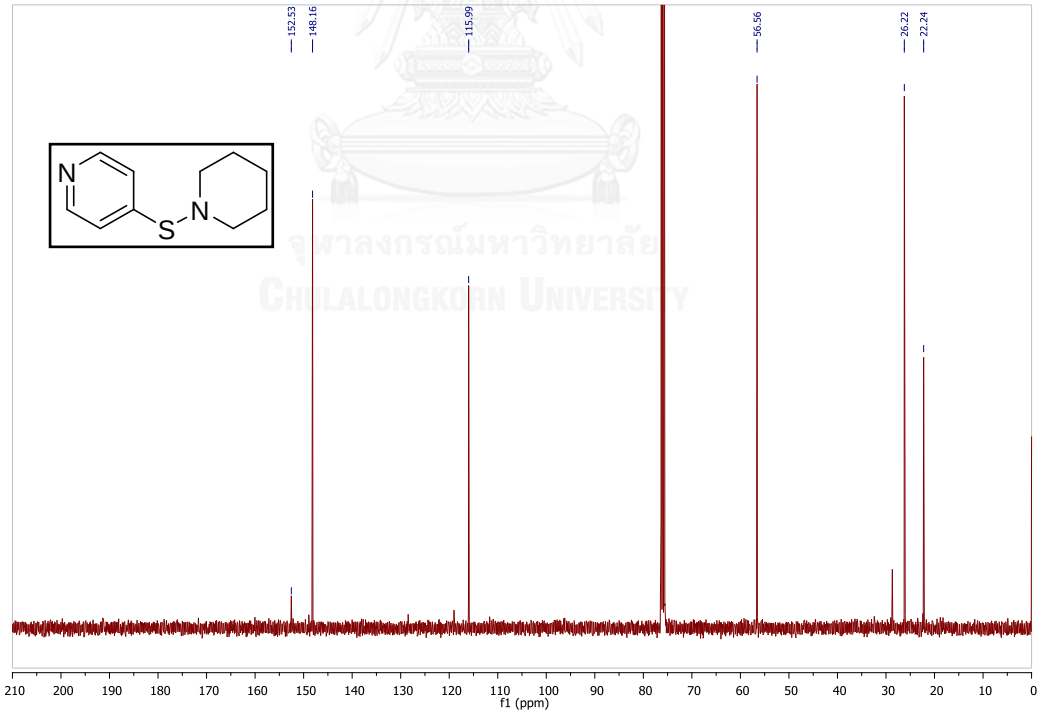

Figure A.123 ^{13}C NMR spectrum of **5.14d** ($CDCl_3$)

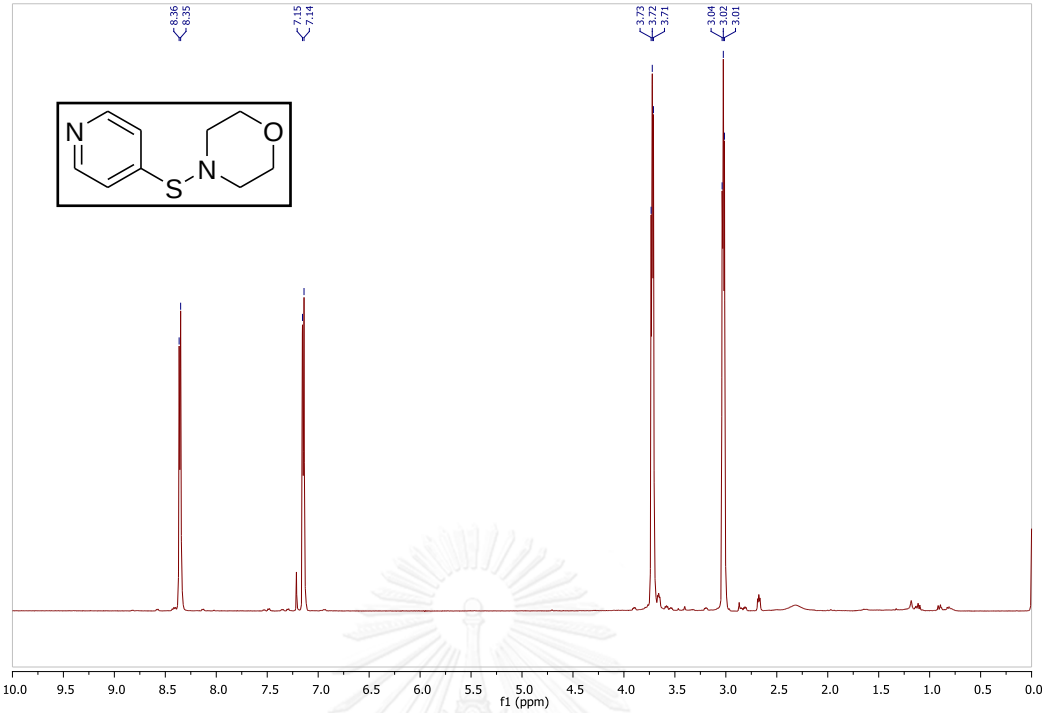

Figure A.124 ^{1}H NMR spectrum of **5.14e** ($CDCl_3$)

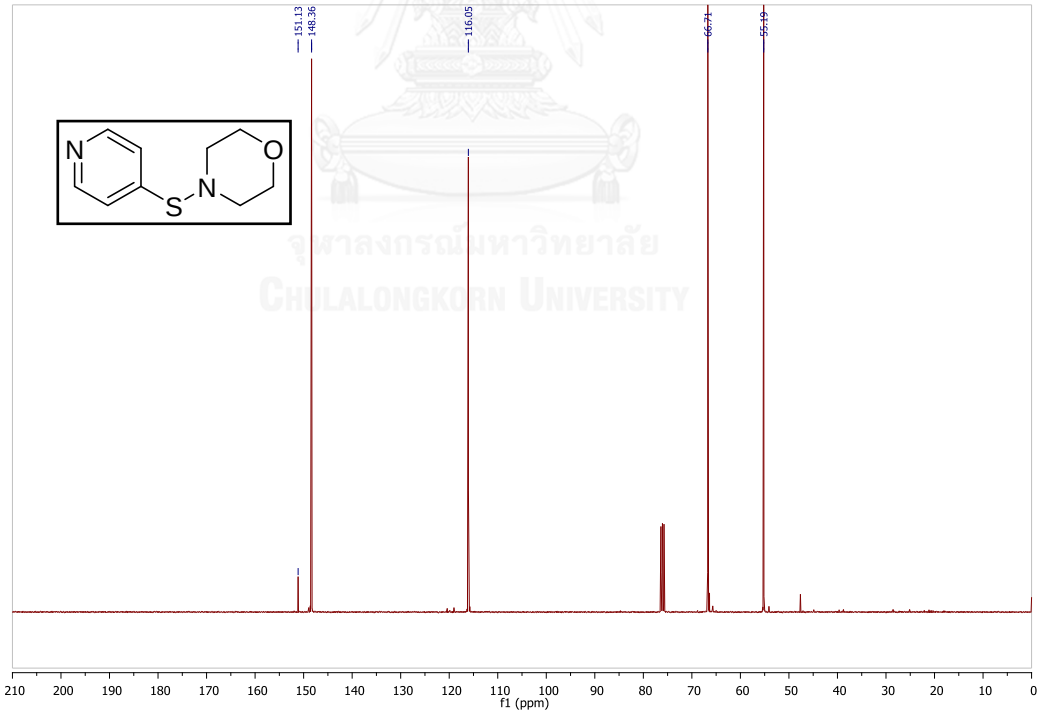

Figure A.125 ^{13}C NMR spectrum of **5.14e** ($CDCl_3$)

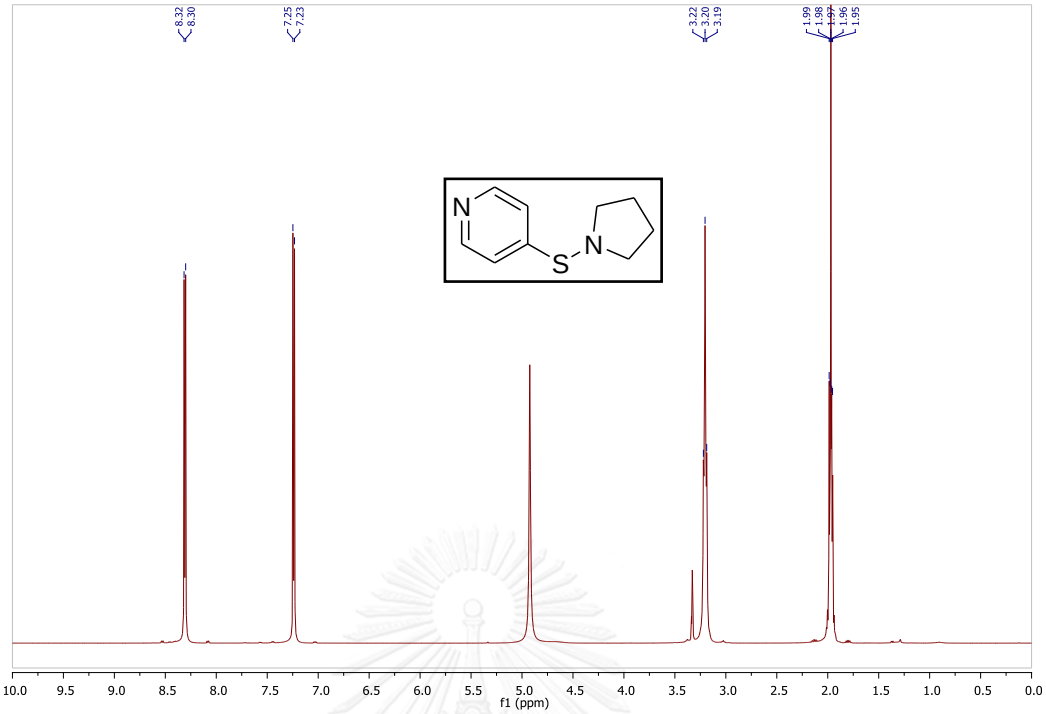

Figure A.126 ^{1}H NMR spectrum of **5.14f (CD_3OD)**

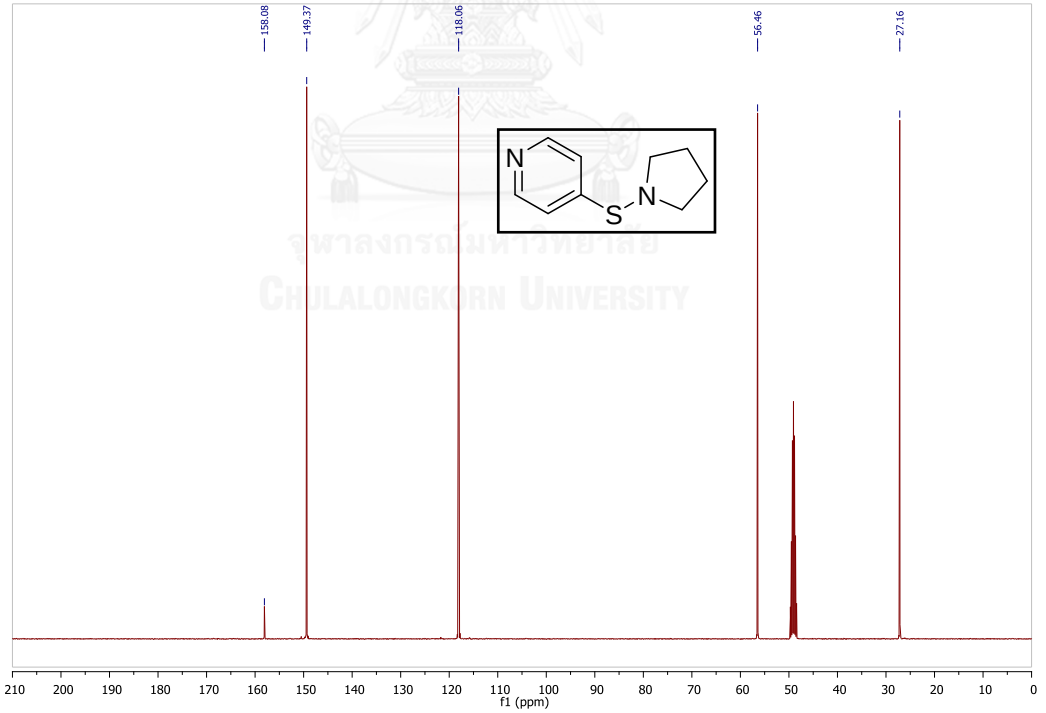

Figure A.127 ^{13}C NMR spectrum of **5.14f (CD_3OD)**

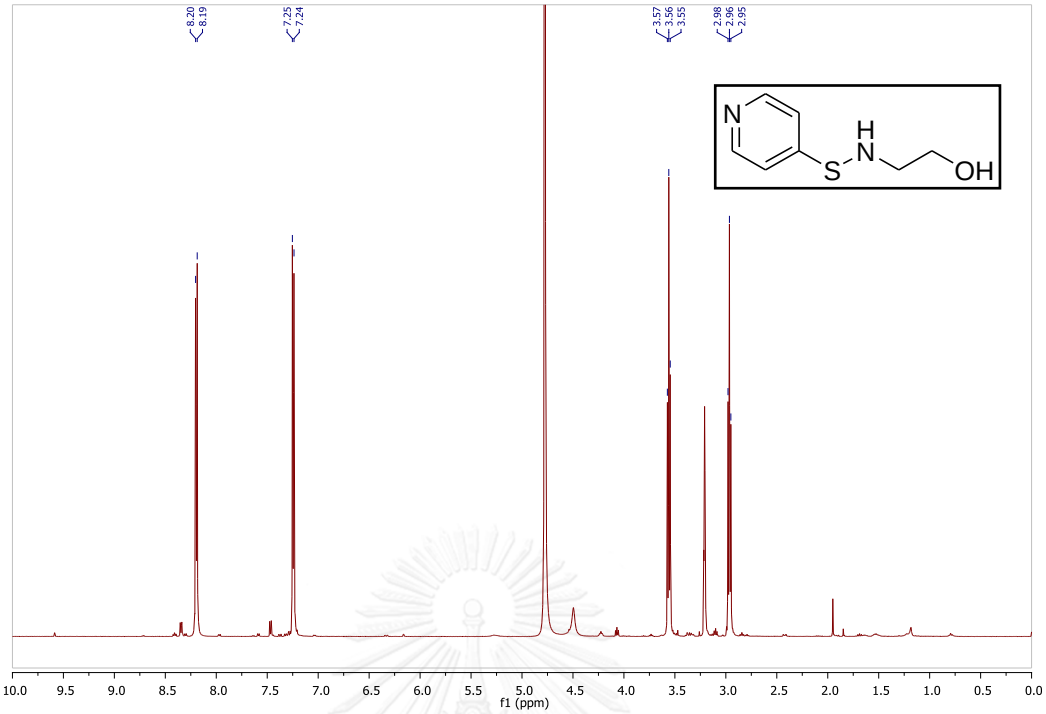

Figure A.128 ^{1}H NMR spectrum of **5.14g** (CD_3OD)

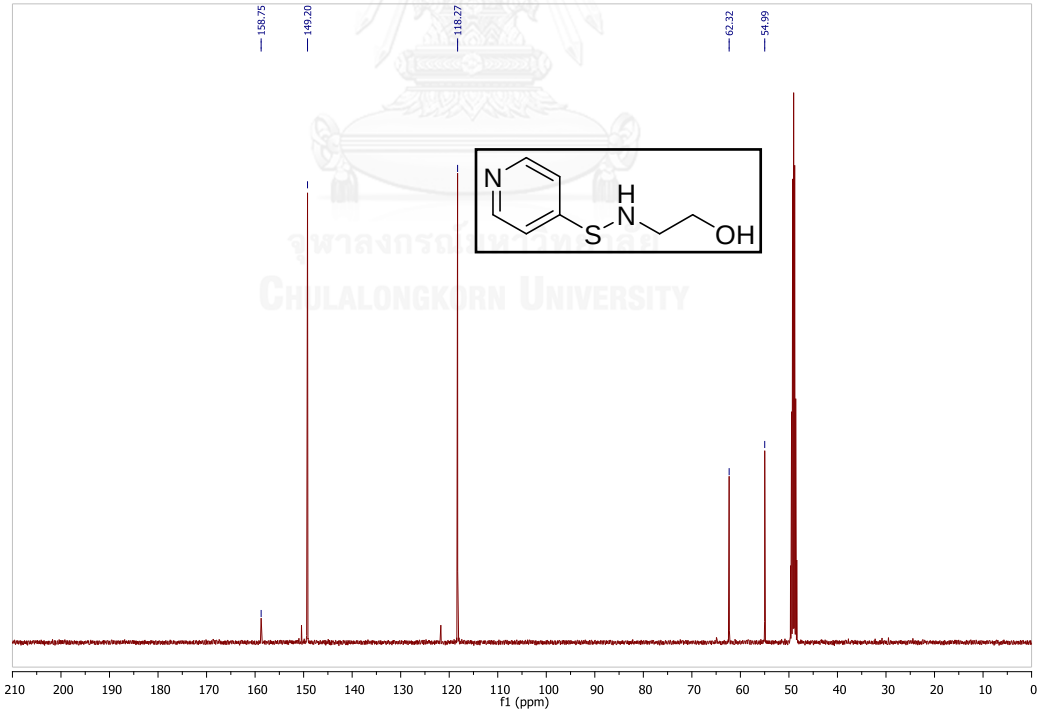

Figure A.129 ^{13}C NMR spectrum of **5.14g** (CD_3OD)

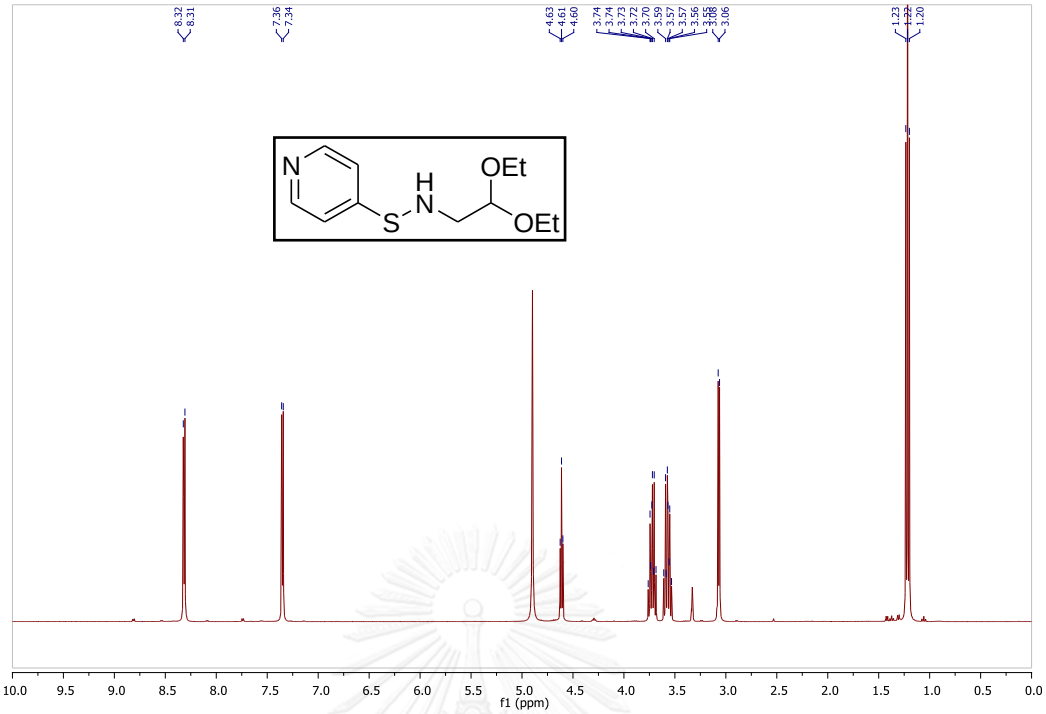

Figure A.130 ^{1}H NMR spectrum of **5.14h** (CD_3OD)

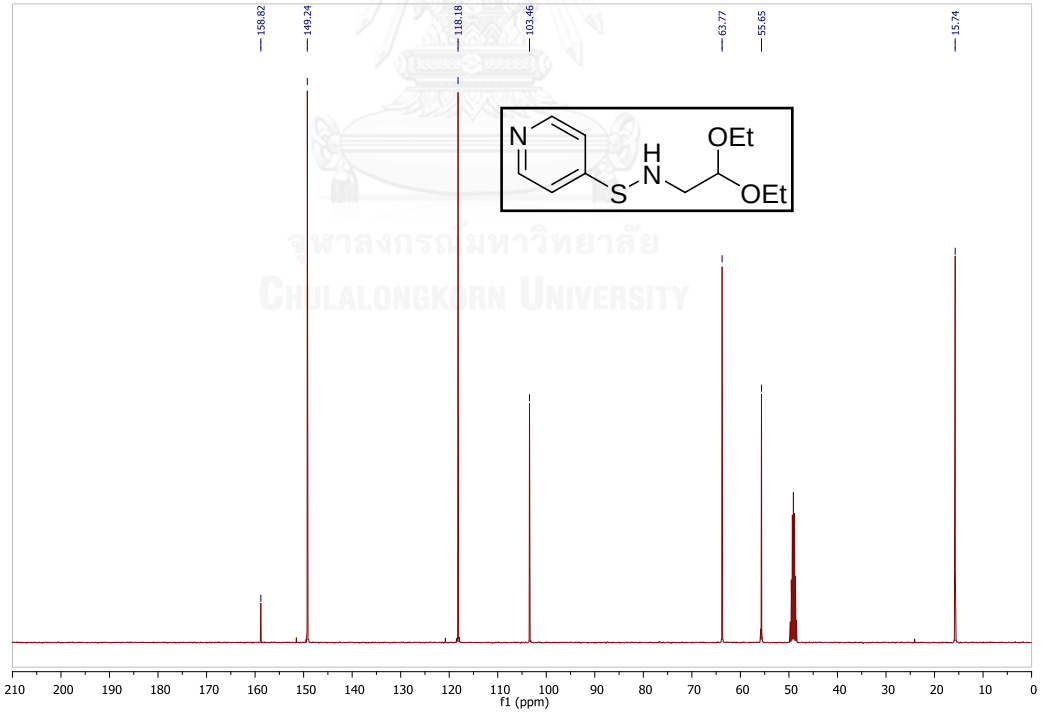

Figure A.131 ^{13}C NMR spectrum of **5.14h** (CD_3OD)

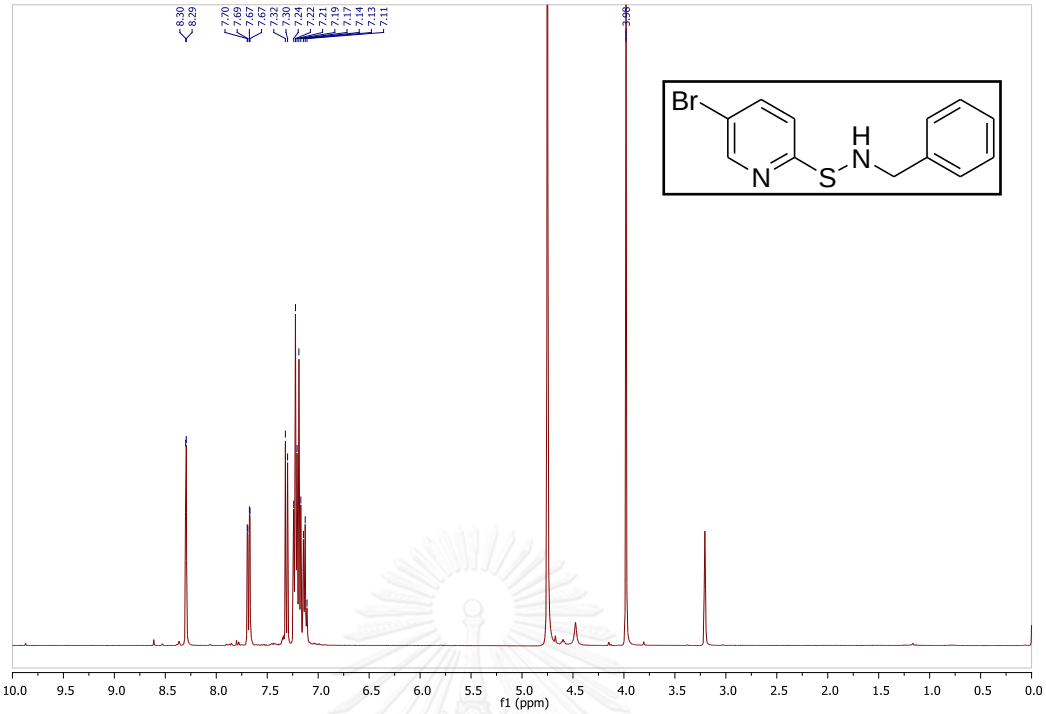

Figure A.132 ^{1}H NMR spectrum of **5.21b** (CD_3OD)

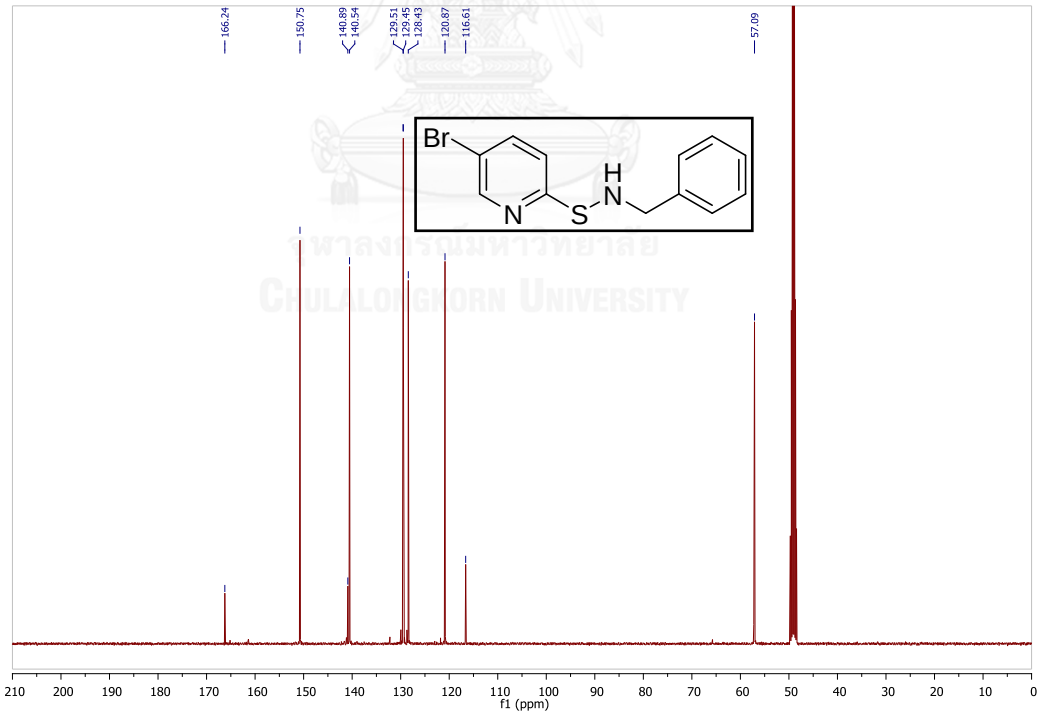

Figure A.133 ^{13}C NMR spectrum of **5.21b** (CD_3OD)

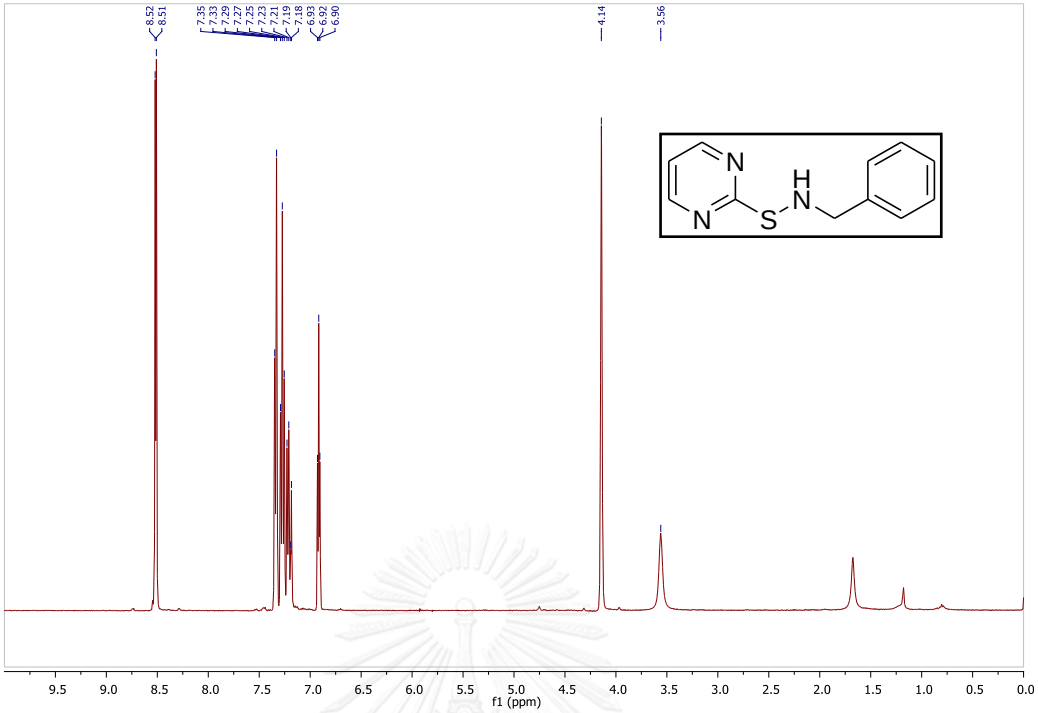

Figure A.134 ^{1}H NMR spectrum of **5.22b** ($CDCl_3$)

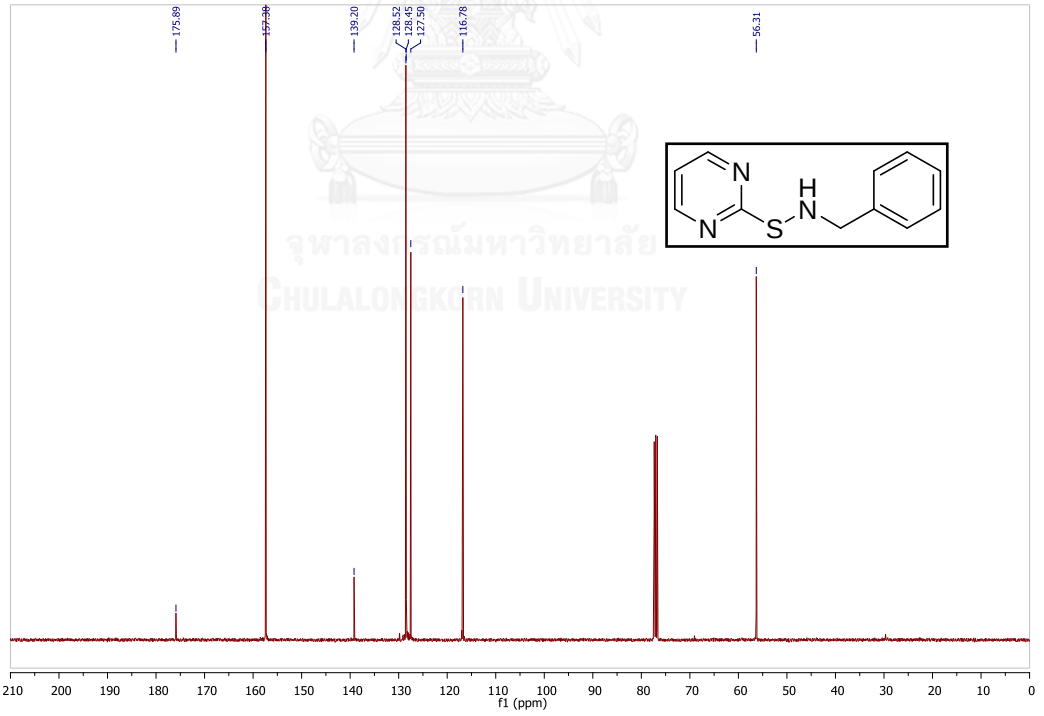

Figure A.135 ^{13}C NMR spectrum of **5.22b** ($CDCl_3$)

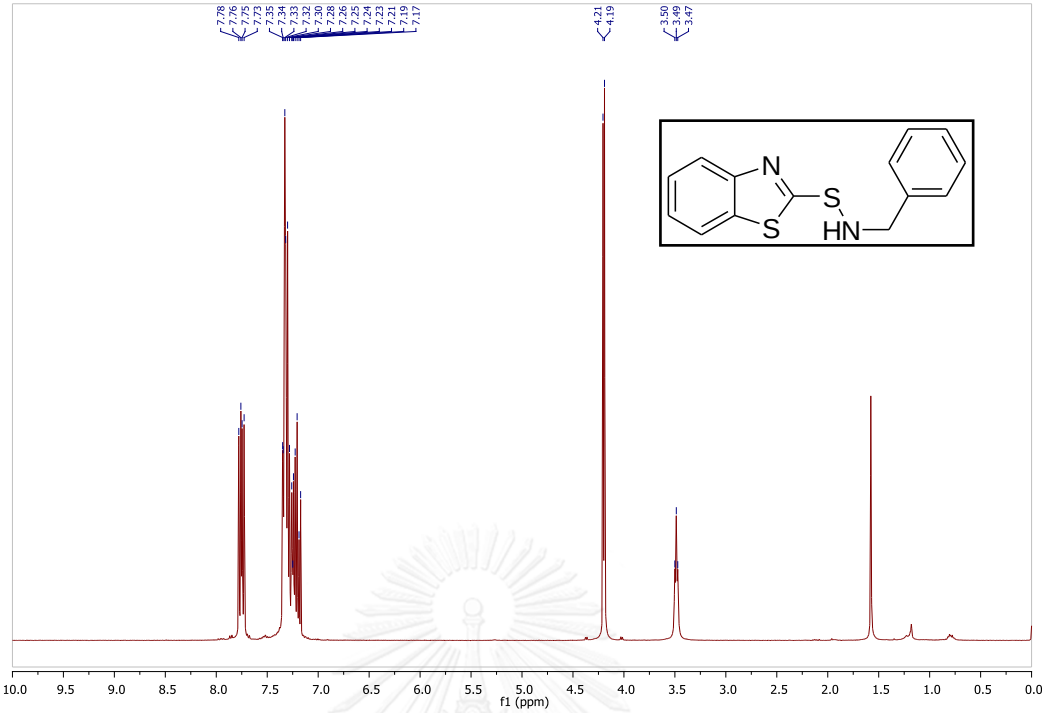

Figure A.136 ^{1}H NMR spectrum of **5.23b** ($CDCl_3$)

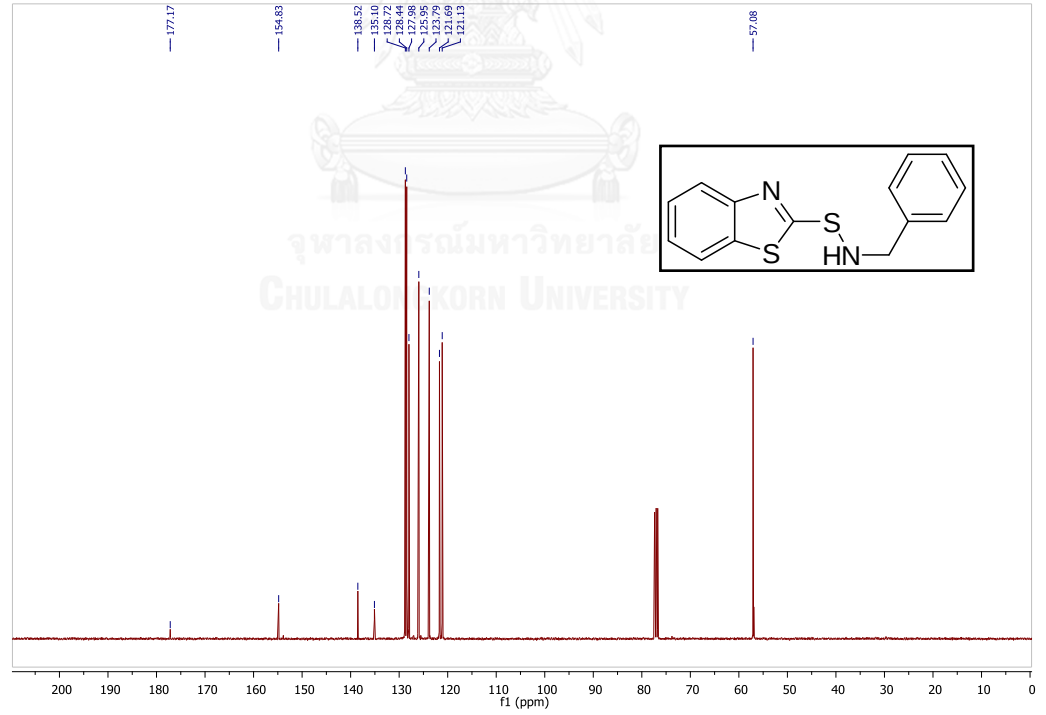

Figure A.137 ^{13}C NMR spectrum of **5.23b** ($CDCl_3$)

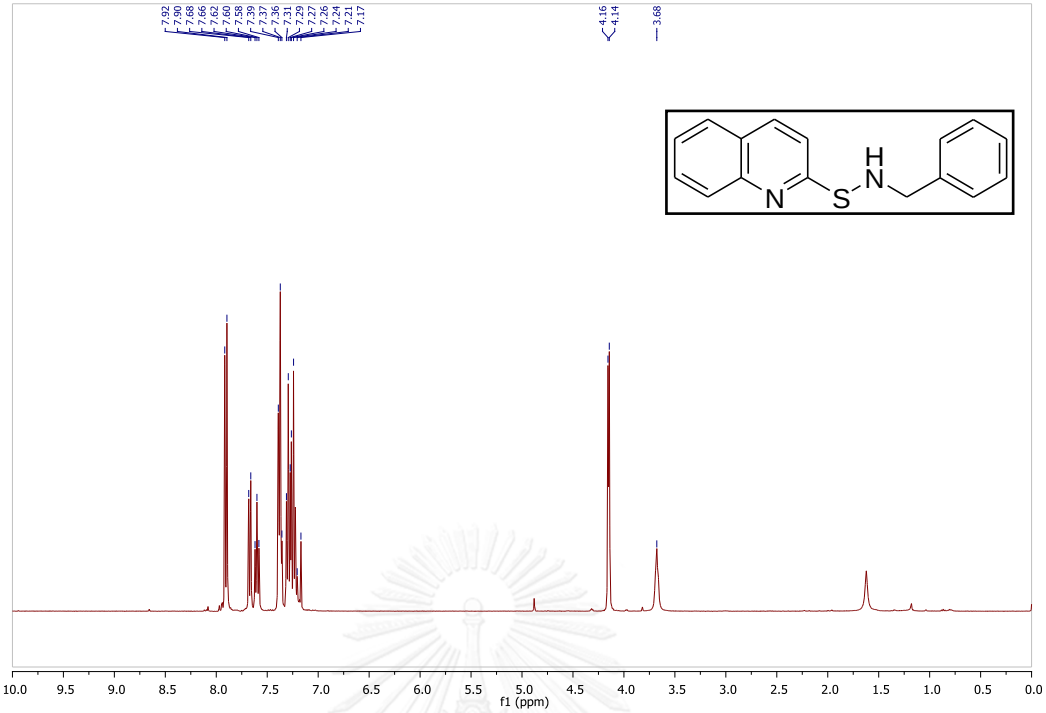

Figure A.138 ^{1}H NMR spectrum of **5.24b** ($CDCl_3$)

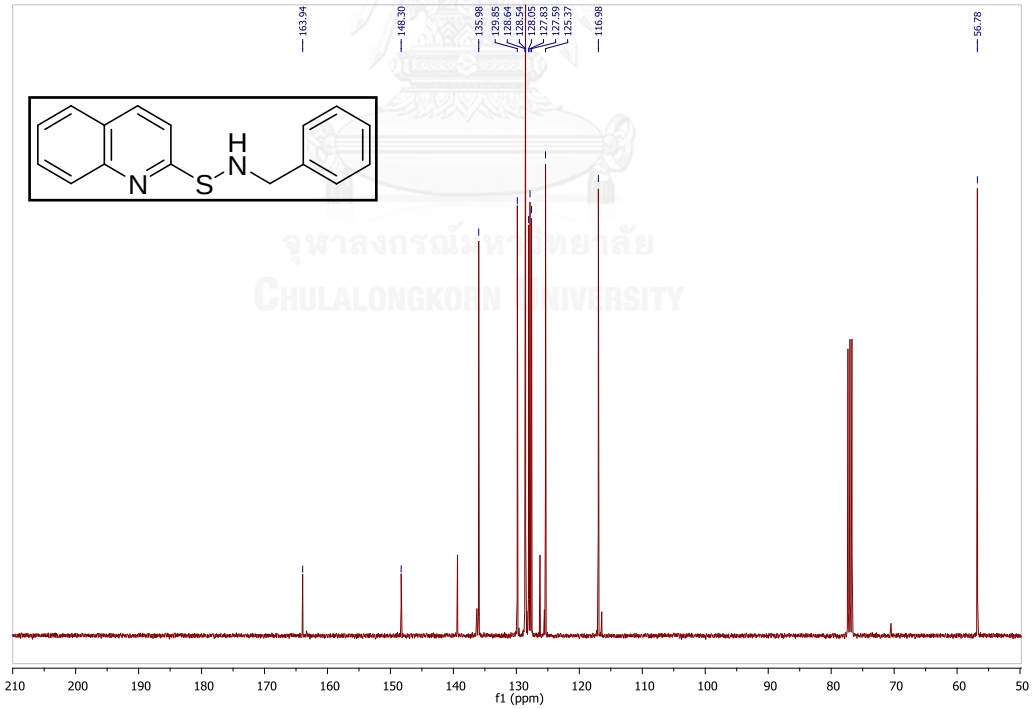

Figure A.139 ^{13}C NMR spectrum of **5.24b** ($CDCl_3$)

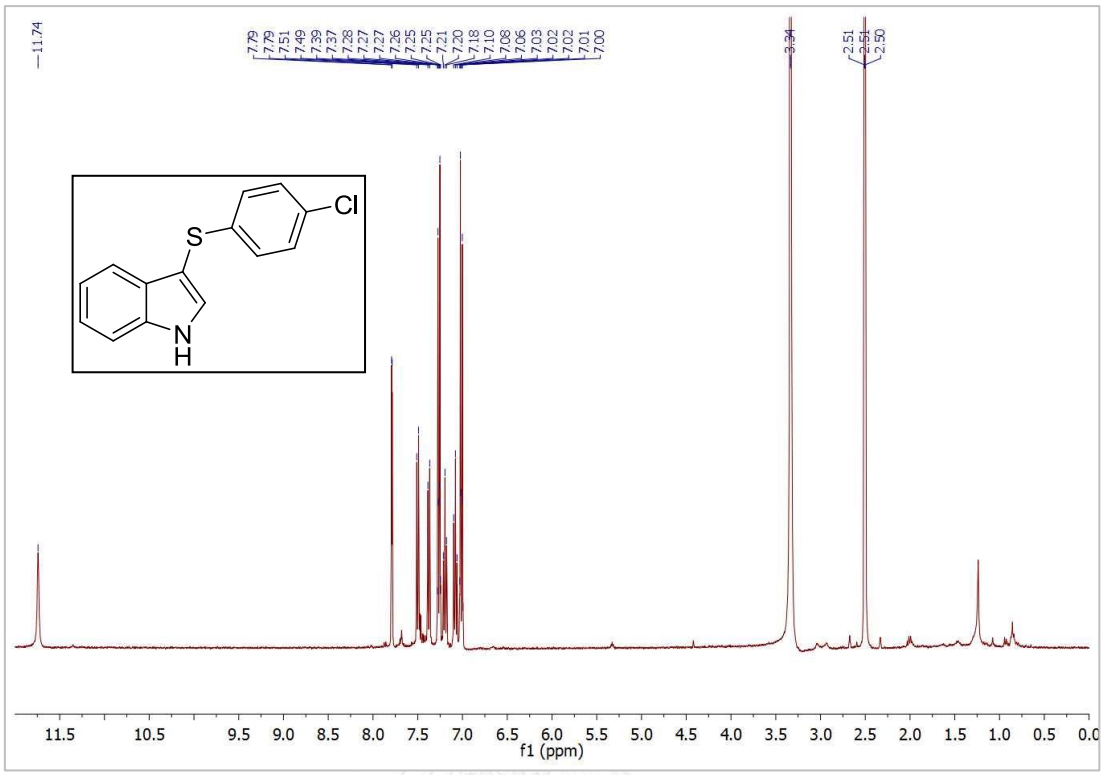

Figure A.140 ^{1}H NMR spectrum of **5.25 (DMSO-d_6)**

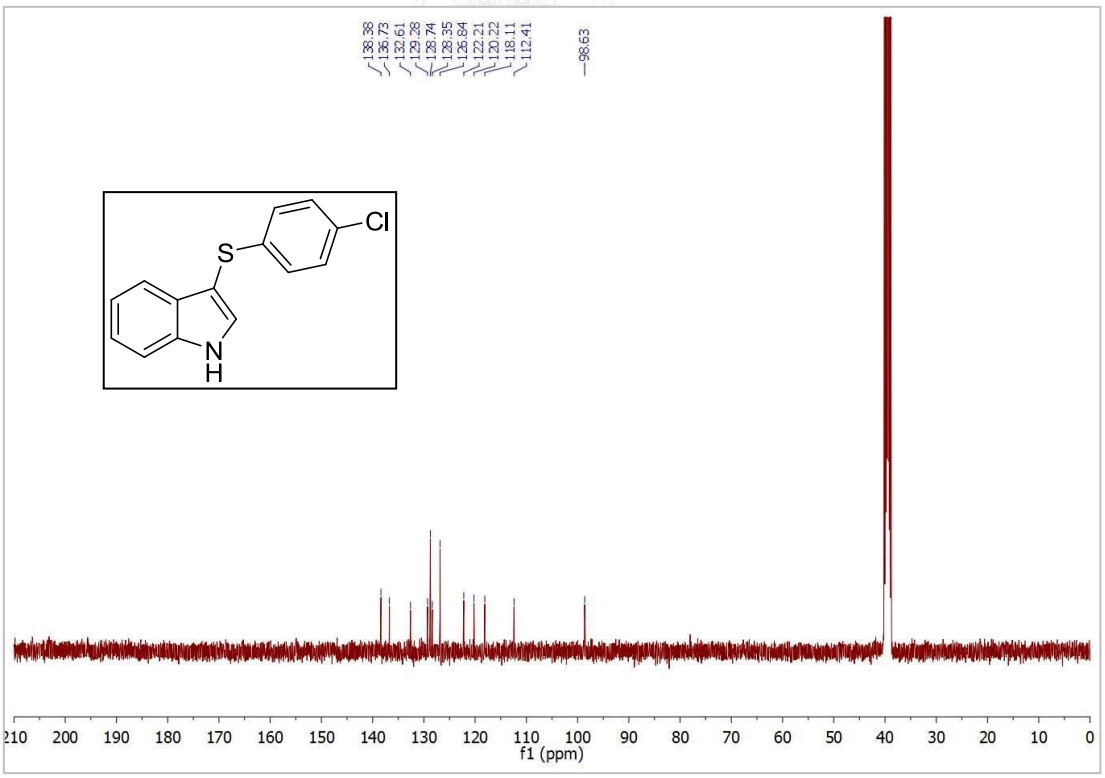

Figure A.141 ^{13}C NMR spectrum of **5.25 (DMSO-d_6)**

Table A.1 The docking of x-ray human NtMGAM model and compound **2.8AS.**

Cluster rank	Binding Energy (kcal/mole)	Cluster rank	Binding Energy (kcal/mole)	Cluster rank	Binding Energy (kcal/mole)
1	-7.03	4	-6.28	4	-5.81
	-7.01		-6.28		-5.8
	-6.99		-6.28		-5.8
	-6.83		-6.26		-5.8
	-6.76		-6.23		-5.79
	-6.76		-6.23		-5.78
	-6.73		-6.22		-5.74
	-6.23		-6.2		-5.74
	-5.4		-6.14		-5.74
2	-6.39		-6.11		-5.73
	-6.15		-6.08		-5.73
	-5.94		-6.04		-5.71
	-5.94		-6.02		-5.71
	-5.92		-6.01		-5.71
	-5.9		-5.97		-5.69
	-5.88		-5.97		-5.69
	-5.81		-5.95		-5.68
	-5.81		-5.95		-5.67
3	-6.36		-5.92		-5.66
	-4.66		-5.92		-5.66
4	-6.35		-5.87		-5.64
	-6.34		-5.86		-5.63
	-6.33		-5.86		-5.63
	-6.3		-5.85		-5.63
	-6.3		-5.84		-5.62
	-6.29		-5.83		-5.61

Table A.1 The docking of x-ray human NtMGAM model and compound **2.8AS** (continuous).

Cluster rank	Binding Energy (kcal/mole)	Cluster rank	Binding Energy (kcal/mole)	Cluster rank	Binding Energy (kcal/mole)
4	-5.6	5	-5.54	6	-5.12
	-5.57		-5.52		-5.1
	-5.55		-5.41		-5.08
	-5.53		-4.94		-5.07
	-5.5		-4.9		-5.06
	-5.5		-4.87		-5.06
	-5.48		-4.87		-5.04
	-5.27		-4.81		-5.04
	-5.26		-4.79		-5.03
	-5.21		-4.69		-5.03
	-5.14		-4.68		-5.03
	-5.12		-4.63		-5.01
	-5.09		-3.96		-5.01
	-5.08	6	-5.48		-5
	-5.02		-5.46		-5
	-4.98		-5.36		-5
	-4.73		-5.35		-4.97
	-4.57		-5.32		-4.97
	-4.42		-5.31		-4.96
	-4.4		-5.29		-4.95
	-4.35		-5.29		-4.95
	-4.33		-5.26		-4.95
	-4.27		-5.2		-4.94
	-4.23		-5.19		-4.93
	-4.21		-5.14		-4.93
	-4.07		-5.13		-4.93

Table A.1 The docking of x-ray human NtMGAM model and compound **2.8AS** (continuous).

Cluster rank	Binding Energy (kcal/mole)	Cluster rank	Binding Energy (kcal/mole)	Cluster rank	Binding Energy (kcal/mole)
6	-4.92	6	-4.62	8	-5.33
	-4.92		-4.6		-5.33
	-4.91		-4.58		-4.96
	-4.91		-4.55		-4.94
	-4.9		-4.48		-4.64
	-4.9		-4.44		-4.11
	-4.9		-4.42	9	-5.29
	-4.89		-4.4		-4.94
	-4.89		-4.37		-4.85
	-4.86		-4.31		-4.81
	-4.85		-4.3		-4.78
	-4.85		-3.99		-4.76
	-4.84		-3.8		-4.71
	-4.83	7	-5.38		-4.71
	-4.79		-4.97		-4.68
	-4.79		-4.95		-4.66
	-4.78		-4.8		-4.47
	-4.77		-4.77		-4.45
	-4.74		-4.67		-4.44
	-4.72		-4.65		-4.27
	-4.72		-4.41		-4.17
	-4.68		-4.4		-4.08
	-4.67		-4.21		-3.99
	-4.66		-4.16		-3.92
	-4.65		-3.88		-3.9
	-4.64	8	-5.36		-3.48

Table A.1 The docking of x-ray human NtMGAM model and compound **2.8AS** (continuous).

Cluster rank	Binding Energy (kcal/mole)
10	-5.27
	-4.94
	-4.93
	-4.9
	-4.89
	-4.77
	-4.76
	-4.73
	-4.63
	-4.55
	-4.48
	-4.35
	-4.19

Table A.2 The docking of homology rat NtMGAM model and compound **2.8AS**

Cluster rank	Binding Energy (kcal/mole)	Cluster rank	Binding Energy (kcal/mole)	Cluster rank	Binding Energy (kcal/mole)
1	-7.27	1	-5.81	4	-5.54
	-7.26		-5.81		-5.36
	-7.21		-5.78		-5.22
	-7.14		-5.77		-5.05
	-7.07		-5.73		-5.02
	-6.8		-5.68		-4.86
	-6.78		-5.61		-4.85
	-6.77		-5.34		-4.81
	-6.77		-5.1		-4.72
	-6.73		-4.65		-4.65
	-6.63		-4.52		-4.55
	-6.55	2	-5.73		-4.21
	-6.45		-5.68		-4.21
	-6.45		-5.54		-4.13
	-6.4		-5.48		-4.07
	-6.37		-5.46		-4.04
	-6.36		-5.38		-4.04
	-6.34		-5.38		-3.89
	-6.34		-5.32	5	-5.43
	-6.31		-5.2		-5.3
	-6.3		-4.18		-5.16
	-6.26		-2.96		-5.16
	-6.26	3	-5.71		-5.15
	-6.24		-5.61		-5.11
	-6.23		-5.51		-5.09
	-6.16		-4.73		-5.08

Table A.2 The docking of homology rat NtMGAM model and compound **2.8AS** (continous).

Cluster rank	Binding Energy (kcal/mole)	Cluster rank	Binding Energy (kcal/mole)	Cluster rank	Binding Energy (kcal/mole)
5	-5.04	5	-3.98	7	-4.63
	-4.99		-3.64		-4.6
	-4.98	6	-5.24		-4.5
	-4.97		-5.2		-4.41
	-4.9		-5.16		-4.4
	-4.9		-5.1		-4.39
	-4.86		-5.1		-4.38
	-4.85		-5.04		-4.1
	-4.85		-5.02		-3.96
	-4.83		-4.99		-3.61
	-4.75		-4.96	8	-5.08
	-4.75		-4.92		-4.97
	-4.74		-4.91		-4.96
	-4.71		-4.88		-4.75
	-4.71		-4.77		-4.74
	-4.71		-4.76		-4.62
	-4.65		-4.17		-4.58
	-4.63		-4.06		-4.54
	-4.61		-4.04		-4.52
	-4.52		-3.9		-4.5
	-4.48	7	-5.12		-4.46
	-4.47		-4.94		-4.46
	-4.44		-4.89		-4.41
	-4.38		-4.79		-4.36
	-4.24		-4.67		-4.01
	-4.1		-4.66		-3.95

Table A.2 The docking of homology rat NtMGAM model and compound **2.8AS** (continous).

Cluster rank	Binding Energy (kcal/mole)
8	**-3.94**
	-3.87
9	**-5.05**
	-4.81
	-4.73
	-4.73
	-4.66
10	**-5.03**
	-4.92
	-4.92
	-4.87
	-4.64
	-4.63
	-4.39
	-4.2
	-4.08
	-3.91
	-3.83
	-3.78

Table A.3 Fpocket results

Human (2QLY)		Rat (homology)	
Rank	Pocket score	Rank	Pocket score
1	40.6198	1	39.7893
2	24.3316	2	26.3544
3	23.9379	3	26.1438
4	22.7107	4	25.8207
5	19.0911	5	23.6258
6	16.9132	6	23.0038
7	15.8819	7	21.4583
8	14.5601	8	20.9685
9	14.3890	9	17.9303
10	14.3760	10	17.3478
11	13.5752	11	17.1288
12	12.4564	12	15.8245
13	12.4529	13	15.4024
14	12.4280	14	15.0978
15	11.8928	15	14.5059
16	11.8148	16	14.3946
17	11.6288	17	14.3685
18	10.7631	18	13.2492
19	9.8124	19	13.1511
20	9.7770	20	13.0672
21	9.5181	21	13.0021
22	9.2242	22	12.8104
23	8.7699	23	12.1916
24	8.3241	24	11.3377
25	8.2389	25	10.7970
26	7.9878	26	9.3377
27	7.5561	27	8.4079

Table A.3 Fpocket results (continous)

Human (2QLY)		Rat (homology)	
Rank	Pocket score	Rank	Pocket score
28	7.0416	28	8.1180
29	6.1509	29	8.1032
30	5.9082	30	7.9926
31	5.0941	31	7.9411
32	4.7106	32	7.8577
33	3.2301	33	7.7063
34	2.7461	34	7.3675
35	2.6612	35	7.3142
36	1.8512	36	7.3137
37	1.7317	37	6.4650
38	1.0398	38	6.4403
39	1.0109	39	6.1921
40	0.9528	40	6.0217
41	0.2078	41	5.2574
42	-0.0380	42	5.1822
		43	4.6946
		44	4.4323
		45	4.4013
		46	4.3645
		47	3.6335
		48	3.4728
		49	3.2856
		50	3.0963
		51	3.0629
		52	-0.8797

VITA

Education:

2015 Ph.D. (Organic Chemistry, Chulalongkorn University)

2009 B.Sc. (Chemistry, Chulalongkorn University)

Scholarships:

2010-2015 Chulalongkorn University Dutsadi Phiphat Scholarship

2009-2010 The Graduate School of Chulalongkorn University

Publications:

Worawalai, W.; Rattanangkool, E.; Vanitcha, A.; Phuwapraisirisan, P. and Wacharasindhu, S. Concise synthesis of (+)-conduritol F and inositol analogues from naturally available (+)-proto-quercitol and their α-glucosidase inhibitory activity. Bioorg. Med. Chem. Lett. 2012, 22, 1538-1540.

Rattanangkool, E.; Kittikhunnatham, P.; Damsud, T.; Wacharasindhu, S. and Phuwapraisirisan, P. Quercitylcinnamates, a new series of antidiabetic bioconjugates possessing α-glucosidase inhibition and antioxidant. Eur. J. Med. Chem. 2013, 66, 296-304.

Rattanangkool, E.; Krailat, W.; Vilaivan, T.; Phuwapraisirisan, P.; Sukwattanasinitt, M. and Wacharasindhu, S. Hypervalent iodine(III)-promoted metal-free S–H activation: New approach for the construction of S–S, S–N and S–C bonds. Eur. J. Org. Chem. 2014, 2014, 4795-4804.

Busacca, C.A.; Miligan, J.A.; Rattanangkool, E.; Ramavarapu, C.; Chen, A.; Saha, A.K.; Li, Z.; Lee, H.; Geib, S.; Wang, G.; Senanayake, C.H. and Wipf, P. Synthesis of phosphoguanidines by hydrophosphination of carbodiimides with phosphine boranes. J. Org. Chem. 2014, 79, 9878-9887.